Late Cretaceous to Cenozoic Reactivation of Central Scotian Slope Salt Bodies and the Impact on Slope Depositional Systems

by

Andrea Christians

Submitted in partial fulfilment of the requirements
for the degree of Master of Science

at

Dalhousie University
Halifax, Nova Scotia
April 2015

Table of Contents

List of Tables

List of Figures

Abstract

The history of younger (Late Cretaceous to present) salt-related deformation is largely unknown on the Scotian Margin. This study investigates the style and timing of Late Cretaceous to Cenozoic salt tectonic rejuvenation on the upper Scotian Slope and related effects on depositional systems using two 3D seismic surveys. Salt bodies were passively extruded between the Cenomanian/Turonian and Ypresian followed by a period of quiescence and drape between the Ypresian and Rupelian. Compressional rejuvenation began at different times in two structural provinces. In the vertical salt diapir province (west), compression began in the Bartonian (Late Eocene) and in the allochthonous tongue province (east) it began in the Rupelian (Early Oligocene). At some point between Pliocene and today, compression rates waned and a period of slope regrading took place, planing off much slope relief. This was succeeded by a series of mass transport deposits and erosive canyons to yield the modern-day seafloor.

Acknowledgements

I would like acknowledge my supervisors Mark Deptuck, Andrew MacRae and Nicholas Culshaw for their encouragement and guidance. I would also like to thank the Canada-Nova Scotia Offshore Petroleum Board and all their employees for sponsoring this project and their continuous support throughout. I would like to thank the Pengrowth/Nova Scotia Department of Energy and Geological Society of America for additional funding.

Additionally, I would like to thank Encana and Shell and partners for collecting such excellent data-sets. I express great gratitude to Becky Jamieson for her help throughout my master's and to my examining committee Calvin Campbell, Martin Gibling and Dave Mosher for their helpful feedback.

Finally, I would like to thank my parents, Luc Cormier, Brad Stout and Sharane Simon for the continuous support they have given me throughout my graduate degree. Lastly, my cats Luci and Demon Christians for always being the cutest cats.

Chapter 1: Introduction

1.1 The problem

The continental margin of Nova Scotia, Canada (the Scotian Margin) rifted during the Late Triassic to Early Jurassic, during which a narrow Central Atlantic Ocean allowed salt and other evaporites to be deposited. Today, it is estimated that approximately half of the margin is affected by salt tectonics (Ings and Shimeld 2006). Although a major control on slope morphology, the younger (Late Cretaceous to Cenozoic) history of salt deformation remains largely undocumented. This study analyzes the history of salt movement from the Late Cretaceous and Cenozoic, including periods of quiescence, passive extrusion and compressional active diapirism on the central Scotian Slope. Documenting salt movement during this time may have broader implications for the understanding of other salt structures across the Scotian Slope. Besides scientific interest, variation in the style and timing of salt tectonism and the depositional processes affected by it ultimately have implications for hydrocarbon traps in the central Scotian Slope, and thus are economically interesting as well.

The study area is located in the central Scotian Slope between two different salt tectonic structural domains. The western study area is a region of isolated, generally vertical salt diapirs (salt province II of Shimeld 2004). These salt bodies are generally circular to elliptical in plan view with vertical stalks and salt wings, the latter providing evidence of passive extrusion during their formation (see sections 2.1.1 and 2.1.2). The area of vertical salt diapirs changes into amalgamated allochthonous salt tongues (sheet-like canopies) in the eastern part of the study area **(**salt province III of Shimeld 2004; see section 4.3) **(**Fig. 1.1). Allochthonous tongues in the east are sub-horizontal and elongate in the downslope direction.

Overlying strata in both structural provinces are commonly folded immediately above vertical diapirs and salt tongues with some intervals showing stratigraphic thinning above salt crests, indicating rejuvenation of the salt structures and providing constraints on the timing of fold growth. Deformation of this type can be linked to active diapirism, whereby the salt forcefully pushes upward, deforming its overburden (see section 3.3) (Hudec and Jackson 2011). Although previously noted by Shimeld (2004) and Deptuck et al. (2009), active diapirism in this younger interval was not investigated in detail by prior authors.

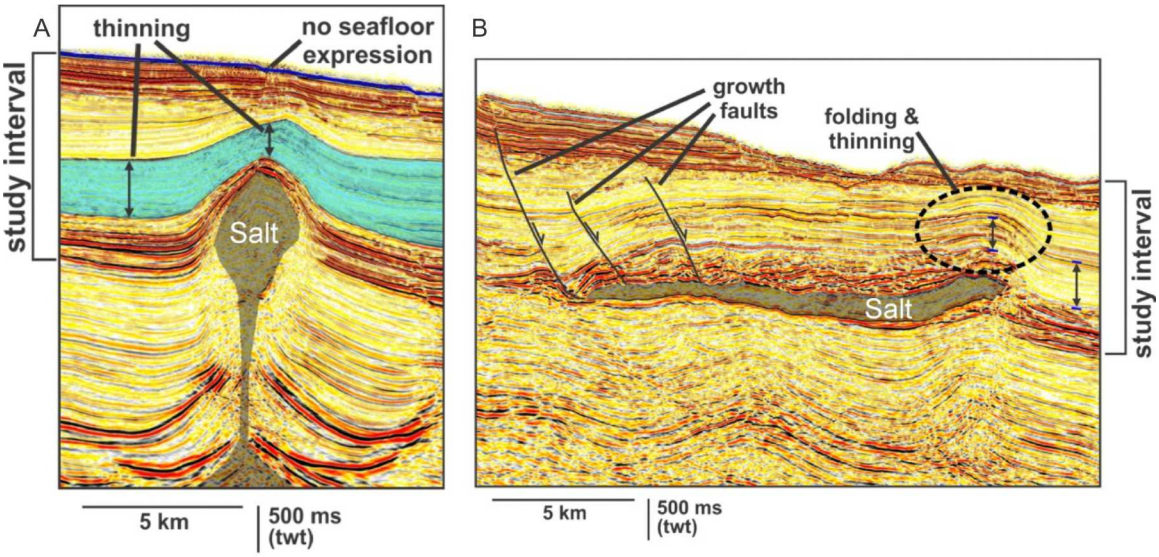

Figure 1.1: A seismic section across the study area depicting the salt structures in the vertical diapir structural-province (A) and the allochthonous tongue province (B) and the features that indicate the timing of salt structure deformation.

Active diapirism can be subdivided into two types: halokinetic active diapirism and compressional active diapirism (Hudec and Jackson 2011). Distinguishing between them is often difficult (see section 3.3). Halokinetic active diapirism is the upward movement of buried salt diapirs in response to adjacent sediment loading (downbuilding) whereas compressional active diapirism is the upward movement of buried salt diapirs from periods of broader

regional/tectonic lateral squeezing. Determining the type of active diapirism can further constrain the origin of slope changes in the study area.

Processes driving active diapirism are varied and poorly understood, however, a period of lateral compression in the downslope area may be related to processes occurring on the shelf or uppermost slope, such as increased loading from rapidly depositing sediments (Rowan et al. 2004).

Near the study area and during the study time interval, the Scotian Shelf has been host to shelf-edge deltas, shelf-crossing glaciations and more than 1500 m of upper slope contourite deposits that may be responsible for downslope contraction (Piper et al. 1994; Fensome et al. 2008; Campbell 2011; Deptuck 2011a; Weston et al. 2012). Other studies based on apatite fission track thermal modeling indicate a period of post-Paleocene uplift in the onshore and shelf areas in the region (Grist and Zentilli 2003). A period of uplift could have increased the tilt of the margin which could trigger downslope compression. It is expected that the timing of lateral compression was synchronous with the timing of active diapirism. Thus, linking the timing of compression will help determine (or at least narrow down) the possible processes driving active diapirism and reaekctivation of salt structures in the study area.

1.2 Objectives

The objectives of this study are as follows:

1.) To define a seismic stratigraphic framework for the Late Cretaceous and Cenozoic strata on the central Scotian Slope, calibrated to available wells in the study area. What are the major changes in slope sedimentation? How does the sedimentary system respond to changing salt-related bathymetric relief?

2.) To determine the history of salt-related sediment deformation:

   a. Unravel the history of passive diapirism in the study area. Were diapirs passively extruded onto the seafloor? If so, when did it start and when did it stop? Why did it stop?

   b. Study the timing and style of active diapirism in the study area. Is it halokinetic or compressional active diapirism? Was it a solitary event or several? Is deformation uniform throughout or does it vary over the study area?

3.) If evidence of compressional active diapirism exists, to determine the possible causes behind such an event. Are there several different processes driving lateral compression or is it solely linked to one system (e.g. upslope contourite deposition, localized linked system).

1.3 Thesis organization

This thesis is subdivided into 7 chapters: Introduction, Background, Methods, Seismic Stratigraphic Framework, Reconstructing Salt-related Deformation, Discussion and Conclusions.

Chapter 2 presents the previously-published background material on salt tectonics, slope stratigraphy and the Scotian Margin, including what is known about the movement of salt. Chapter 3 focuses on the datasets and techniques used to identify passive and active diapirism and the necessary steps of mapping and analyzing the 3D surveys in this study.

Chapters 4 and 5 describe the seismic stratigraphy and salt-related deformation i.e. mapping of horizons, identifying depositional trends, and documenting salt deformation based on the Late Cretaceous to present day stratigraphy. Chapter 7 discusses the implications of active diapirism on the central Scotian Slope and explores the possible origins of rejuvenated salt

deformation on the Scotian Margin. Finally, Chapter 7 summarizes the main points from the preceding chapters.

1.4 Study area

The study area is located on the central Scotian Slope where 21 salt bodies occur within the boundary of 2 overlapping 3D surveys (Fig. 1.2). The surveys cover approximately 5300 km^2 and extend from the outer shelf (in present-day water depths as shallow as 70 m) to the middle slope (in present-day water depths up to 3200 m). The interval of interest is the Late Cretaceous to present day stratigraphy, consisting of a downslope-thickening succession of up to 2 seconds TWTT (two-way travel time).

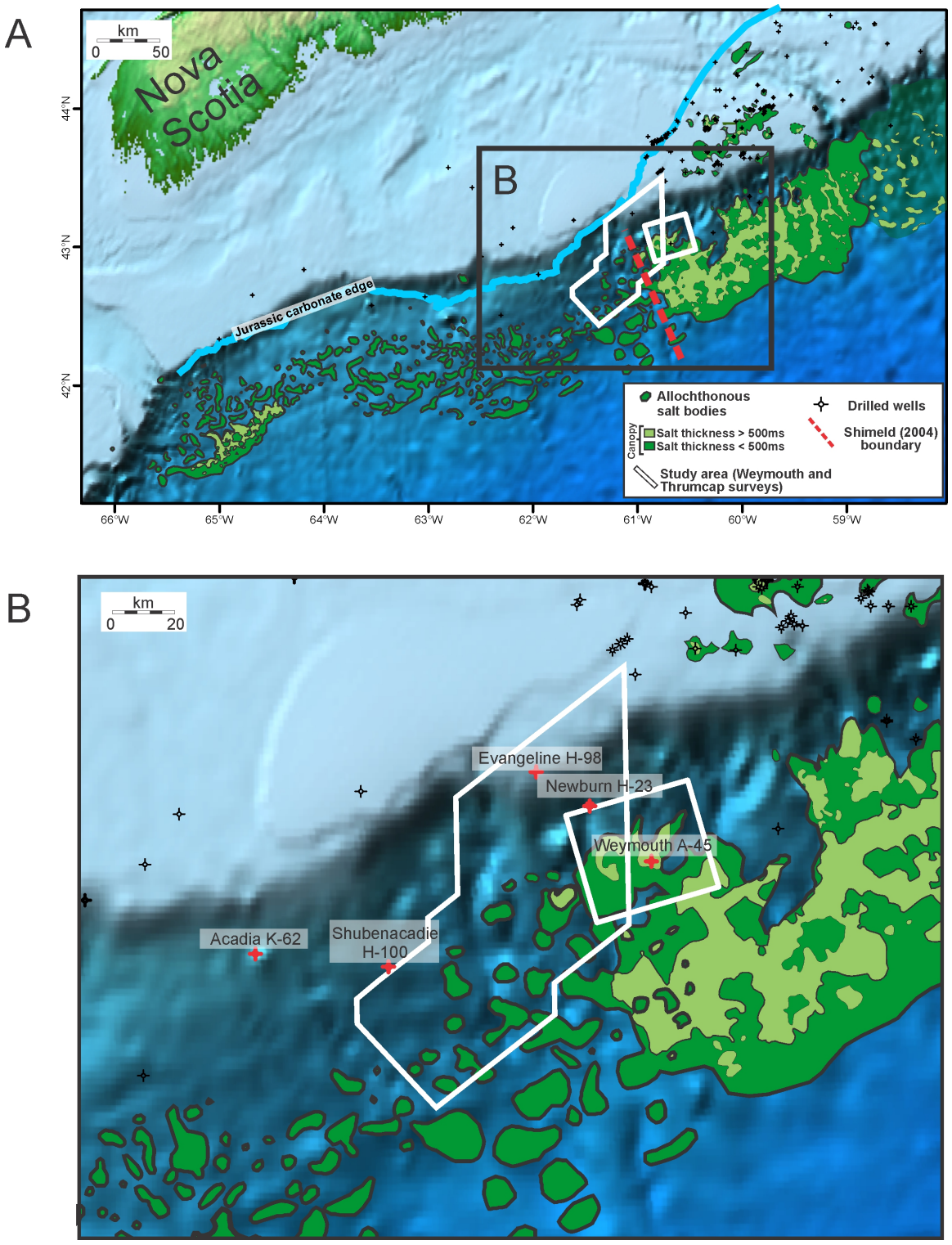

Figure 1.2: A) Present day bathymetry and salt distribution of the Scotian Margin (modified from Deptuck and Kendell 2011). The study area is highlighted in white and salt bodies in green. Dotted red line marks the boundary between structural provinces of Shimeld (2004); B) An enlarged version showing local salt distribution and wells of interest highlighted in red.

Chapter 2: Background

2.1 Salt tectonics

Salt (halite) and other evaporite minerals are generally deposited in warm climates within restricted basins (e.g. lagoonal or narrow ocean basins) allowing evaporites to precipitate from seawater or saline lakes over time, depositing on the basin floor. Such deposits are mechanically weak, in contrast to the stronger, rigid overburden (Hudec and Jackson 2007). For this main reason, salt commonly experiences ductile deformation in comparison to brittle sediments (Hudec and Jackson 2007; Dooley et al. 2009). The ductile deformation of salt results in a variety of geometries, often forming discordant contacts with surrounding strata as it moves. Such a structure is called a salt diapir (Hudec and Jackson 2011).

Until the 1980s, salt diapirism was thought to be initiated by buoyancy, however more recent work shows that differential pressure is the primary driving force and density plays only a secondary role (Jackson 1995; Hudec and Jackson 2007; Dooley et al. 2009). This change came with the realization that overburden is significantly stronger and more brittle in comparison to the salt. Changes in pressure and the consequent flow of the salt are related to the rheological contrast between the surrounding overburden that is brittle and the incompressibility of the salt that is ductile (Jackson 1995; Hudec and Jackson 2007).

Salt that has moved from its original depositional position is called allochthonous salt. In contrast, autochthonous salt has not moved from its original site (i.e. in terms of its stratigraphic position, autochthonous salt always underlies younger stratigraphic layers). The migration of salt from its autochthonous position due to pressure gradients is called ‘salt withdrawal’ or ‘salt expulsion’ (Hudec and Jackson 2007). Salt withdrawal can result in large (kilometre) scale

subsidence basins due to source layer depletion (Jackson et al. 1994). The loading of salt and resulting generation of pressure gradients can be triggered by a variety of forces (see below).

2.1.1 Forces behind differential loading of salt

The three dominant driving forces for deformation of salt are gravitational displacement, displacement loading (lateral extension or compression) and thermal loading. Gravitational displacement occurs when the weight of overburden exerts differential force on the underlying salt and sediment (Hudec and Jackson 2007). Gravity can also drive lateral forces on salt from processes such as crustal-scale tilting (e.g. gravity gliding) (Rowan et al. 2004). Displacement loading is the forceful displacement of a rock boundary relative to another either through extensional or compressional tectonism (Hudec and Jackson 2007). This is common in areas with pre-existing salt structures that are further deformed because they focus regional strain and are the weakest part of the system (Hudec and Jackson 2007). Thermal loading is the response of salt to temperature because higher temperature salt is generally more buoyant, mechanically weaker and prone to rise via intra-salt convection (Hudec and Jackson 2007).

Types of salt structures

Salt structures are map-scale bodies that have deformed from their original depositional layer e.g. vertical salt diapirs, salt walls, salt anticlines and salt sheets/canopies (Fig. 2.1; Hudec and Jackson 2007, 2011). All salt diapirs are a ductile mass of salt that have disconcordant contacts with overburden (Hudec and Jackson 2011). The term *vertical salt diapir* is a generic term used to describe all salt structures with a circular to sub-circular planform shape. Vertical diapirs generally have an upper (wider) portion called the bulb and a lower (narrower) portion called a stem (Fig. 2.1). The downward-flaring portion of the diapir stem is called a salt pedestal.

A salt sheet is sourced from a single feeder and characterized as being several times longer than it is thick (Fig. 2.2; Hudec and Jackson 2011). A salt tongue or sheet is defined as an asymmetric salt sheet elongate in the dip direction and a salt canopy is an amalgamation of two or more salt sheets/tongues.

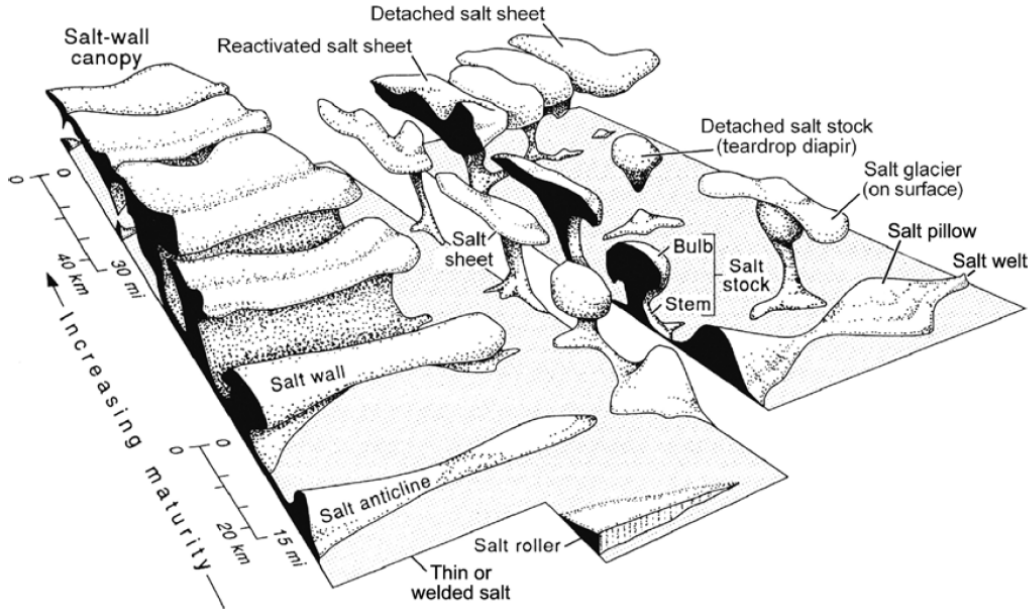

Figure 2.1: Different varieties of salt structures from Hudec and Jackson (2007).

Salt-cored anticlines are the result of buckling of overburden and the flow of salt into the low-pressure core of the anticlines due to lateral compression (Hudec and Jackson 2007). Since salt is the weakest part of the system, shortening is accommodated in the roofs of pre-existing salt structures versus the adjacent rigid overburden (Hudec and Jackson 2007). They can produce significant topographic or bathymetric relief.

Welds and roho systems

A salt weld is a contact where salt has been removed by creep flow and dissolution, allowing sediment formerly separated by the salt body to be in direct contact. A salt weld is an area where salt contacts above and below the salt merge via evacuation of the salt through creep flow and dissolution (Rowan et al. 1999; Hudec and Jackson 2007). Welds separate discordant or disconformable strata and are the remnants leftover from salt expulsion (Jackson et al. 1994). Roho systems are a group of basinward dipping growth faults that sole into allochthonous salt sheets, canopies or salt welds (Hudec and Jackson 2011).

2.1.2 Modes of salt diapir deformation

Salt structures form from three different processes: reactive, passive and active diapirism (Fig. 2.2). Reactive diapirism is the rise of salt in response to thinning of overburden by lateral extension and normal faulting (Vendeville and Jackson 1992).As the overburden is extended, salt can then rise between extensional blocks to create a salt structure (Hudec and Jackson 2007). Active diapirism is the forcible rise of a buried diapir relative to its overburden due to either the pressure generated on the salt in adjacent minibasins or from regional lateral compression (Schultz-Ela et al. 1993; Hudec and Jackson 2007, 2011; Dooley et al. 2009). In comparison to active diapirism, passive diapirs are not buried but rather exposed on the surface with only a thin sediment drape preventing dissolution. Passive diapirism is the syn-depositional vertical rise of a diapir relative to sediments around it (Hudec and Jackson 2007, 2011). If salt vertical extrusion rates are equal to the surrounding vertical sedimentation rates, the salt diapir will maintain its exposure on the surface, and if at any point during extrusion, salt extrusion rates exceed sedimentation rates, an allochthonous tongue forms.

Passive diapirism is driven by the weight of the surrounding overburden acting on the source layer below. The autochthonous salt layer subsides with the surrounding sediments and this synchronous process is called downbuilding (Fig. 2.2; Hudec and Jackson 2007, 2011).

Whether a passive diapir becomes buried or not is dependent on the rate of vertical salt movement versus the rate of local sedimentation and as such, if sedimentation rates exceed the rate of salt movement it will facilitate burial (i.e. relatively rapid sedimentation rates are required to bury a salt diapir that is still actively being supplied from the primary salt layer). In contrast, when salt movement rates equal or exceed sedimentation rates, the salt extrudes on the surface.

The presence of allochthonous tongues and vertical salt diapirs in this study area indicates that active and passive diapirism are the most important mechanisms behind salt movement in the study area during the Late Cretaceous and Cenozoic. Active diapirism can be subdivided into halokinetic and compressional active diapirism.

2.1.3 Differentiating halokinetic from compressional active diapirism

Distinguishing halokinetic from compressional active diapirism is commonly difficult. The presence of pinched stems, a thick overburden and salt pedestals at the base of the diapir can differentiate compressional active diapirism from halokinetic (Table 2.1) (Vendeville and Nilsen 1996; Hudec and Jackson 2011). These features imply lateral shortening of a vertical salt stalk to the point that salt was expelled entirely (salt weld formation) and the folding of overburden thicker than is plausible from halokinetic processes (e.g., >100m). See section 3.3.1 for a full description of the techniques used to differentiate halokinetic from compressional active diapirism.

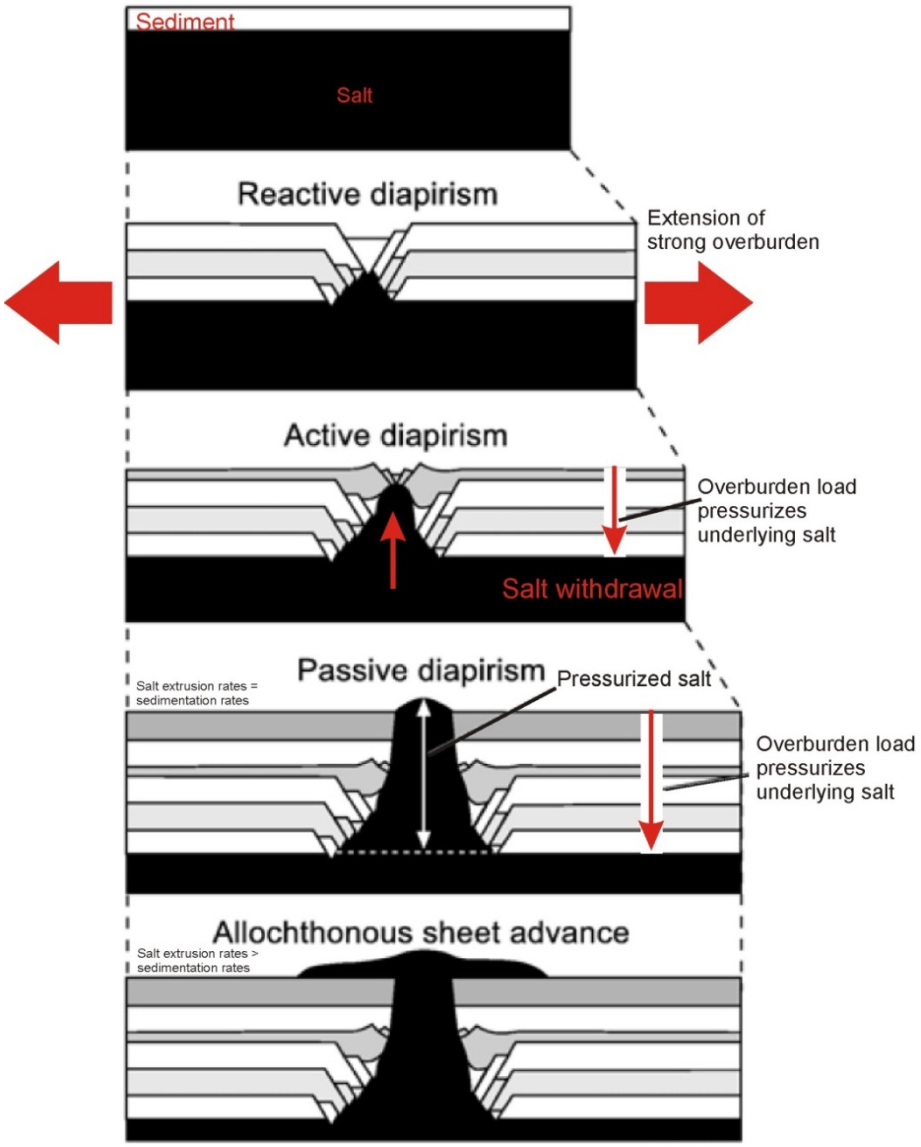

Figure 2.2: A cartoon depiction of the different methods of diapir initiation (active, passive and reactive) modified from Hudec and Jackson (2007). Often, diapirs undergo several variations of each of these mechanisms throughout their history. Reactive diapirism is driven primarily by regional extension (see Vendeville and Jackson 1991). Active diapirism can be compressional or halokinetic (see section 3.3). In this schematic, halokinetic active diapirism is sourced from the downward pressure of surrounding sediment, displacing overburden as the salt is forced upward. Once the diapir pierces the surface, it is passive and driven by downbuilding from the weight of surrounding sediments. If salt rates exceed sedimentation rates, it can extrude onto the seafloor creating an allochthonous sheet or tongue.

	Compressional	Halokinetic
Stratal thinning above salt diapir crests	Yes	Yes
Crestal radial faults	Yes	Yes
Pinched diapir stem	Yes	No
Salt growth after welded-out source layer	Yes	No

Table 2.1: Differentiating characteristics of halokinetic versus compressional active diapirism.

2.2 Dominant depositional and erosional processes and products on continental slopes

A sediment-gravity flow is the downslope transport of a water-sediment mixture under the force of gravity (Mulder 2011). The efficiency of a gravity flow is dependent on the flow composition and slope gradient (Shanmugam 2006; Jackson et al. 2008). Gravity flows are initiated by many different processes, such eustatic fluctuations (i.e. lowering of sea level), prograding carbonate systems or deltas (oversteepening), earthquakes, storm waves and hyperpycnal flows (Normark and Piper 1991; Ross et al. 1994; Shanmugam 2006; Jackson et al. 2008).

Initiation of a sediment failure event depends on the local sediment strength (cohesion) and seabed slope and in order for a given sediment layer to move, it must overcome the frictional force of sediment grains (Carter 1975; Postma 1986; Normark and Piper 1991; Nelson et al. 2011). For example, the prograding unconsolidated sediments from a delta or glacial deposit are more prone to failure both because they are relatively uncompacted initially (less cohesion), and because the deposition process creates a slope where gravity-driven shear stress can exceed the sediment's shear strength.

Sediment gravity deposits can be subdivided into two main categories: mass transport deposits or turbidites (Shanmugam 2006).

Mass transport deposits

Mass transport deposit (MTD) is a general term used to describe slumps, slides and debris flow deposits emplaced by gravity flows (excluding turbidity flows) (Fig. 2.3; Carter 1975 Lowe 1982; Postma 1986; Nelson et al. 2011).

Slumps are deposits with rotational deformation (Lowe 1982; Shanmugam 2006; Nelson et al. 2011). Mass transport deposits can also initiate as slides and break up the internal structure of the rock/sediment as they continue downslope forming a debris flow with a more laminar flow regime (Nelson et al. 2011). Debris flows consist of a higher density of particles in upwards of 50% of the flow (Lowe 1982; Mulder 2011).

Mass transport deposits have varying geometries. In plan view, they generally have elongate, sometimes discontinuous tongue-shaped geometries and are generally very mud-prone on slopes. In cross section, they are typically mounded with steep margins and rugose tops (Bull et al. 2009; Meckell 2011; Mulder 2011). They can be large-scale spanning 10 to 800 km in length, 1-300 km wide and 10-600 m thick. Smaller scale deposits are on the order of 0.1-20 km long, 0.1-15 km wide and 5-50 m thick (Bull et al. 2009).

A headwall scarp marks the upslope margin of many mass transport deposits. Headwall scarps in essence represent the extensional domain of the MTD and often form extensional faults (Bull et al. 2009; Dalla Valle 2013). Scarps can vary widely in height from 10 m to > 1000 m (Bull et al. 2009).

The central part of the flow is referred to the as the translation domain which can experience large amounts of deformation as it travels downslope. Generally the toe domain of the deposit shows thrust, folds and pressure ridges (Fig. 2.3; Bull et al. 2009; Dalla Valle 2013).

Folds can help constrain the paleodirection of the flow (i.e. fold axes are perpendicular to the direction to the flow) in addition to identifying and differentiating the deposit from others. Thrust faults are common, generally affecting the overall thickness of the MTD (Bull et al. 2009). These thrusts are often densely spaced and the spatial difference between fault throws can create an irregular surface on the top of the MTD.

Mass transport deposits can conform to slope morphology. Basal surfaces have been known to ramp up or down to a new stratigraphic level between intervening flats (Bull et al. 2009; Mulder 2011). Ramps can be scarps, faults or any linear feature that has sharp topographic variations, generally trending perpendicular to the flow direction (Bull et al. 2009).

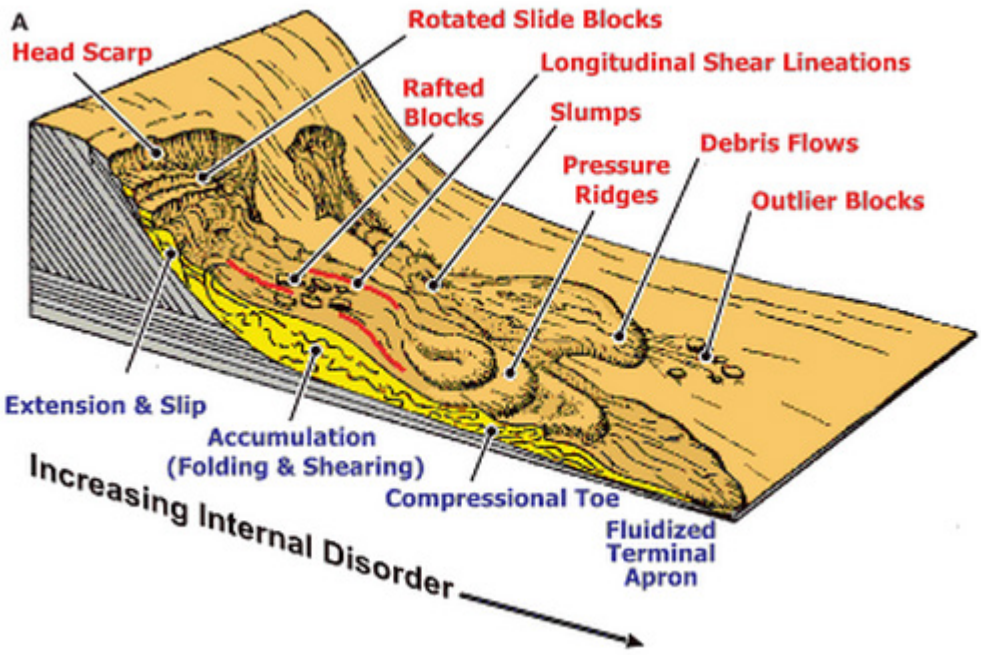

Figure 2.3: Image showing different types of mass transport deposits. From Meckell (2011), previously modified from (Prior 1984) and Galloway and Hobday (1996).

Turbidites

Turbidites are deposits that contain graded sand, silt, and mud beds deposited by turbidity currents (Nelson et al. 2011). Turbidity flows are defined as the local downslope flow of sediment lifted by the upward movement of suspended particles via fluid turbulence (Lowe 1982; Bouma 1962, 2004). Such flows are turbulent at the head of the flow, followed by a more laminar flow body that sorts sediments in a diagnostic fining-upward sequence known as the Bouma Sequence (Fig. 2.4; Bouma 1962). Flows are short-lived, generally on the scale of hours to days (Normark and Piper 1991; Shanmugam 2006). Turbidity currents can be further subdivided into high (coarse sand to cobble-dominated) or low (clay to medium sand-dominated) density flows (Lowe 1976; Lowe 1982; Bouma 2004). When deposited as a turbidite and when all parts of the succession are present, they are characterised by an erosive base, massive sandstones fining upward into laminar beds, grading into current ripples and finally into laminar (concordant) hemipelagic to pelagic muds (Bouma 1962).

Turbidity flows can be triggered by different types of events, for example, storm surges can increase the rate of failure by creating rip currents that cannibalize sands from canyon heads and trigger slope failure by locally increasing slope angle, increasing shear stress on the sediment bottom, and/or increasing pore fluid pressure by loading (which decreases shear strength; Normark and Piper 1991). These rip currents can channel coastal sands down submarine canyons most commonly in lowstands (Normark and Piper 1991). Contour currents can form contourite sheet deposit

Hyperpycnal flows are density flows that can also trigger turbidity currents from the rapid input of dense cold and sediment-laden water (Normark and Piper 1991). These flows are a product of high river water sediment concentrations and the resulting density and temperature

differences. Shelf-edge deltas can also act as gateways for hyperpycnal flows as the rivers discharge cold fresh water during a lowstand onto the slope (Normark and Piper 1991).

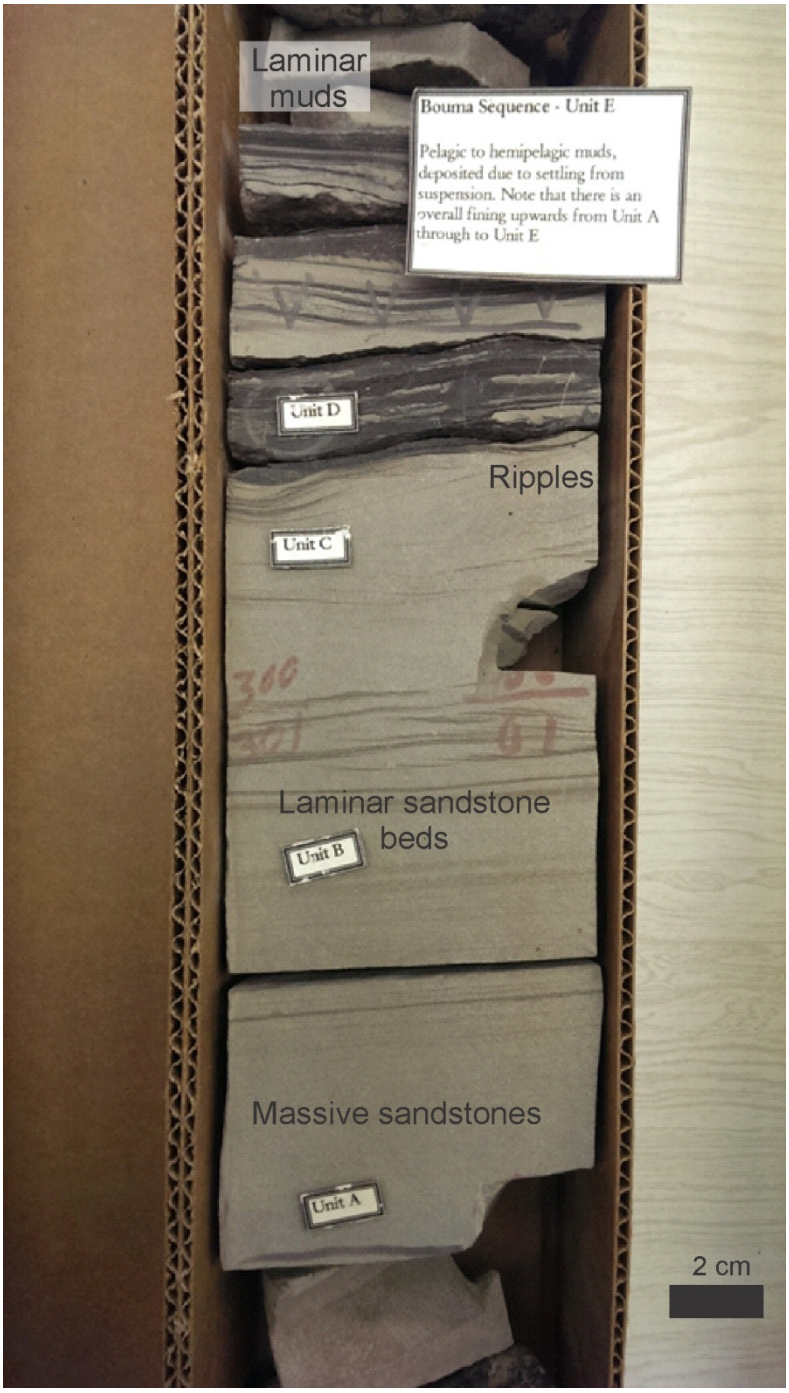

Figure 2.4: A typical Bouma fining-upward sequence. Photo taken at the Bureau of Economic Geology (BEG) Core Center, Houston, Texas.

2.2.1 Submarine canyons and channels

Turbidity currents (and other mass wasting processes) are responsible for the formation of submarine canyons, channels and fan systems (Hay 1987; Normark and Piper 1991). Submarine channels are studied worldwide and are oil and gas exploration targets in deepwater settings because they commonly contain reservoir sands (Deptuck et al. 2003, 2005; Cronin et al. 2005; Jackson et al. 2008, McHargue et al. 2011). Although the process is not fully understood, gravity flows generally follow topographic lows, carving out a channel over repeated use of a given flow corridor. These channels are produced by confined flows that generally occur on slopes with bathymetric relief. Changes in relief can be as low as 1° to 3° for a gravity flow to respond and react by diverting or depositing sediments around it.

In contrast to submarine channels, submarine canyons are notably larger (km scale) and confined to the upper slope. These canyons can be initiated by headward backstepping from the upper slope to the eventual shelf-edge, trapping and funnelling turbidite deposits (Cronin et al. 2005). Other causes include erosion from turbidity currents, glacial processes, and mass wasting events.

Slumps and debris flows are common in submarine canyons and their products consist of muddy matrices with channel fill ranging from muddy to clean sands that generally are not reservoir grade targets (Mayall et al. 2006). Slumps are generally common along canyon walls on the upper slope and shelf-edge where canyons are usually at their steepest (Cronin et al. 2005; Deptuck et al. 2012).

2.2.2 Contour currents

Although down-slope gravity-related processes are major influences, contour currents also exert a strong influence on the stratigraphic development of continental slopes. Contour

currents are deep-water (300 to ≥ 2000 metres) bottom currents formed by worldwide thermohaline circulation and are directly related to the global climate and continent positions (Viana et al. 2007). Accumulations from such currents are called 'contourite drifts' and are often interbedded with turbidites (Faugeres et al. 1999; Stow and Mayall 2000). Contourite drifts vary in scale from several metres to tens of kilometers in length and the flow velocity responsible for them can change at different depths within the water column (Stow and Holbrook 1984). They are found worldwide and have recently been recognized as potential prospects for oil and gas exploration (Stow and Mayall 2000; Viana et al. 2007).

The main factors controlling contourite deposition are: intensity and duration of the bottom-current; available sediment supply; sea-floor morphology and the general margin configuration (Viana et al. 2007). Paleoceanographic data can be extracted from cyclicity that is often preserved in long-term deposits from bottom-water currents. For example, bottom water activity generally increases through inter-glacial cycles with faster flow rates and larger grained sediments, and in contrast, glacial periods see significantly lower flow rates and finer grained sediments (Stow and Holbrook 1984; Brackenridge et al. 2007).

The distribution of contourites is directly to bottom-current intensity (Viana et al. 2007; Brackenridge et al. 2011). Strong bottom water currents (> 100 cm/s) are often localized and short-lived (Stow and Holbrook 1984; Viana et al. 2007; Brackenridge et al. 2011). Contour currents can flow downslope or along slope, forming eddies at right angles to flow direction (Stow and Holbrook 1984; Brackenridge et al. 2007). Contour currents can form contourite sheet deposits with uniform thickness and slightly tapered ends (Faugeres et al. 1999). These sheets can consist internally of large fields of sediment waves (Faugeres et al. 1999).

Continental slopes are often areas of complex bathymetry, especially on a slope with salt tectonics. The distribution of contourites is directly related to local interaction of contour currents with the margin morphology and the effect of a readily available sediment supply (Viana et al. 2007; Brackenridge et al. 2011). Large scale margin changes related to tectonic or depositional processes can cause changes in the intensity and consequently the configuration of bottom currents and their deposits (Viana et al. 2007).

2.3 Slope morphology and its impact on sedimentation

In response to increased or decreased accommodation space (available space for sediment deposition) on an irregular slope, basins undergo different types of slope sedimentation and erosion to reach equilibrium eventually (Fig. 2.6; Ross et al. 1994; Prather 2000, 2003; Kneller 2003; Olafiranye et al. 2013).

Trapping of sediment in a three-dimensional closure on a slope is referred to as ponding. This process mainly occurs on irregular slopes with complex bathymetric relief. On these bumpy slopes, gravity flows follow the path of least resistance and flow into areas of local topographic lows where the slowing flows deposit as fans. Tectonic and depositional relief in the upper slope are therefore potential mechanisms for trapping reservoir grade sands on the upper and middle slope which would have otherwise been a bypass zone to the basin floor (Fig. 2.5) (Prather 2000; Prather 2003; Olafiranye et al. 2013). For example, the presence of salt domes will divert flows, allowing sediment to preferentially deposit in adjacent minibasins. A minibasin is a subset of a larger basin and can be defined as a three or four-way closure related to withdrawal of underlying salt. These minibasins are significantly smaller than regional-scale basins and are generally on the scale of tens of kilometres wide. Minibasins have increased accommodation

space and in order for a slope to reach its equilibrium profile, will preferentially fill and stack multiple gravity flows over time. Once the basin is filled, and the equilibrium profile is restored, the flows will continue downslope unimpeded. The same principle applies to salt domes which will preferentially erode (as a high) in order to eventually reach regional equilibrium. Bathymetric highs preferentially erode due to higher slopes on the flanks of the structure (gravity flow trigger), or because turbidite flows and/or contourite flows increase in velocity due to the focusing of the flows over the bathymetric relief.

Once local bathymetric highs and lows are smoothed over by either sedimentation or erosion (from passing gravity flows), sands are generally more easily transferred by sediment gravity flows to the lower slope or abyssal plain (Fig. 2.10) (Booth et al. 2003; Prather 2003).

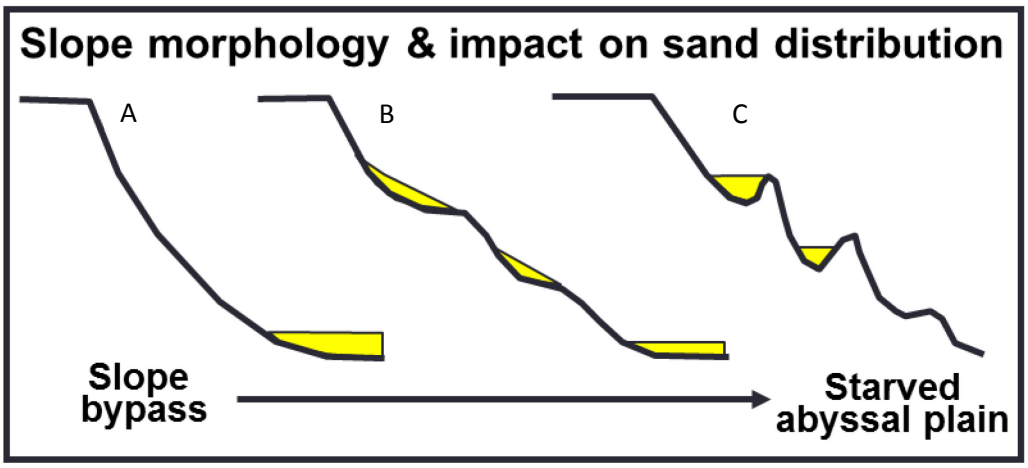

Figure 2.5: Irregular slopes allow sediment to be trapped in topographic lows on the upper/middle slope (B and C) whereas concave up (graded) slopes force sediment to bypass to the toe of the slope (A) (from Deptuck 2011b).

2.4 Lithostratigraphy of the Scotian Margin

The Scotian Slope experienced continental rifting in the Late Triassic to Early Jurassic, and transitioned to a post-rift margin by the Middle Jurassic (Fig 2.6; Wade and MacLean 1990).

Rift-stage sedimentation, including salt units, is described in more detail below (See Chapter 2.5). Middle Jurassic to Lower Cretaceous strata in the southwestern Scotian Margin are dominated by marine carbonates (Abenaki Formation). These carbonates grade laterally to the northeast into clastic deltaic deposits (Mic Mac, Missisauga, and Logan Canyon formations) in a setting collectively referred to as the "Sable Island Delta". These clastic units ultimately grade distally into marine shales (Verrill Canyon Formation; Wade and MacLean 1990; Weston et al. 2012**)**. Input from this and earlier deltaic clastics were the main drivers of salt expulsion from the Jurassic to Cretaceous (Deptuck 2011a; Kendell 2012). These delta systems waned in the Late Cretaceous (Cenomanian) with the deposition of shales (Dawson Canyon Formation) and a thin transgressive limestone called the Petrel Member (Weston et al. 2012). A widespread transgressive chalk was also deposited from the Early Campanian to at least the Maastrichtian across the Scotian Margin, called the Wyandot Formation (Wade and MacLean 1990; Weston et al. 2012). The overlying Banquereau Formation is a mix of interbedded sandstones, mudstones, conglomerates, and some chalk units deposited during the late Cretaceous to Neogene. Chalks are present intermittently between the Paleocene and Eocene, with the most prominent and widespread chalk depositing in the Ypresian (the informal "Ypresian Chalk" unit; Weston et al. 2012). A large bolide impact known as the Montagnais impact occurred around 51 Ma, immediately preceding the Ypresian Chalk, and it initiated widespread mass wasting associated with slope failure (Deptuck and Campbell 2012).

The margin experienced an overall regression and progradation phase during the Tertiary, superimposed with a series of smaller-scale transgressive-regressive cycles (Wade and MacLean 1990). The "Banquereau delta" was a delta system that prograded to the shelf edge of the central Scotian Margin (Campanian-Maastrichtian), later switching to the eastern Scotian Margin in the

Paleocene (Fensome et al. 2008). Overall, a global climatic cooling phase commenced in the Middle Eocene to Present day (Zachos et al. 2001, 2009). The Oligocene experienced a more significant cooling period associated with establishment of Antarctic ice sheets and with a regression that created widespread erosion across the Scotian Margin (Wade and MacLean 1990; Zachos et al. 2001, 2009). The final phases of deposition on the Scotian Margin in the Neogene and Quaternary have been dominated by glacial and glacio-marine conditions related to high frequency (~100 ka) glacial-interglacial cycles from Milankovich cyclicity (Hilgen et al., 2004). Shelf crossing glaciations began post-0.5 Ma with the last major glaciation beginning at about 75 ka (Piper et al. 1994; Stea et al., 1998).

This study focuses primarily on the younger periods of salt-related deformation (Late Cretaceous to Cenozoic) corresponding to the deposition of the Dawson Canyon, Wyandot and Banquereau formations. As such, these formations are described in more detail below, as is the history of the salt that forms the structures affecting the younger stratigraphy.

2.5 Salt tectonics on the Scotian Margin

A widespread series of rift basins formed during the breakup of Pangaea in the Late Triassic to Early Jurassic, including along the Scotian Margin as Nova Scotia rifted from Morocco (Wade and MacLean 1990). Salt and other evaporites of the Osprey and Argo formations were deposited within the narrow rift basin until seafloor spreading had widened the ocean enough for normal marine conditions to occur, probably within the Early Jurassic (Wade and MacLean, 1990; Labails et al. 2010; MacRae et al. 2014). The Scotian Margin has been a postrift margin since at least the Middle Jurassic, and today, it is an area of interest for hydrocarbon exploration largely because of a wide variety of structures that formed in response to the postrift movement of salt (Wade and MacLean 1990).

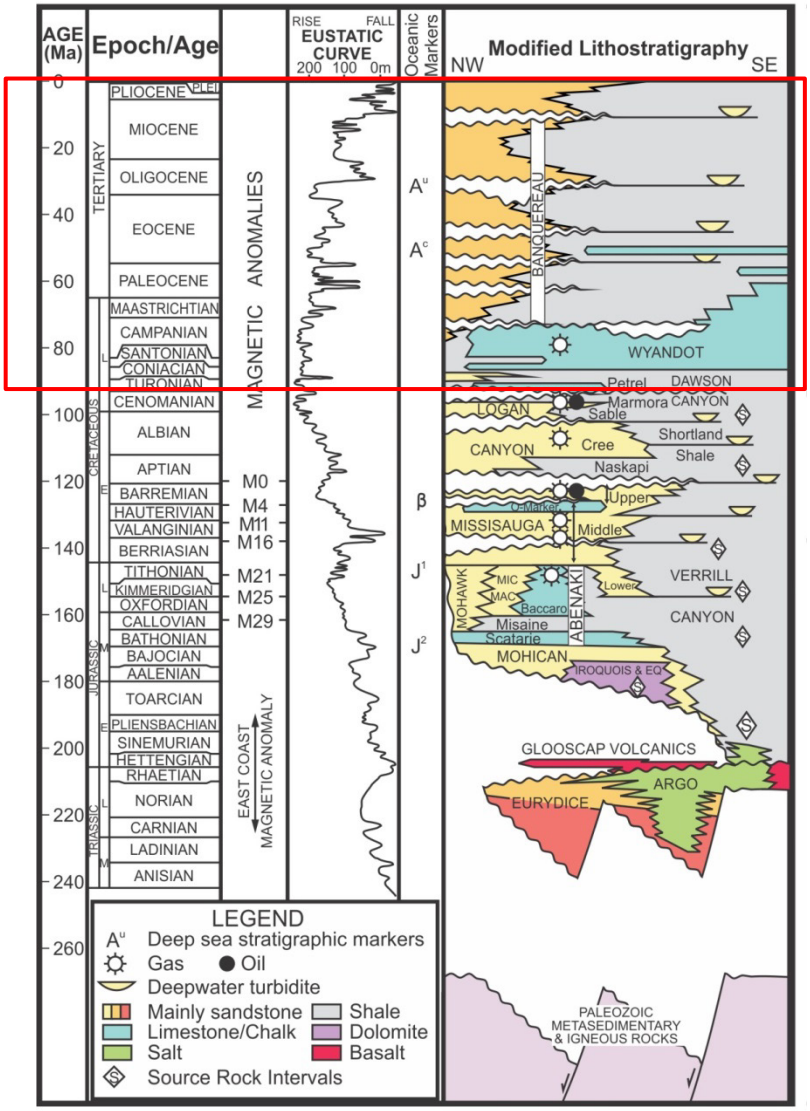

Figure 2.6: Stratigraphic column modified from Weston et al. (2012). The red box highlights the study interval. Although labelled as the Argo Formation, the salt units in the region include both the Argo and Osprey formations. See text for details.

2.5.1 Argo and Osprey formations

During the early Atlantic rift stage in the Late Triassic to Early Jurassic, red beds (Eurydice Formation) and evaporites (Osprey and Argo formations) were deposited on top of Paleozoic basement of the Scotian Margin (Wade and MacLean 1990; Weston et al. 2012; MacRae et al. 2014). The salt on the Scotian Margin is referred to as the Argo Formation (Wade

and MacLean 1990; Shimeld 2004; Ings and Shimeld 2006), although recent studies have hypothesized that the Osprey Formation (originally recognized on the Grand Banks) is also present (MacRae et al. 2014).

The oldest Mesozoic sediments on the Scotian Margin are red clastics of the Eurydice Formation dated late Norian to Hettangian-Sinemurian. The Eurydice interfingers with the salt of the Argo and Osprey formation and is thus coeval with evaporite deposition. Both salt formations contain minor amounts of shale, limestone, and dolostone.

The original thickness of the autochthonous salt on the Scotian Margin is estimated to be at least 2000 m. Since deposition, salt has flowed across the margin in response to sediment loading (OETR 2011). Today, the Scotian Slope is host to a series of different salt structures (e.g. salt pillows, canopies and vertical salt bodies) (OETR 2011).

2.5.2 Salt evolution on the Scotian Margin (Jurassic-Cretaceous)

Previous studies have focused on the Triassic to Early Cretaceous salt tectonics (Jansa and Wade 1975; Wade and MacLean 1990; Shimeld 2004; Ings and Shimeld 2006; Albertz et al. 2010; Deptuck 2011a; Kendell 2012), however, minimal work has been done to document the impact of salt tectonics in the Upper Cretaceous to Cenozoic interval.

Salt structures have been recognized on the Scotian Margin since the early days of petroleum exploration in the 1960s and 1970s. Jansa and Wade (1975) described the “Slope Diapiric Province” stretching along the entire Scotian Slope. More recent work by Shimeld (2004) subdivided the salt structures of the Scotian Slope into five structural provinces (I to V) based on the morphology of the salt structures in each area (Fig. 2.7). Each province shows varying salt geometries: Subprovince I and II are salt walls and vertical diapirs; Subprovince III

is composed of allochthonous salt tongues/canopies; Subprovince IV is a detachment system with little salt left (salt was expelled seaward from the base layer – see Ings and Shimeld 2006; Deptuck et al. 2014); and Subprovince V consists of allochthonous tongues and diapirs (Shimeld 2004). Shimeld (2004) notes a period of late (Cenozoic) salt activity in the vertical salt stock provinces (structural subprovinces I and II) evident by uplift at the crest of some salt bodies continuing until present day, albeit at slower rates.

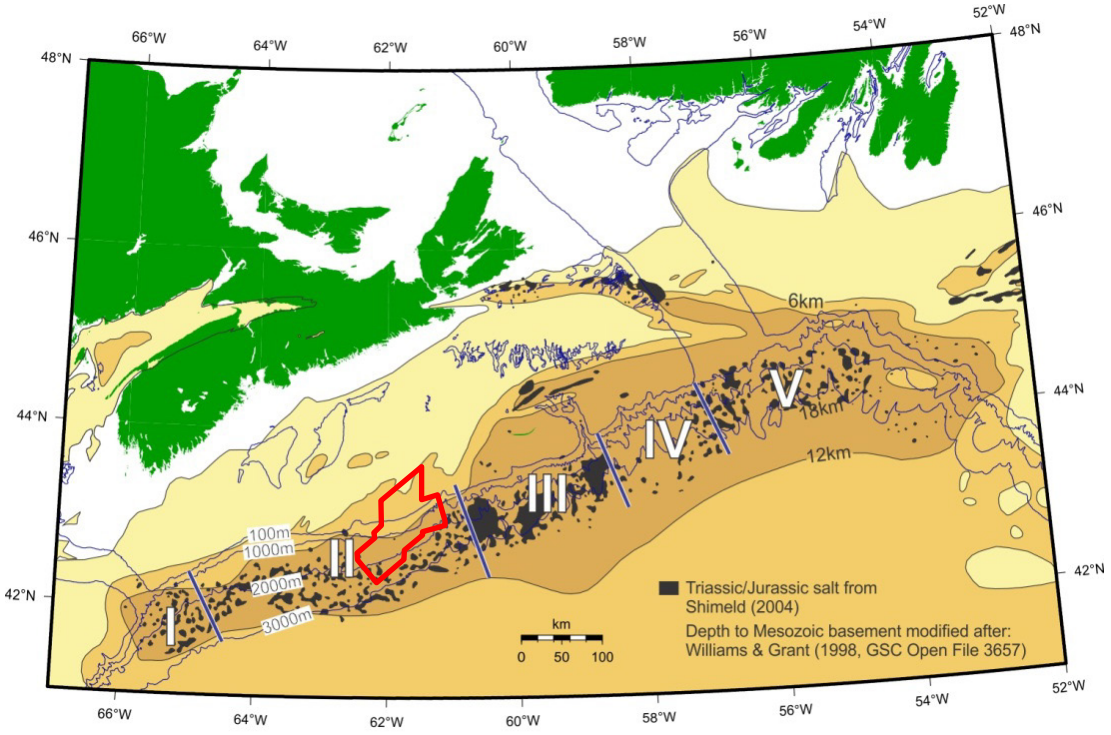

Figure 2.7: Salt mapped by Shimeld (2004) in black and the corresponding Subprovinces I to V overlain on a basement structure map from Williams and Grant (1998). The red outline marks the extent of the study area. Drawing compiled by A. MacRae (Pers. Comm. 2013).

On the central Scotian Slope, Kendell (2012) studied the Sable Canopy Complex (Fig. 2.8; Subprovince III of Shimeld 2004) in greater detail, and determined it is composed of two allochthonous tongue provinces: the Sable Shelf Canopy and the Sable Slope Canopy. While the

Sable Shelf Complex was generally assembled in the Middle Jurassic, the process of completion of the Slope Complex is estimated to extend into the Tertiary (Kendell 2012).

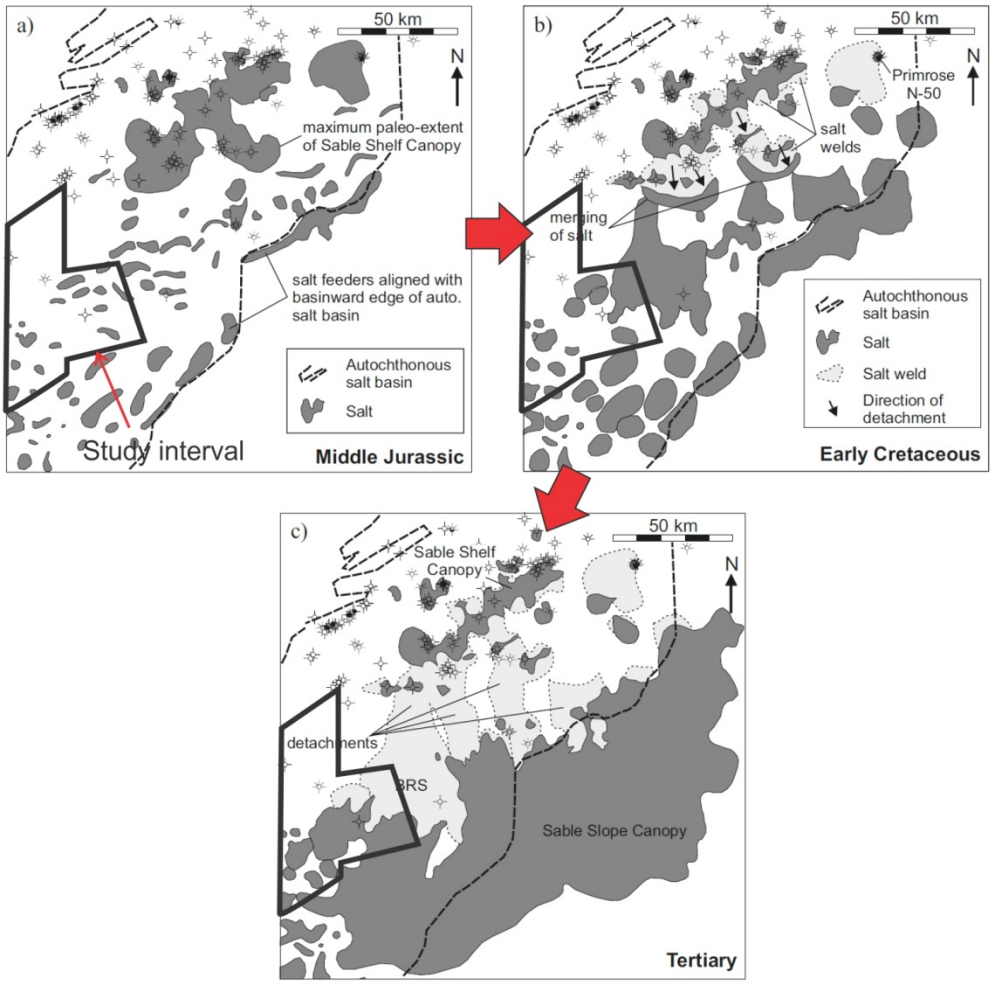

Figure 2.8: Interpreted Jurassic to early Tertiary evolution of salt canopies on the central Scotian Margin by Kendell (2012). The black outline reflects the overlapping extent of the present study area in the west. BRS abbreviates the Balvenie Roho System (Deptuck et al. 2009) and the dashed black line indicates the maximum extent of autochthonous salt.

By the Jurassic, the Sable Shelf Canopy system had reached its maximum paleo-extent. In the Late Cretaceous salt was expelled downslope away from the Sable Shelf Canopy system, creating a series of new salt canopies. By the Tertiary, these salt structures amalgamate on the slope forming the Sable Slope Canopy Complex. This salt migration was primarily controlled by

a series of large roho systems, the largest known as the Balvenie Roho System that merges with the salt stock province in the west, and occurs at the eastern part of the current study area.

Deptuck et al. (2009) and Deptuck (2011a) studied salt tectonics and other processes on the western Scotian Slope (Subprovince I & II of Shimeld 2004) detailing the impact of updip extension and downdip shortening (i.e. gravity gliding) on this part of the margin. Deptuck (2011) divided the shelf and slope into several structural zones. Other work by Deptuck et al. (2009) studied fault and fold geometries on the central Scotian Slope and inteprets two possible directions of shortening that are reflected in a region of complexity around allochthonous tongues and vertical salt diapirs (Fig. 2.9).

In order to understand the interplay between deposition and salt tectonics in the region, numerical modelling has been performed on the eastern part of the Scotian Slope by Ings and Shimeld (2004) and for parts of the whole margin by Albertz et al. (2010). Ings and Shimeld (2004) modeled Shimeld's (2004) Subprovince IV, the salt detachment zone where salt has been expelled downslope over time through gravity gliding and gravity spreading. Results show that a large detachment surface is present from the Jurassic in the northeast Scotian Margin and the seaward migration of salt was driven by deltaic sedimentation. The detachment was reactivated during the Late Cretaceous and present day creating a zone of extension beneath the shelf break and resulting contraction near the toe of the syn-kinematic wedge.

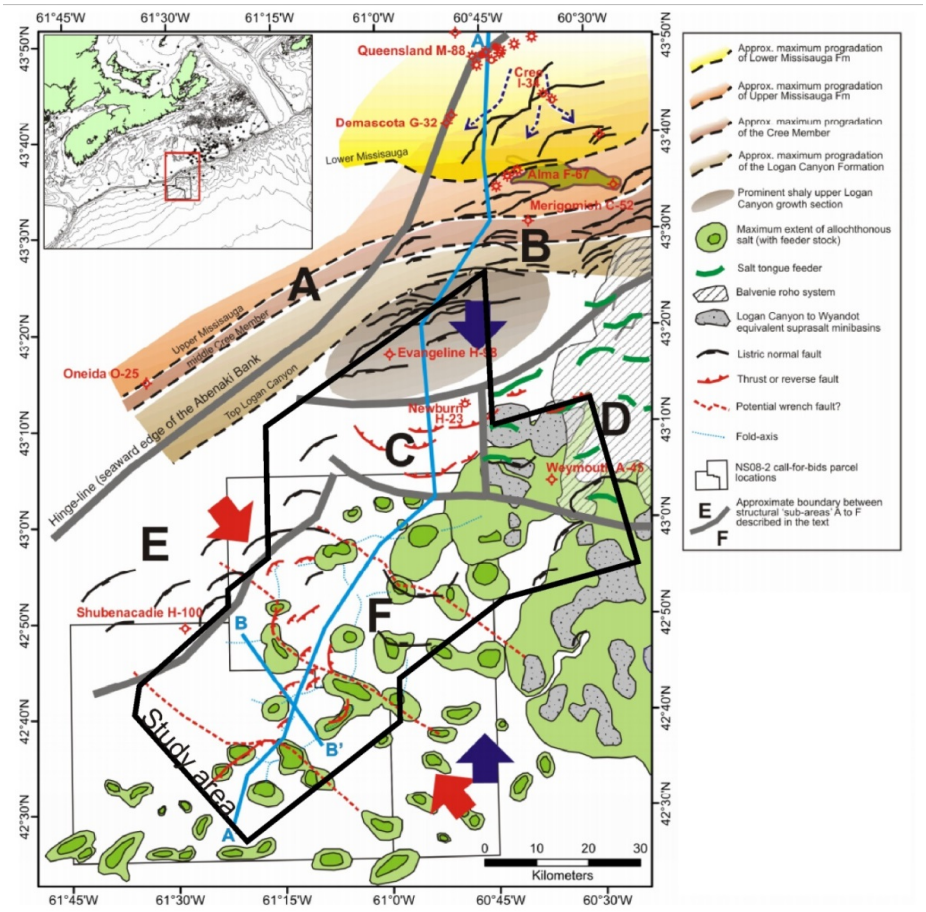

Figure 2.9: Directions of compression inferred for the study region by Deptuck et al. (2009)**.** Deptuck et al. (2009) suggests at least 2 different directions of compression in the study area region. Note the Balvenie Roho System and Cretaceous faults that extend outside of the study area to the northeast. Figure modified from Deptuck et al. (2009) overlain by an outline of the study area (thick black outline).

Albertz et al. (2010) modelled the Scotian Margin (Subprovinces II, III and IV of Shimeld 2004) from the Jurassic to Cretaceous subdividing it into three structural domains and compared it with modern day seismic data. These three domains are a salt detachment ("roho") system with a syn-kinematic wedge (Structural Style A, Subprovince IV), a linked tectonic system with normal faulting and allochthonous salt sheets (Structural Style B, Subprovince III) and salt diapirs with intervening minibasins (structural style C, Subprovince II). This roho system extends to the northeastern section of the study area more formally known as the Balvenie Roho System. When compared to modern day seismic, results in Albertz et al. (2010)

revealed that the Structural Style A (open ended roho system) is the result of early deltaic progradation triggering a seaward spreading/gravity gliding system. Structural Style B had a combination of initial aggradation followed by progradation from the Sable Delta forcing salt to form as sheets. Contrastingly, Structural Style C required large amounts of aggradation in addition to thick overburdens and low density overburden sediments (to allow buoyancy of salt to rise), ultimately forming isolated vertical diapirs with intervening basins.

2.6 Previous work on seismic stratigraphy on the central Scotian Slope (Late Cretaceous to Cenozoic)

The study interval commences in the Late Cretaceous (Cenomanian) around the Petrel Member of the Dawson Canyon Formation, corresponding to seismic marker K94 by Deptuck and Campbell 2012. The Petrel Member is a thin but widespread limestone on the Scotian Margin found at the base of the Turonian interval (Wade and McLean 1990; Weston et al. 2012). Overlying the Petrel Member of the Dawson Canyon Formation is the Wyandot Formation which begins at the base of the Coniacian and extends upwards into the Campanian (Wade and McLean 1990; Weston et al. 2012). Overlying the Wyandot is the Banquereau Formation that continues into the Tertiary. The Banquereau is described as mainly consisting of predominately mudstones with minor chalk and grades upwards into increasing amounts of sandstone and minor conglomerate interbedded with the mudstone (Wade and McLean 1990).

Although parts of the Late Cretaceous to Cenozoic interval consist of the Banquereau Formation, it is host a series of complex events, such as contourite drifts, paleocanyon development, recurring glaciations and even a bolide impact. Multiple studies have attempted to unravel this complexity (Swift 1987; Wade and MacLean 1990; Mosher et al. 2004; MacDonald 2005; Campbell 2011; Campbell and Deptuck 2012; Deptuck and Campbell 2012).

From the Campanian to Paleocene, the "Banquereau delta" deposited north of the study area and eventually reached the shelf edge (Fensome et al. 2008). Clinoforms prograde basinward and overlie and intertongue with the Wyandot Formation, in some areas with an erosive contact (Fensome et al. 2008).

From the Late Cretaceous to the Early Eocene, global sea levels were generally at a long-term highstand, and began to fall around the middle Eocene, consistent with the increasing shelf progradation seen in the Banquerau Formation (MacDonald 2005; Weston et al 2012). The Late Cretaceous (Coniacian/Santonian) to Eocene (Priabonian) interval on the Scotian Slope is dominated by a series of unconformities caused by repeated canyon erosion (Fig. 2.10; Swift 1987; Campbell 2011; Deptuck and Campbell 2012). These canyons are mainly areas of sediment bypass and deposition on inter-canyon erosional remnants. These inter-canyon erosional remnants are mainly composed of interbedded hemipelagic muds and chalks (Swift 1987; Deptuck and Campbell 2012).

During late Early Eocene, a bolide impacted the southwestern part of the Scotian Shelf (formally known as the Montagnais Impact; 51 Ma) ultimately causing extensive slope failures across the Scotian Margin (Jansa and PePiper 1987; Deptuck and Campbell 2012). The slope experienced mass failure as a result of the impact in the form of a large band of regional deformation (12-24 km x 250+ km), parallel to the structural hinge zone in the upper slope called the Upper Slope Slide Complex (Deptuck and Campbell 2012; Fig. 2.11). The Upper Slide Slope Complex deformation spans the northern part of the study area in the Early Eocene. Deptuck and Campbell (2012) mapped the interval above and below the impact event in detail (Late Cretaceous to Oligocene) and subdivided it into 3 sub-units (Fig. 2.10).

The middle Oligocene on the Scotian Margin has a widespread unconformity and canyon incision that is interpreted as the product of a significant fall in sea level (Wade and MacLean 1990; Piper et al. 1987; MacDonald 2005). The Oligocene also generally marks the onset of increased bottom water activity on the Scotian Slope and resulting erosion and contourite deposition. Bottom water currents have been documented by several authors on the Scotian

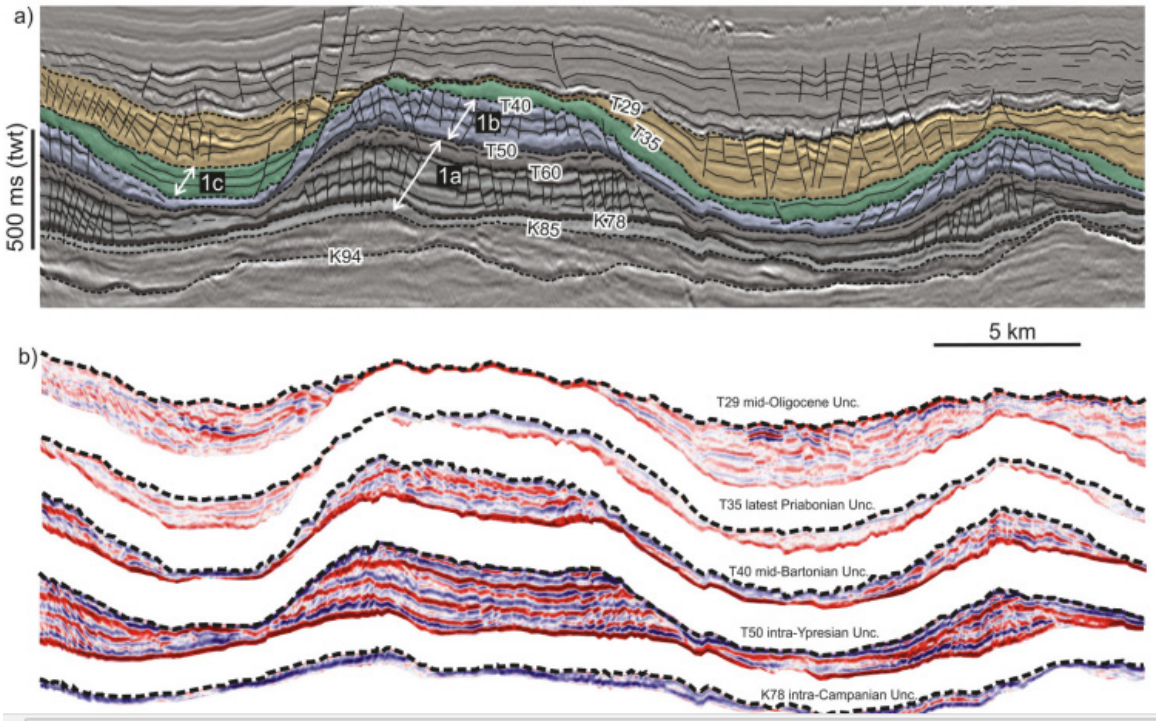

Figure 2.10: Phases of canyon development between the Late Cretaceous and Eocene (horizons K94 to T35) with eventual infill during the Oligocene (T35 to T29), as interpreted by Deptuck and Campbell (2012).

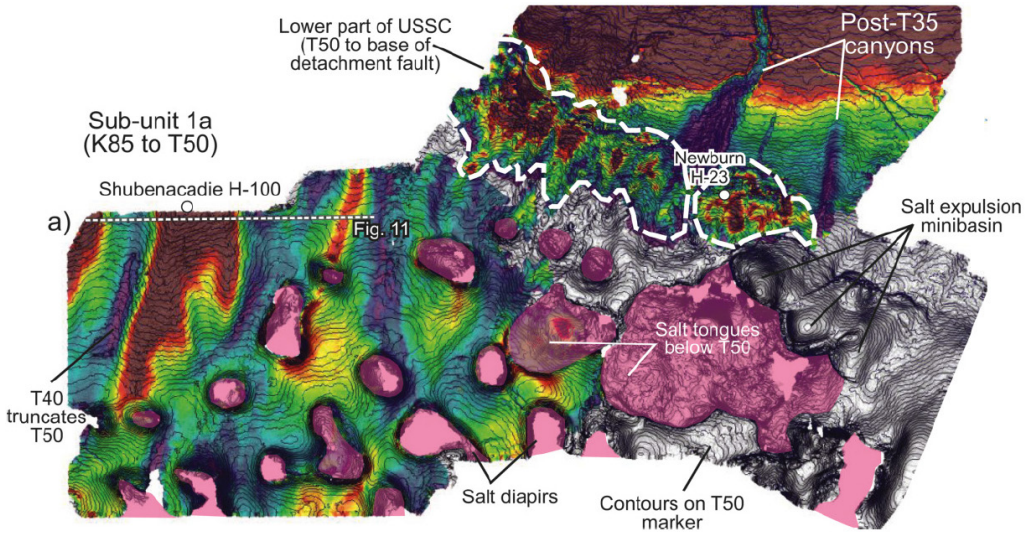

Figure 2.11: Time-thickness map from Deptuck and Campbell (2011) showing deformation from the Upper Slope Slide Complex (USSC) related to the Montagnais Impact.

Slope between the Oligocene to Pliocene (Swift 1987; MacDonald 2006; Campbell 2011; Campbell and Deptuck 2012). Currents trend from northeast to southwest and are responsible for up to 1500 m of deposition on the slope between the Oligocene and Pliocene (Campbell 2011). These contour currents form deposits expressed as low to moderate amplitude/wavy parallel reflections in seismic section and favour bathymetric highs (MacDonald 2005; Campbell 2011).

The late Middle Miocene shows signs of a significant drop in sea level in the form of erosion at the shelf edge and canyon incision (Wade and MacLean 1990; Piper et al. 1987; MacDonald 2005). Previous authors have recognized a thick and widespread succession of Miocene deposits linked to contourite deposition (Campbell 2005; MacDonald 2005). During this time, large contourite deposits such as the Shubenacadie Drift deposited on the central Scotian Slope (Campbell 2011). These drifts have been known to divert around topographic

highs (e.g. salt structures) and preferentially infill paleocanyons in the study area (Campbell 2011).

By the time of the Pliocene, eustatic sea levels fluctuated significantly as a result of numerous glacial-interglacial cycles thought to be related to Milankovich cyclicity (Zachos et al. 2001). At least three lowstands were recognized between the Middle to Late Pliocene on the central Scotian Slope (Piper et al. 1987). The first was marked by erosion of an ancestral valley (Middle-Late Pliocene), the second has a series of small scale gullies and the final unconformity is a more widespread gullied horizon at the Plio-Pleistocene boundary (Piper et al. 1987; MacDonald 2005). These lowstands were followed by low sediment aggradation on inter-canyon highs and finally, an episode of increased sedimentation in the Early Pleistocene that was confined to the upper slope and probably sourced from the margin of grounded ice sheets (Piper et al. 1987).

Glaciations have been noted on the Scotian Margin by several authors (Piper et al. 1987; Gauley 2001; Piper and DeWolfe 2003; Mosher et al. 2004; MacDonald 2006; Shaw et al. 2006). Initial estimates for the first shelf-crossing glaciations on the Atlantic Margin are around 500 ka (marine isotopic stage 12) derived from detrital petrography and palynology on the Grand Banks (Piper et al. 1987; Mosher et al. 2004). The latest major glaciation began at about 75 ka and was initiated in Maritime Canada during a cooling period (marine isotopic stage 4/5 boundary) (Stea et al., 1998).

There are four main phases within the latest glaciation in eastern Canada: the Caledonian (75-40 ka), Escuminac (22-16 ka), Scotian (18-16 ka) and Chignecto (13-12.5 ka) Phases (Stea et al., 1998). During these periods, local sea level fluctuated drastically and formed a series of

trangressional and regressional sequences on the Scotian Shelf causing a series of large-scale mass wasting processes (Stea et al. 1998; Gauley 2001; Mosher et al. 2004).

Today, the central Scotian Slope is host to several large-scale canyons, slides, slumps, scarps and downslope mass transport deposits likely related to previous glaciations. All of these features are exceptionally well imaged in the 3D seismic datasets used for this study. Deeply incised modern canyons with depths up to 1200 m (such as Verrill and Dawson Canyon) were conduits for expulsion of sediments from the shelf edge and down the slope during glaciations (Mosher et al. 2004). Canyons such as these commonly have steep walls (upwards of 40°) and rotational slumps that have amphitheatre-like failure surfaces with incoherent seismic-reflection character (Mosher et al. 2004). Average slope angles vary from 2° to 4° in this area.

The modern seafloor is scattered with modern and buried scarps upwards of 100 m high related to repeated mass wasting events (Mosher et al. 2004). Additionally, there is abundant evidence of turbidity currents taken from cores, seismic and bathymetry data. Mosher et al. (2004) argues that one of the possibilities behind these failure events may be due to slope oversteepening and faulting related to salt domes, among other reasons.

In conclusion, it is clear that the lithostratigraphic unit known formally as the Banquereau Formation does not adequately describe the complexity of the Late Cretaceous to Cenozoic interval on the Scotian Shelf or Slope. This study further investigates the interval and the important role of salt tectonics on slope bathymetry and depositional patterns.

2.7 Marine reflection seismic data

Reflection seismology measures reflected seismic waves to generate a representative cross section of the subsurface. The main factor determining the acoustic character is the acoustic impedance. Acoustic impedance is the velocity and density in a given lithology (Eqn. 1; Yilmaz 1987). The impedance contrast occurs at the interface between two units with different physical properties i.e. a larger contrast yields a strong seismic reflection and vice versa (Fig. 2.12). Seismic reflections are generated from an interaction between the sound source and the contrast in acoustic impedances from the passage of a source wavelet through an interface (Brown 2011).

The boundary between salt and sediment is typically a strong reflection because of the usually high impedance contrast between the two materials. Deformed salt has little to no internal continuity in seismic facies because it distorts the horizons below due to its high velocity (~4400 m/s; often twice the velocity of surrounding sediments).

$$\boldsymbol{I} = \rho\upsilon \qquad \textbf{(1)}$$

Acoustic impendence (***I***) is defined as the product of rock density (ρ) and seismic velocity (υ; Yilmaz 1987).

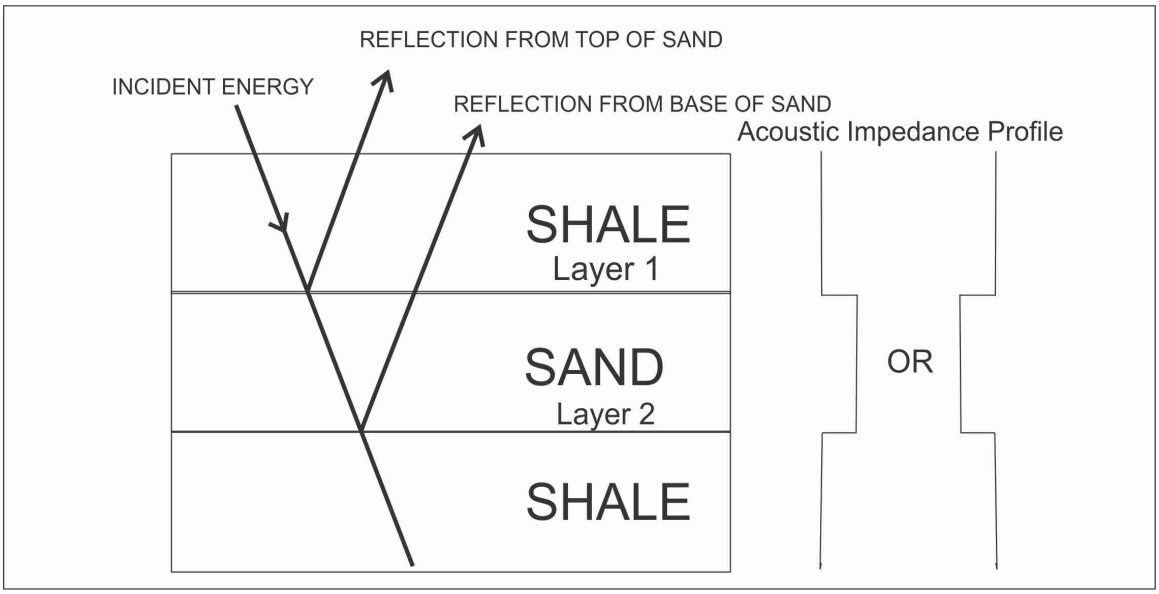

Figure 2.12: Schematic showing the different variances in acoustic impedance as seismic waves encounters a stratigraphic boundary (modified from Brown 2011).

For a seismic wave interacting with two stratigraphic layers at normal incidence, the reflection coefficient (R) is determined by the impedance contrast between each layer (Eqn. 2; Yilmaz 1987). Finally, the reflection coefficient is multiplied by a wavelet (i.e. a basic sound response from a single reflector) to generate a reflection amplitude. The strength of the reflection is proportional to the reflection coefficent and other factors such as the sound source, signal attenuation with distance etc.

$$\boldsymbol{R} = \frac{\rho_2 v_2 - \rho_1 v_1}{\rho_2 v_2 + \rho_1 v_1} \qquad \textbf{(2)}$$

Equation for calculating the reflection coefficient (R), where $\rho_2 v_2$ and $\rho_1 v_1$ are the acoustic impedances for each layer (layers 1 and 2 in this case; Yilmaz 1987; Brown 2011).

2.7.1 Resolution

If a sediment bed of interest is not thick enough or laterally extensive enough, then the bed will not be visible as a clear reflection or other signature. The resolution of seismic is

generally dependent on the wavelength of the dataset (Brown 2011). The wavelength is a function of velocity and frequency and therefore it can be said that at its basic, seismic resolution is also a function of velocity and frequency (Brown 2011). Resolution is commonly measured vertically and horizontally.

Vertical Resolution

Vertical resolution is dependent on the thickness of the layer, the impedance contrast of its bounding interfaces, the average velocity of the material, and the frequency content (or wavelength) of the sound passing through it (Yilmaz 2001). The vertical resolution is a function of the dominant wavelength (λ) and can be calculated by dividing the value (of the dominant wavelength) by 4 (Eqn. 3 & 4).

$$\lambda = \frac{\upsilon}{f} \qquad \textbf{(3)}$$

The dominant wavelength (λ), is a function of velocity (υ) and the dominant frequency (*f*) (from Yilmaz 1987, 2001).

Average seismic velocities in sedimentary rocks generally vary between 2000-5000 m/s, mostly increasing with depth, and dominant frequencies for deep (kilometre-scale) industry seismic generally vary between 50 and 20Hz (decreasing with depth; Yilmaz 2001). With this in mind, typical seismic wavelengths for industry seismic will vary from 40 to 250m, and the vertical seismic resolution will be on the order of 10 to 62.5m (Yilmaz 2001).

$$\text{V. R.} = \frac{\upsilon}{f}/4 \qquad \textbf{(4)}$$

The vertical resolution is a function of velocity (υ) and the dominant frequency (f) (from Yilmaz 1987, 2001).

Horizontal Resolution

Horizontal resolution is the ability to resolve objects in the horizontal plain with respect to one another. It is generally dependent on the area of the Fresnel Zone in unmigrated data. The Fresnel Zone is a frequency and range-dependant circular area where the reflector in the circular area transmits a reflection to the receiver within half a cycle of the first reflection. The size of the Fresnel Zone can be calculated to determine the minimum resolvable feature i.e. features smaller than the width of the Fresnel Zone cannot be detected (Brown 2011). Resolution can be improved by a process called migration. Migration is the movement of reflections to their correct locations in 3D space (Brown 2011) and both the Thrumcap and Weymouth surveys have been migrated to reduce diffractions and out-of-plane artifacts.

2.7.2 Seismic stratigraphy

Stratigraphy can be divided into chronological units called sequences. A sequence is identified as a relatively conformable succession bounded by unconformities or their correlative conformities (sequence boundaries) (Mitchum et al. 1977; Catuneanu et al. 2009). Sequence stratigraphy is the study of these chronological units and is further defined by Catuneanu et al. (2009) as a succession of strata deposited during a full cycle of change in accommodation space or sediment supply. Stratigraphic sequence boundaries therefore include both unconformable boundaries and their time-equivalent correlative surfaces (Catuneanu et al. 2009).

Mitchum et al. (1977) defines seismic stratigraphy as the study of stratigraphy and depositional facies interpreted from seismic data. Seismic facies are identified by their reflection geometry, strength and continuity. Identifying and interpreting these reflections is vital to identifying depositional environments in seismic data (Figs. 2.13 and 2.14).

Seismic reflections can have many geometries, the ones discussed in this study area are concordant (parallel), hummocky (shingled), chaotic (no organized orientation), progradational (basinward migration of sediments) and climbing waves (ripples that aggrade) (Fig. 2.15). Cut and fill configurations are limited to channel systems in the study area.

There are four main reflection geometries between sets of discordant reflections below and a more continuous reflection above: onlap, downlap, toplap and truncation (Fig. 2.14). Onlap is the horizontal truncation of reflections against an inclined surface (Mitchum et al. 1977; Catuneanu et al. 2009). Downlap is the termination of inclined reflections against an inclined or horizontal surface (Mitchum et al. 1977; Catuneanu et al. 2009). Toplap is the termination of reflections against an overlying surface and finally, truncation is the erosion of reflections along an unconformity (Mitchum et al. 1977; Catuneanu et al. 2009). Drape is the uniform accumulation of strata above a pre-existing structure.

Submarine channels can exhibit a linear (straight), sinuous (slight bends) or meandering (significant bends) geometries in plan view, and in cross section, channels can have erosional bases that are V or U-shaped (Fig. 2.14).

A mound is a symmetrical positive relief bathymetric extrusion. A lens is a flatter and more elongated mound. A wedge is an asymmetrical, triangular extrusion with tapering reflections on one side.

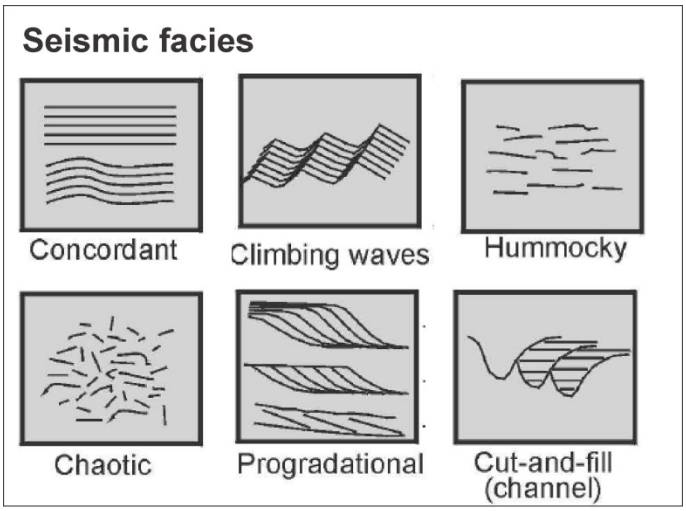

Figure 2.13: Seismic facies in the study area, modified from Deptuck (2003).

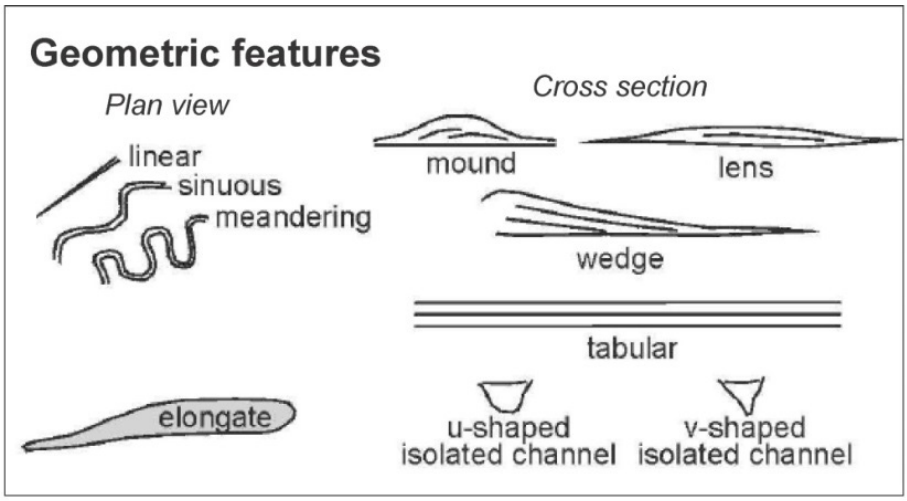

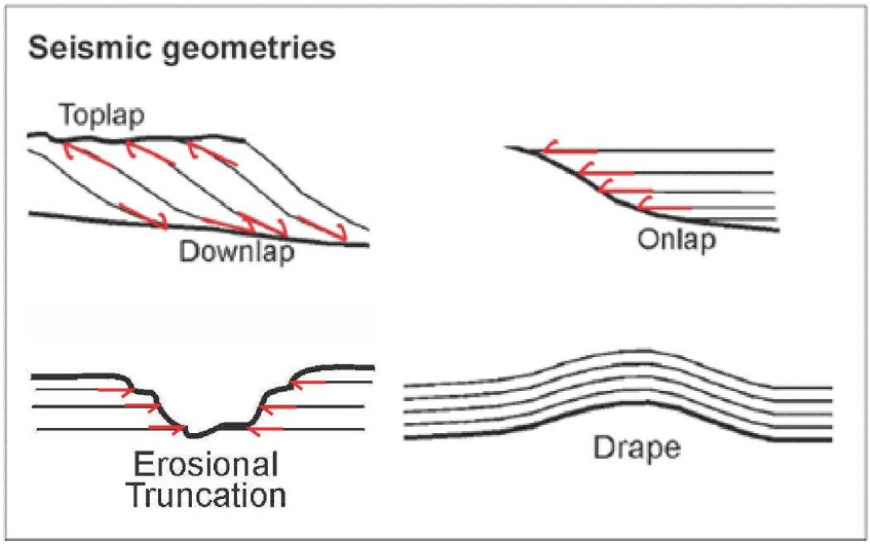

Figure 2.14: Various seismic geometries in cross-section and plan-view, modified from Deptuck (2003).

Chapter 3: Datasets and Methods

3.1 Interpretation of 3D seismic data

3D seismic data is collected by shooting closely spaced parallel seismic lines. The shooting direction is called the *inline* track and perpendicular to the shooting direction is called the *crossline* direction (Brown 2011). Typical line spacing in 3D is much more dense (up to 25m) in comparison to 2D lines (1 kilometer plus; Brown 2011) and modern 3D surveys contain more than 100 000 traces (data recorded for one single seismic channel) (Brown 2011). In 3D data, traces are collected into a common-cell gather called a bin (Yilmaz 2001). A bin consists of x,y (shot point distances) and z values (samples) with an assigned trace value.

3D seismic bins allow the user to view a seismic line at any orientation (Brown 2011). Generally in-lines and cross-lines (vertical transects) allow the user to scroll through the data volume in the X and Y dimensions (Fig. 3.1). 3D surveys also enable an interpreter to generate seismic sections in the z-plane (a horizontal timeslice; Fig. 3.1). Timeslices allow the user to slice across the volume parallel to a specific time (two-way travel time; TWTT). From this, structures such as channels and faults are resolvable in plan view. The ability to pick a line in any orientation allows the user to select profiles oriented normal to the trend of structures, which commonly do not align with the in-line or cross-line directions.

3.2 The Thrumcap and Weymouth surveys

Two 3D surveys, Thrumcap (NS24-S006-001E, 002E; Shell Geophysical Report, 2002) and Weymouth (NS24-P003-004E, Barrington Geophysical Report, 2002), were mapped at the Canada-Nova Scotia Offshore Petroleum Board using Schlumberger's GeoQuest-IESX software package. These 3D surveys encompass a combined area of 5300 km^2 and provide good imaging

of individual salt bodies in comparison to sparsely-spaced 2D grids used in previous regional studies (e.g. Shimeld 2004).

The dominant frequencies in these two surveys are between 25Hz and 60Hz and are between 30 and 60Hz in the study interval. Using velocity estimates for the study interval (sediment at seafloor =1500m/s, Wyandot=1800m/s), the resulting vertical resolution ranges between 6.25m (optimally) and 15 m in these surveys when divided by 4 (Eqn. 5). Bin spacing for Thrumcap is 12.5 x 25m and for Weymouth is 12.5 x 37.5m which are the maximum horizontal resolution of the dataset. Both surveys have a time sampling rate of 4 ms two-way travel time.

3.2.1 Attribute analysis

A wide variety of standard 3D seismic interpretation methods were used throughout this project. Picking or autopicking (tracking reflections from manual seeds) yields a horizon that is the interpretation of a seismic surface in two-way travel time (TWTT) (Brown 2011). A horizon can also be flattened along a horizontal plane in TWTT in order to remove effects of later deformation and compare subtle angular relationships with respect to the flattened surface.

Isopach (thickness) or isochron (time-thickness) maps represent an interval of sediment or its seismic response between two mapped horizons. They are widely utilized in many seismic stratigraphic studies. Isochron/Isopach maps are generated by subtracting a shallower mapped horizon from a deeper mapped horizon showing the thickness variations between these two maps.

Dip maps are used to identify faults and fractures in a seismic volume (Fig. 3.1). In order to do this, the angle of a dipping plane is measured in relation to the horizontal plane (Brown 2011). The resulting output is a magnitude of a trace with respect to the adjacent traces.

In order to generate a dip map, the horizon had to be picked either manually or by the autopicker (See Chapter 3.2.1). The selected map area would run through an algorithm in GeoFrame to calculate the dips of that horizon.

A coherence algorithm converts a volume of reflectors into a volume that highlights discontinuities by calculating the differences between a given trace and the laterally adjacent seismic traces (Brown 2011; Fig. 3.1). When the amplitude and polarity of a trace is similar to its surroundings, it is given a high coherence value and when it differs, it is given a low value (Yilmaz 1987; Hart 2000). Coherence attributes are normally derived from amplitude data and allow for excellent imaging of faults, channels and other amplitude discontinuities (Hart 2000).

Amplitude extractions are a widely used technique used mainly along a non-standard plane such as a picked horizon (Hart 2000; Fig. 3.1). It is a measure of polarity strength and phase of a reflection and is directly related to its acoustic impedance (Deptuck 2003). Variations in amplitude can indicate changes in lithology as well as many other things, such as fluid pressure, porosity, thickness (tuning), etc. Amplitude extractions can locate changes in reflection character from deposits like turbidite channels, canyons or hydrocarbons (e.g. potential gas chimneys or direct hydrocarbon indicators).

3.2.2 Seismic marker interpretation

Eleven horizons were mapped from Upper Cretaceous strata to the present day seafloor (~2.5 second succession). These horizons were continuously revised from the manual interpretation grid and then autopicked (where possible) to fill in interpretation gaps (Fig. 3.2).

The initial manual grid used for Thrumcap was at intervals of 50 (inline), 100 (cross-line) and for Weymouth at spaces of 25 (inline) and 50 (cross-line; Fig. 3.2). A denser manual interpretation grid was generated in cases where the autotrackers were unable to properly correlate seismic markers.

Subsurface maps such as time-structure, isochron, dip, amplitude extraction and coherence attributes were used to analyze the dataset. Time-structure maps were gridded on a 50 m by 50 m resolution. These maps show the horizon surface in the time domain. Isochron maps were gridded from two seismic horizons with an interval of 50 m by 50 m Contours were generated at 50 ms intervals for both isochron and time-structures.

3.3 Salt interpretation and documenting the history of salt-related deformation

The Thrumcap and Weymouth 3D seismic volumes were used to document the distribution and structure of different salt bodies in the study area. The top, and where possible base, of salt bodies were mapped, and salt thickness maps were generated. Evidence such as onlap onto salt structures, location and timing of salt wings/overhangs, distribution of pinched stems, the timing and distribution of stratal thinning, as well as identifying other kinematic evidence like the diversion of canyons and channels around salt structures, and the timing of fault growth, were all used to unravel the nature and history of salt-related deformation.

Active diapirism is believed to be a main component of salt deformation in the Cenozoic in the study area (Deptuck et al. 2009). Hudec and Jackson (2011) distinguish between two types of active diapirism: halokinetic active diapirism and compressional active diapirism (Fig. 2.2: active diapirism from downbuilding; Fig. 3.3: active diapirism from compression).

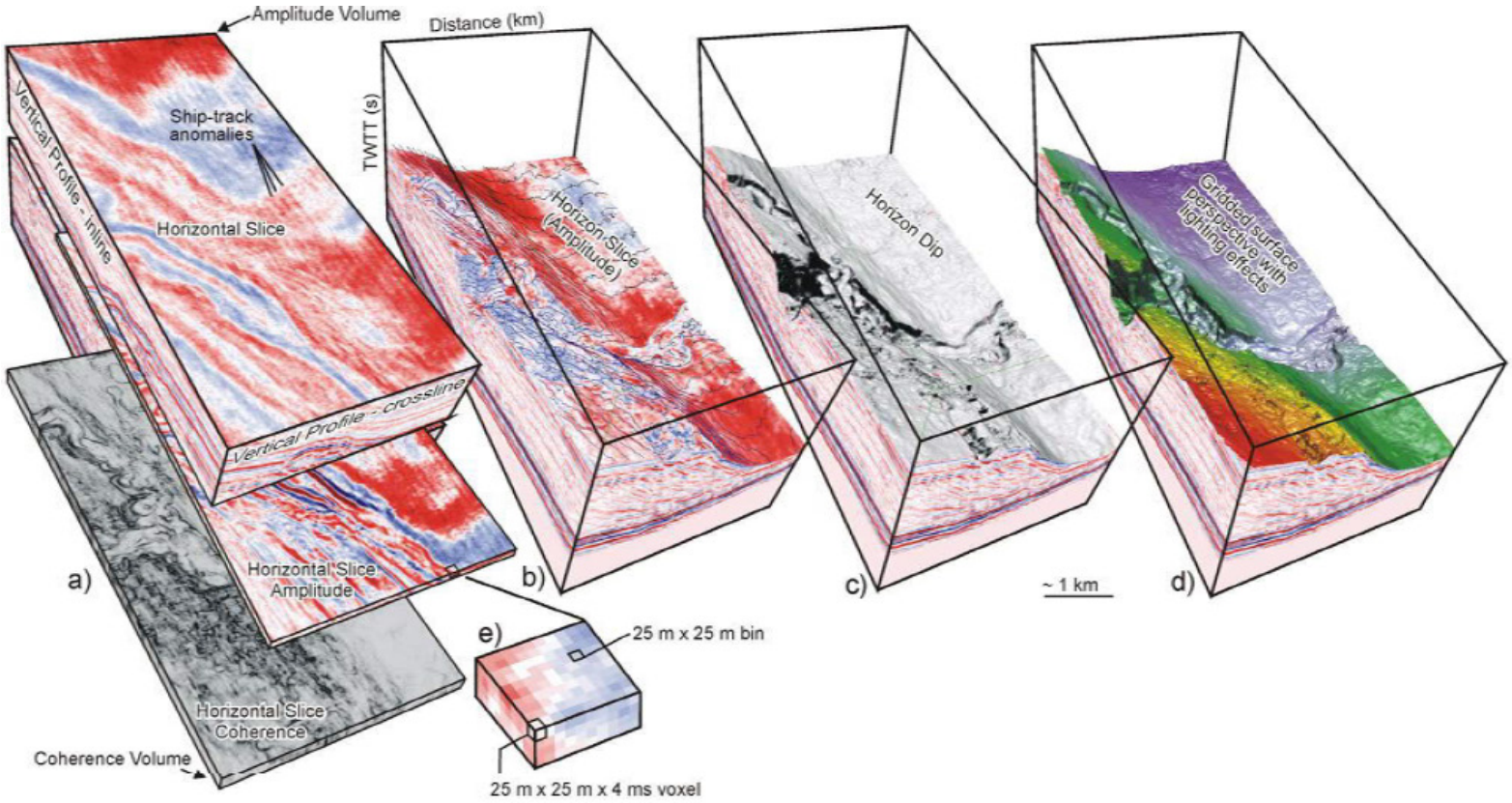

Figure 3.1: Summary figure of 3D seismic attributes from Deptuck (2003) showing: a) Vertical in-line or crosslines and horizontal time-slices through a 3D coherence and amplitude volume, b) an amplitude extraction along a mapped horizon, c) A dip section along a mapped horizon, d) gridded time-structure map, and e) an example of a 3D voxel (comprising of bins).

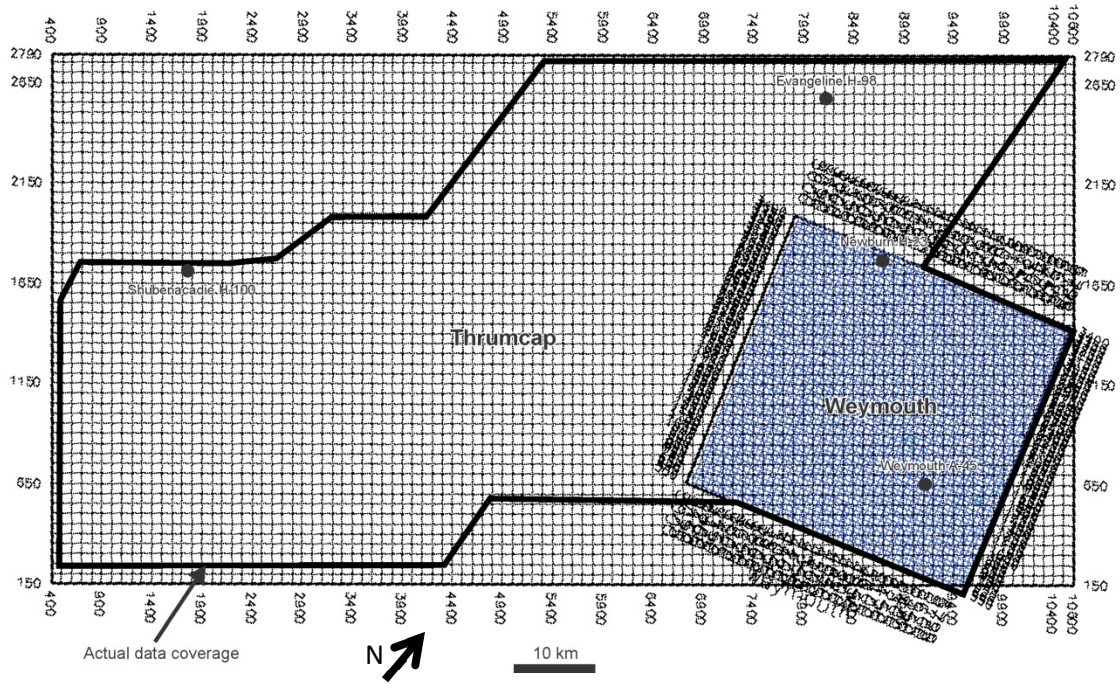

Figure 3.2: Original grid distribution in the study area.

Halokinetic active diapirism is active salt movement driven by overlying pressures from the overburden load onto the underlying source layer (Hudec and Jackson 2011). In the case where overburden density is greater than salt, a relatively thin roof can also be pushed upwards (Hudec and Jackson 2011).

In contrast, compressional active diapirism is driven by lateral compression. This mechanism is driven by tectonics at a broader scale (i.e. not related to local salt tectonic processes but rather an external structural mechanism further away) and although active diapirism is optimal with thin or weak overburden (i.e. less resistance to pressure from the upward-pushing salt), compressional active diapirism can deform "thick" roofs and can do so even when the source layer has been depleted (Dooley et al. 2009). After the primary source layer has welded out, roofs greater than several hundred metres thick are unlikely to deform without tectonic compression or extension (Vendeville and Nilsen 1995; Hudec and Jackon

2007). Therefore, upward movement of salt after source layer depletion is a clear sign of compressional diapirism, especially when in combination with folding of thick overlying strata (Vendeville and Nilsen 1995; Hudec and Jackson 2007).

Compressional active diapirism can form buckle folds, reverse faults or thrusts above the diapir roof. In comparison, halokinetic active diapirs generally form monoclinal folds at the diapir shoulder (Vendeville and Nilsen 1995).

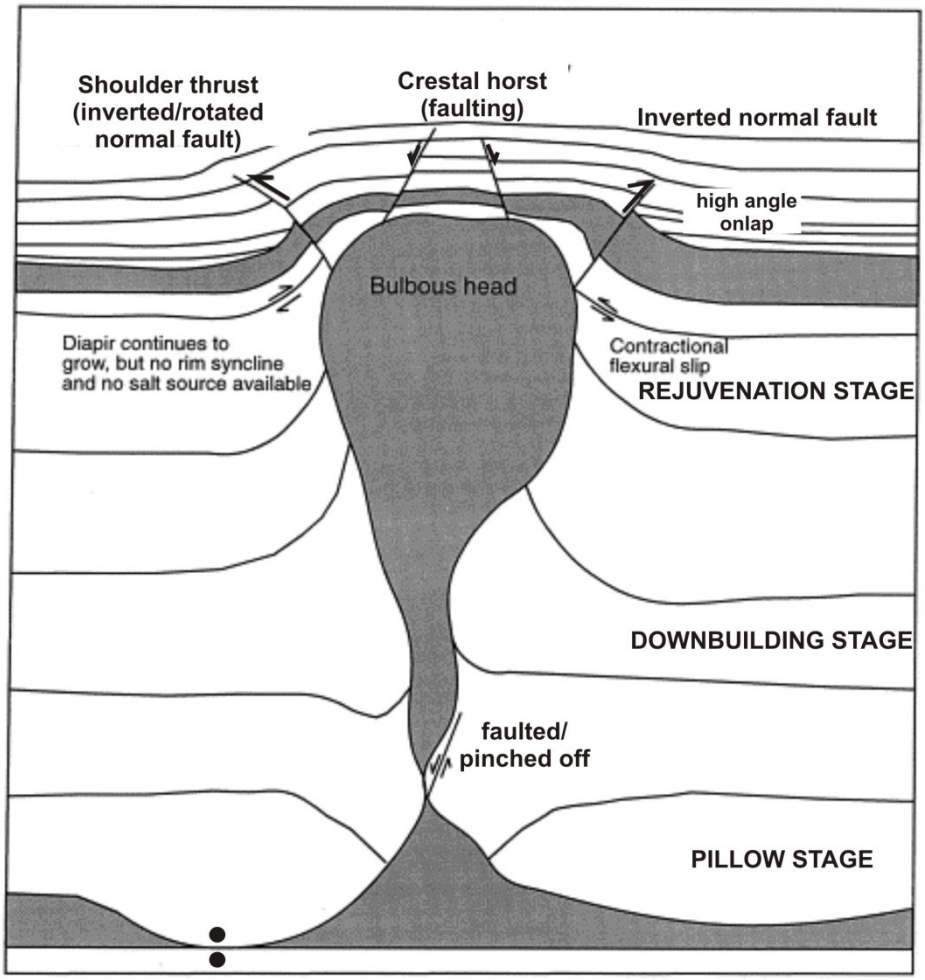

Figure 3.3: Characteristics of a typical rejuvenated diapir from compressional active diapirism (modified from Davison et al. 2000).

Uplift of salt through active diapirism (from halokinetic or compressional**)** triggers extensional crestal faults commonly in the form of growth faults that root into the diapir crests creating central grabens (Rowan et al. 1999). These faults form in response to flexural shear rather than regional extension associated with reactive diapirism. Crestal faults are formed around diapirs in response to upward displacement of overburden (Fig. 3.4). The extent of crestal faulting is proportional to the degree of uplift of the salt dome (Schultz-Ela et al. 1993; Jackson et al. 1994; Hudec and Jackson 2007; Carruthers et al. 2013). Crestal faulting can be in the form of one or two large "master faults" offsetting smaller radial faults (Yin et al. 2009; Carruthers et al. 2013) which are diagnostic of active diapirism. These Master faults and the associated folding can be reactivated several times through a process called rejuvenation.

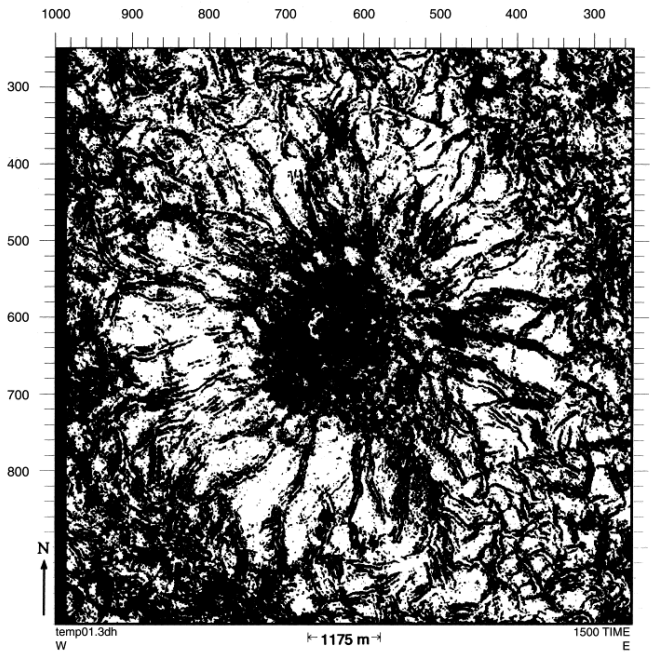

Figure 3.4: Horizontal coherency slice showing radial crestal faulting above a salt diapir that experienced compressional active diapirism in the North Sea (Davison et al. 2000).

3.3.1 Rejuvenation

Rejuvenation periods are defined as a reactivation of salt tectonic motion after a period of quiescence (i.e. minimal or no activity). Specifically, rejuvenation due to compressional active diapirism is commonly episodic and has several indicators such as a narrow or pinched stem of a vertical diapir (teardrop diapir), crestal growth faults, crestal anticlines with positive seafloor relief and evidence for growth after the salt has been expelled and depleted from the base layer (i.e. after passive diapirism ceases) (Fig. 3.5; Vendeville and Nilsen 1995; Hudec and Jackson 2007). These diapirs can cause bathymetric uplift due to repeated lateral shortening events and subsequent uplift of salt.

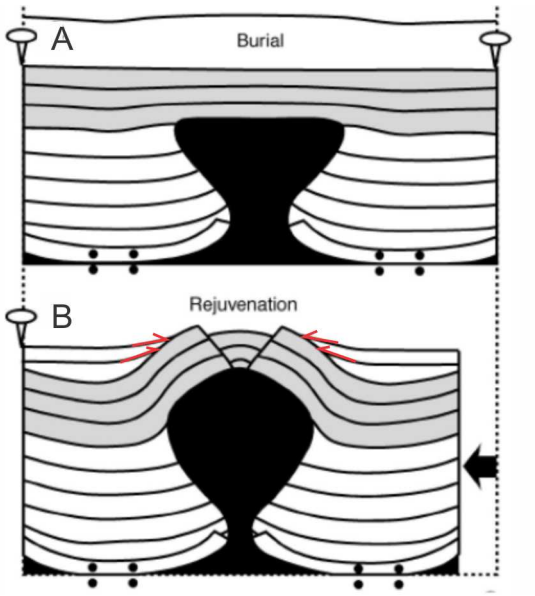

Figure 3.5: (A) A schematic of a buried, dormant diapir (B) The same diapir has been subsequently rejuvenated by lateral compression (Vendeville and Nilsen 1995). The mode of deformation during this reactivation phase was compressional active diapirism. Note the bathymetric uplift of the grey layer and onlap of sediments that post-date the syn-kinematic rejuvenation period. The onlap relationship (red arrows) constrains the timing of uplift. The two adjacent dots at the base of each diapir indicate that source layer has been welded out.

During lateral compression, syn-kinematic intervals show stratal thinning (thinner stratigraphic thickness relative to their surroundings) or onlap above salt crests (Davison et al.

2000; Fig. 3.6). Packages showing no paleoslope expression and uniform stratigraphic thickness over the crest of the salt structures indicate that salt movement had ceased during that period of time, whereas, strata showing thinning and truncation indicate that the diapir was likely active during the corresponding period creating a paleo-topographic high (Vendeville and Nilsen 1995; Davison et al. 2000).

3.4 Age calibration

Matching wells to seismic is essential in order to determine the timing of horizons and more importantly, constrain the ages of salt movement in the study area.

Synthetic seismograms are used to tie well data (collected in depth) to seismic data (collected in two-way travel time). A synthetic seismic section is derived from well data and allows the lithostratigraphy in the well to be matched to seismic facies and the sonic velocities to be calibrated to stratigraphic horizons from the seismic data (in TWTT) (Fig. 3.7).

Sonic well logs measure changes in the velocity of sound in a formation by measuring the time it takes for a sound from the source (top of the tool) to reach the receiver at the bottom of the tool through the surrounding formation (Brown 2011). Density-neutron measures a formation's bulk density by emitting a beam of neutrons and measuring the rate and energy of return (Brown 2011). An increasing amount of neutrons in the receiver corresponds to an increase in density. Sonic and density logs can be used to calculate the acoustic impedance (Eqn. 1, Figs. 3.7 and 3.8) which is the product of density and velocity in a rock. The reflection coefficient is the difference in the acoustic impedance between a type of rock and the next (i.e. a positive or negative number).

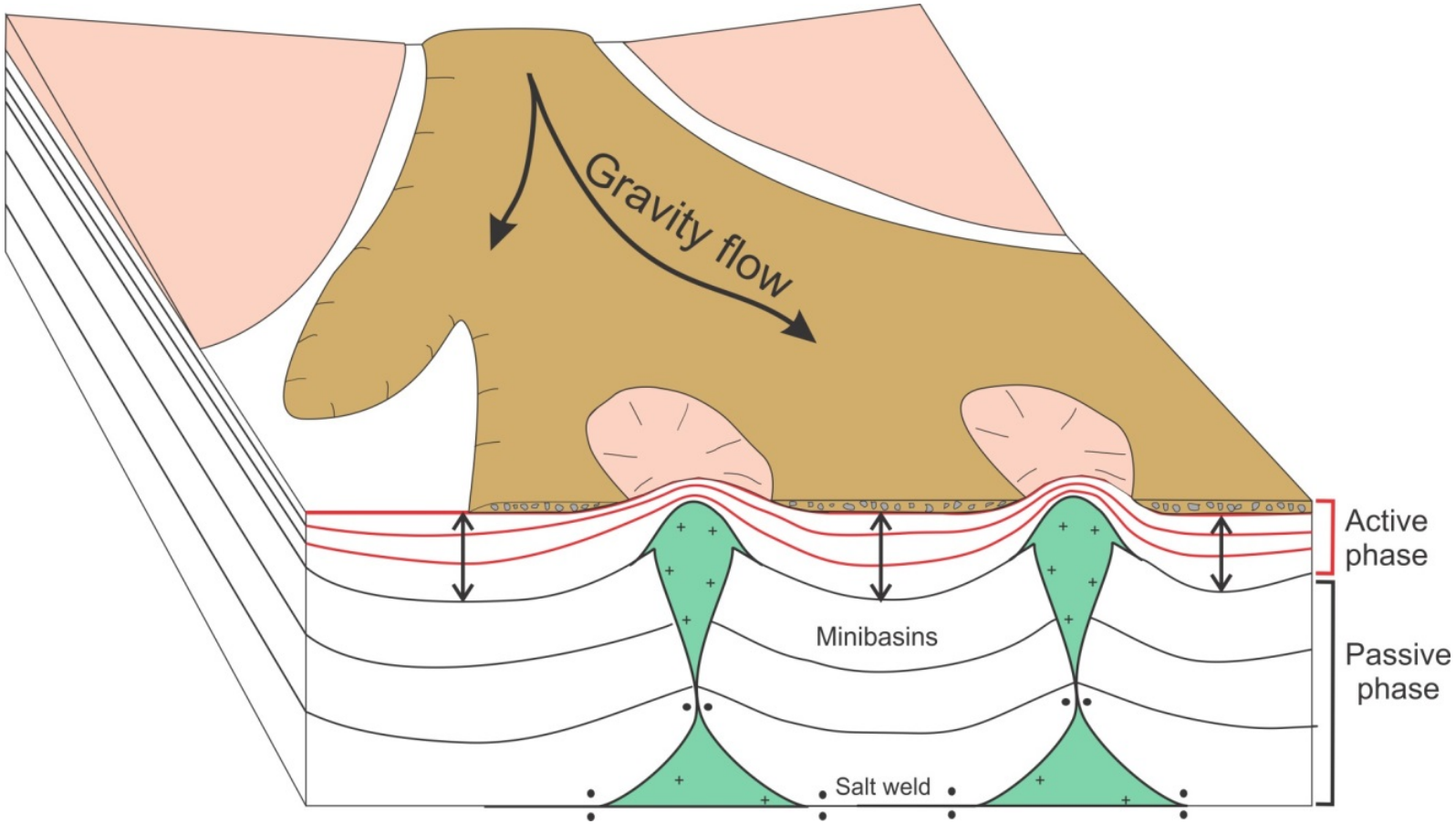

Figure 3.6: Cartoon depicting a gravity flow (brown) diverting around two rejuvenated salt bodies (bathymetric highs in pink) and depositing on the flanks. Note the onlap relationship of the gravity flow along flanks of these salt bodies as it preferentially deposits in lows.

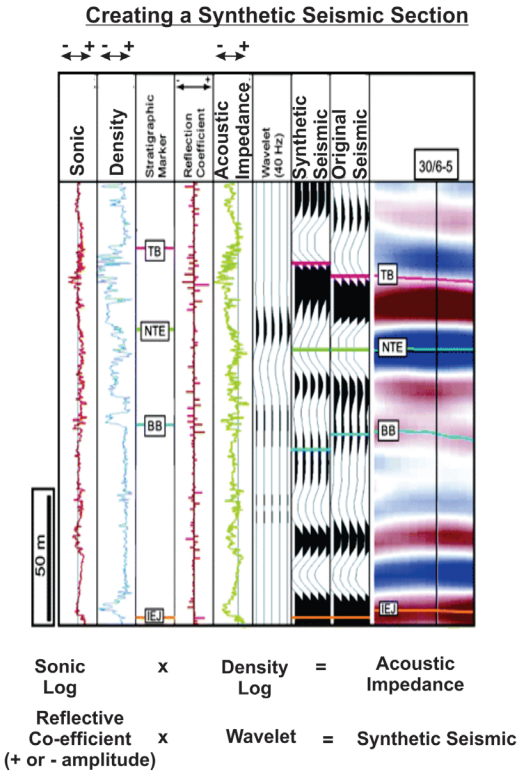

Figure 3.7: An example well synthetic seismic section that ties to original seismic data (known as a "well tie") modified rom Jackson et al. (2010). The synthetic seismogram is derived by using sonic and density logs to produce reflection coefficients that are then integrated with a wavelet representing the source sound signal.

The synthetic seismic section is generated from the integration of a wavelet (a model of the source sound) (30 Hz Ricker wavelet in this study) and the reflection coefficient. A synthetic seismogram is then compared to the *original* (collected) seismic section and matched up by comparing the acoustic characteristics of the trace amplitudes. This allows development of a detailed velocity model (a time: depth relationship) where features in the well (that are expressed in depth) can be matched to features in the original seismic section (in the time domain). The match is known as a "well tie".

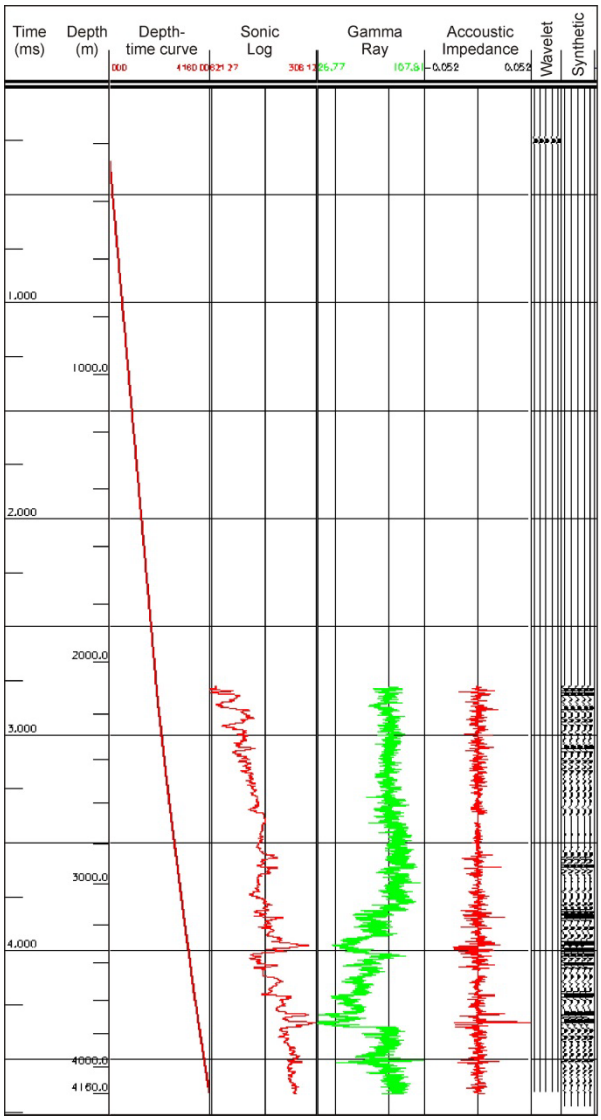

Figure 3.8: Example synthetic seismogram from the Shubenacadie H-100 well. The Ricker wavelet to generate the synthetic in this study was at a frequency of 30 Hz.

Well tie inaccuracies

Although well ties between the seismic and depth domain can have significant uncertainties, well data generally gives more detail (higher frequency data) than the reflection seismic used in typical industry surveys. Seismic surveys process for a frequency range of around 5-200 Hz and sonic logs effectively record information at about 10-12 kHz (Lines and Newrick 2005). Problems with sonic logs include velocity dispersion i.e. cycle skipping, a noisy seismogram,

and modification of the rock properties around the borehole due to drilling etc. Another issue with logs is the tilting of the instrument downhole giving false or incorrect readings in travel time. Newer sonic tools have two geophones (receivers) that will allow for a correction between an offset of the two arrival times. Although more detailed, there is no guarantee that the sonic measured at the borehole is representative of the average velocity over an interval comparable to seismic data. Furthermore, no checkshot data was used in this study. All of these caveats mean that the well:seismic tie is a key limitation in the integration of well data with the seismic interpretation.

Chapter 4: Salt and seismic stratigraphic framework

In order to establish geological age constraints within the study interval, stratigraphic ties have been made from well data using the most recent biostratigraphic results (Fensome et al. 2008; OETR 2011; Weston et al. 2012), which are based on palynology, foraminifera, and nannofossils. There are five wells in the immediate study area (from east to west): Weymouth A-45, Newburn H-23, Evangeline H-98, Shubenacadie H-100 and Acadia K-62 (Fig 4.1). These well ties constrain the age of stratigraphic horizons and additionally, have been combined with other local studies (Swift 1987; Campbell 2011, the Play Fairway Analysis (OETR 2011) and Deptuck and Campbell 2012) to accurately gauge the chronology of salt deformation from the Late Cretaceous to Cenozoic (Fig. 4.2).

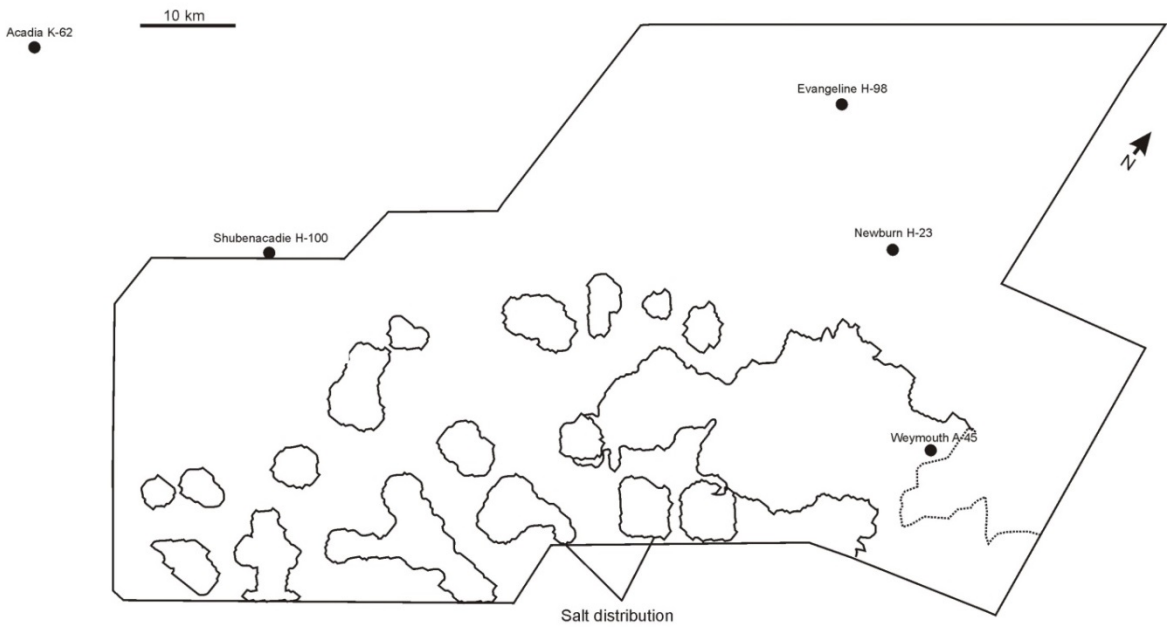

Figure 4.1: Distribution of wells in the study area.

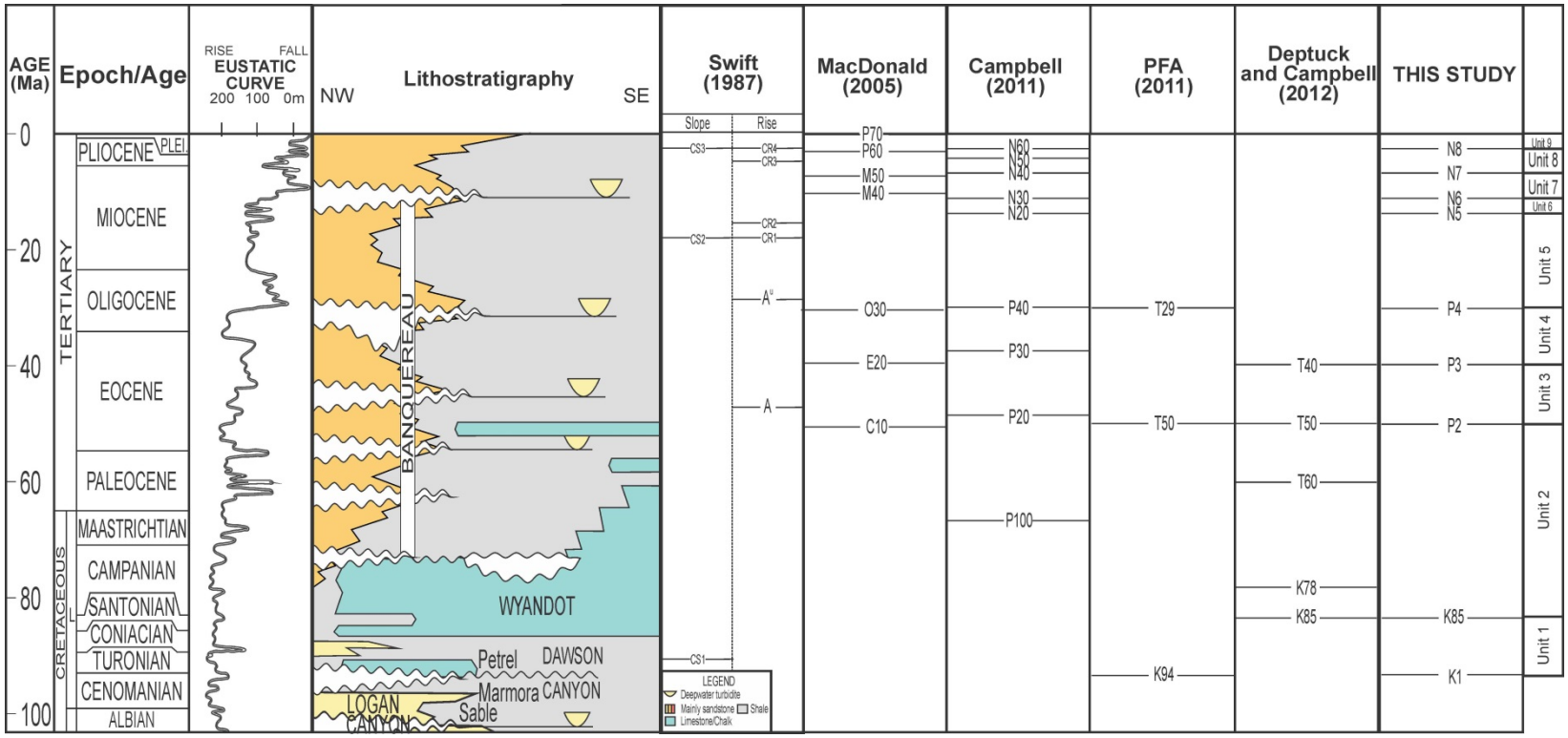

Figure 4.2: Figure comparing the relative ages of horizons and units in this study with other work done on the central Scotian Slope. Lithostratigraphy and timescale modified from Weston et al. (2012).

4.1 Well ties

Recent biostratigraphic data for well ties and ages were used (Fensome et al. 2008; OETR 2011; Weston et al. 2012), however, the amount available from the Cenozoic is generally limited. In some cases this is due to limited biostratigraphic study, and in others it is due to lack of sample recovery at the time of drilling.

Well plots are listed below with corresponding horizon names. Although shown here, horizons mapped in this study will be discussed in section 4.5 below.

Weymouth A-45

No Cenozoic age data are available for Weymouth A-45 which penetrates an allochthonous salt tongue/canopy in the eastern study area (Fig. 4.3) (OETR 2011). The salt canopy is underlain by Aptian-Albian strata (Shortland Shale).

Chalks and marls overlie the top of the salt resembling the Ypresian Chalk of Weston et al. (2012) or possibly chalks of the Late Cretaceous Wyandot Formation. The K1 (Cenomanian/Turonian), P3 (Bartonian), N6 (Tortonian) and N7 (Tortonian) horizons are absent in this well (Fig. 4.4).

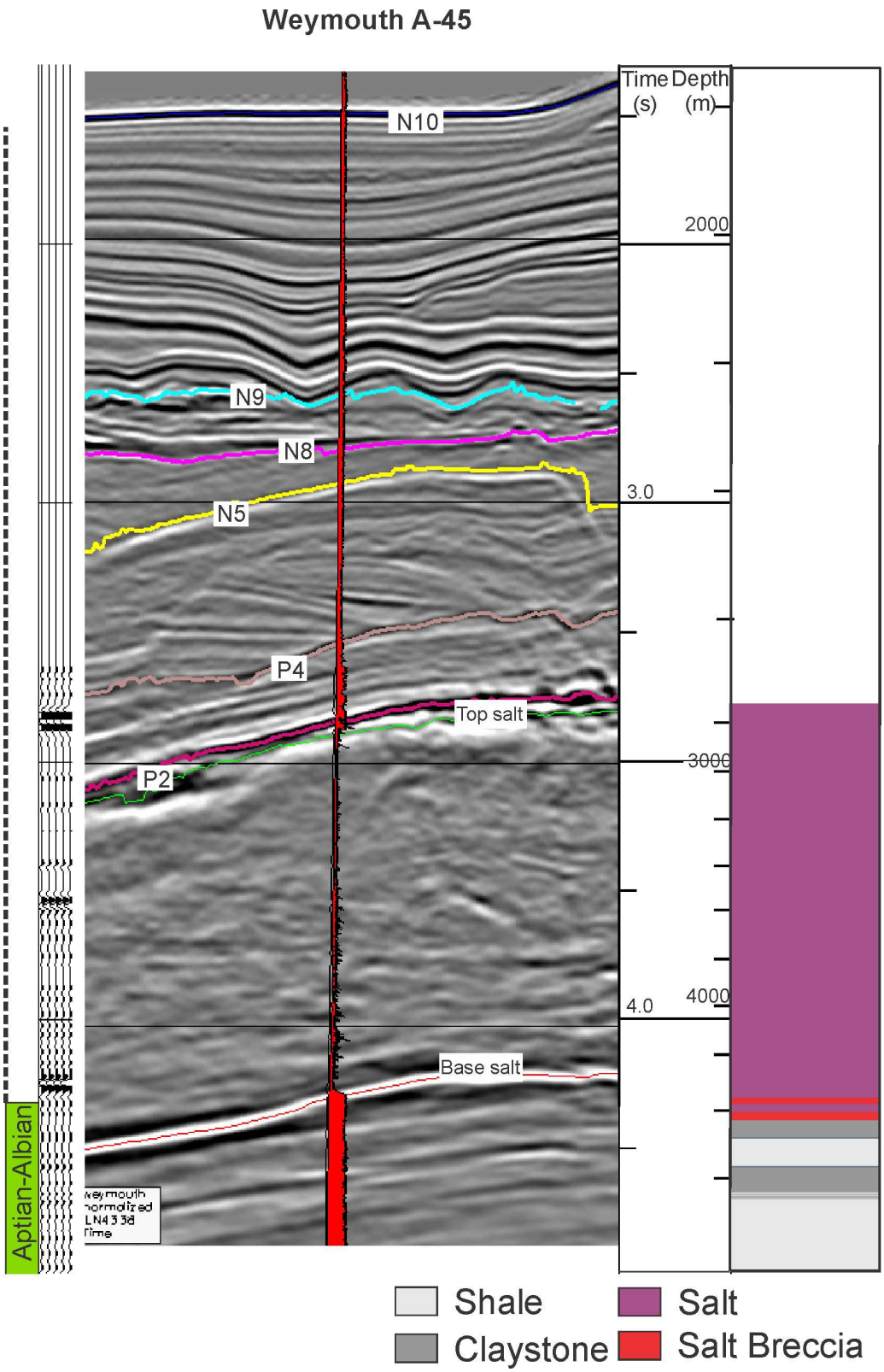

Figure 4.3: Well calibration for the Weymouth A-45 well. GR= Gamma Ray.

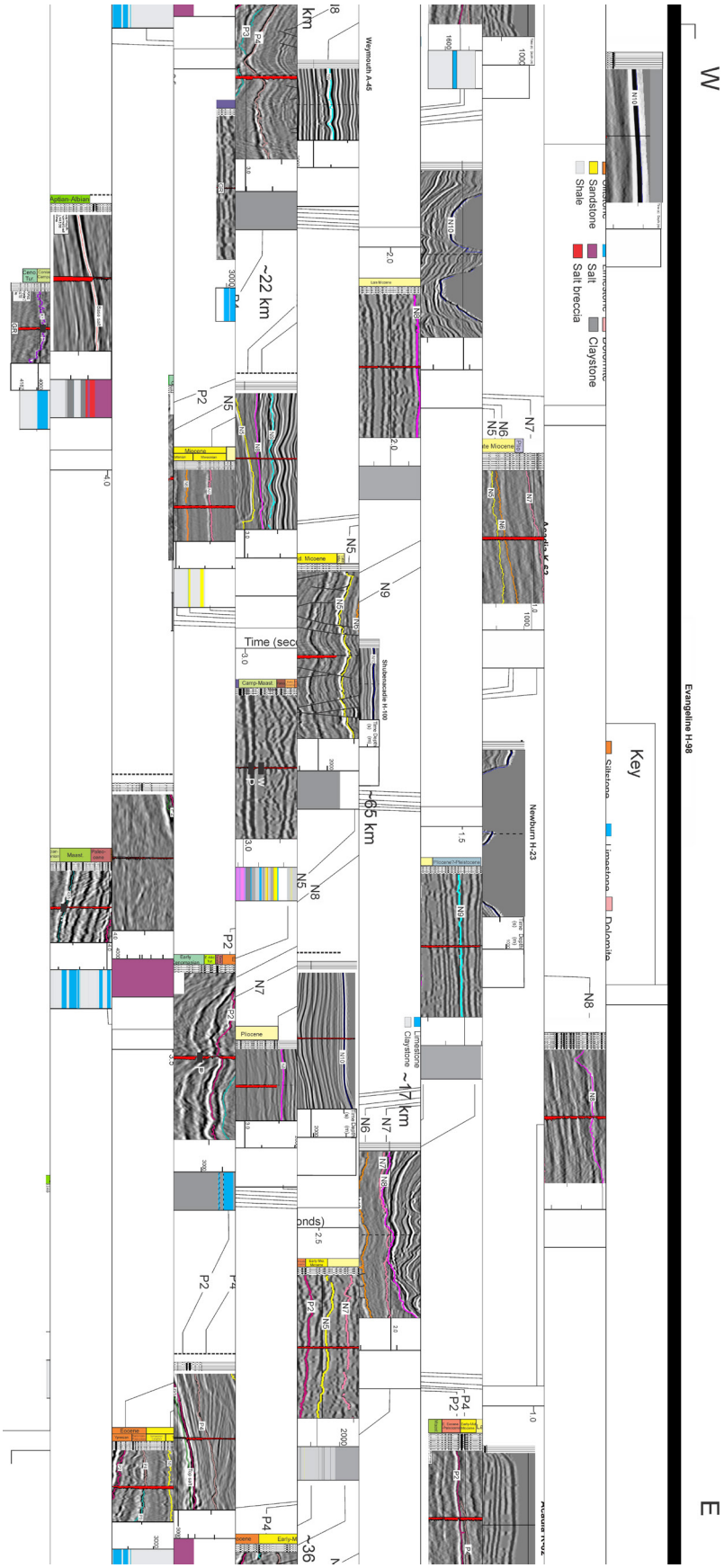

Figure 4.4: Lithostratigraphic correlations across the study area.

Newburn H-23

Newburn is located on the shelf-edge and targeted Cretaceous sands sourced from the Sable Delta (Kidston et al. 2007). All markers were resolvable in this well except for the K1 (Cenomanian/Turonian) and N9 (Pliocene) markers (Fig. 4.4). The well notably intersects a modern day canyon and a fault glide block between 2849 m and 3024 m (Early Eocene to Turonian succession).

Biostratigraphy (from Weston et al. 2012) for Newburn H-23 extends from the Hauterivian to the Late Miocene using palynology and nanofossil data (Fig. 4.5).

The Aptian to Early-Middle Turonian comprises bedded mudstones with small amounts of sands and limestone (in the lower Albian). The onset of the Eocene marks a change to a series of thick chalks and marls (Ypresian Chalk; ~2760-2840 m) that unconformably overlie claystone from the Late Cretaceous where the well penetrates the Upper Slope Slide Complex (USSC) (Deptuck and Campbell 2012). These uniform claystones continue upward through the Eocene until the Late Miocene where sampling ends.

Most of the Upper Cretaceous to Paleocene and Oligocene have been eroded away in this well, leaving parts of the Eocene and Miocene.

Evangeline H-98

The primary target was a marine/deltaic sands of Logan Canyon and Missisauga formations (Kidston et al. 2007). Evangeline is located on the modern shelf edge and intersects all horizons aside from the K1 (Cenomanian/Turonian), P3 (Bartonian) and N9 (Pliocene) markers (Fig. 4.4).

Biostratigraphy (from Thomas 1991 and Weston et al. 2012) collected from the Evangeline H-98 well extends from the Aptian to the Early to Middle Miocene (Fig. 4.6). It intersects a USSC glide block (2849 m to 3029 m) on the downthrown side of a listric fault.

Biostratigraphy (from Weston et al. 2012) from the Aptian-Early Albian indicate a prodelta, paralic and shallow marine origin with some continental deposits. The Cenomanian (Dawson Canyon Fm) is composed of shales in the lower portion transitioning to chalks, shales and some silts in the upper half. Continuing upwards, the frequency of chalks and mudstone deposits (Wyandot Fm) increase from the Turonian to Campanian changing to dominantly mudstones (Banquereau Fm) by the Maastrichtian. The Paleocene to Early Eocene consists of mudstones, interbedded with shales and some limestone and chalks (i.e Ypresian Chalk, 1515 m to 1524 m). These grade into dominantly mudstones until the Middle Miocene. Wireline logs continue upwards into the shallow interval implying a transition to sandier intervals at approximately 1000 m.

Age dating (from Weston et al. 2012) extends from the Maastrichtian to the Early-Middle Miocene. Upwards from the Late Miocene, palynology data from Williams (1991) was utilized. This interpretation moves the N7 horizon to at least the Pliocene, conflicting with Shubenacadie H-100 interpretation of the N7 in the Late Miocene. This conflict in the timing may be due to the limited methods (solely palynology) used in that particular study (Williams 1991). Further dating is required to refine this upper interval and confirm their interpretation.

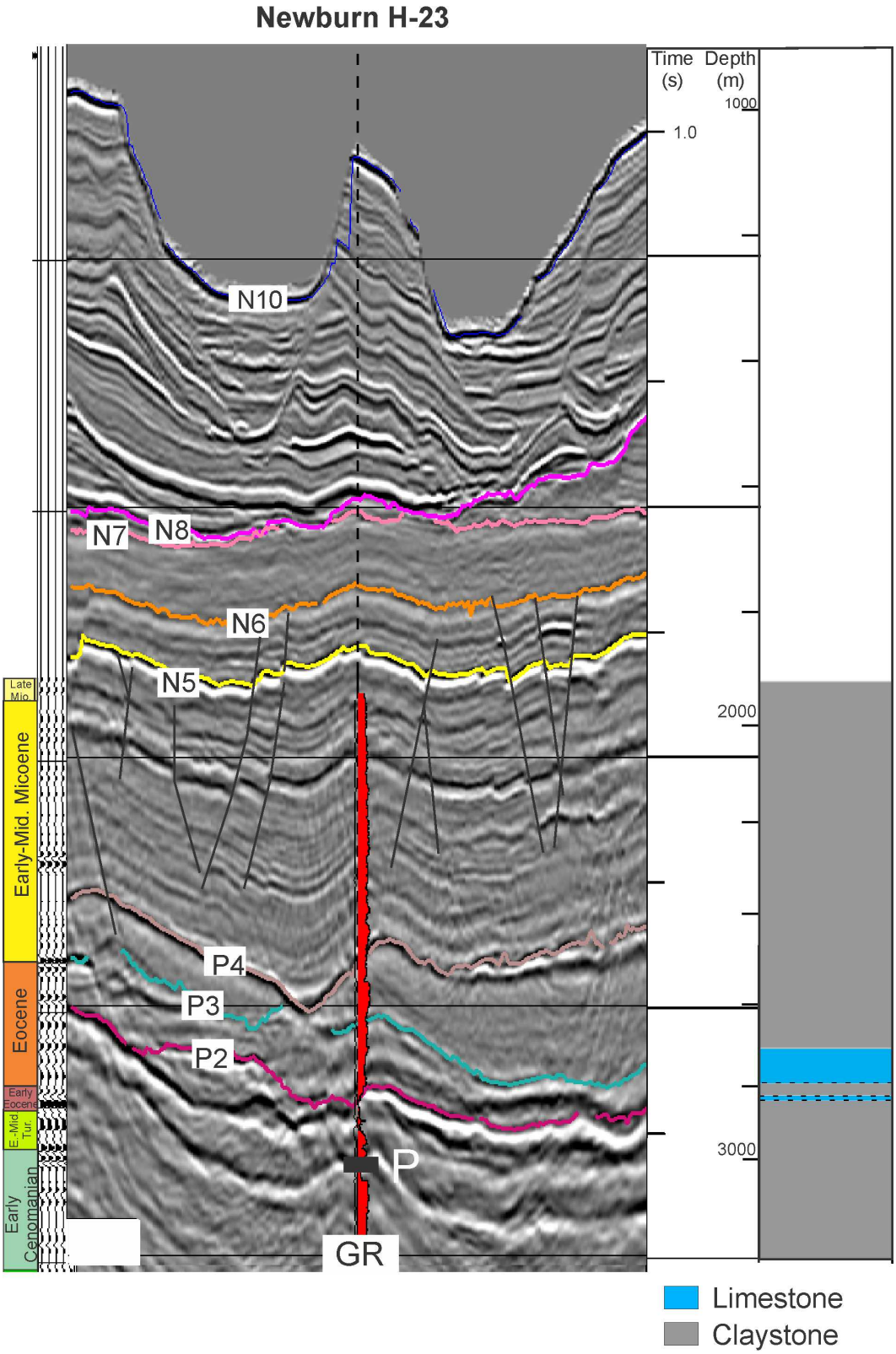

Figure 4.5: Well calibration for the Newburn H-23 well. P = Petrel Member.

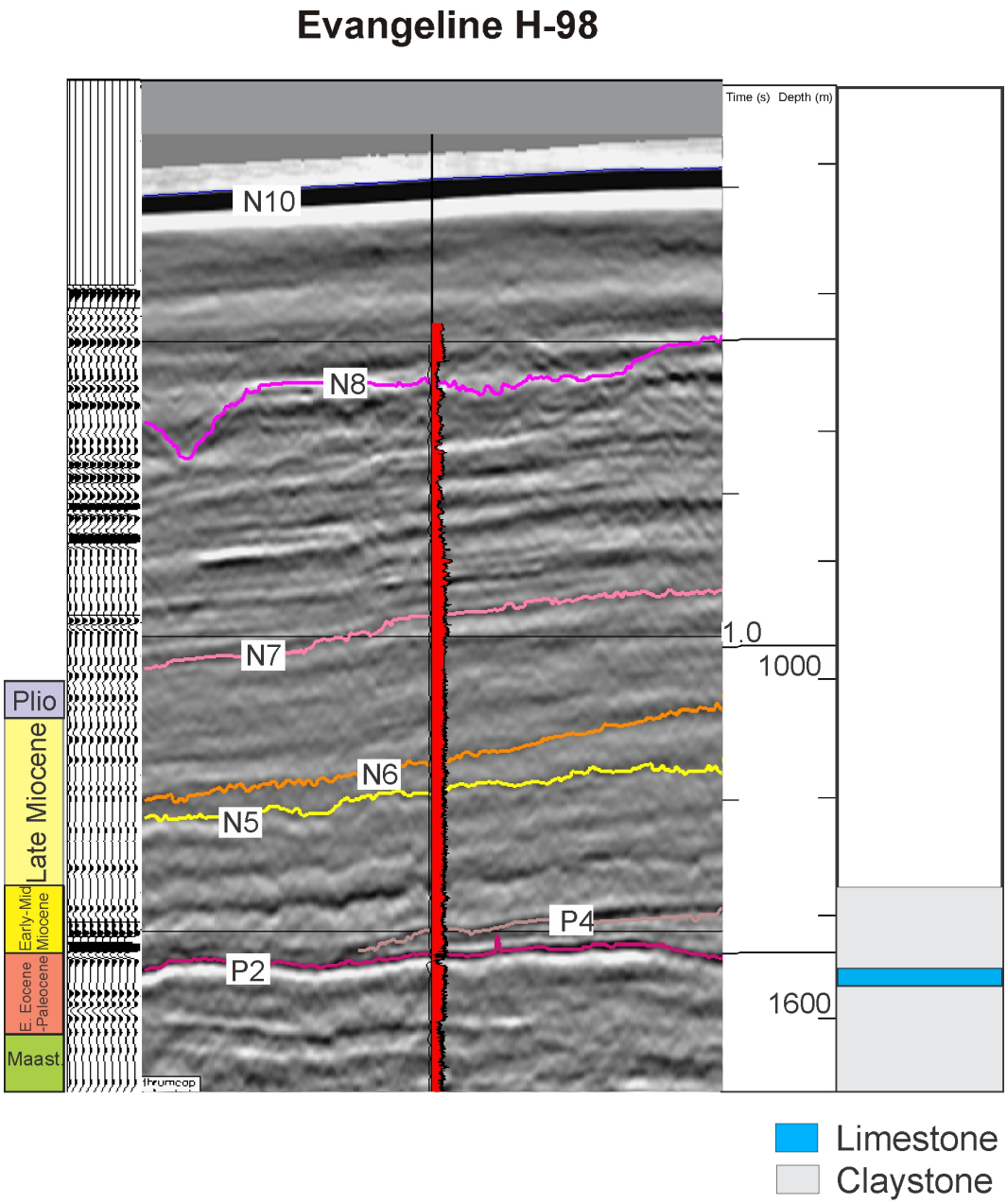

Figure 4.6: Well calibration for the Evangeline H-98 well. GR= Gamma Ray.

Shubenacadie H-100

Shubenacadie H-100 is located on the upper slope and drilled in 1982. It targeted a lower Tertiary turbidite fan and a secondary 'bright spot' in the Miocene. This well has the most refined biostratigraphy in the study area and was drilled to a depth of 4200 m (MD) reaching the Middle Cenomanian (Kidston et al. 2007). Recent work dated the strata in this well from the

Cenomanian to the Pliocene (Fensome et al. 2008; OETR 2011; Weston et al. 2012) (Fig. 4.7). It penetrates all horizons except for P3 (Bartonian) which merges with the P4 horizon in this area (Figs. 4.4 and 4.7).

The well has penetrated several unconformities, most notable an Early Miocene unconformity with a 23 Ma time gap eroding into Middle Eocene and Oligocene strata. A younger 4 Ma unconformity is also present in the Late Miocene (Tortonian) (Kidston et. al. 2007). The primary target was a fan complex which turned out to be erosional remnants between canyons in the Late Cretaceous and Paleogene. Sediments consists of shales, chalks and marls.

Biostratigraphy data (from Weston et al. 2012) indicates an open marine, prodelta and outer neretic environment during the Cenomanian changing to open marine and outer neretic around the Turonian boundary. This depositional trend continues until the beginning of the Paleocene. Biostratigraphy from the Paleocene through to the Early to Middle Miocene indicates prodelta with inner, middle and outer neretic deposits.

Data from the Late Miocene to Pliocene shows an upper slope depositional environment while the early Eocene to Paleocene is a deeper middle slope transgressional setting.

Lithologically, the Cenomanian interval is dominantly shales (of the Shortland Shale) transitioning to interbedded mudstones, shales and mostly limestones at the Turonian-Campanian boundary (equivalent to the Dawson Canyon, Wyandot and Banquereau formations). This trend of interbedded lithologies continues into the Maastrichtian where shales become more dominant upwards. By the Paleocene, the lower-half consists of dominantly shales changing to interbedded limestone and mudstones in the upper-half of the interval. Similarly, the Eocene lower half consists of limestones transitioning to mudstones in the upper section. These mudstones continue upwards becoming interbedded with sand in the Late Micoene. Lithological logs end in the Late

Miocene and there is no available data for the Pliocene lithologies. Wireline logs hint at shales upwards grading into interbedded sands towards the Pliocene.

Acadia K-62

Acadia K-62 is located at the shelf edge above the Abenaki carbonate bank. Biostratigraphy (from Thomas 2001) in the Acadia well is limited and extends from the Jurassic to the Early to Middle Miocene (Fig. 4.8). The well intersects the Jurassic Abenaki Carbonate at the shelf hinge and because horizons merge in this area or are truncated, correlation to this well was difficult. Since the well is located near the shelf-edge, horizons tended to merge around this area and therefore, the well only penetrates a few horizons (P2, N5, N7, N8 and N9) (Fig. 4.4). Horizons K1 (Cenomanian/Turonian), P3 (Bartonian), P4 (Rupelian) and N6 (Tortonian) are absent in this area. The well also notably intersects the USSC previously studied by Deptuck and Campbell (2012) that caused widespread mass wasting in the early Eocene from the Montagnais Impact.

Biostratigraphy for Acadia (from Thomas 1991) is generally limited in the upper section and ties to the N5 and N8 horizon appear to be different from other well correlations in this study, specifically the Shubenacadie H-100 or Evangeline H-98 wells. The N8 horizon correlates to at least the Pliocene (or post-Pliocene) in the Shubenacadie H-100 well and in the Acadia well it appears to tie the Upper Miocene. The N5 horizon ties to the Late Miocene (Tortonian) in the Shubenacadie H-100 well and Early-Middle Miocene in the Acadia well. These differences may be due to issues with the seismic interpretation (i.e. Acadia is outside of both 3D datasets and therefore horizons were correlated across using 2D seismic) or with the accuracy of the biostratigraphy based solely on foraminfera.

In terms of depositional environment in the Acadia well, there is a gradual change from outer neretic to inner and then to coastal marginal marine between the Aalenian-Bajocian and the Albian. At around the Paleocene, the depositional environment switches to open marine all the way until the around the late Miocene which shows a change to outer-neretic/open marine continuing upwards until the Plio-Pleistocene where data ends.

Fill of the older intervals largely consist of carbonate material until the Albian. The Albian marks a transition to limestones changing to shales with small amounts of interbedded limestones in the Barremian to Maastrichtian. The Eocene to Early-Middle Miocene generally consists of interbedded sandstone, shales and siltstone progressing into purely shales by the Late Miocene that continue upwards into Pliocene-Pleistocene.

4.2 Salt distribution in the study area

Numerous salt bodies are recognized in the study area, and although they have been previously mapped by other studies (e.g. Shimeld 2004; Deptuck et al. 2011), salt bodies were remapped in this study in order to confirm previous interpretations (Figs. 4.9A, 4.10-4.12). Salt structures have been mapped further downslope but are not included in this study since they are outside of the study area (see Deptuck et al. 2009; Fig. 2.9).

The top salt horizon is a positive high amplitude reflector (Fig. 4.10). The base salt horizon, although not always resolvable, is a negative amplitude reflection (Fig. 4.12). There are 21 salt bodies in the study area; 18 salt bodies are classified as vertical salt diapirs, with three salt bodies forming salt tongues that are entirely allochthonous (Figs. 4.9A, 4.10). The western, generally vertical salt bodies are found within Shimeld's (2004) Subprovince II whereas the allocthonous salt tongues belong to Subprovince III (see section 2.4.2). A naming scheme for individual salt structures is explained below.

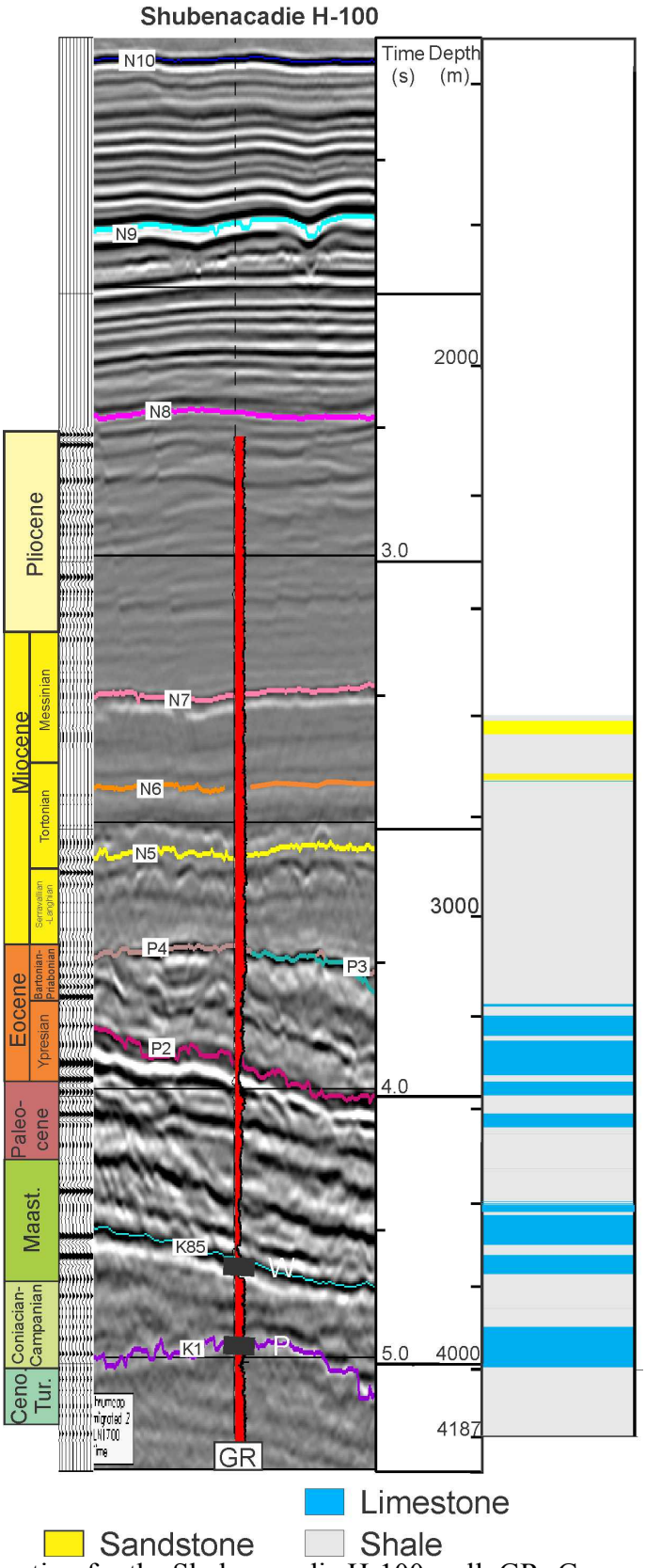

Figure 4.7: Well calibration for the Shubenacadie H-100 well. GR=Gamma Ray; W=Wyandot Formation (top); P=Petrel Member.

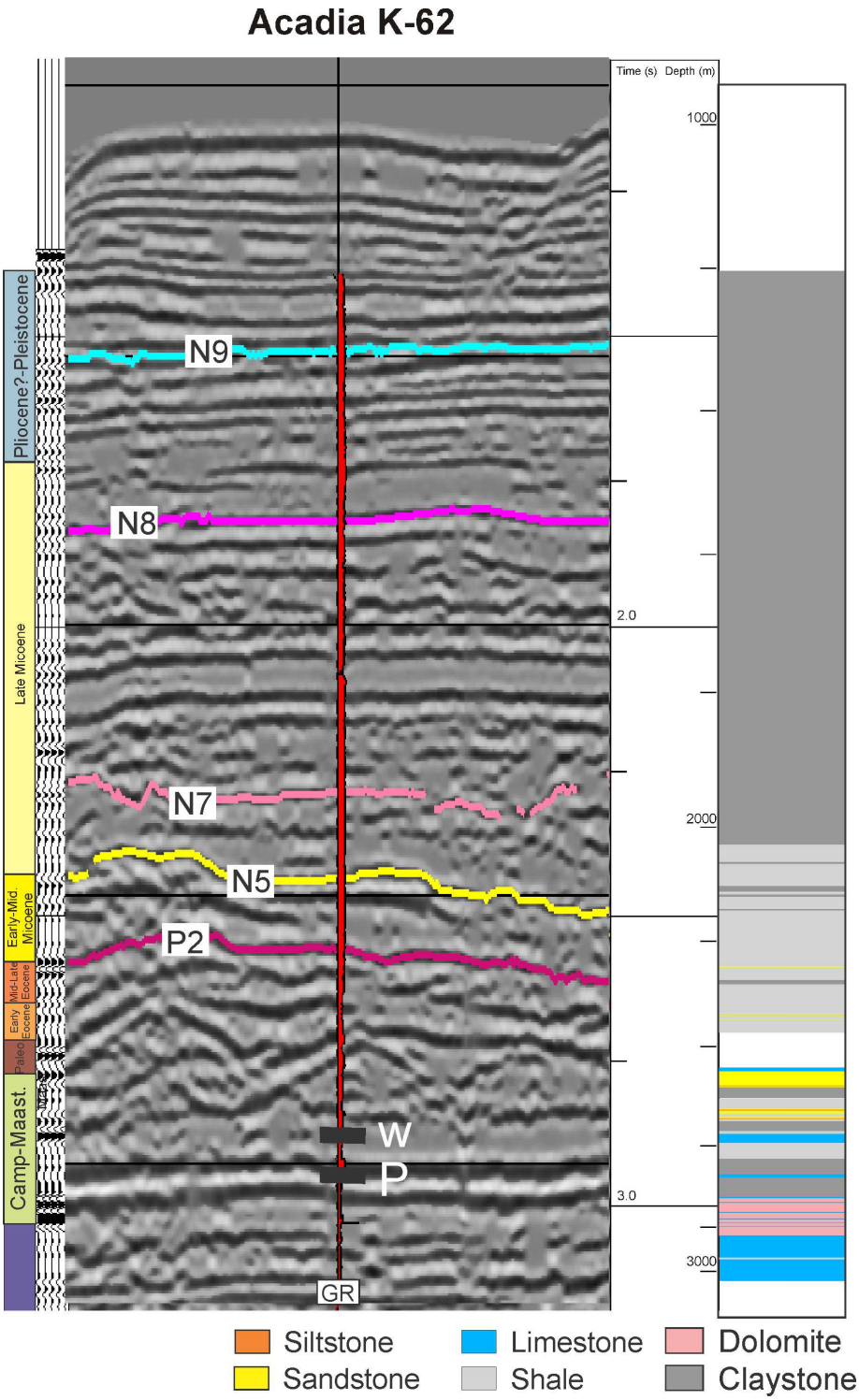

Figure 4.8: Well calibration for the Acadia K-62 well. GR=Gamma Ray; W=Wyandot Formation; P=Petrel Member.

4.2.1 Vertical salt diapirs

These diapirs are typically circular to elliptical in plan view (Fig. 4.10). In cross section, they typically have a rounded bulb with salt wings and pinched stem structure (Figs. 4.13-4.14). The vertical salt diapir province in the western study area is further subdivided into 3 groups: proximal, medial and distal (Figs. 4.9A, 4.15-4.18). Diapirs P1 to P6 are located nearest the shelf edge and diapirs D1 to D8 are located furthest from the shelf edge, with diapirs M1 to M5 located in a medial position.

4.2.2 Allochthonous tongues

The allochthonous tongues in the eastern sector of the study are named from west to east: salt bodies A1, A2, and A3, all having separate feeders (Fig. 4. 9A). The A3 tongue has generally been omitted from this study because it extends beyond the study area limits, hindering its interpretation (Fig. 4.9A). Salt tongues in the east are elongate and generally folded with extensional faults in the upslope portion and thrusts in the downslope portion (Fig. 4.14).

Length and width values were taken perpendicular to the maximum extent of each diapir in plan view. At their lengths, A1 and A2 measure at 13.5 km and 36.5 km respectively (Figs. 4.10 and 4.19). Large regional growth faults and associated minibasins are present landward of both the A1 and A2 salt bodies. The minibasins are labelled B1, B2 and B3 (Fig. 4.20). These growth faults were most active from the Oligocene-Pliocene and are a result of salt withdrawal as the salt evacuated seaward over time allowing landward minibasins (salt withdrawal basins) to form.

The allochthonous tongues have been further subdivided into structural zones i.e. withdrawal basins, salt highs, rafts and a roho system (Fig. 4.10). Withdrawal basins are areas

where salt has evacuated due to overburden pressures creating bathymetric lows. These lows preferentially trap sediments and create areas of thick sedimentation (`thicks`) in isochrons.

Adjacent to withdrawal basins are areas where salt was expelled (Fig 4.10-4.11). These regions form the salt highs where younger stratigraphic units thin onto their resulting positive relief. The A1 salt tongue has a salt high surrounding a withdrawal basin in the middle and the A2 tongue has two salt-highs on the eastern and northwestern areas sections of its extent (Fig. 4.19A, 4.10-4.11).

4.3 Salt body characteristics

4.3.1 Overburden in the study area

All of the salt bodies in this study are buried (Fig. 4.21). Overburden thicknesses range from 660 m to 1374 m at the thickest when using a simple velocity conversion (assuming sediment velocity of 1750 m/s) derived from the Shell Geophysical Report in the Thrumcap survey area (Porter et al. 2002; Table 4.1).

Generally distal diapirs in the southern section of the study area have lower overburden values than proximal diapirs due to increased erosion and landward tapering of stratigraphic packages in the Cenozoic succession (Figs. 4.15 and, 4.18 and 4.18). Salt crests that are intersected by modern-day canyons are P3, P4, D2 (partial) and D4 thus having lower overburden values (Figs. 4.14-4.19, 4.21). The salt structure with the thinnest overburden (>500 ms or 500 m) is the D4 diapir that intersects a modern canyon system in addition to being in the distal section of the study area where overburden thicknesses are less. The diapir with the

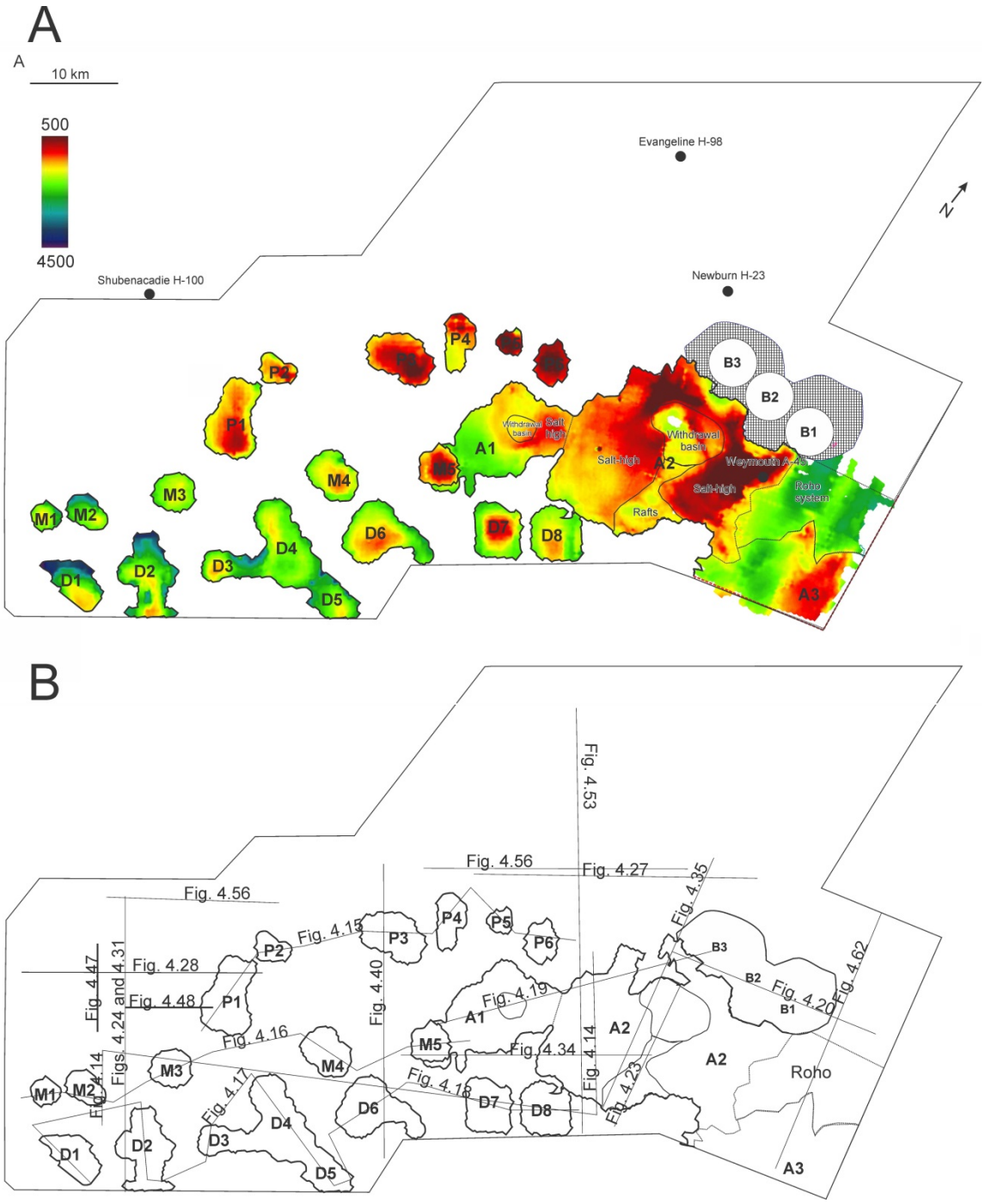

Figure 4.9: A) Time-structure map showing the distribution of the 21 salt bodies in the study area and allocated names and structural zones. "A" labels represent allochthonous tongues in the east and "P", "M" and "D" labels represent proximal, medial and distal vertical salt bodies in the west, respectively. B) Seismic location map for profiles from 4.14 to 4.63.

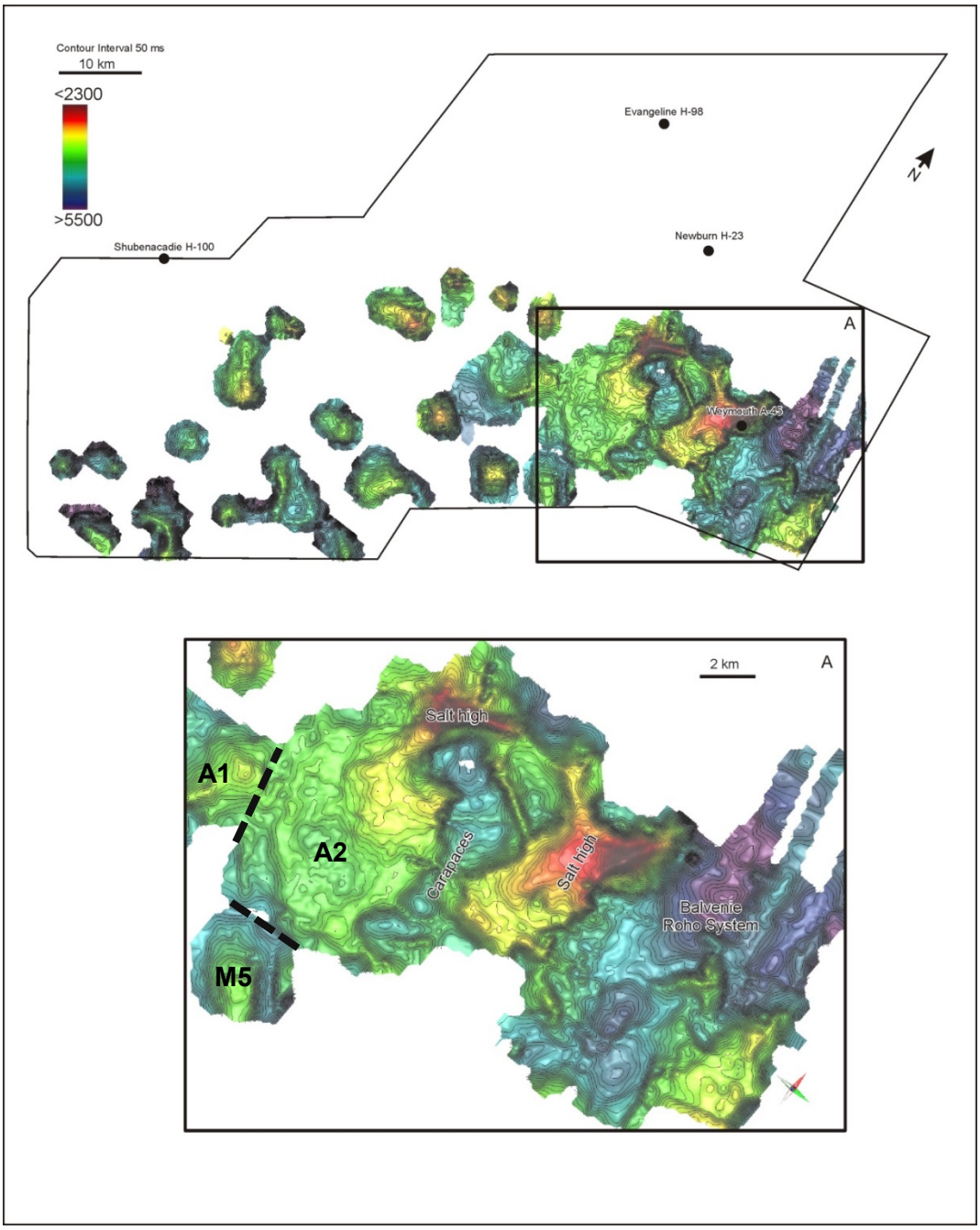

Figure 4.10: Figure showing the time-structure of the 'top salt' horizon (top). Enlarged below is the allochthonous tongue salt tongue A2 (and part of A3) that has salt highs, internal minibasins, carapaces, and part of the Balvenie Roho System in the east.

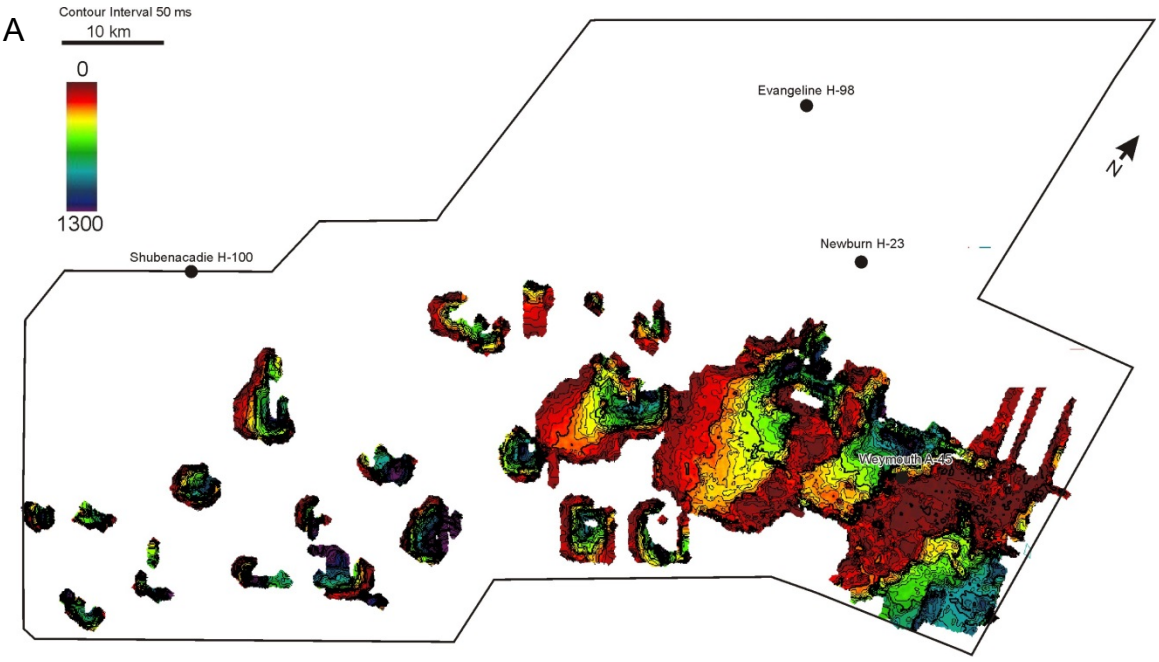

Figure 4.11: Time-thickness map of salt in the study area (isochron map from top salt to base salt).

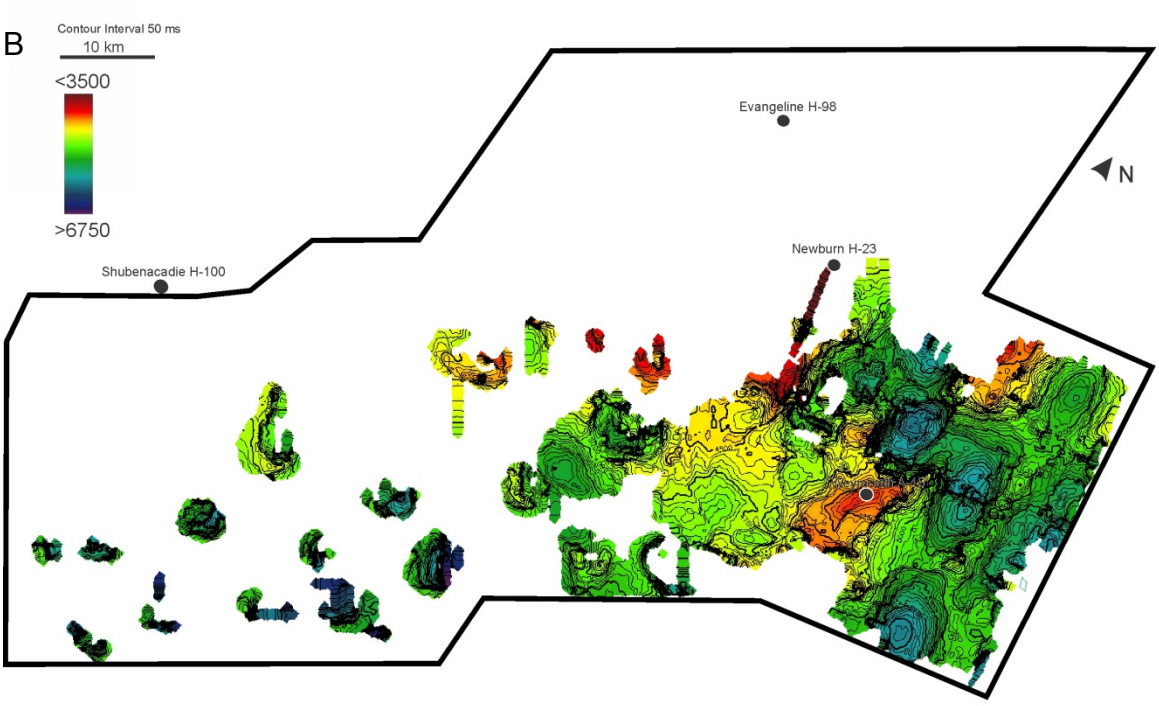

Figure 4.12: Time-structure map of the `base salt` Horizon.

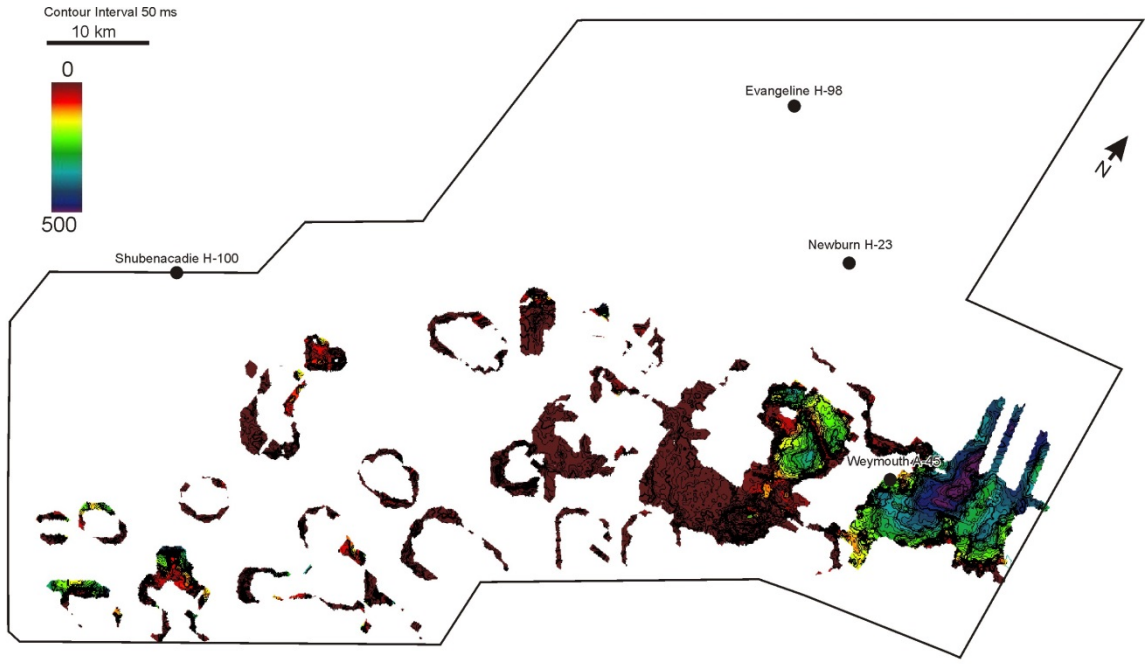

Figure 4.13: Salt overhangs in the study area (isochron map of top salt to K1).

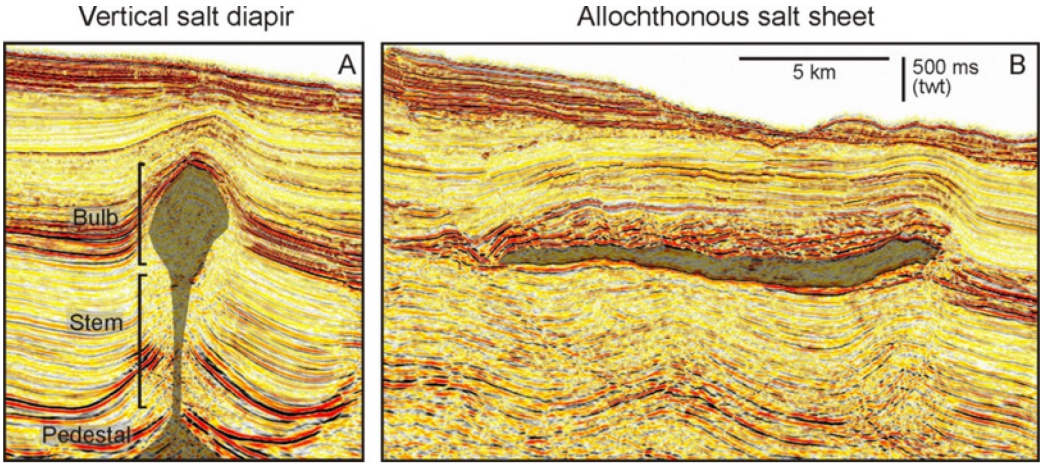

Figure 4.14: Type section through a vertical salt diapir (west) and allochthonous tongue (east) in the study area.

thickest overburden is P6 diapir, in part due to the presence of a Miocene paleocanyon system with significant infill (> 1800 ms or approximately 1800 m) and being in the proximal part of the study area where the Cenozoic succession is the thickest (Fig. 4.1, 4.18 and 4.19).

Overburdens in the allochthonous tongue province vary considerably from one part of the tongue to another (ranging from 500 to 2500 ms TWTT). Generally, thinning is associated with salt highs and thick packages correspond to areas where salt withdrawal has taken place (i,e. withdrawal basins or welds).

4.3.2 Length:width ratios

To better define the map geometry of the diapirs, lengths and widths have been measured. A maximum length value was recorded in the P1 diapir (9.2 km) and a minimum value in P6 (2.2 km). In terms of width, maximum and minimum values are 8.13 km for the D4 diapir and 2.81 km for the P5 diapir respectively. When calculating the surface area, the D4 diapir covers the greatest area (~83 km^2) in contrast to the P5 diapir that covers about ~8km^2. Generally the proximal diapirs are smaller than other salt structures in the study area with the exception of P1.

Length:width ratios closer to 1.0 are more circular and ratios closer to 2.0 are more elongated (Fig. 4.9A and Table 4.1). Most diapirs in the study area have length:width ratios ranging between 1 and 2, but the the P3 diapir with a ratio of 2.31 is the most elongated in plan-view. In contrast to the P3 diapir, the P5 diapir has a circular plan view ratio of 1.0. There appears to be no distinguishable trend in the plan view shape of vertical salt structures and values vary widely across the study area (Table 4.1).

4.3.3 Salt extrusion, rafts and carapaces in the study area

Carapaces in this study are defined as blocks of older hemipelagic-pelagic sediments that have been detached and uplifted since deposition. These blocks sit above the salt diapir crests and are fault-bounded. They have a low amplitude discordant facies and are common throughout the study area, generally including older (pre-K1) strata that have subsequently been exhumed by

salt since deposition. In cases where the K1 horizon is present as a raft/carapace, it conformably overlies older horizons. Diapirs that have the most prominent rafts/carapaces are P2, M1, M2, M4, D1, D4 and D5 (Figs. 4.15-4.18, 4.21), although they appear to be apparent above all salt bodies.

The presence of salt wings in the study area is a distinctive indication of passive diapirism whereby salt from the source layer was extruded onto the seafloor and flowed over the sediment surface. Salt appears to have extruded between the lower units 1 to 2 (Cenomanian-Ypresian) (indicated by horizons that are truncated by the salt in this interval) and then draped by overlying units once the extrusion ceased (for more detail see Chapter 6.2).

All proximal diapirs show signs of having been extruded in addition to some medial (M3, M5) and distal diapirs (D2, D3, D6, D7 and D8) (Figs. 4.15- 4.19). There appears to be no regional trend between periods of salt extrusion and rafts/carapaces in the study area (Table 4.1).

Salt stems

Where resolvable, all vertical diapirs show pinched stems (i.e. narrowed) (Figs. 4.15-4.19). The welding out of the stem creates a teardrop-shaped structure in cross section. Diapirs with dramatically pinched or welded salt stems are diagnostic of active diapirism driven by lateral compression (see section 3.3.1).

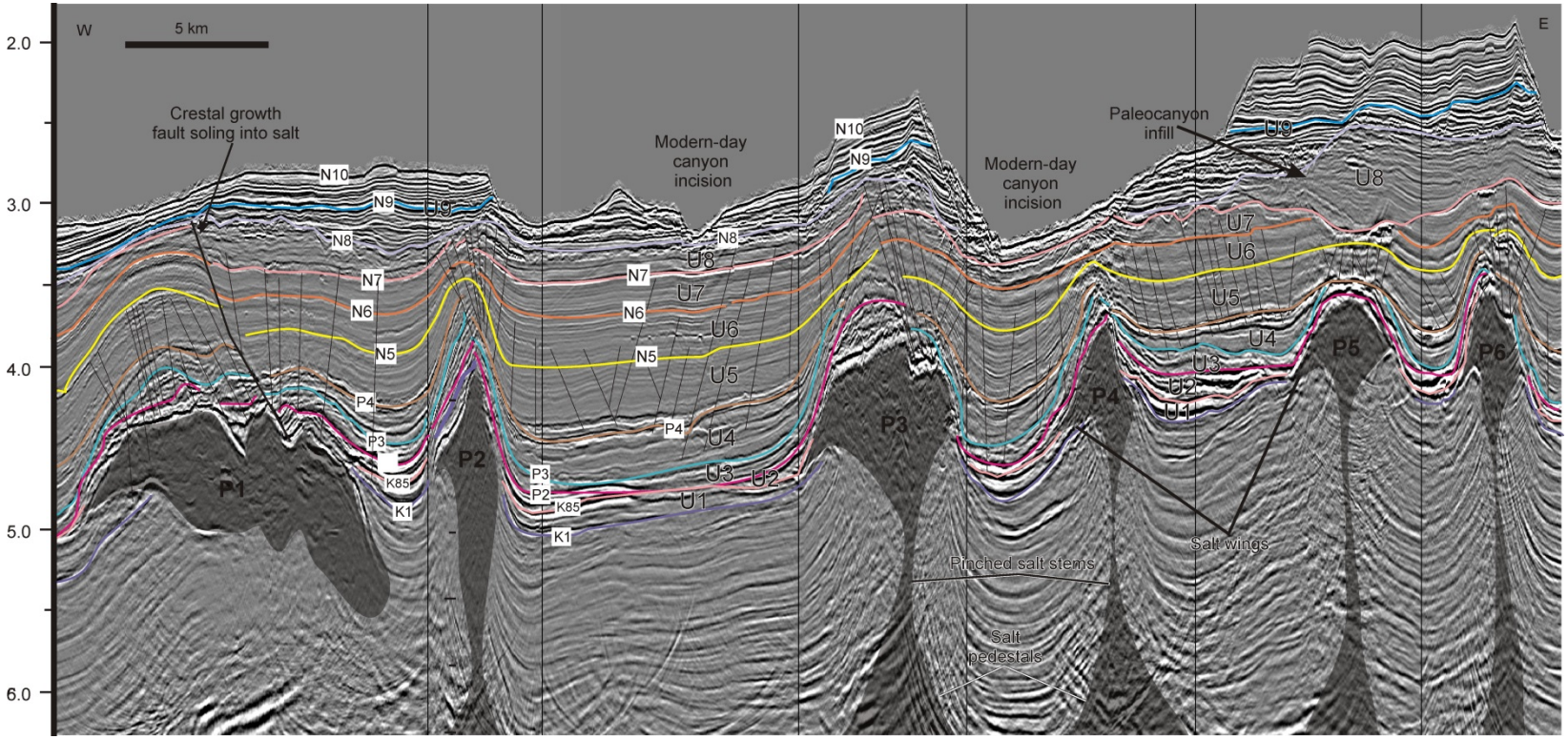

Figure 4.15: A cross section through the *proximal* diapirs. See Figure 4.9B for the location of this transect.
transect.

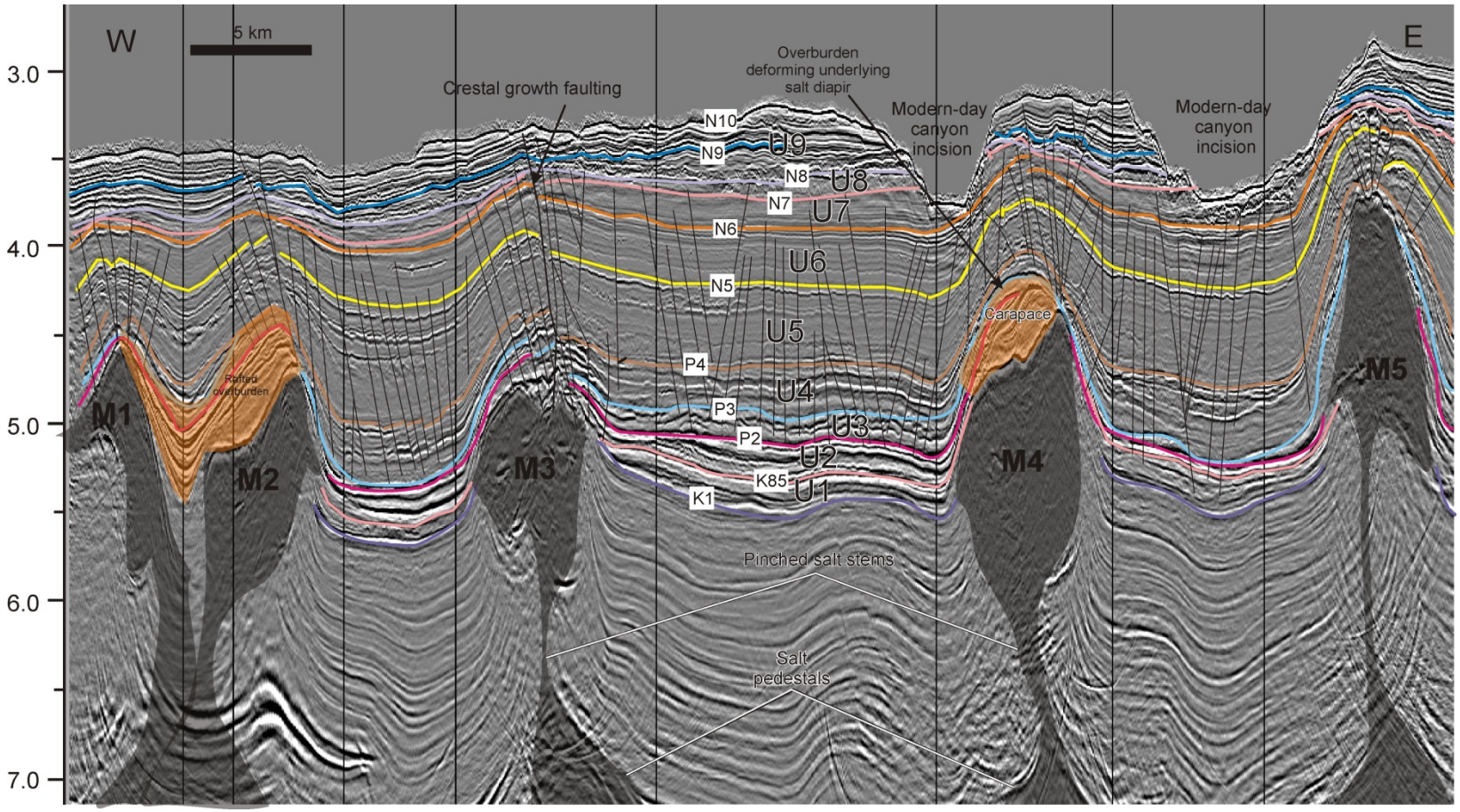

Figure 4.16: A cross section through the *medial* diapirs. See Figure 4.9B for the location of this transect. Rafts are indicated in orange.

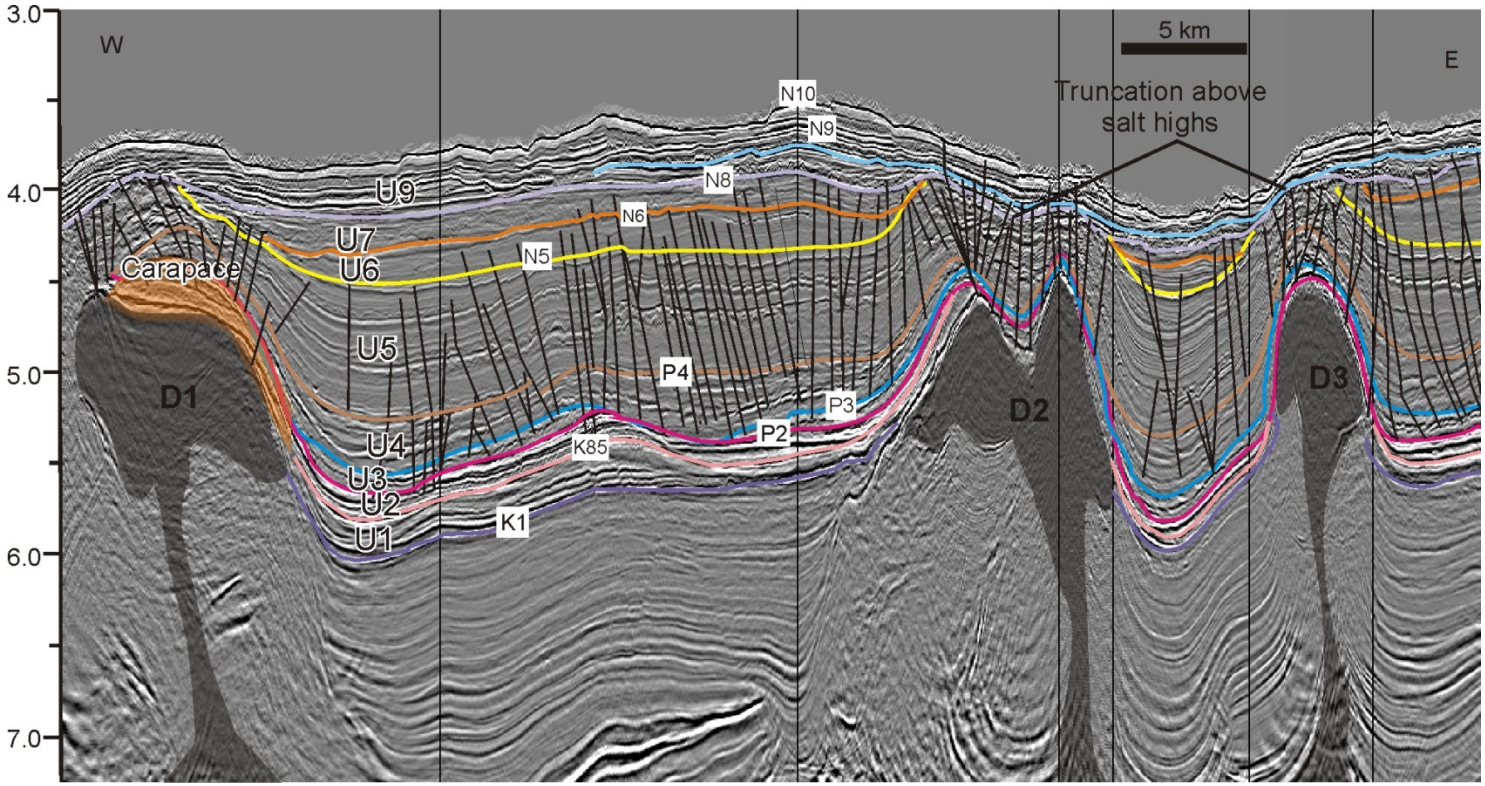

Figure 4.17: A cross section through the *distal* diapirs D1-D3. See Figure 4.9B for the location of this transect. transect.

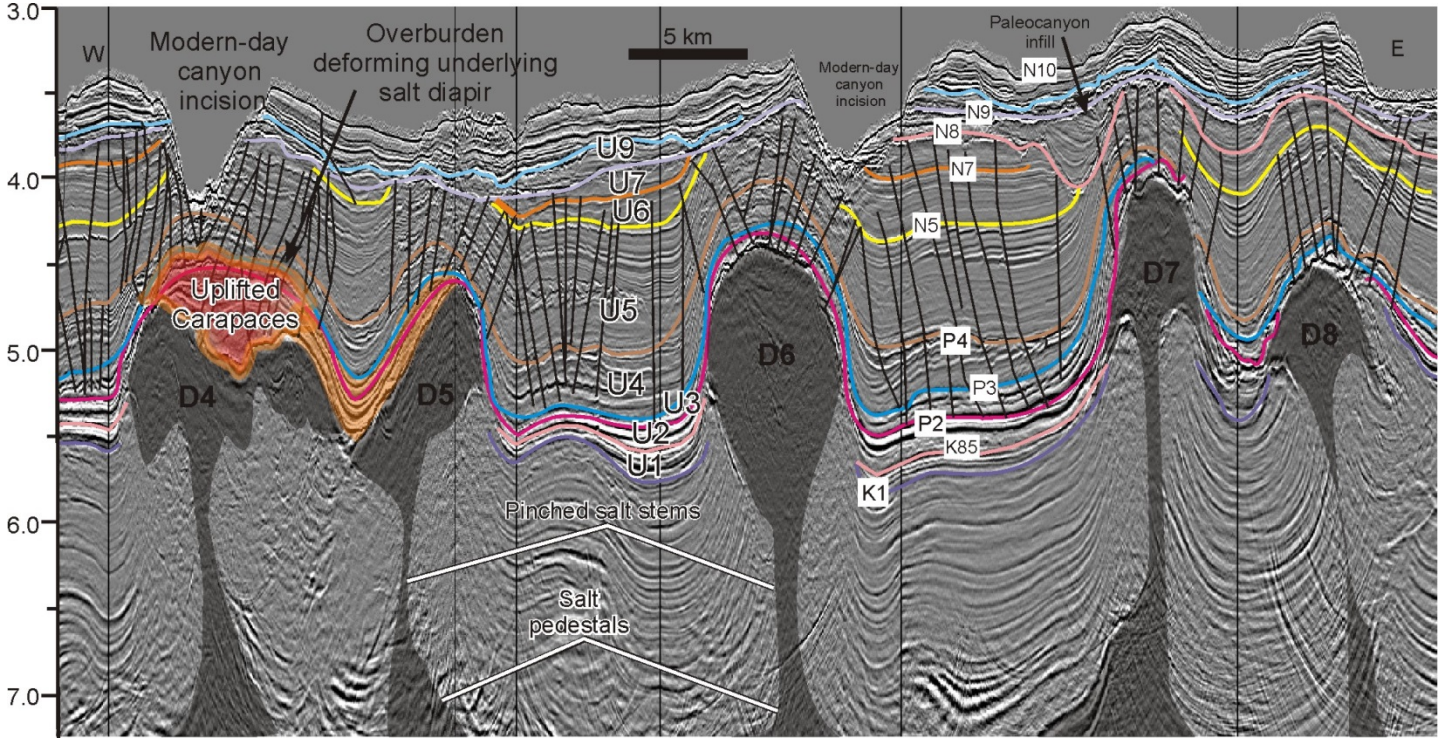

Figure 4.18: A cross section through the widest parts of the *distal* diapirs D4-D8. See Figure 4.9B for the location of this transect.

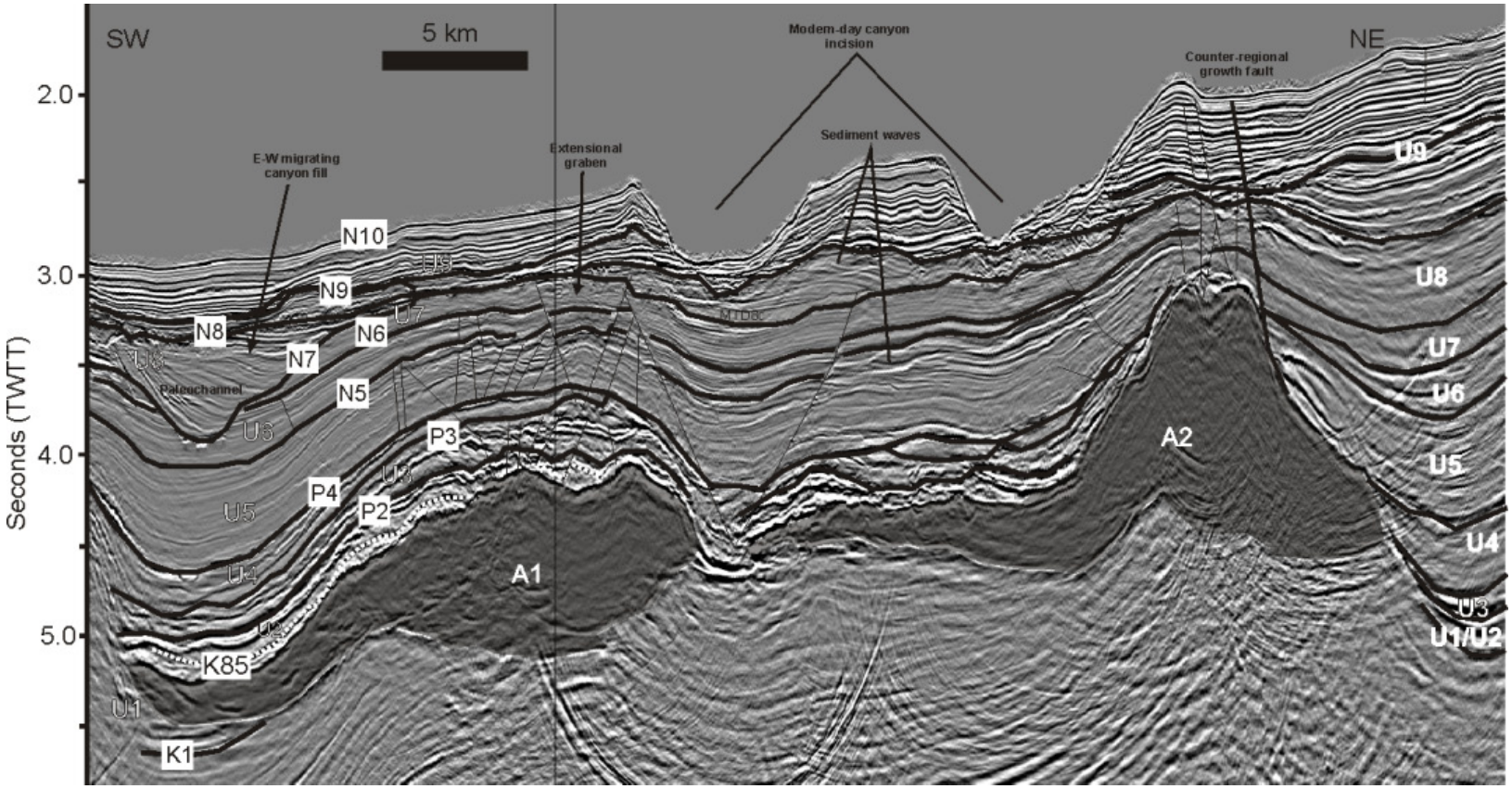

Figure 4.19: Allochthonous tongues A1 and A2. See Figure 4.9B for the location of this transect.

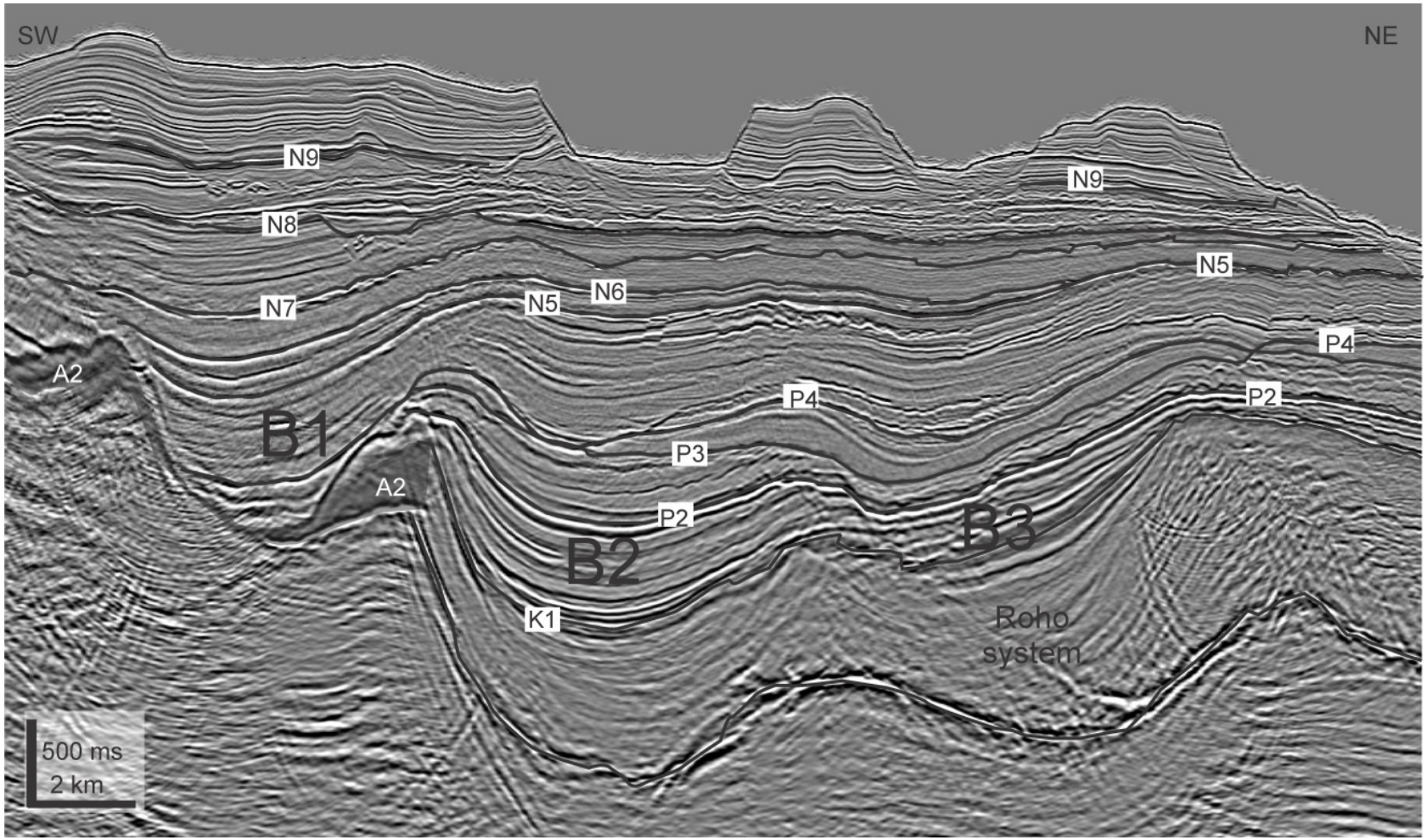

Figure 4.20: Profile through minibasins B1, B2 and B3. See Figure 4.9B for the location of this transect.

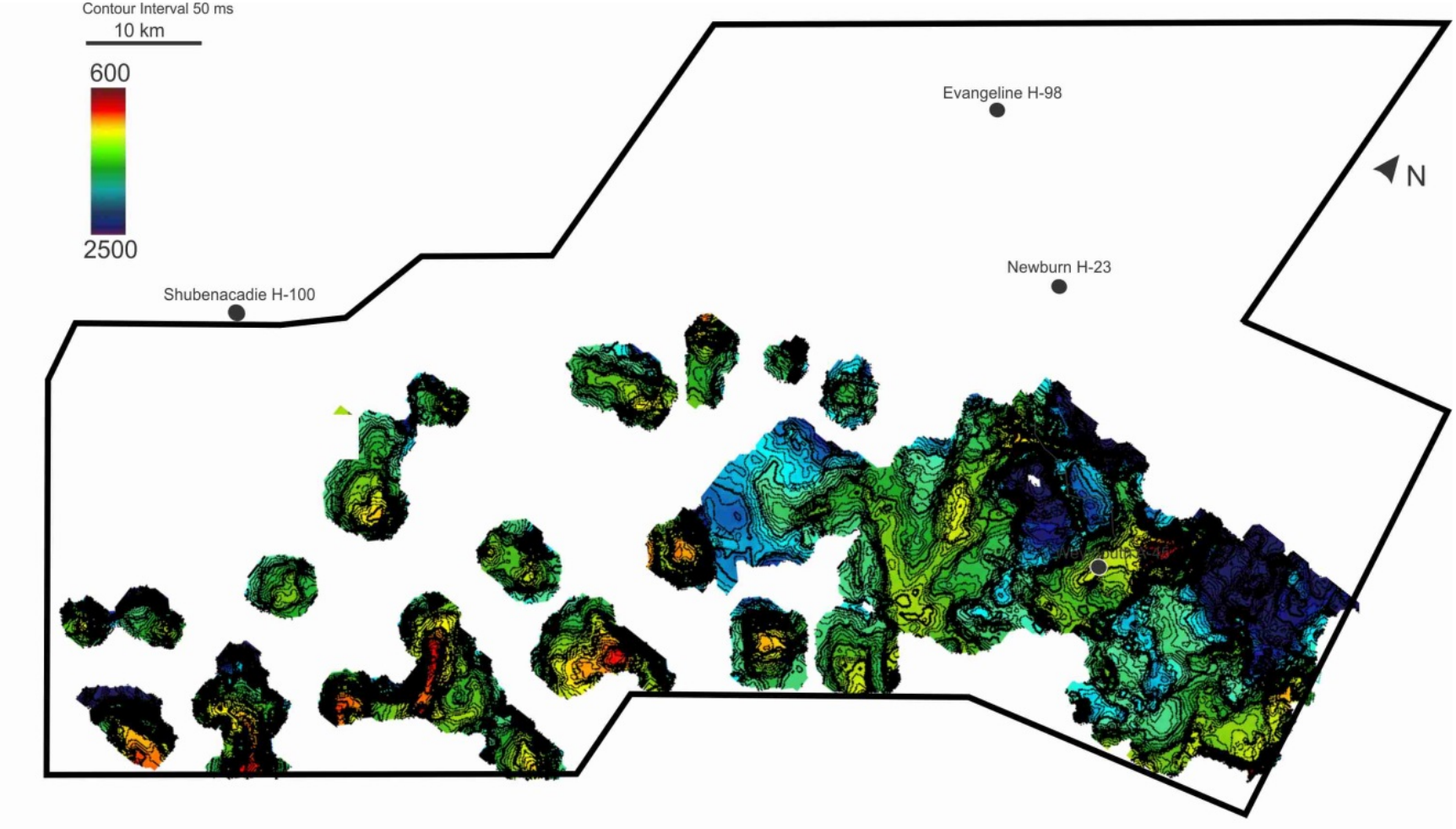

Figure 4.21: Overburden isochron from *top salt* horizon to present day seafloor. Minibasins overlying the allochthonous salt tongues in the east are evidence as the blue "thick" areas.

Table 4.1: Recorded measurements from each vertical salt body.

Diapir Name	Length (km)	Width (km)	Ratio (length:width)	Map shape	Max overburden thickness (TWTT seconds)	Approximate depth* (m)	Salt wings	Additional comments
P1	11.88	5.63	2.11	ELONGATED	1.47	1282	Y	CRESTAL GROWTH FAULTING
P2	4.25	2.50	1.70	CIRCULAR	1.39	1212	N	CRESTAL GROWTH FAULTING
P3	11.56	5.00	2.31	ELONGATED	1.44	1256	Y	CRESTAL GROWTH FAULTING
P4	6.25	3.13	2.00	ELONGATED	0.75	654	Y	CRESTAL GROWTH FAULTING
P5	2.81	2.81	1.00	CIRCULAR	1.56	1361	Y	CRESTAL GROWTH FAULTING
P6	4.69	3.63	1.29	CIRCULAR	1.58	1378	Y	CRESTAL GROWTH FAULTING
M1	3.44	3.13	1.10	CIRCULAR	1.07	933	N	CRESTAL GROWTH FAULTING
M2	5.00	3.44	1.45	ELONGATED	1.2	1047	N	CRESTAL GROWTH FAULTING
M3	5.13	4.38	1.17	CIRCULAR	1.575	1374	Y	CRESTAL GROWTH FAULTING
M4	6.56	4.38	1.50	ELONGATED	1.35	1177	N	CRESTAL GROWTH FAULTING
M5	5.31	5.00	1.06	CIRCULAR	1	872	Y	CRESTAL GROWTH FAULTING
D1	6.88	4.06	1.69	ELONGATED	0.95	828	N	COVER STRATA ERODED
D2	10.31	6.25	1.65	ELONGATED	0.57	497	Y	COVER ERODED
D3	6.25	3.25	1.92	ELONGATED	0.81	706	Y	COVER STRATA ERODED
D4	10.31	8.13	1.27	ELONGATED	0.76	663	N	COVER STRATA ERODED
D5	5.94	5.63	1.06	ELONGATED	1	872	N	COVER STRATA ERODED
D6	10.31	6.88	1.50	ELONGATED	1.04	907	Y	COVER STRATA ERODED
D7	6.56	5.31	1.24	CIRCULAR	0.95	828	Y	COVER STRATA ERODED

D8	6.25	5.63	1.11	CIRCULAR	1.44	1256	Y	COVER STRATA ERODED

An older (pre-K1) roho system (see section 3.1.1) is located in the northeast section of the study area, referred to as the Balvenie Roho System by Deptuck et al. (2009) and Deptuck and Kendell (2012) (Figs. 2.10, 4.9A, 4.22). This roho system is a remnant of seaward salt migration from the Jurassic to Cretaceous.

A large system of rafts in the study area is located in the southeastern section of the A2 allochthonous tongue (Fig 4.10A, 4.11 and 4.23). This raft system is a thick section of pre-study interval strata adjacent to the two salt highs and south of a withdrawal basin.

4.4 Seismic stratigraphic framework

Slope stratigraphy

Eleven seismic markers were correlated from the Upper Cretaceous to Cenozoic succession in the study area (Fig. 4.24). Each marker was mapped according to its acoustic character. The basal horizon of the study interval is the K1 marker. Horizons with names that have a “K” are Cretaceous strata; markers starting with a “P” are found within Paleogene strata and markers beginning with an “N” originate from Neogene strata. In addition, two additional markers were correlated by Mark Deptuck and contributed to this study (K85 marker and the modern seafloor reflection). Units are named U1 to U9 from stratigraphically oldest to youngest and are defined between each pair of horizons, with the exception of U9 which is an amalgamated interval between horizons N8 and the sea floor.

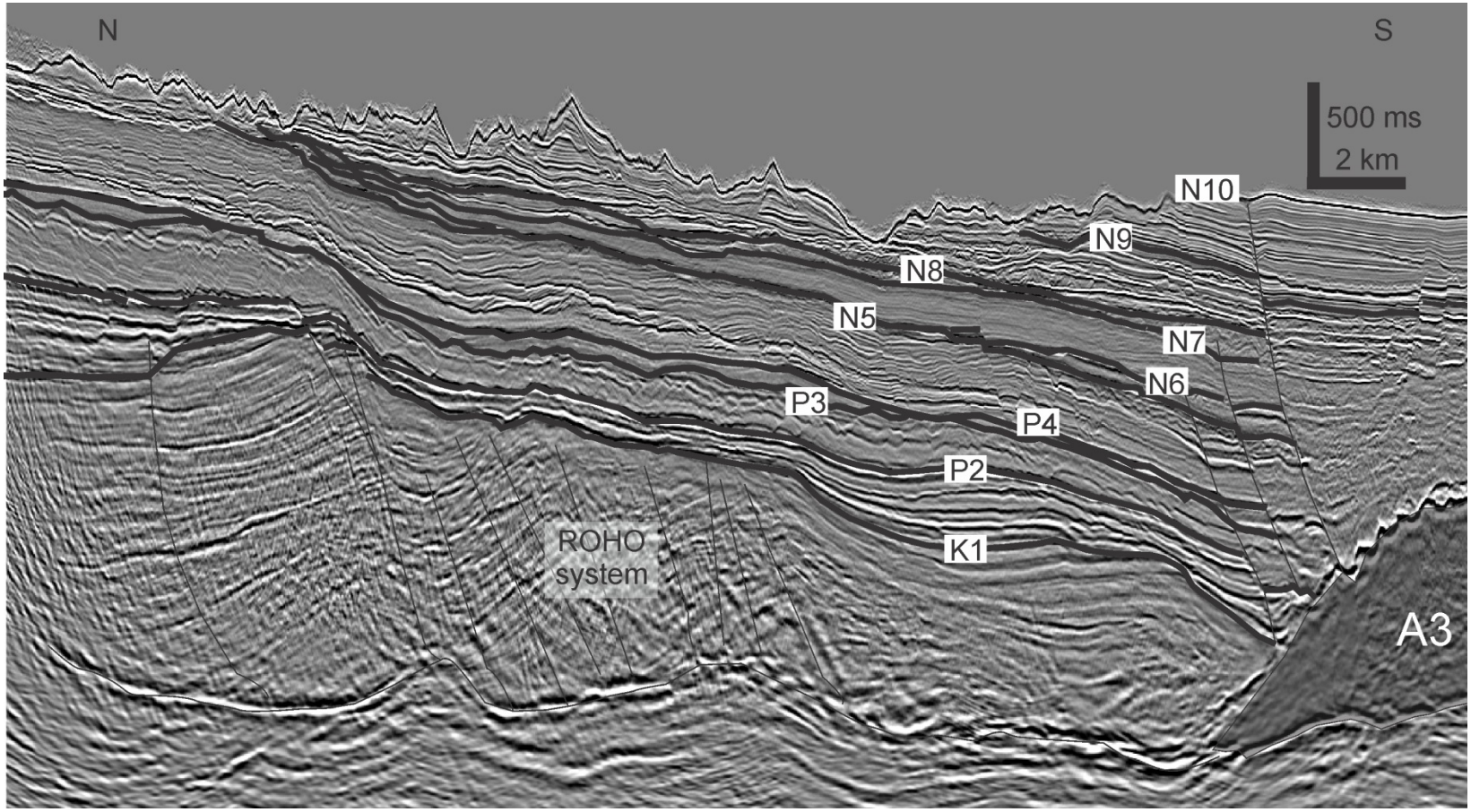

Figure 4.22: A cross section of the roho system located in the northeastern section of the study area. See Figure 4.9B for the location of this transect.

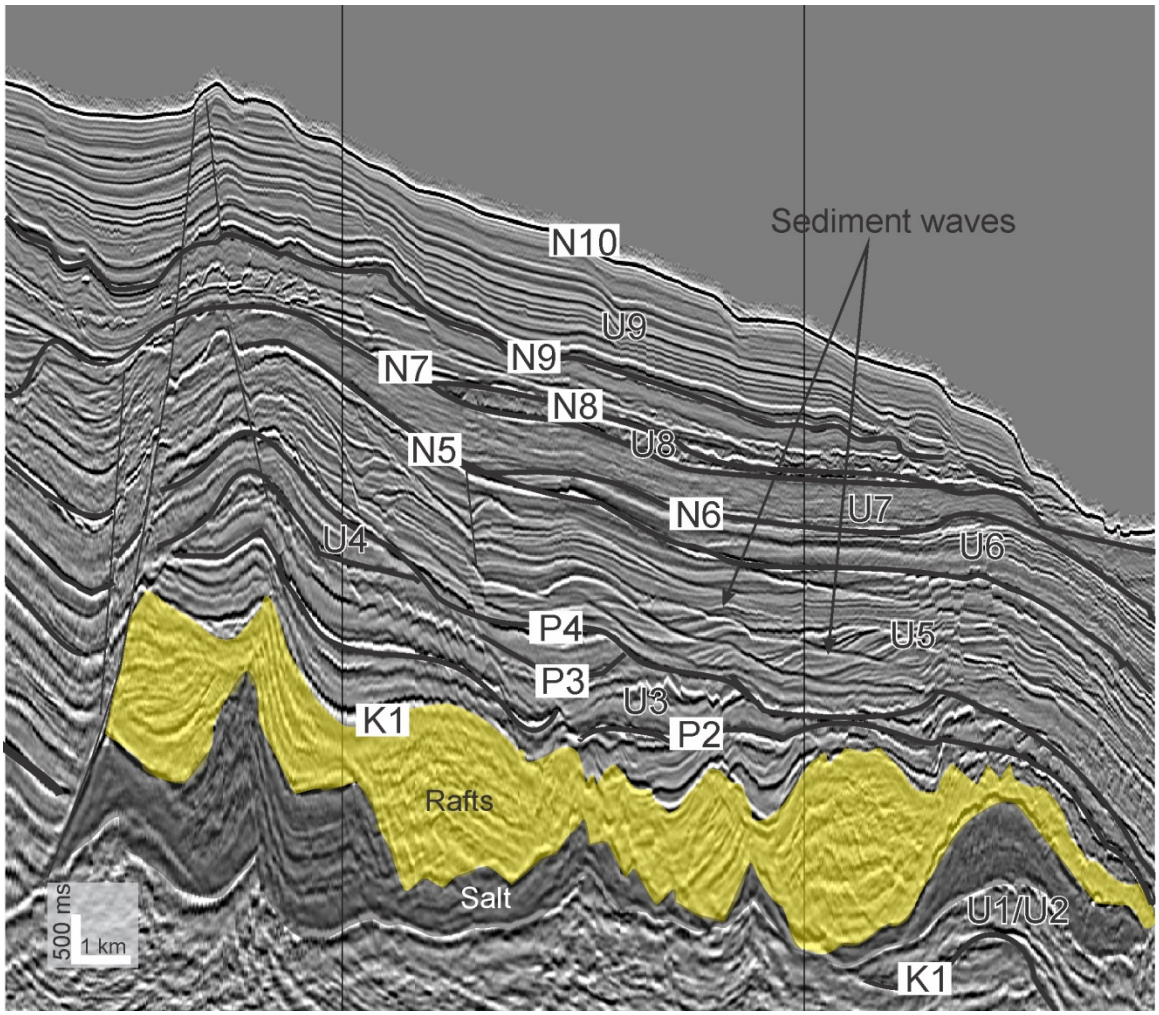

Figure 4.23: A series of conjoined rafts above the A2 salt tongue. See Figure 4.9B for the location of this transect.

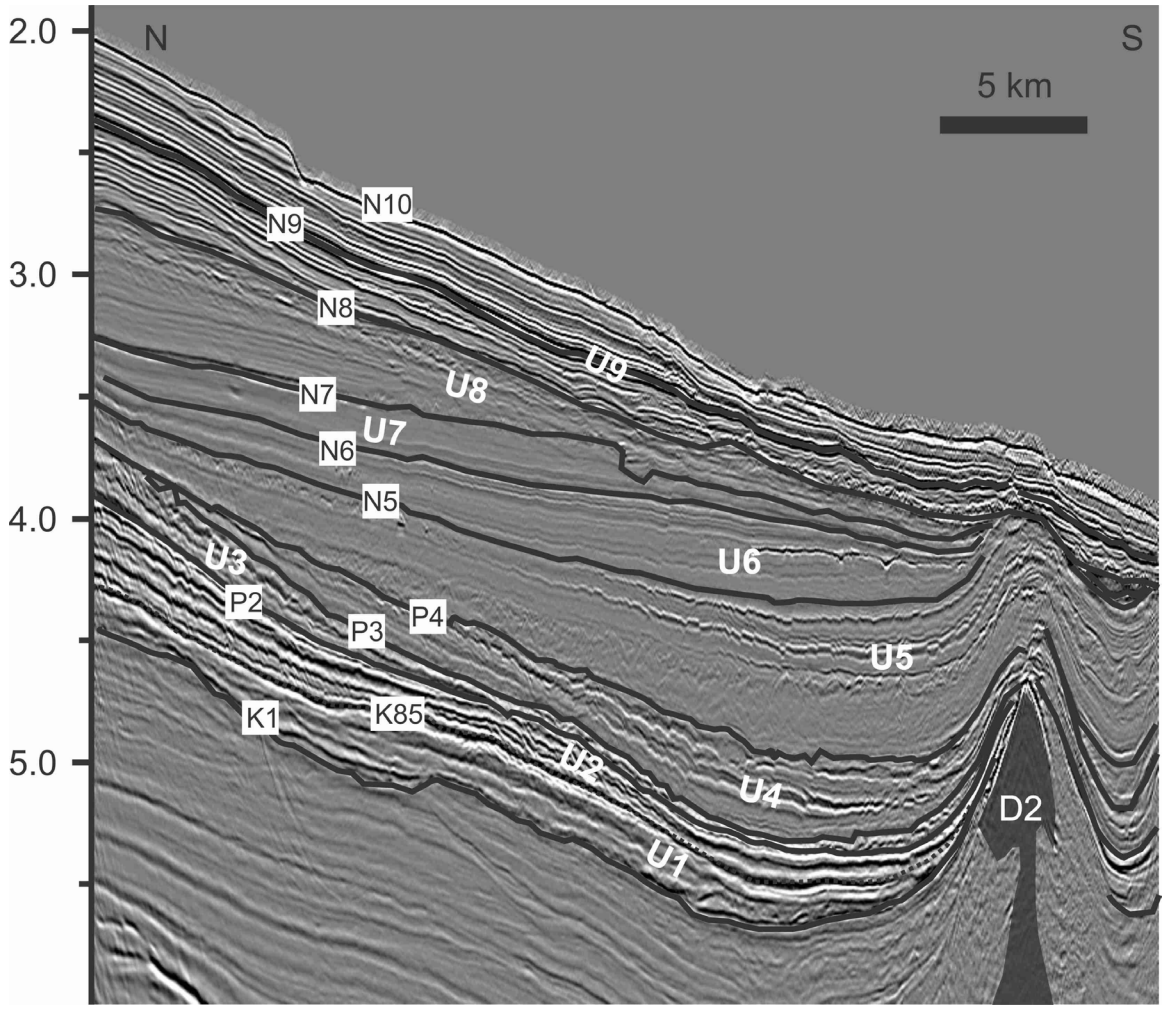

Figure 4.24: A representative dipline showing the 11 horizons and the subdivision of units. See Figure 4.9B for the location of this transect.

Unit 1: K1 to K85 (Cenomanian/Turonian-Coniacian/Santonian)

Unit 1 is bound below by the K1 and above by the K85 horizon (Figs. 4.25-4.26). The K1 marker is a medium to high amplitude negative reflection that truncates underlying parallel reflectors. This horizon is confined to intervening basins between salt bodies and salt tongues and corresponds closely to the K94 marker of OETR (2011) (Fig. 4.2). It is eventually truncated as it approaches the Upper Slope Slide Complex in the northeast of the study area (Fig. 4.27).

Deptuck and Campbell's (2012) K85 marker is a medium to high amplitude negative marker mapped in the western study area only. It is also truncated in the east/northeast by overlying reflections as it approaches the Upper Slope Slide Complex and salt tongues (Deptuck and Campbell 2012; Fig. 4.27).

Both the K1 and K85 horizons generally are truncated by or underlie vertical salt structures. In cases where the unit is part of a raft/carapace, it is densely faulted and often difficult to interpret. The K1 marker extends below both the A1 and A2 salt tongues i.e. below the *base salt* horizon indicating the distribution/seaward extent of the salt at K1 time. This marker is also present above the A2 salt diapir (and rafts/carapaces) likely indicating that it kept flowing across the seafloor after the K1 deposited (Figs. 4.10, 4.11 and 4.19).

The K1 and K85 markers are both erosive, and cut into underlying strata (Fig. 4.28). Between these markers, Unit 1 consists of generally low amplitude shingled truncated reflectors.

Generally, the unit thins towards the shelf-edge due to increased truncation by the younger canyon systems (Fig. 4.29). A thick in the northwest exceeding 300 ms is an area of increased incision of the K1 horizon into underlying strata (Fig. 4.28).

Unit 2: K85 to P2 (Coniacian/Santonian-Ypresian)

Unit 2 is bound below by the K85 and above by the P2 horizon (Fig. 4.30). The transition from units 1 to 2 marks a significant change between shingled low amplitudes to mounded high amplitude reflections (Fig. 4.31). The P2 Horizon corresponds to the T50 marker previously mapped by Deptuck and Campbell (2012) and the PFA (OETR 2011). Additionally, Unit 2 corresponds to Sub-unit 1a of Deptuck and Campbell (2012).

The P2 horizon is a high amplitude positive reflection that was mapped across most of the study area. In places where the marker merges with other horizons, it was difficult to correlate across. For example, along the axes of canyons where incision is the greatest, it merges with the K85 and other markers. Due to its strong positive amplitude, it was a relatively easy marker to map in the vertical salt diapir and allochthonous tongue province. Some challenges arose from reflections often merging and diverging in the area of the USSC, the incision of an Oligocene canyon system in the east and seafloor multiples from modern-day canyons around the upper slope (Fig. 4.27).

In both salt provinces, some areas show what appears to be 'onlap' of the P2 marker onto salt (See Figs. 4.27, diapirs P3, P6, M2, M5, D2, D7, D8 and A2). Closer inspection shows that the P2 marker (and horizons above it) are offset by faults with large (>200 ms) amounts of displacements such that the units on the downthrown section of the fault are in contact with the salt.

Paleocanyons intermittently cut through this interval. These paleocanyons are oriented in a north-south direction in plan view, and are preferentially eroded along the axes. Inter-canyon highs show up as thicker packages between canyon axes, in contrast to canyon axes that show up as thinner sediment packages (Figs. 4.28 and 4.32-4.33). Thickness maps show that the inter-canyon highs are elongated in the downslope direction (Fig. 4.32). Where it is best preserved, Unit 2 forms a wedge-shaped deposit that thins from a maximum of 500 ms (TWTT) on the upper slope (e.g. near the Shubenacadie H-100 well) to 300 ms (TWTT), 20 km down the slope. Profiles down the axes of these thick packages show that individual reflections on the upper parts of Unit 1 are high amplitude reflections, and are often offset by faults with less than 100 ms of

throw (Fig. 4.31). In cross section, these erosional remnants form inter-canyon highs (e.g. see figure 2.10; Deptuck and Campbell, 2012). Incision amounts generally vary between 100 to 200 ms between erosional remnants.

Since the K85 marker could not be mapped in the eastern study area, a thickness map between the K1 and P2 markers is used as a proxy to show the thickness distribution of Units 1 and 2 together (Fig. 4.33). As mentioned above, the K1 horizon extends below the salt tongue and the P2 marker drapes the tongue. As a result, the isochron map show an interval of exaggerated thickness due to the intervening salt between these horizons and repeated stratigraphic successions above and below the salt tongues (Fig. 4.34).

Rafts are present on the toe of the A2 salt tongue. This raft is part of a series of adjacent rafts trending north-south above the A2 salt tongue (Figs. 4.10 and 4.25). They consist of older (pre-K1) strata that were lifted and carried seaward above the salt tongue (Figs. 4.23 and 4.35).

Unit 3: P2 to P3 (Ypresian to Bartonian)

Unit 3 is bound below by the P2 and above by the P3 horizon (Fig. 4.36). The P3 horizon is a prominent unconformity with positive medium amplitude reflection. It is truncated in the east and northeast (upper slope) by the overlying P4 horizon that is erosive. Additionally, the horizon merges with the P2 surface along canyon axes. It corresponds to the T40 marker previously mapped by Deptuck and Campbell (2012).

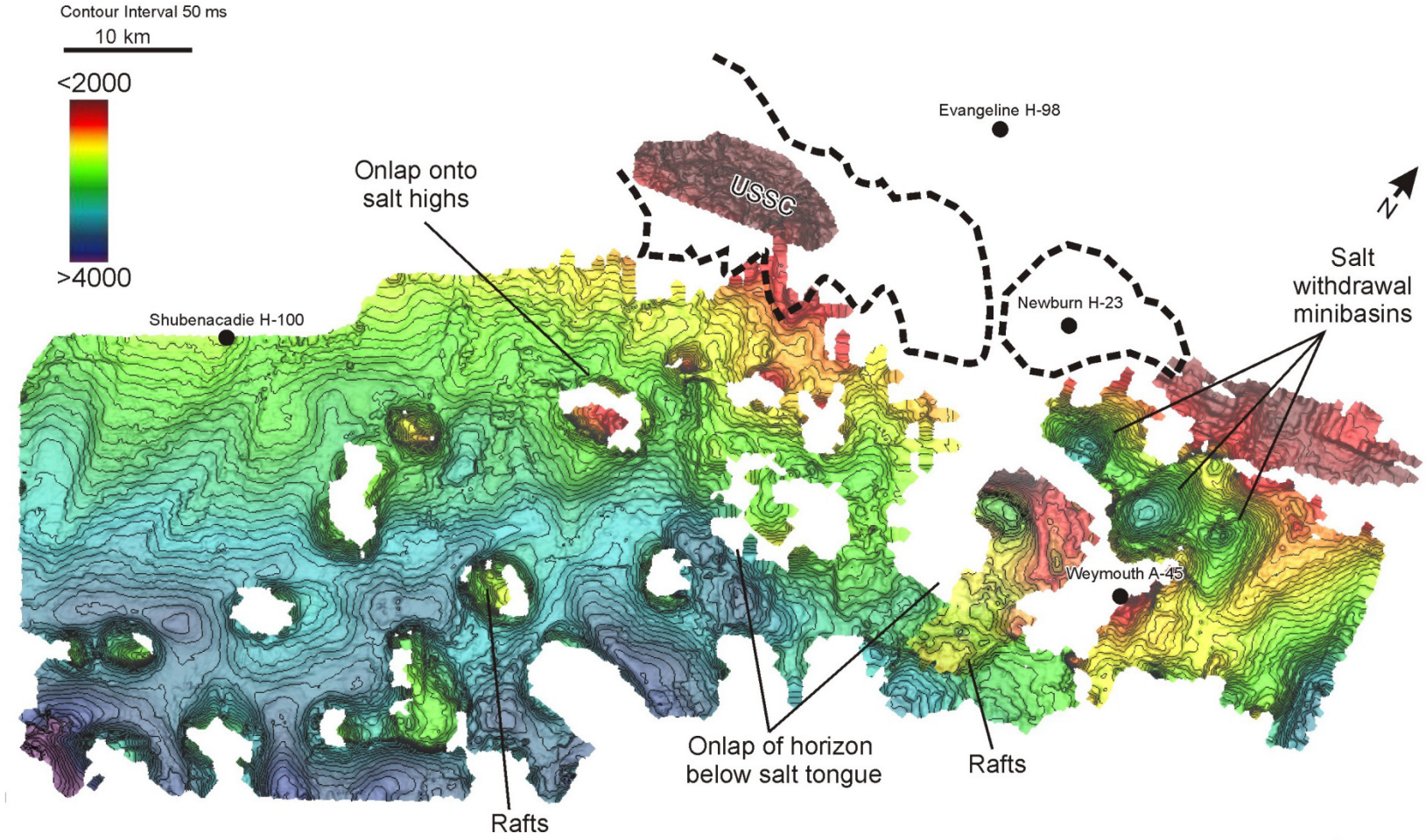

Figure 4.25: Time-structure of the K1 horizon. USSC = Upper Slope Slide Complex (see Deptuck and Campbell, 2012).

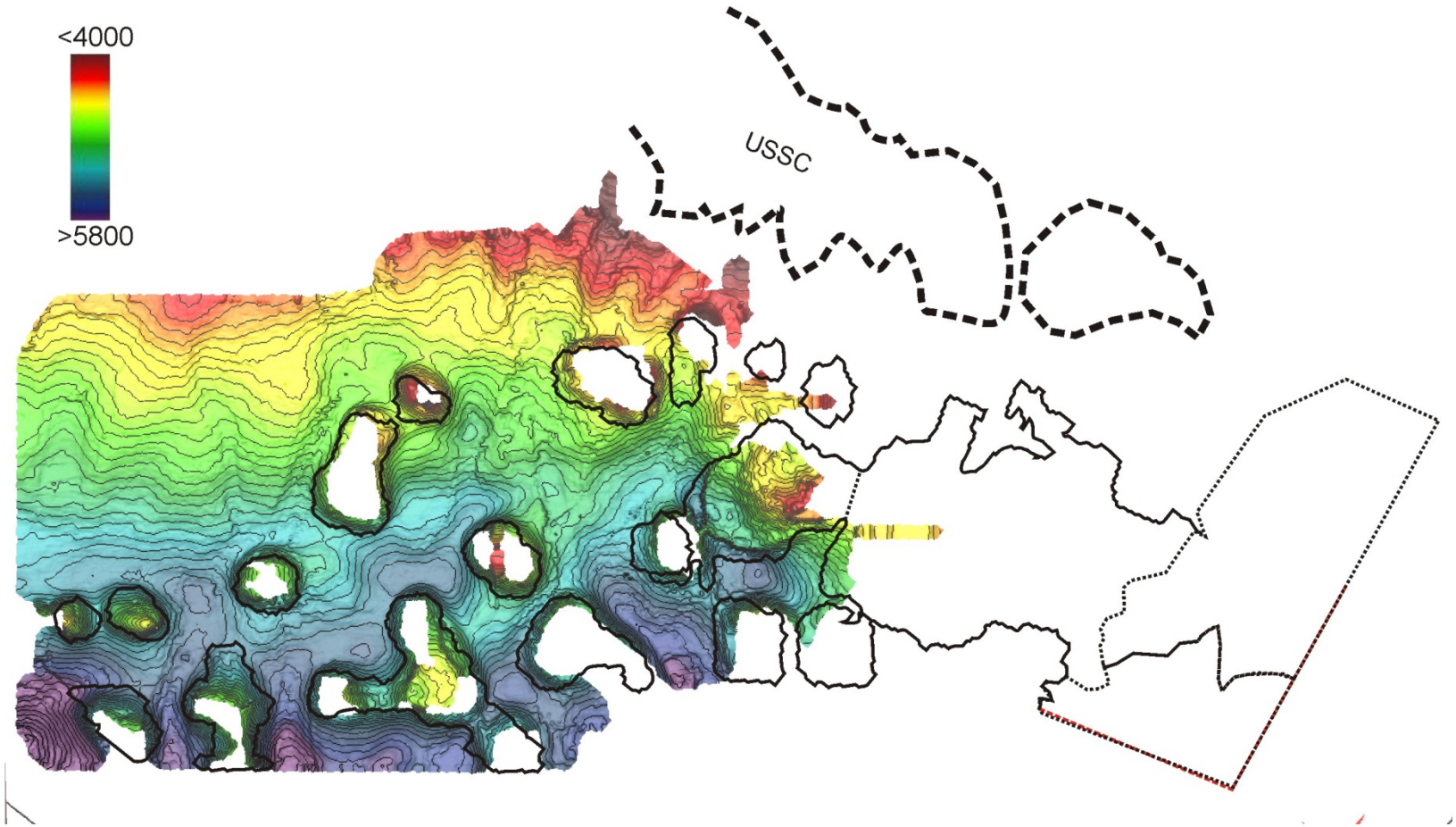

Figure 4.26: Time-structure of the K85 horizon mapped by Mark Deptuck (pers. comm. 2014). Salt structures are indicated with black outlines.

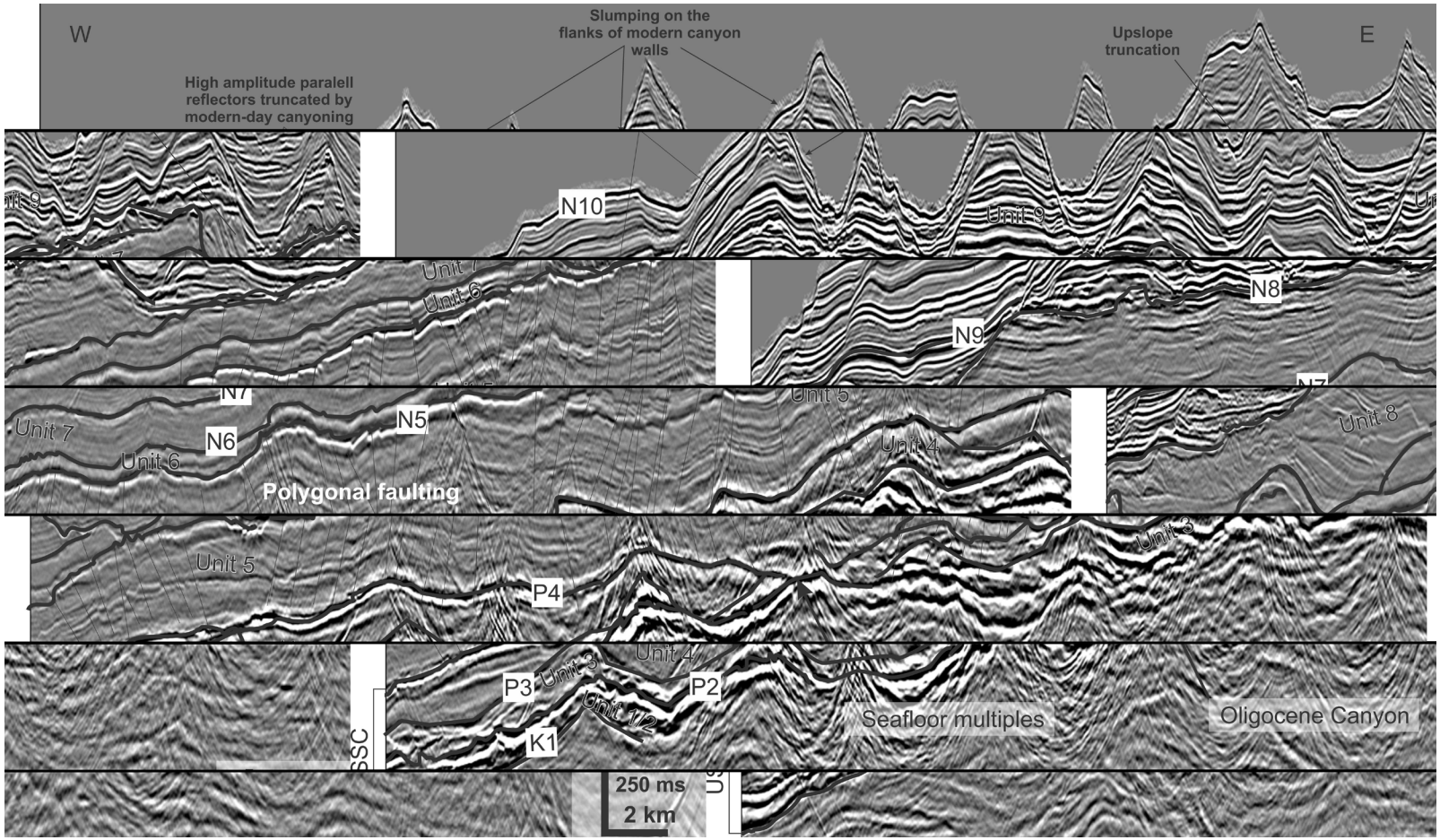

Figure 4.27: Seismic section showing the complexity of the *Upper Slope Slide Complex* (USSC) of Deptuck and Campbell (2012) as well as the seismic character in the upper slope area generally. See Figure 4.9B for the location of this transect.

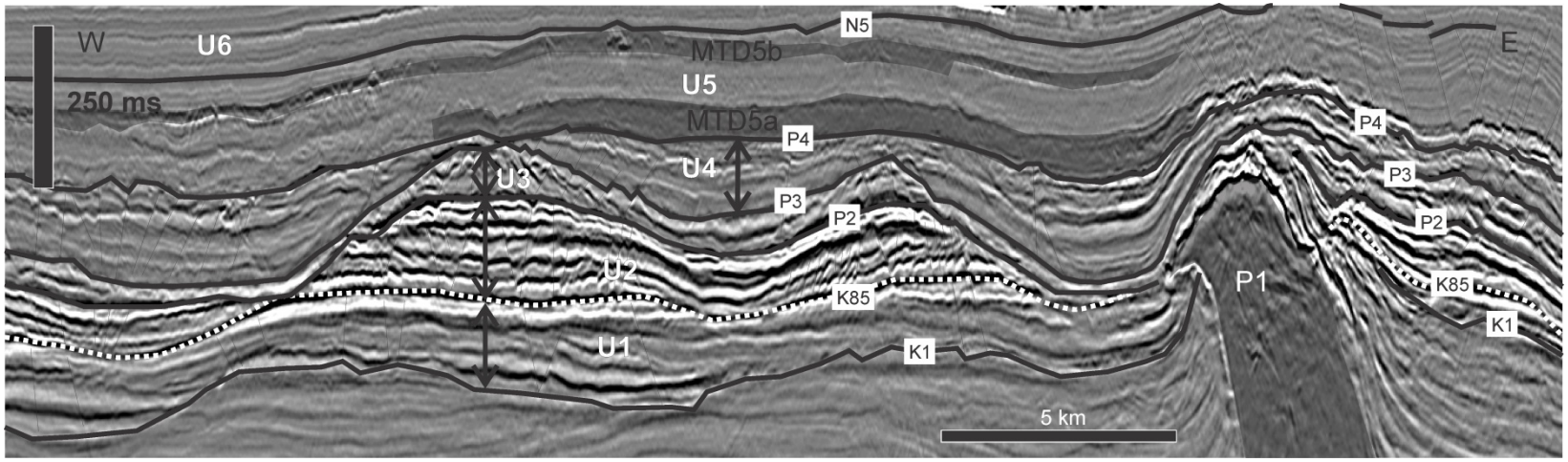

Figure 4.28: Canyons with multiple erosional events. Mapped horizons with preferential erosion along canyon axes are K85, P2 and P3. See Figure 4.10B for the location of this transect.

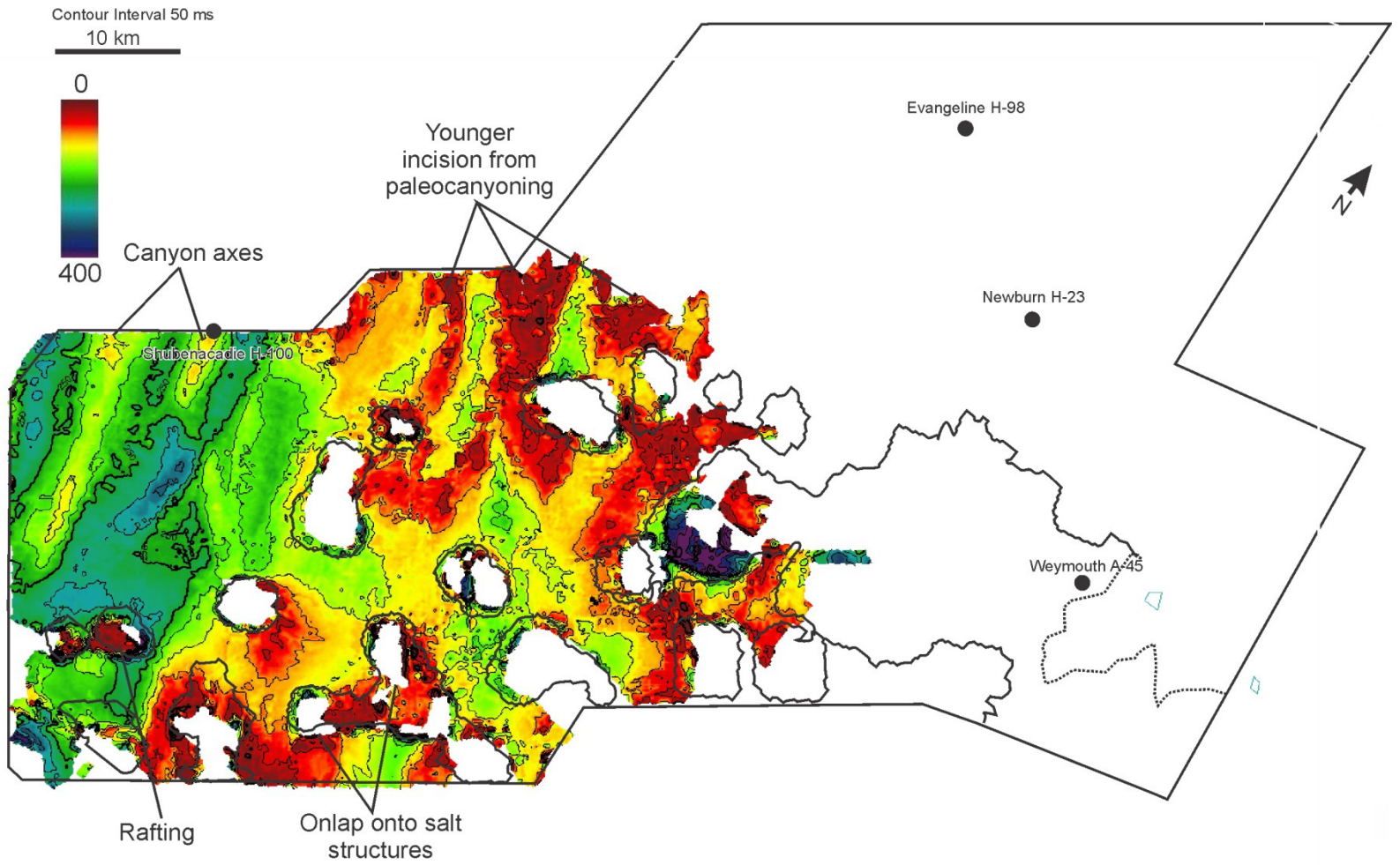

Figure 4.29: Isochron map of Unit 1 encompassing horizons K1 to K85 from the Cenomanian to the Coniacian/Santonian.

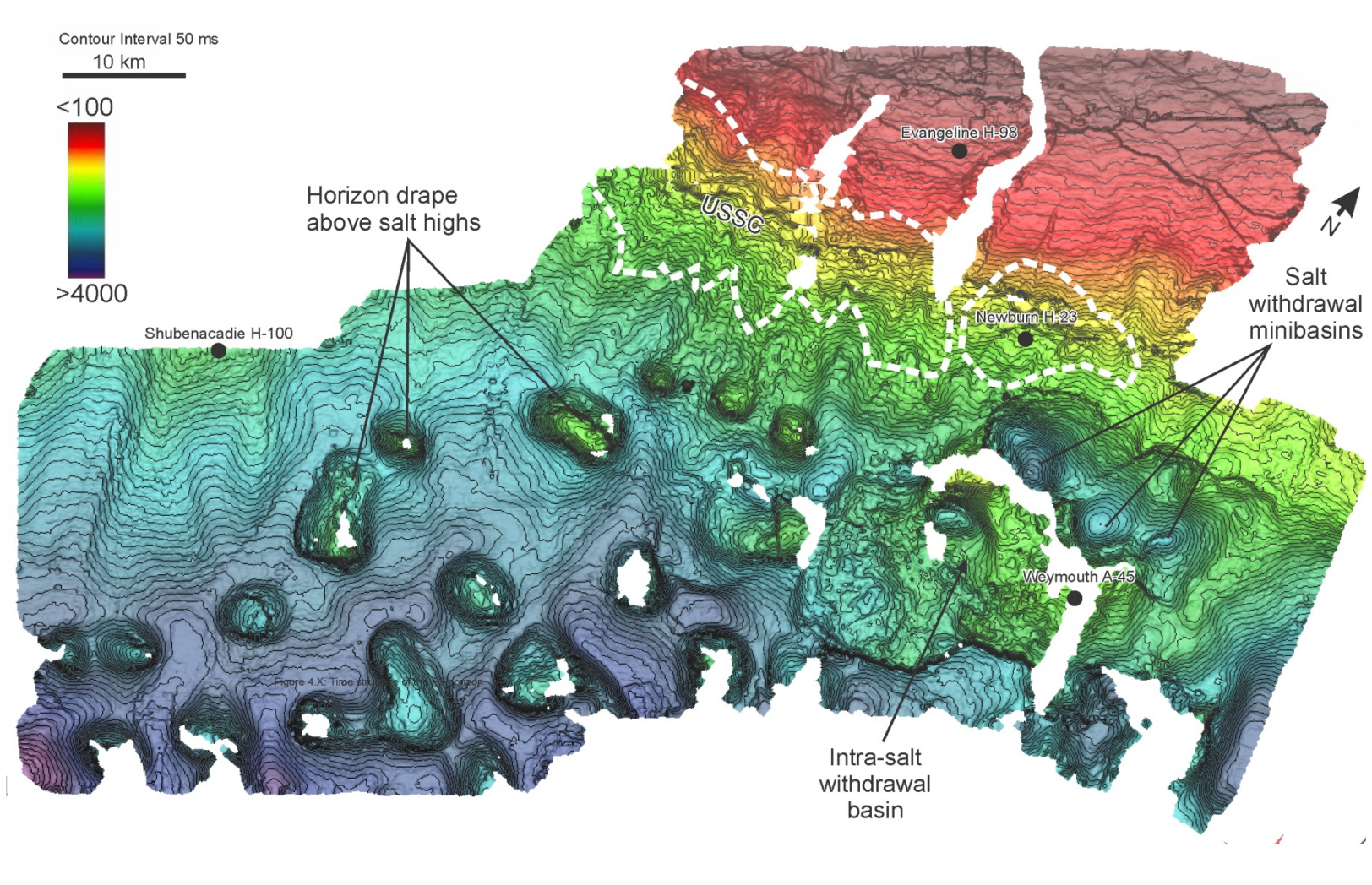

Figure 4.30: Time-structure of the P2 Horizon.

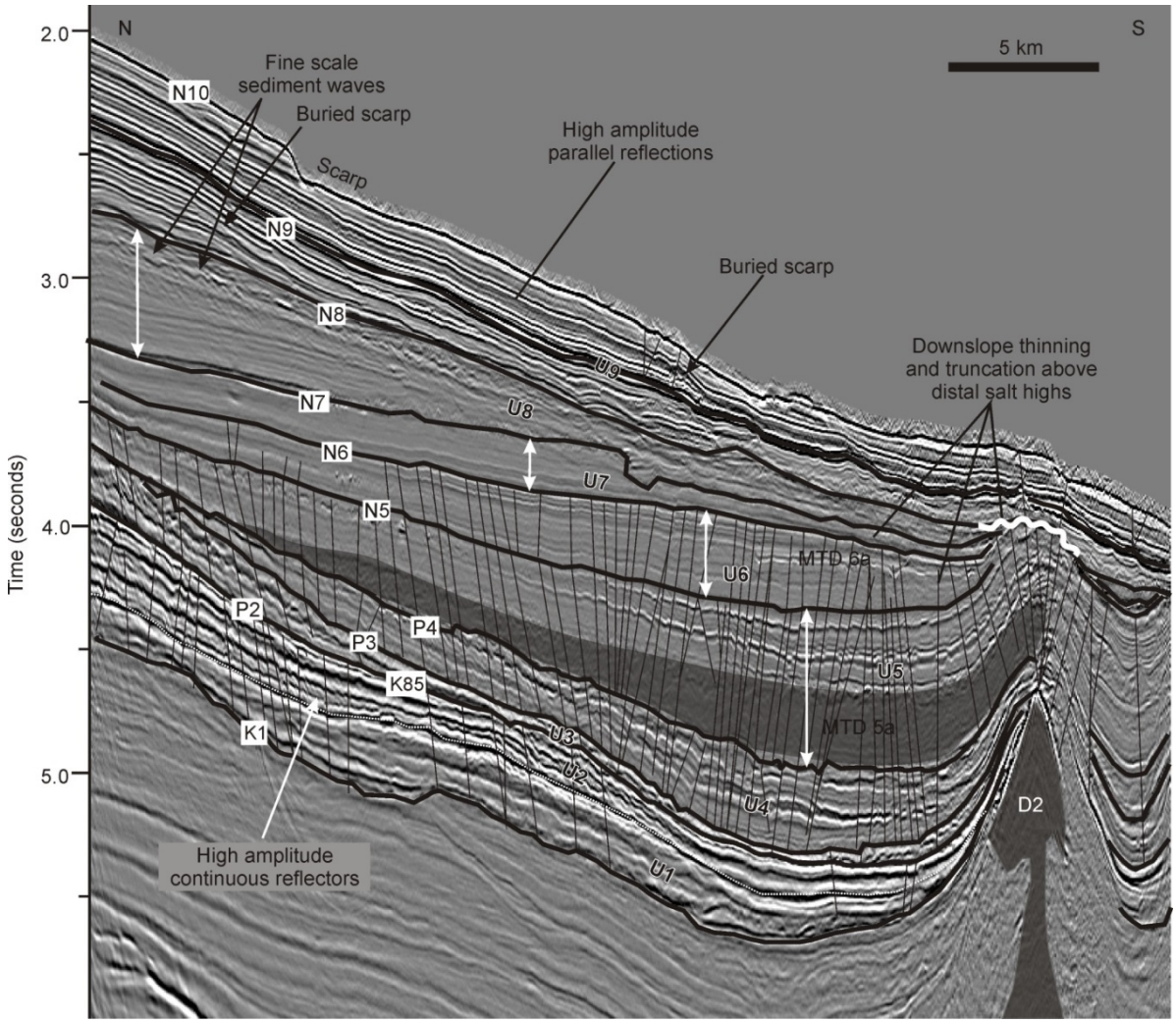

Figure 4.31: Dipline in the study area showing depositional thickness variations such as the landward shift in depocenters, crestal erosion along distal diapirs, downslope changes in MTDs 5a and 6a, dense polygonal faulting, and fine-scale sediment waves. See Figure 4.9B for the location of this transect.

Areas of truncation in the northeast (upper slope) coincide with the onset of the USSC where the P3 horizon is intermittently eroded away (Fig. 4.27). Incision from an Oligocene paleocanyon and deformation across the USSC also made it slightly difficult to tie the P3 marker to the shelf.

Units 2 and 3 contain multiple phases of canyon incision with horizons merging along canyon axes creating thin packages that are elongated in the downslope direction (Fig. 4.26). In the vertical salt diapir province, these bounding horizons (P2 and P3) merge along the canyon

axes where truncation is the most extensive (Fig. 4.28). The merging of these horizons is related to a re-incision event and these canyons appear to be mainly bypass surfaces with no related deposition of channel systems or levees (Fig. 4.28). Maximum thicknesses exceeding 450 ms (TWTT) are located along these inter-canyon highs in the west, thinning to less than 100 ms (TWTT) along canyon axis where incision is the greatest. Like Units 1 and 2, dip profiles taken along inter-canyon highs show that internal reflections are broken by small-scale faults but are otherwise continuous, thinning in the downslope direction (Fig. 4.31).

Canyons in the western section of the study area show minor depth variations above salt or diversion around salt (Fig. 4.35). This observation is discussed in more detail in section 2.6 (also see Deptuck and Campbell 2012). In plan view, these canyons are straight to gently curved and range from 8 to 10 km wide, merging and diverting around the allochthonous tongues in the east (Fig. 4.37).

Unit 4: P3 to P4 (Bartonian-Rupelian)

Unit 4 is bound below by the P3 horizon and above by the P4 horizon (Fig. 4.38). Although the amplitude varies widely throughout the survey, the P3 horizon generally consists of a low amplitude, positive reflection in the west changing to a medium amplitude reflection towards the upper slope and above salt bodies. The P4 marker is absent in areas with large fault offsets and in the northeast due to paleocanyon incision (Fig. 4.38). Due to its erosive nature and dense-polygonal faulting with small offsets (<100 ms), the horizon was difficult to map. Fault density is the greatest west of the P1 salt diapir, above vertical salt structures and on the upper slope (Figs. 4.27, 4.31 and 4.34).

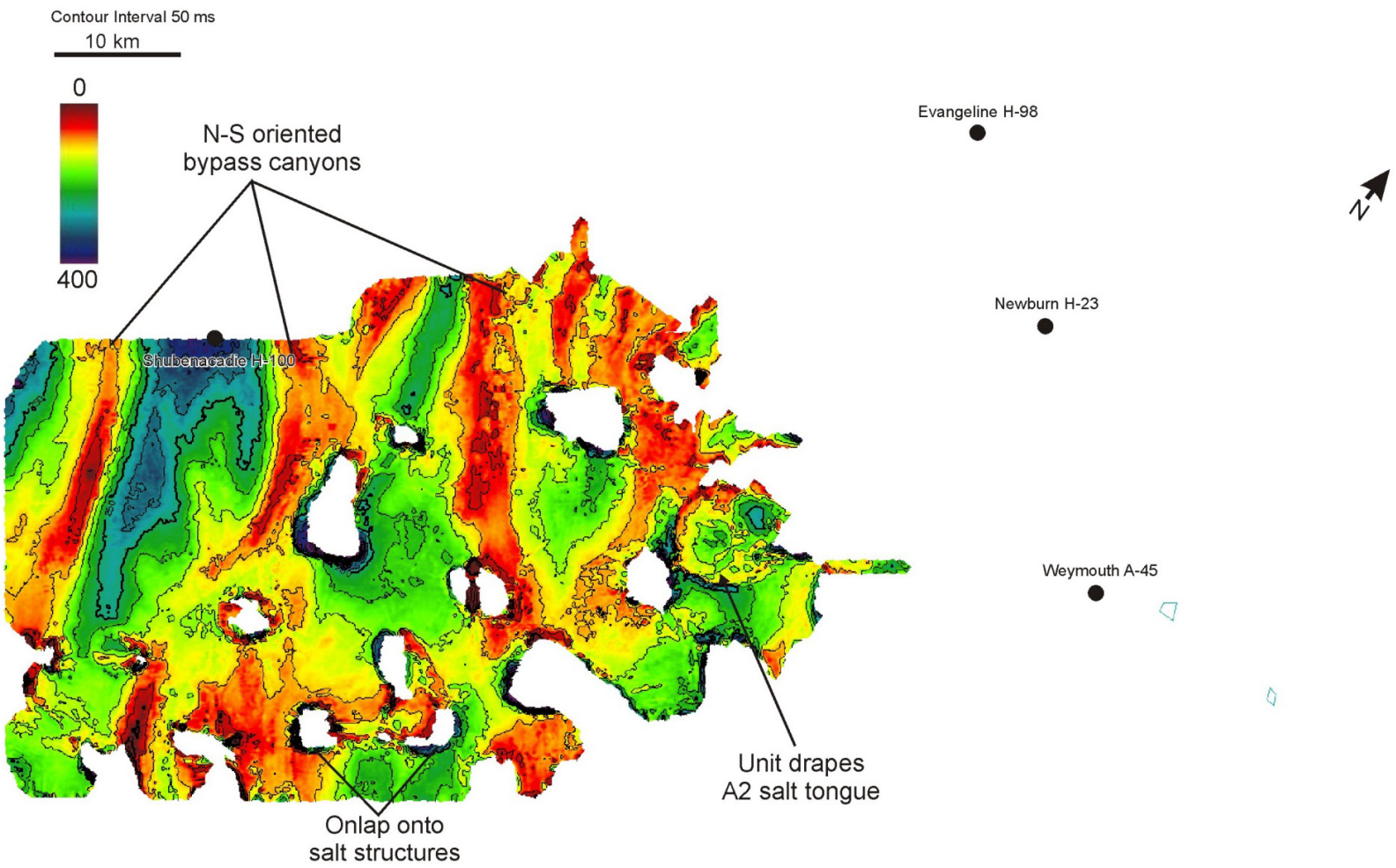

Figure 4.32: Isochron map of Unit 2 encompassing horizons K85 to P2 from the Santonian to the Ypresian.

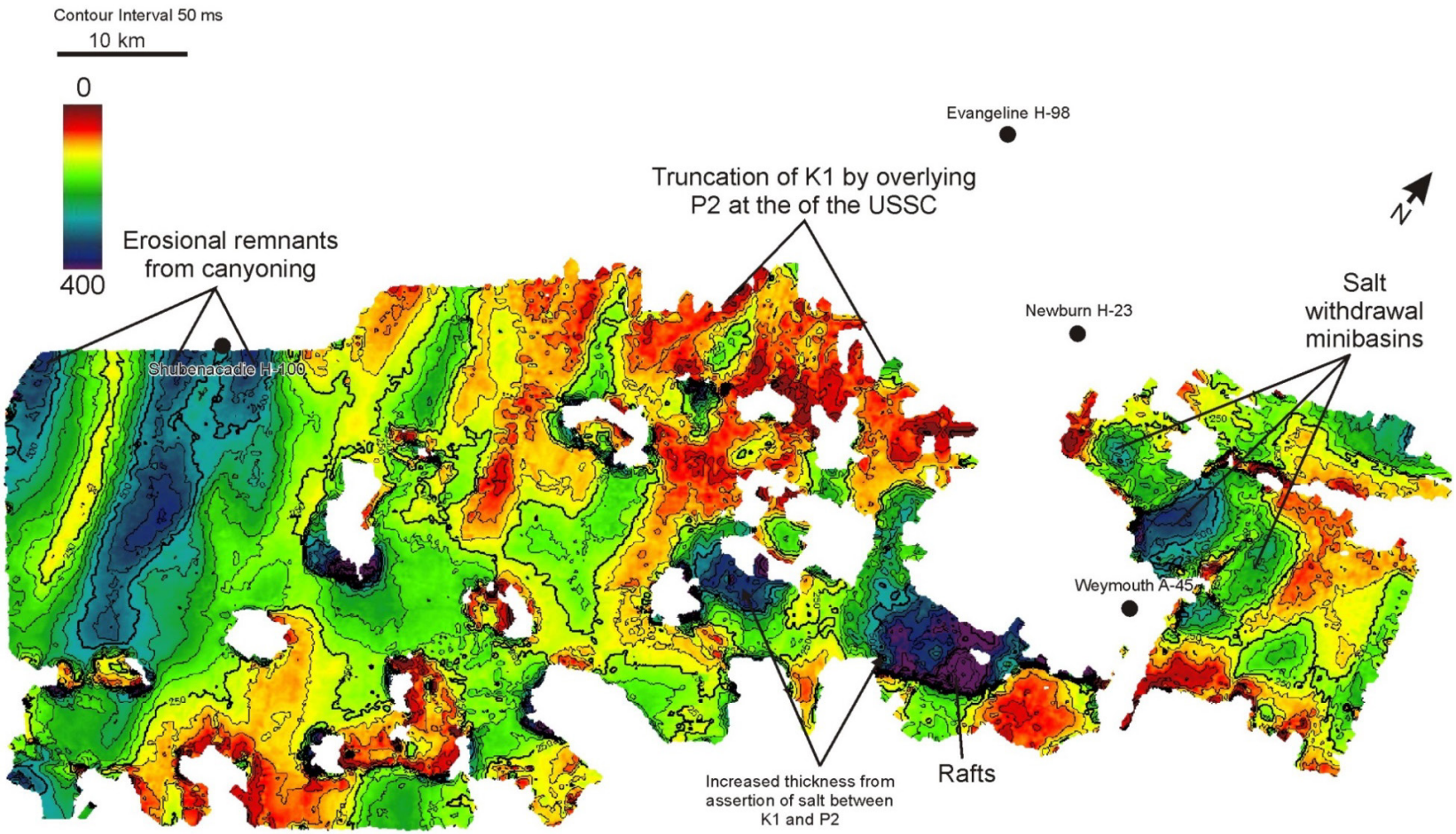

Figure 4.33: Compilation isochron of Units 1 and 2 (i.e. K1 to P2; Cenomanian to Ypresian).transect.

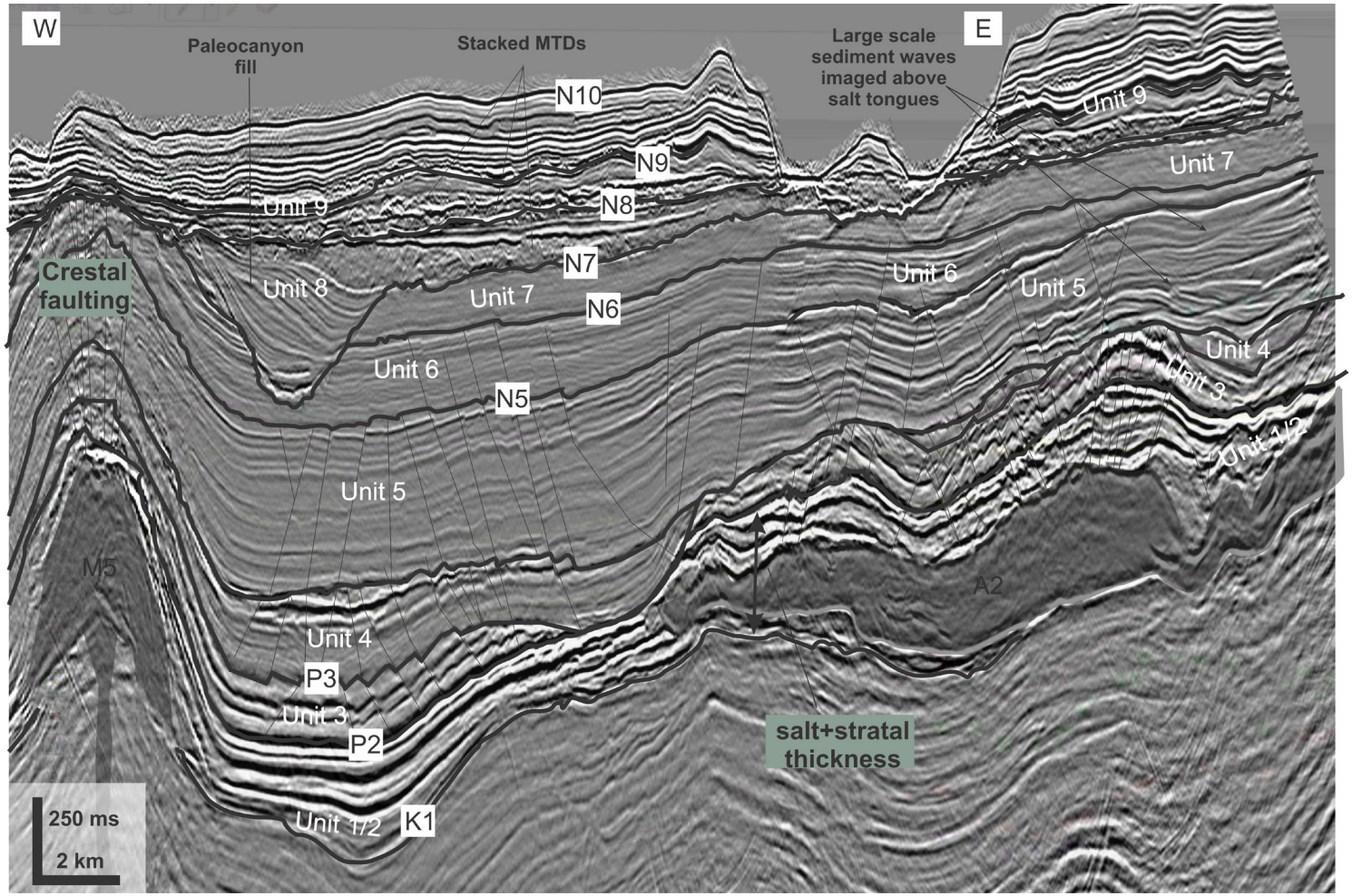

Figure 4.34: This figure shows the anomalous thickness introduced in the merged isochron of units 1 and 2 due to the presence of allochthonous salt between horizons K1 and P2 (labelled "salt + stratal thickness"). Also note the dense crestal faulting, stacked MTDs above a Miocene paleocanyon and sediment waves above the A2 salt tongue. Signifnicant the stratal thinning occurs in Unit 6 above the salt tongue. See Figure 4.9B for the location of this transect.

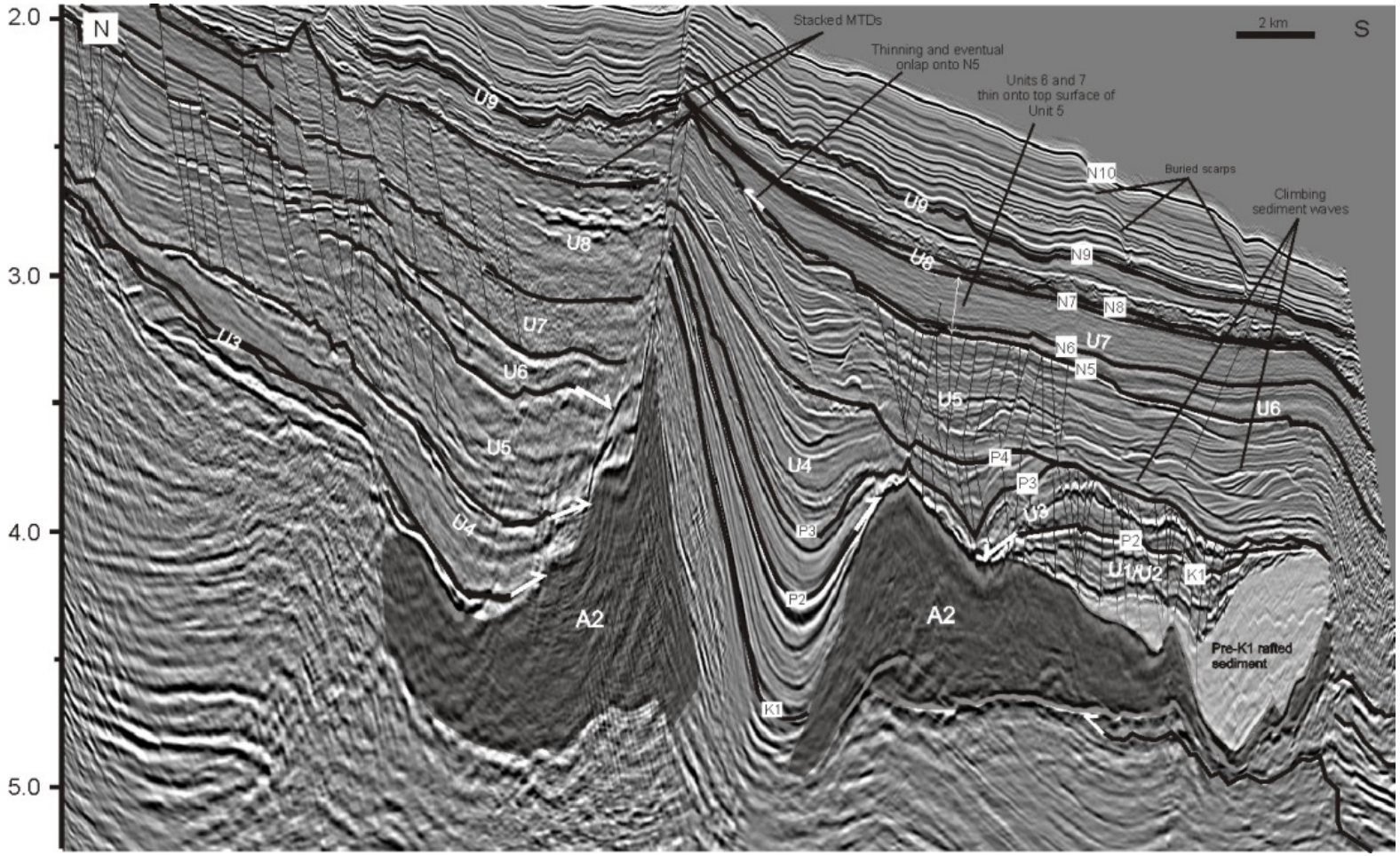

Figure 4.35: Seismic cross section showing the large raft present at the toe of the A2 salt diapir, stratal thinning of units 6, 7 and 8 above salt highs, sediment waves above the salt tongue, ponding of MTDs on the downthrown side of the growth fault (bounding minibasin B3 on the upslope side) and a large withdrawal basin located centrally in A2. Note the onlap of the P2 horizon onto the A2 salt tongue (marked with white arrows on right). See Figure 4.9B for the location of this transect.

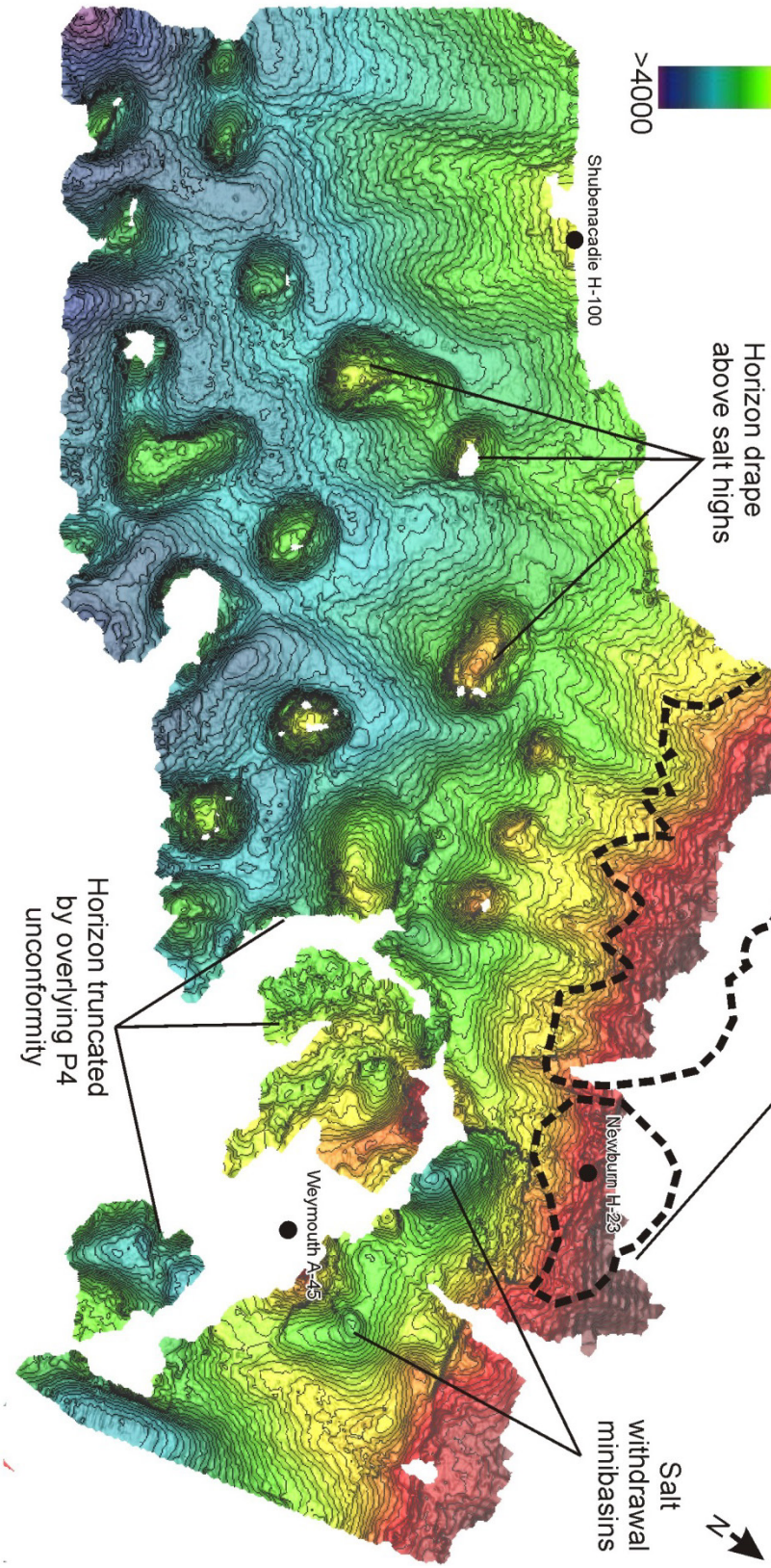

Figure 4.36: Time-structure map of the P3 Horizon.

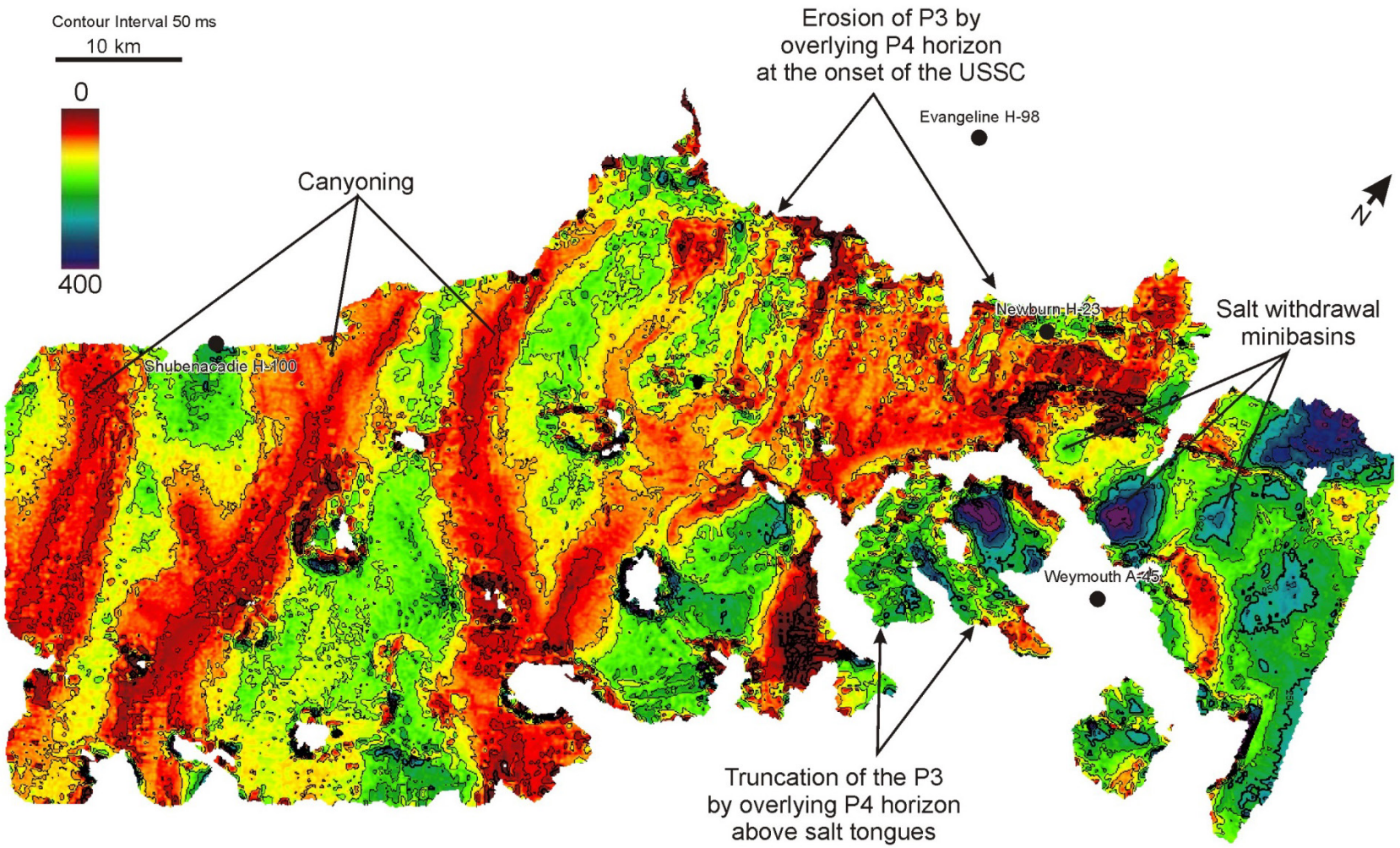

Figure 4.37: Isochron map of Unit 3 encompassing horizons P2 to P3 from the Ypresian to the Bartonian.

Unit 4 consists of generally low amplitude, transparent reflections (Fig. 4.28). It is at least partly co-eval with the Late Eocene mud-belt described by Deptuck and Campbell (2012).

The thickest parts of Unit 4 correspond to the thinnest parts of both Units 2 and 3. As such, there is generally an inverse relationship with respect to preserved sediment thickness (Figs. 4.28, 4.37 and 4.39). Thinning is also evident in the east above the salt tongues where this unit becomes increasingly deformed. In the west, Unit 4 often thins above salt highs ("crestal thinning") in the vertical salt diapir province, notably different to observations in prior units.

Two paleocanyon systems are resolvable in the western section of the study area (Fig. 4.39). These canyons are bypass surfaces in cross section with a maximum incision of approximately 500 ms. In plan view they are linear and less than 5 km wide.

The easternmost canyon intersects a salt high in the allochthonous tongue province. Over the high, the canyon's erosional base structurally inverts changing from a typical concave-upwards profile to straight (Fig. 4.40). The inversion here clearly took place after the canyon was incised and filled and took place in response to the upward movement of underlying salt in post-P4 marker times. The western-most canyon is located northeast of A2 (north of A1), and becomes increasingly difficult to resolve downslope (south of A1). As such, the canyon, and its later inversion, provides a constraint on the timing of active diapirism (Fig. 4.40).

Unit 4 contains one resolvable MTD around the top of Unit 4 (MTD 4a; Figs. 4.41 and 4.42). This deposit is confined to the southwestern half of the study area. In cross section, it has transparent acoustic character with a strong negative reflection and erosion at its base. The MTD generally thickens downslope towards distal diapirs until it encounters a small step (<100 ms) in

the paleoslope that it thins above and eventually tapers. It has an erosional base and extends throughout the southwestern part of the study area between salt diapirs.

When taking a coherence slice through the upper half of Unit 4, a small submarine channel is visible in the western-most portion of the study area (Fig. 4.43). It is also located less than 100 ms under a large unconformity (P4 horizon) in a densely faulted area. The submarine channel belt has a maximum width of approximately 550 m and is sinuous in plan view with meander bends. The channel appears to divert westward downslope around the M1 salt structure. It consists of several channel complexes with multiple incision events. In cross section, the channel was difficult to resolve because of its small scale (<50 ms incision), sinuous nature and dense faulting in the area. Channels show up as small discontinuous reflections (resembling a seismic character similar to a blocky MTD, but with a clearly different planform geometry).

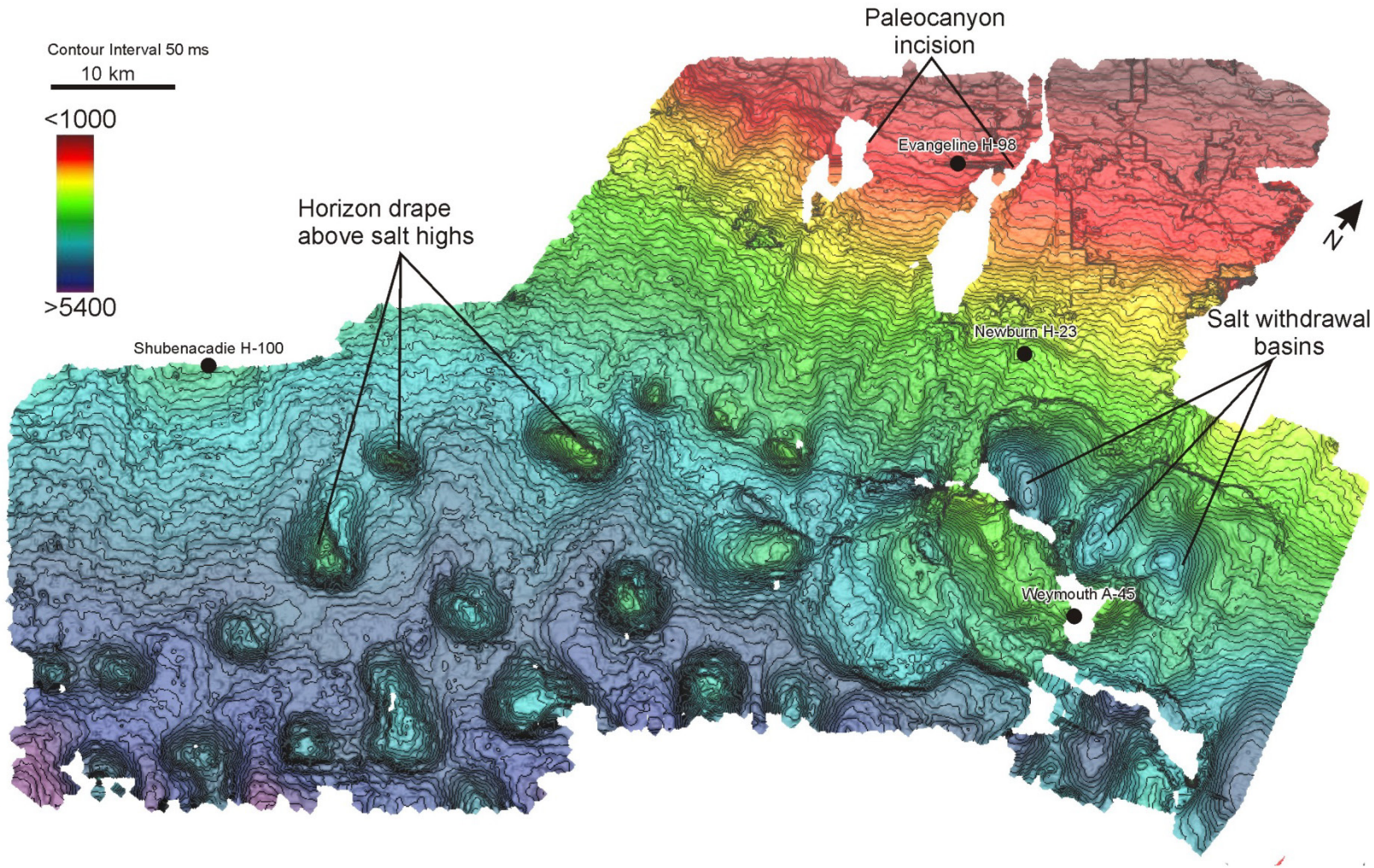

Figure 4.38: Time-structure map of the P4 Horizon.

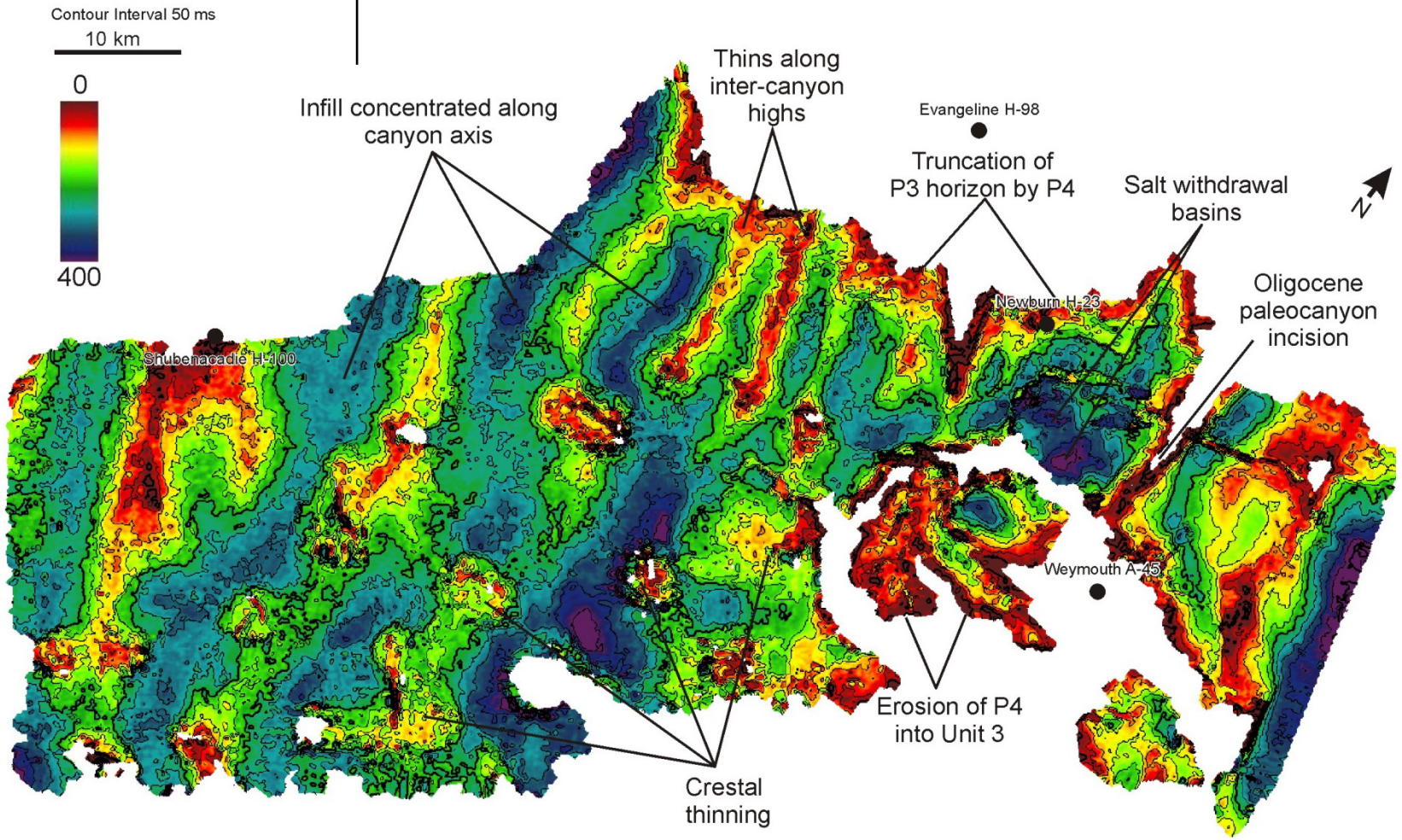

Figure 4.39: Isochron map of Unit 4.

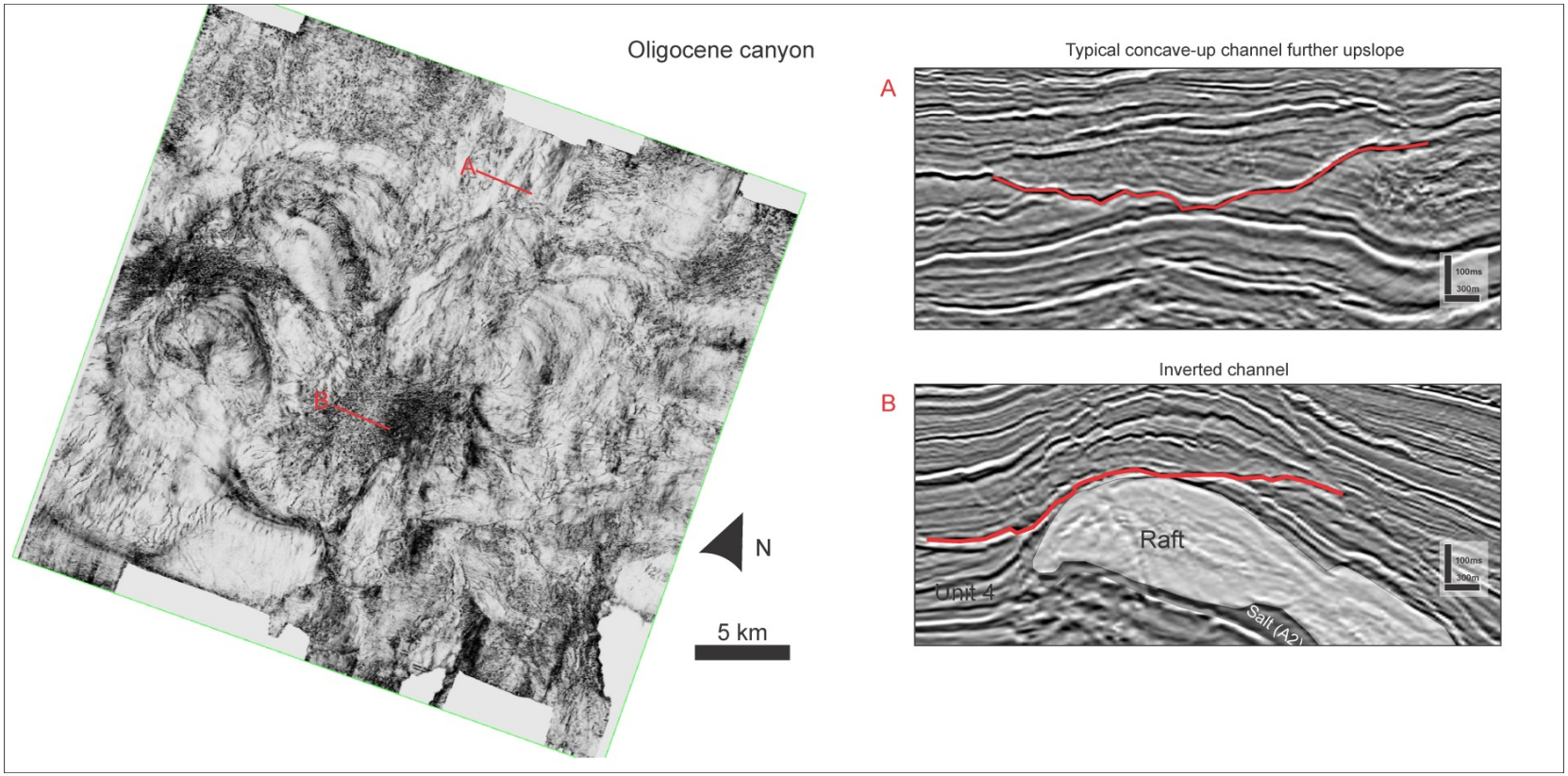

Figure 4.40: Coherence slice taken through the (mapped) canyon axis in the Weymouth survey (left). Profiles A and B (right) show the downslope change in the channel structure from concave-up to planar above the eastern-most A2 salt high.

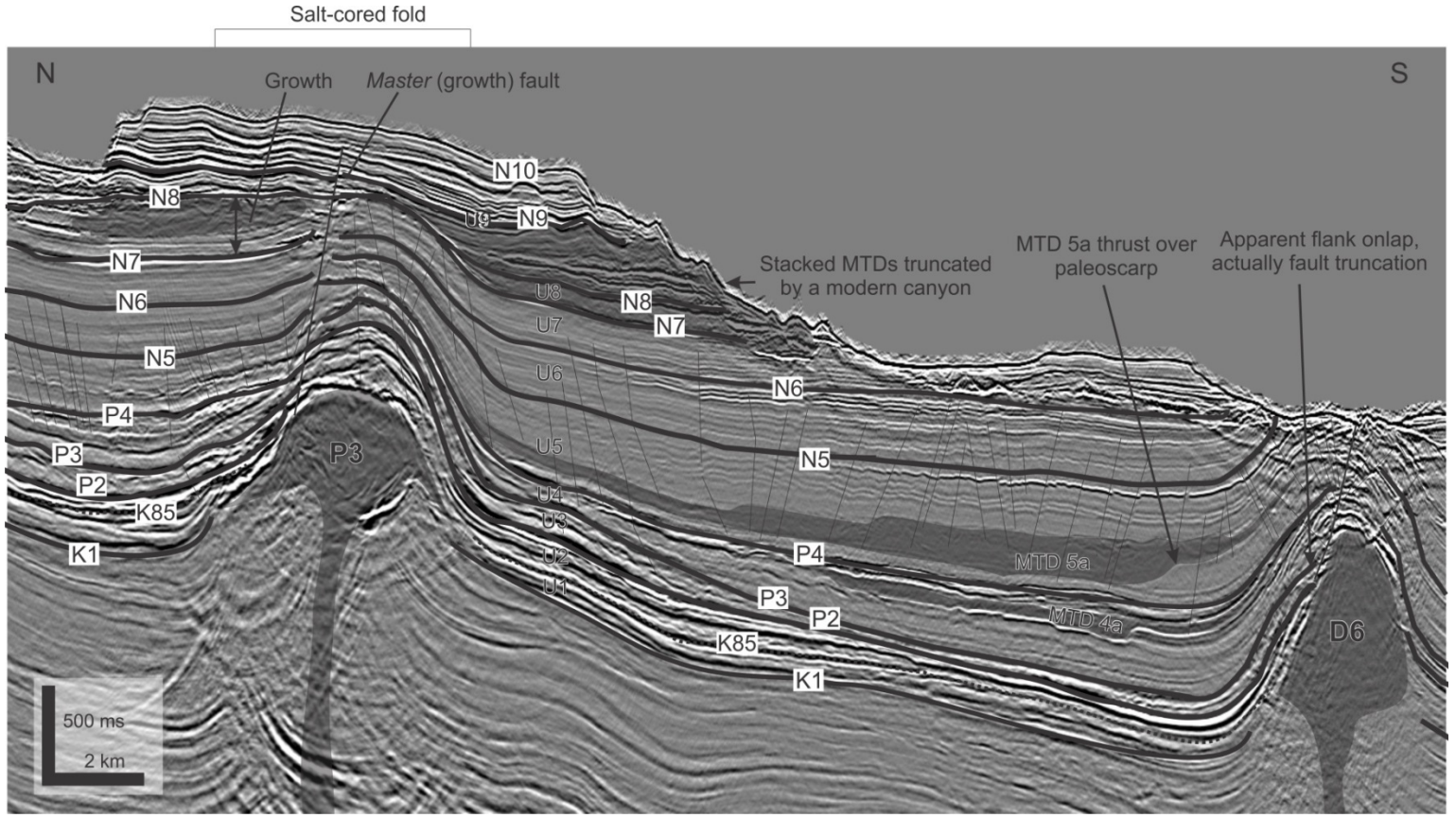

Figure 4.41: Cross section of a salt-cored fold (P3 salt diapir) and downslope truncation by a modern canyon system eroding into the D6 salt high. Note the strong negative reflection from the erosive base on MTD 4a and the less distinct base of MTD 5a. See Figure 4.10B for the location of this transect.

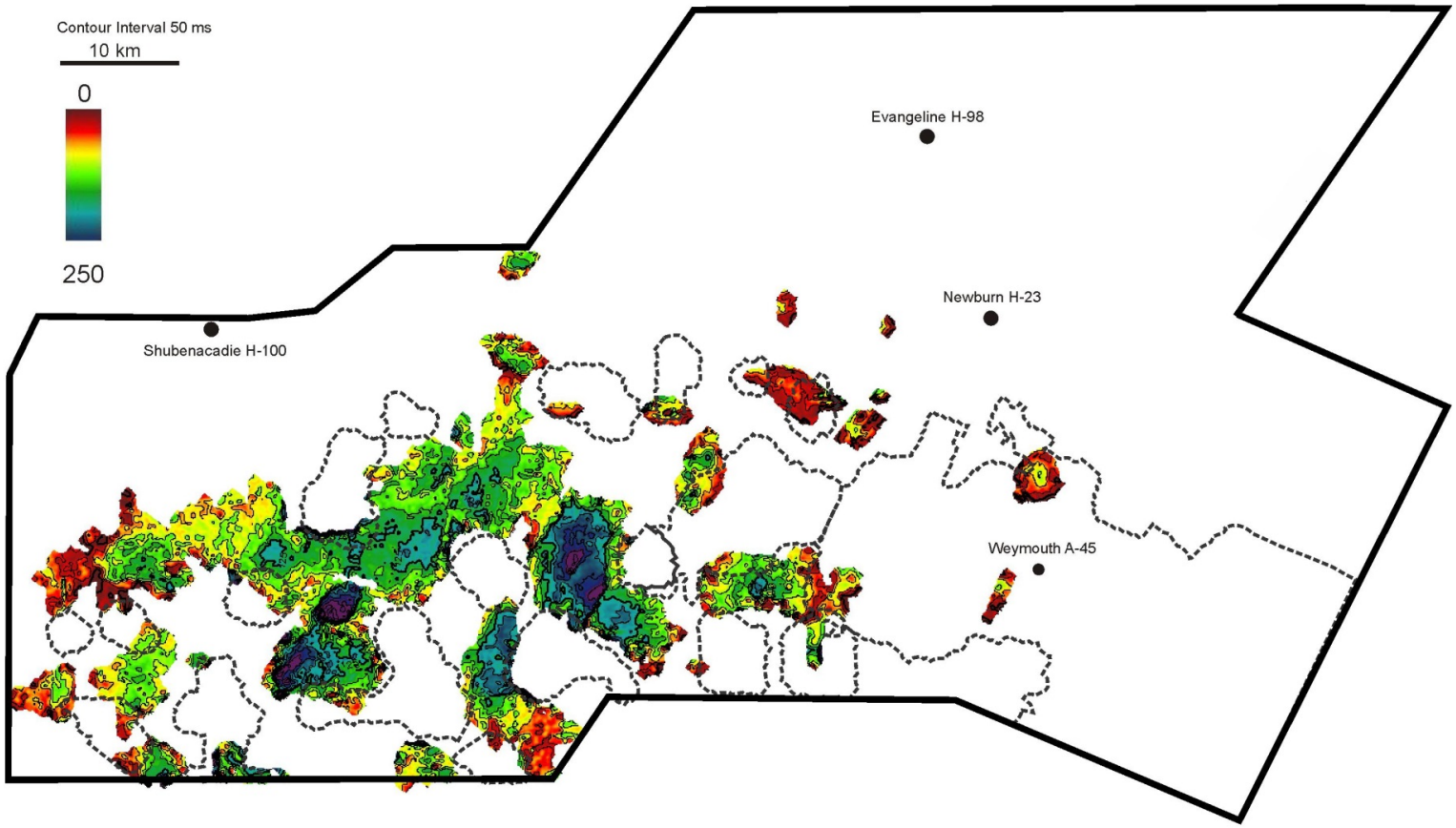

Figure 4.42: Isochron map of MTD 4a distribution in the study area. This is the first mass transport deposit in the study interval. It appears to have preferentially accumulated between salt bodies (in withdrawal basins) where it is the thickest, probably indicating that salt was a topographic high during this time.

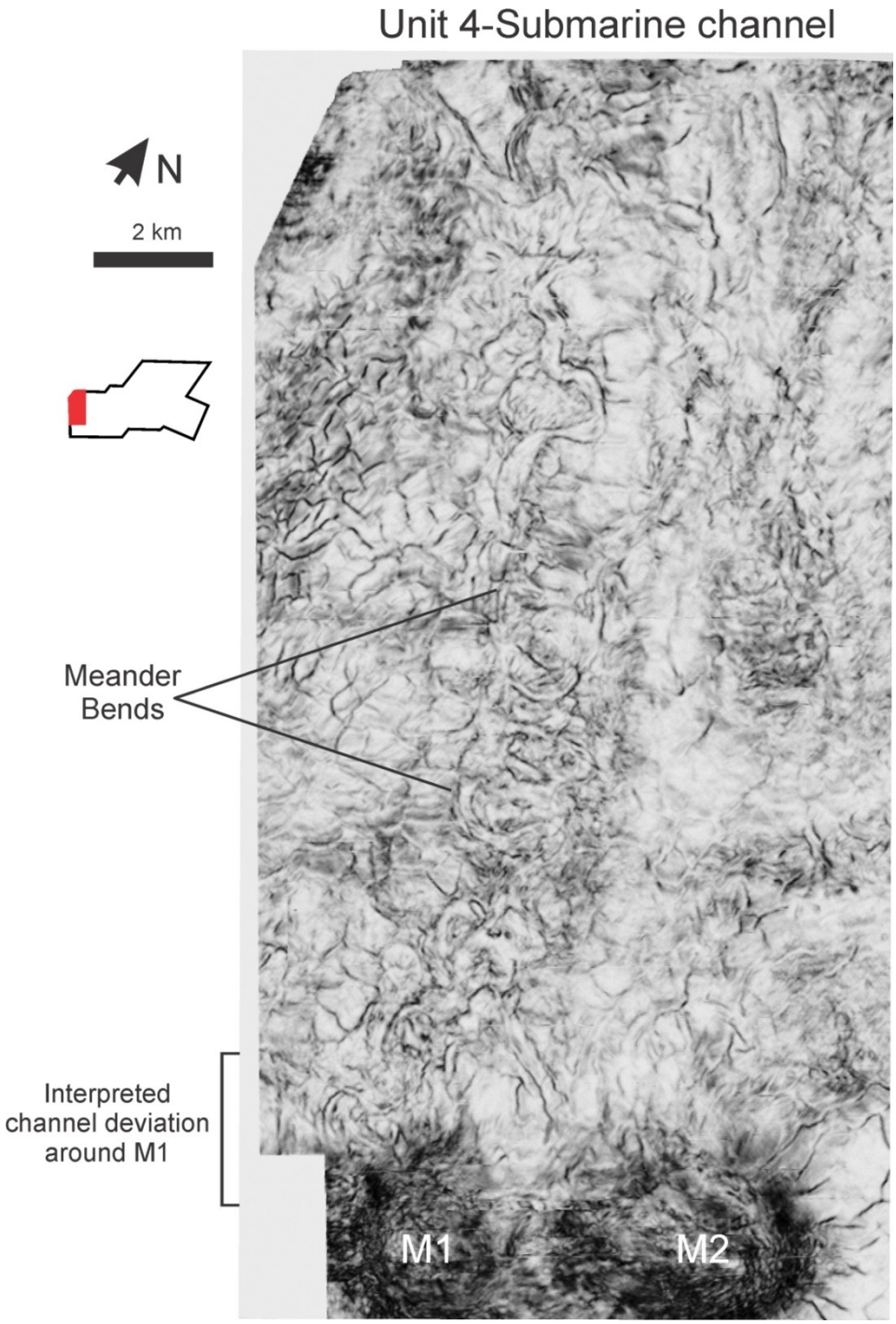

Figure 4.43: A coherence slice of a small, meandering submarine channel system taken 32 ms below the P4 Horizon (Unit 4). The channel appears to divert westward around the M1 diapir downslope. The dense fault pattern surrounding the channel made it difficult to resolve in seismic.

Unit 5: P4-N5 (Rupelian-Tortonian)

Unit 5 is bound below by the P4 Horizon and above by the N5 Horizon (Fig. 4.44). The N5 horizon is a medium-amplitude positive reflection in the east transitioning to a low amplitude reflection in the vertical salt diapir province (west). The horizon is absent in areas with large growth fault offsets, as well as areas with localized erosion above the southwestern *distal* salt crests, incision from a large Miocene paleocanyon or increased erosion while approaching the shelf-edge.

In the western study area, the unit is composed of two distinctive acoustic packages. The lower package is a thick (>400 ms), low amplitude, transparent MTD (MTD 5a-described further below; Fig. 4.31). The upper section of this unit consists of a series of concordant reflections with medium to high amplitudes (Fig. 4.31).

As the unit changes into the allochthonous salt diapir province in the east, it changes to a medium or high amplitude package with large (>5 km in length) sigmoidal climbing bedforms above both salt tongues that resemble sediment waves previously noticed by MacDonald (2006), Campbell (2011), and Campbell and Deptuck (2012) (Figs. 4.34 and 4.35). They are stacked ontop of each other with erosional bases. These bedforms are oriented in a northwest-southeast direction and offset by small scale (<100 ms) faults.

Unit 5 changes in stratal thickening across the study area. In the western study area, the unit thickens seaward. A thick sediment package above the USSC (Fig. 4.27) is located on the upper slope and in the allochthonous tongue province. There are also three linked depocenters in the salt withdrawal basins landward of A2 (Fig. 4.45). Infill from the two canyon systems in Unit 4 are easily resolvable as thick packages in Unit 5 (Fig. 4.45). Thin areas are mostly visible above salt diapirs in the northern-most part of the western study area and approaching the shelf edge (northeast).

There are two MTDs (MTD 5a and 5b) within Unit 5. MTD 5a is the largest MTD in the study area and the lower of the two MTDs in this unit (Figs. 4.31, 4.46A). It is best developed in the southern portion of the vertical salt diapir province (south of the proximal diapirs; Figs. 4.46A), thickening seaward to a maximum of ~300 ms downslope. These thick depocenters are confined to minibasins where it appears to have preferentially deposited between salt. It is thickest (>250 ms) between the P3, P4 and M3 diapirs thinning above the flanks of these diapirs.

In cross section, MTD 5a has low amplitudes containing transparent to chaotic fill with a negative amplitude erosional base reflection. The MTD is thrust over a large (>100 ms) paleo-scarp near the D6 salt body (Fig. 4.40). Fill contains large blocks in some cases greater than 50 ms thick in vertical dimensions and >200 m in horizontal dimensions. Crestal thinning above salt diapirs can often be difficult to resolve in comparison to the lateral depositional tapering of the deposit, however, the MTD does appear to show relatively uniform thickness variations between the flanks and crests of diapirs. The amount of thinning does appear to vary from diapir to diapir and some salt structures show more dramatic thinning than others. MTD 5a is thickest between diapirs P1 and D3 and makes up at least 30% of Unit 5 thickness.

MTD 5b extends over the edge of the Thrumcap survey in the east (east of P1) and generally thickens downslope (Fig. 4.46B) The MTD changes from a high amplitude reflection to a low amplitude reflection westward (Figs. 4.47 and 4.48). The MTD has a strong negative, erosive base changing to a lower amplitude south and westward where it has overlapped over a small (<50 ms) paleo-scarp near P1 (Figs. 4.47 and 4.48). The top of the MTD generally has a high positive amplitude reflection that changes to a low amplitude reflection in the west. Fill is generally chaotic and contains large (upwards of 150 m wide and 75 ms thick) blocks that are mostly scattered in the eastern-most part of the MTD where amplitudes are the highest.

Unit 6: N5 to N6 (Tortonian)

Unit 6 is bound below by the N5 and above by the N6 horizon (Fig. 4.49). The N6 horizon is absent above distal diapir crests, areas with large growth faulting, and where it onlaps the N5 horizon above the A2 salt tongue and on the upper slope. The N6 marker has low amplitudes in the vertical salt diapir province changing to medium amplitudes above salt tongues in east and approaching the shelf-edge.

The unit generally consists of parallel, low amplitude reflections in the western study area, passing into slightly brighter amplitude reflections above salt tongues and in the upslope direction. It contains one MTD (6a) confined to the middle portion of the vertical salt diapir province where it is thickest (Figs. 4.50 and 4.51). MTD 6a appears to intersect and overlap the P1 and P2 salt structures indicating that these salt structures were not a topographic high during this time. In seismic section, fill is generally chaotic with large blocks (>300 m x 50 ms) that have high amplitudes (Fig. 4.48).

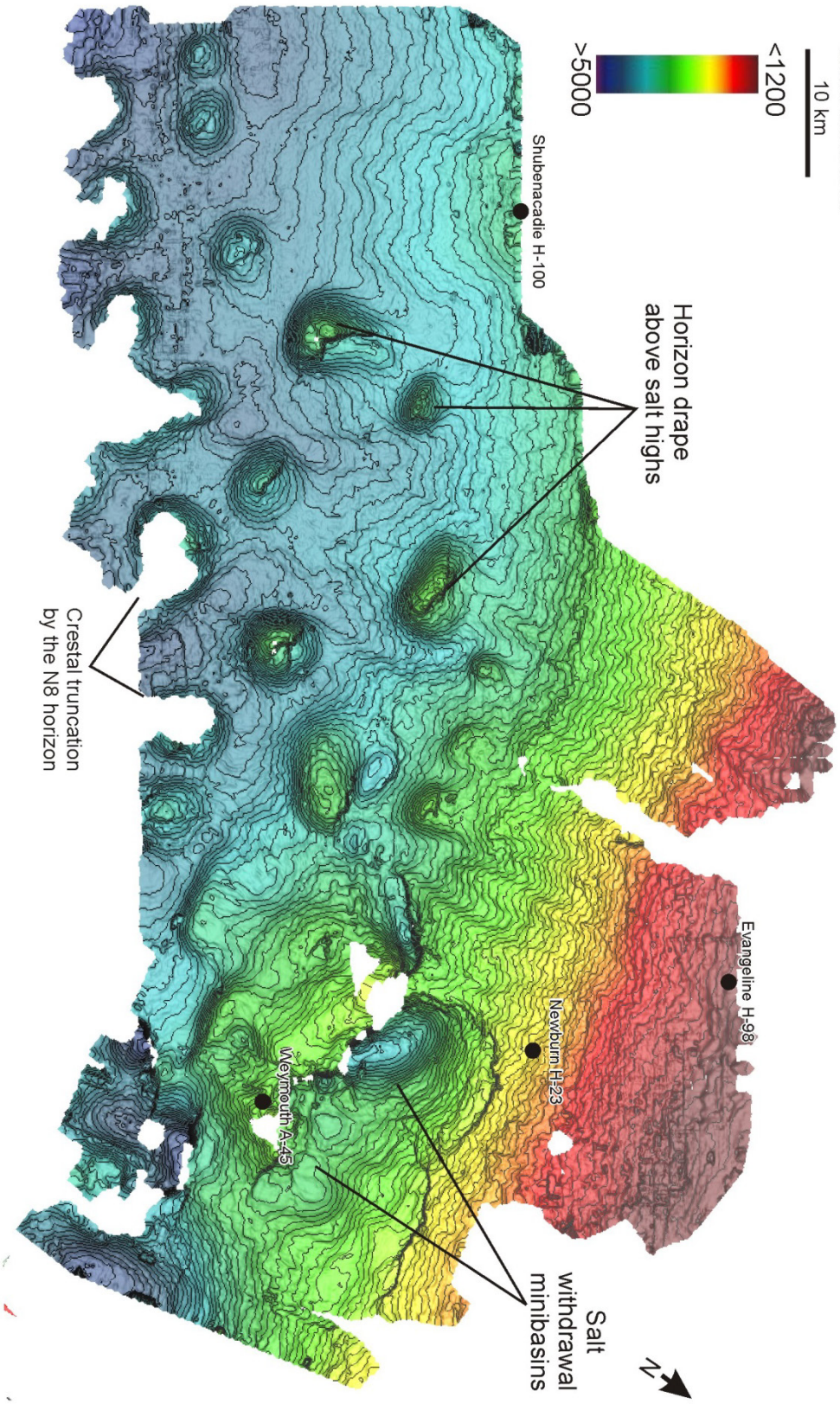

Figure 4.44: Time-structure of the N5 Horizon.

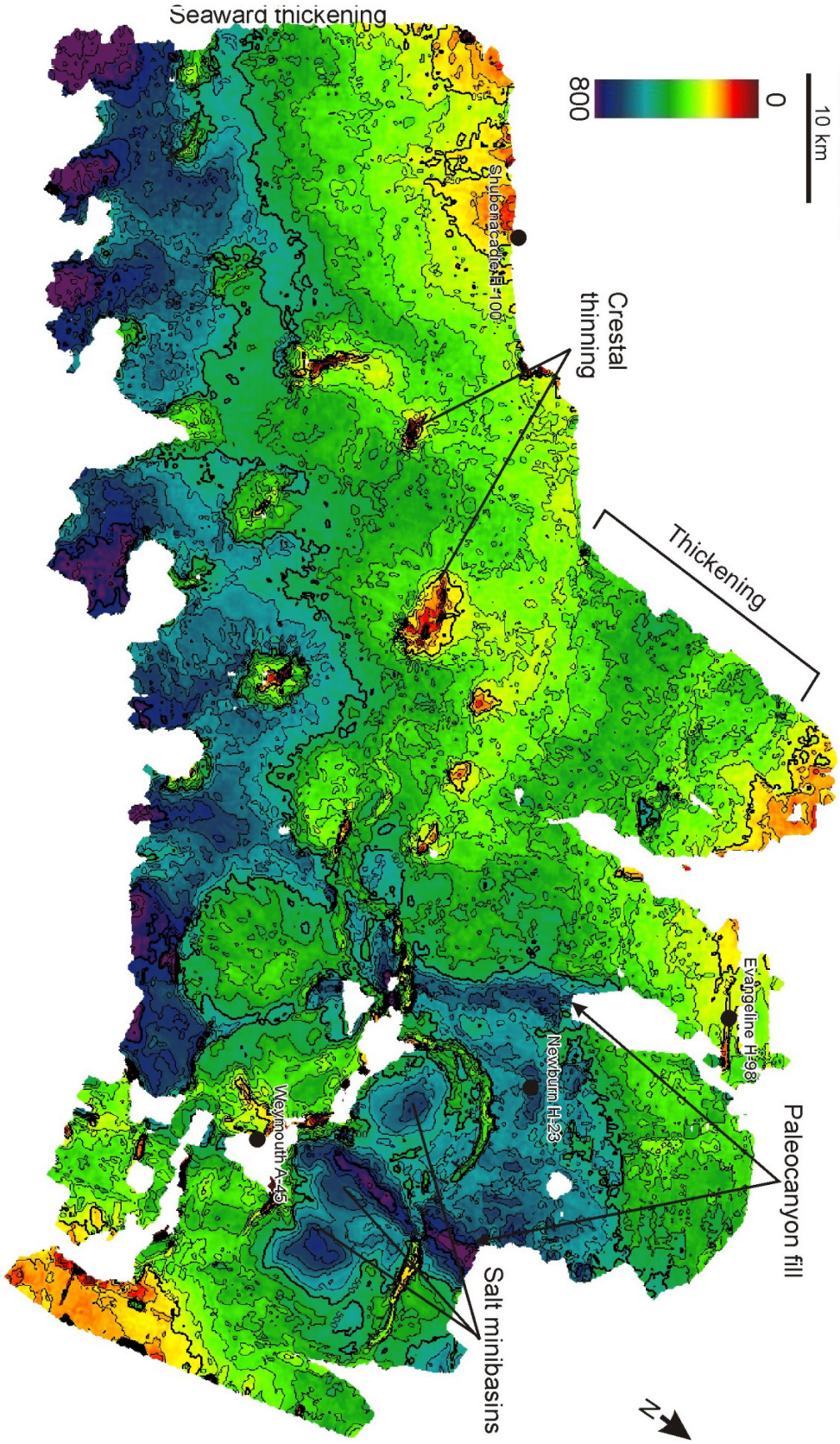

Figure 4.45: Isochron map of Unit 5 between horizons P4 (Rupelian) and N5 (Tortonian).

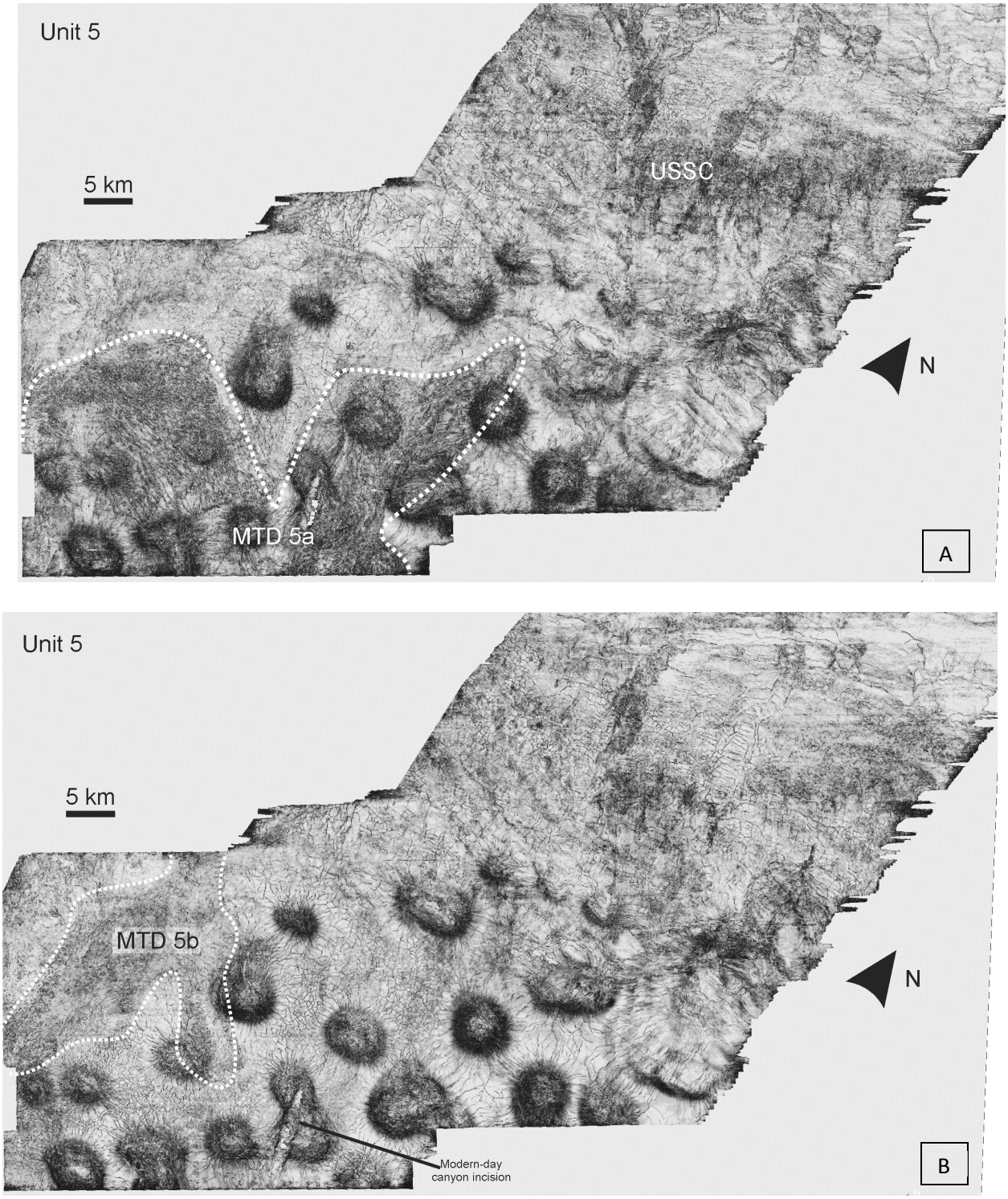

Figure 4.46: Thrumcap coherence slices in Unit 5 showing the distribution of the MTDs 5a (A) taken 50 ms above P4 and 5b (B) 80 ms below N5.

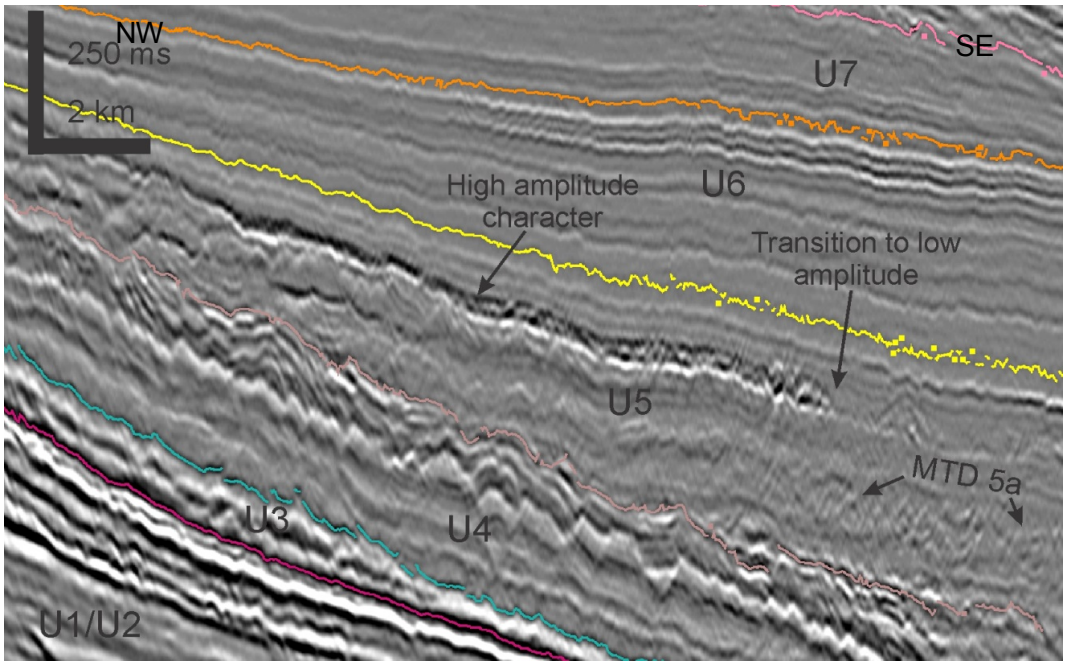

Figure 4.47: MTD 5b changing from high amplitude to low amplitude reflections**.** See Figure 4.9B for the location of this dip-oriented section.

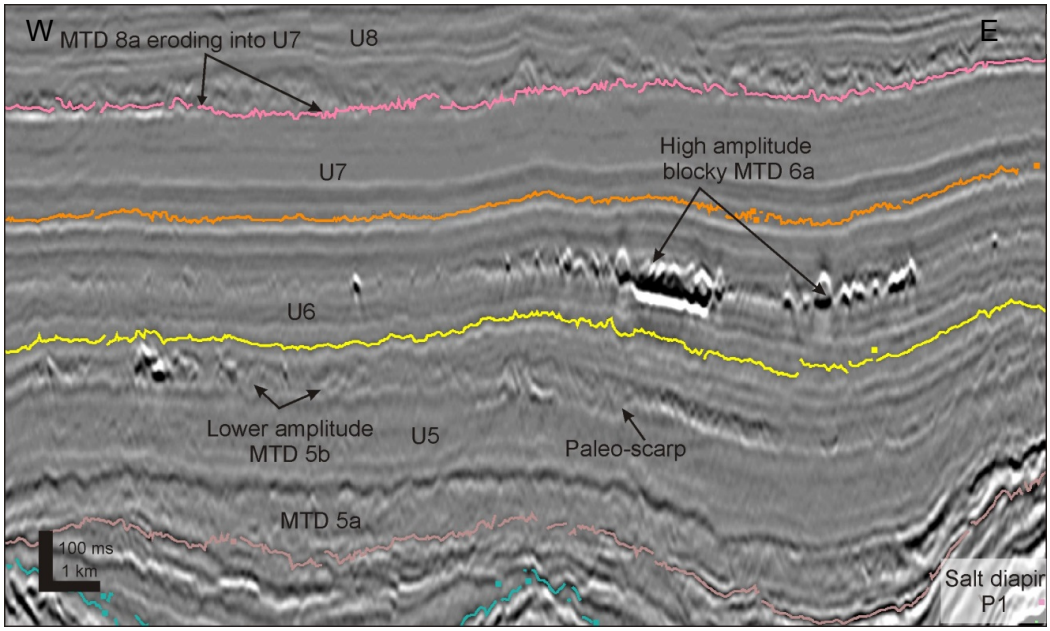

Figure 4.48: A closer look at the main MTDs in the study area. In this strike profile, MTD 5a has a uniform thickness and appears to be thinning above salt body P1. MTD 5b has a lower amplitude with some blocky character and rises over a paleoscarp in this profile. MTD 6a has a very high amplitude blocky character and MTD 8a incises downward into Unit 7 giving it an irregular character. See Figure 4.9B for the location of this transect.

The base has a strong negative reflection and does not appear to be thrust above any paleo-scarps in this area. The top of the MTD is highly irregular in comparison to its base which has a strong negative reflection and is generally continuous.

In the vertical salt diapir province, Unit 6 tapers upslope and downslope away from thick packages (around the medial diapirs; Fig 4.53). These sediment accumulations are in the form of linked depocenters reaching a maximum thickness of 330 ms between medial diapirs M3 and M4 (Fig. 4.53).

In addition to the downslope tapering of the unit, there are strong indications on seismic profiles of increased erosion in the southwestern section of the study area, where Unit 6 is thin or absent (Figs. 4.16, 4.17, 4.29 and 4.52). Unit 6 is also incised from above by a Miocene canyon system (N7 Horizon) in the vertical salt diapir province.

In the eastern study area, Unit 6 dramatically thins above both salt tongues A1 and A2, onlapping above the A2 tongue (Figs. 4.34 and Fig. 4.35). Similarly, the unit tapers on the upper slope until the N6 horizon onlaps the N5 horizon (Fig 4.36). Unit 6 has one large minibasin (i.e. sedimentation is focused uniformly across B1, B2 and B3) in the allochthonous tongue province in contrast to lower units that generally have three separate minibasins landward of the A2 salt tongue.

Unit 7: N6 to N7 (Tortonian-Messinian)

Unit 7 is bounded below by the N6 horizon and above by the N7 horizon (Fig. 4.54). The amplitude of the N7 horizon varies widely throughout the study area, however, it generally has the highest amplitudes in the western study area and the lowest amplitudes in the eastern study

area. This marker is intermittently truncated across the study area by deeply incised modern canyons (e.g. Dawson and Verrill canyons) eroding downward into Unit 6 and older buried paleocanyon systems (Fig. 4.54). Additionally, the horizon is absent in areas with large growth fault offsets i.e. above the crests of diapirs D1-D6 where it has been eroded away (Figs. 4.16, 4.17 and 4.55).

An overlying MTD (MTD 8a) extends over the northwestern portion of the study area incising into the N7 horizon (Figs. 4.52, 4.53 and 4.54). The horizon becomes irregular and has a lower amplitude in this area and was consequently difficult to map. On the Unit 7 isochron map, erosion of from the MTD shows up as a relatively uniform thin surface.

Amplitudes of the reflections in the Unit 7 package are generally low to medium and they are parallel reflections. Unit 7 is also absent where modern canyons erode it, in particular above distal salt bodies that appear to have topographic highs and in areas with large amounts of fault offset. Unit 6 is eroded above distal salt highs due to the overlying N8 unconformity and along a central corridor in the survey (Figs. 4.17, 4.18, 4.49, 4.55 and 4.56).

Unit 7 is generally the thickest (<300 ms) in areas where erosion from the N8 horizon is minimal (Figs. 4.55 and 4.56). Relative to Unit 6, these depocenters thicknesses have shifted landward in the vertical salt diapir province (Figs. 4.52 and 4.55). The unit also tapers downslope when combined with the increased downcutting of the N8 horizon. (Fig. 4.31). It reaches a maximum thickness of <500 ms on the downthrown section of a growth fault landward of A2.

There are no resolvable MTDs in this unit.

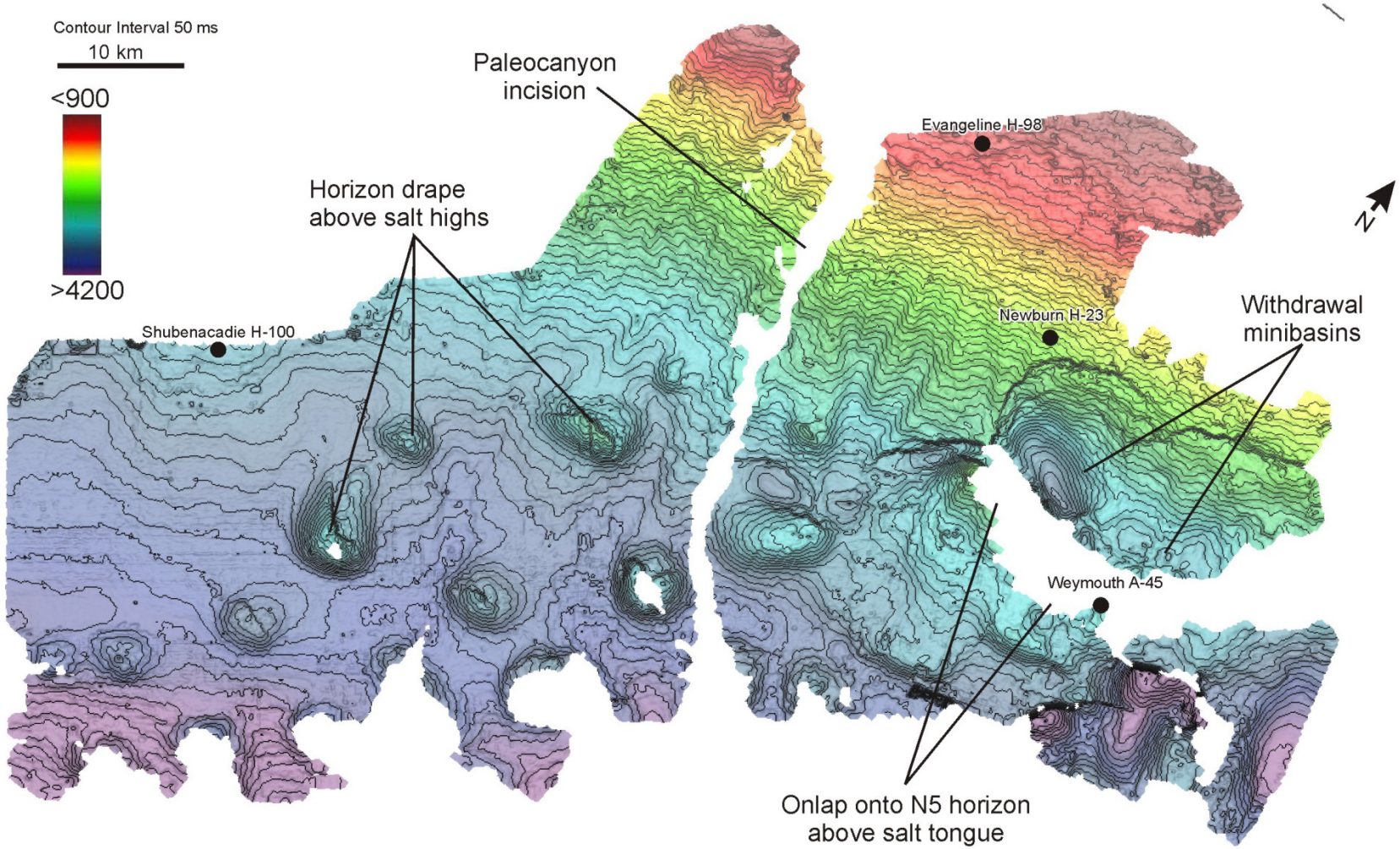

Figure 4.49: Time-structure of the N6 Horizon.

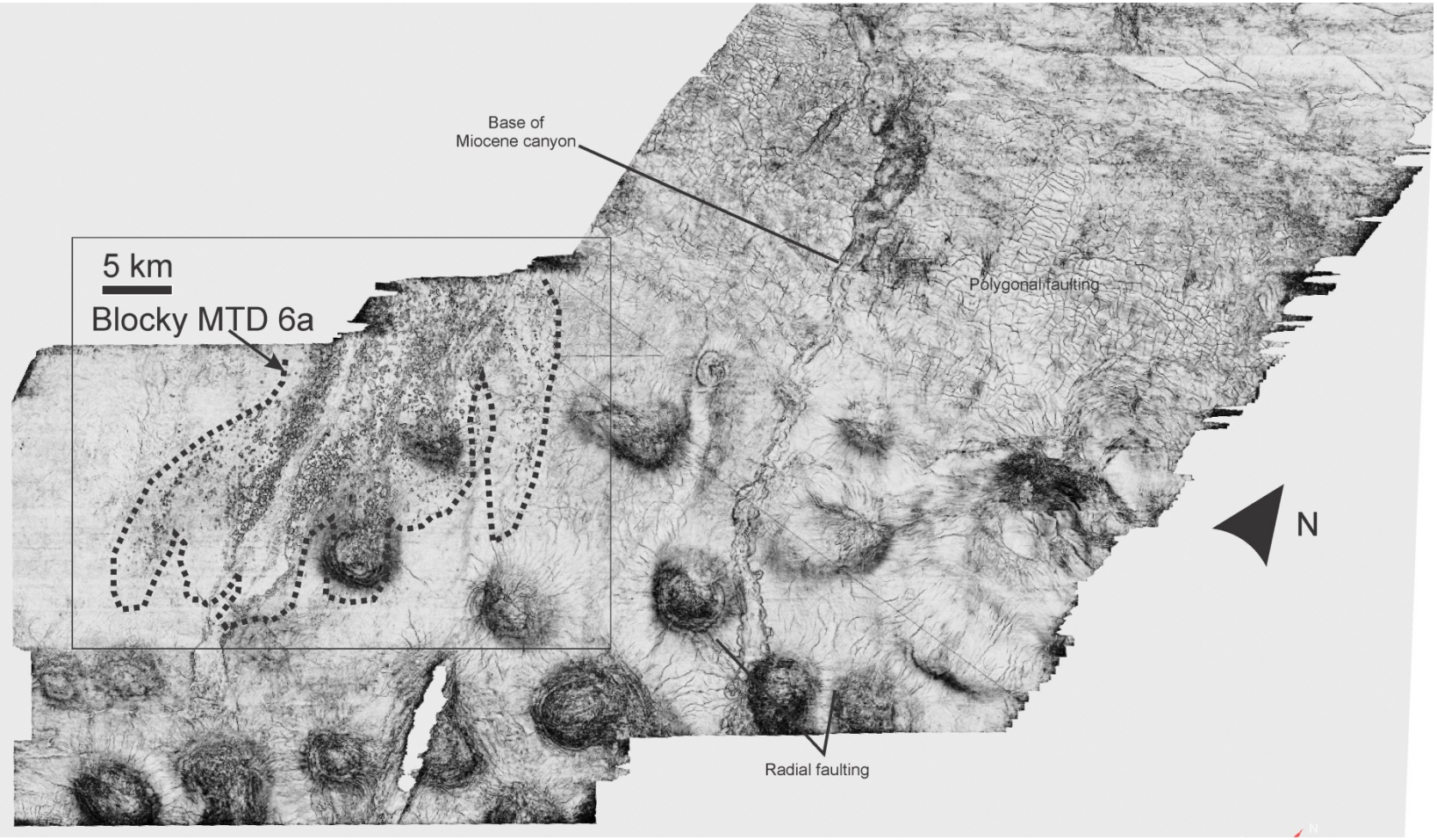

Figure 4.50: A coherence slice in Unit 6, 66 ms below N6 through MTD 6a. The base of the Miocene canyon originates from the down-cutting of the younger N7 Horizon. The black square shows the location of Figure 4.49.

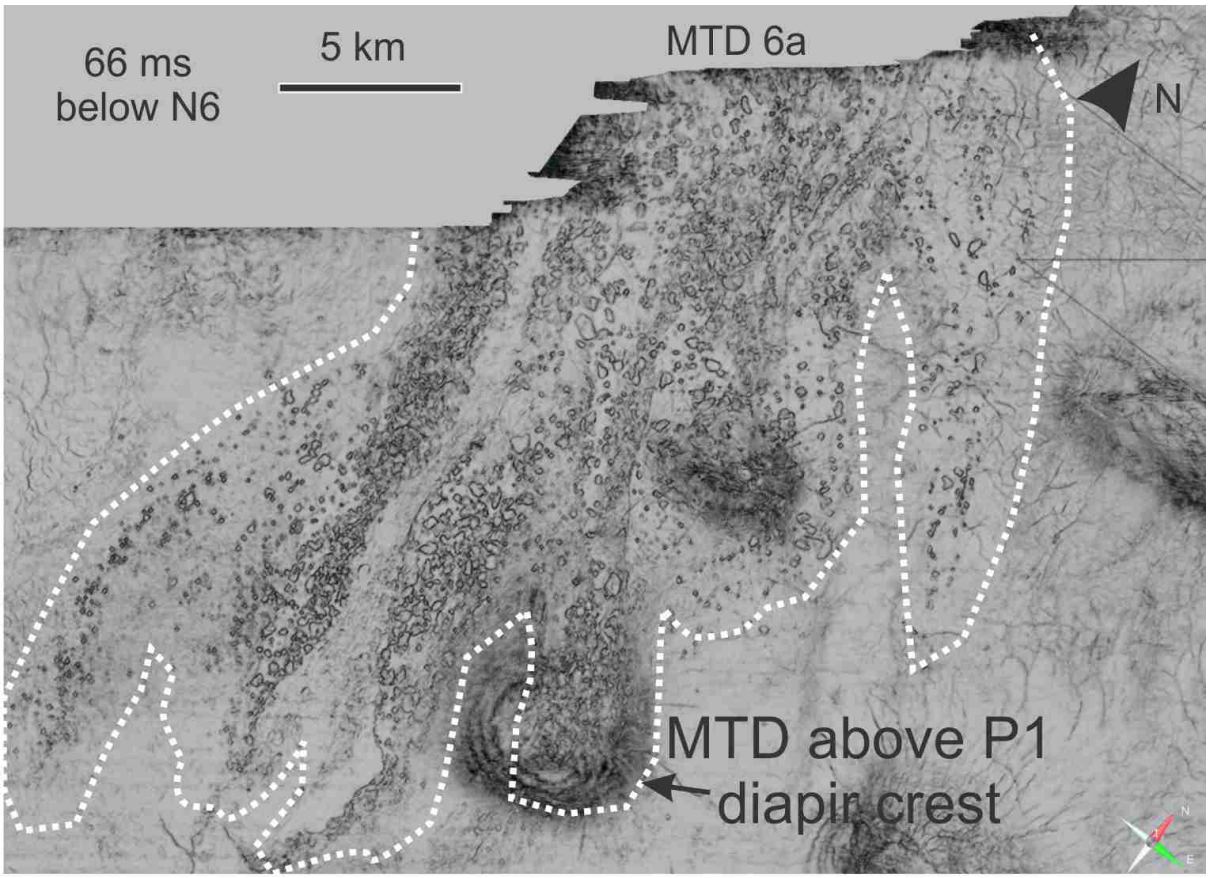

Figure 4.51: A zoomed-in coherence slice of the blocky MTD 6a. See Figure 4.48 for location.

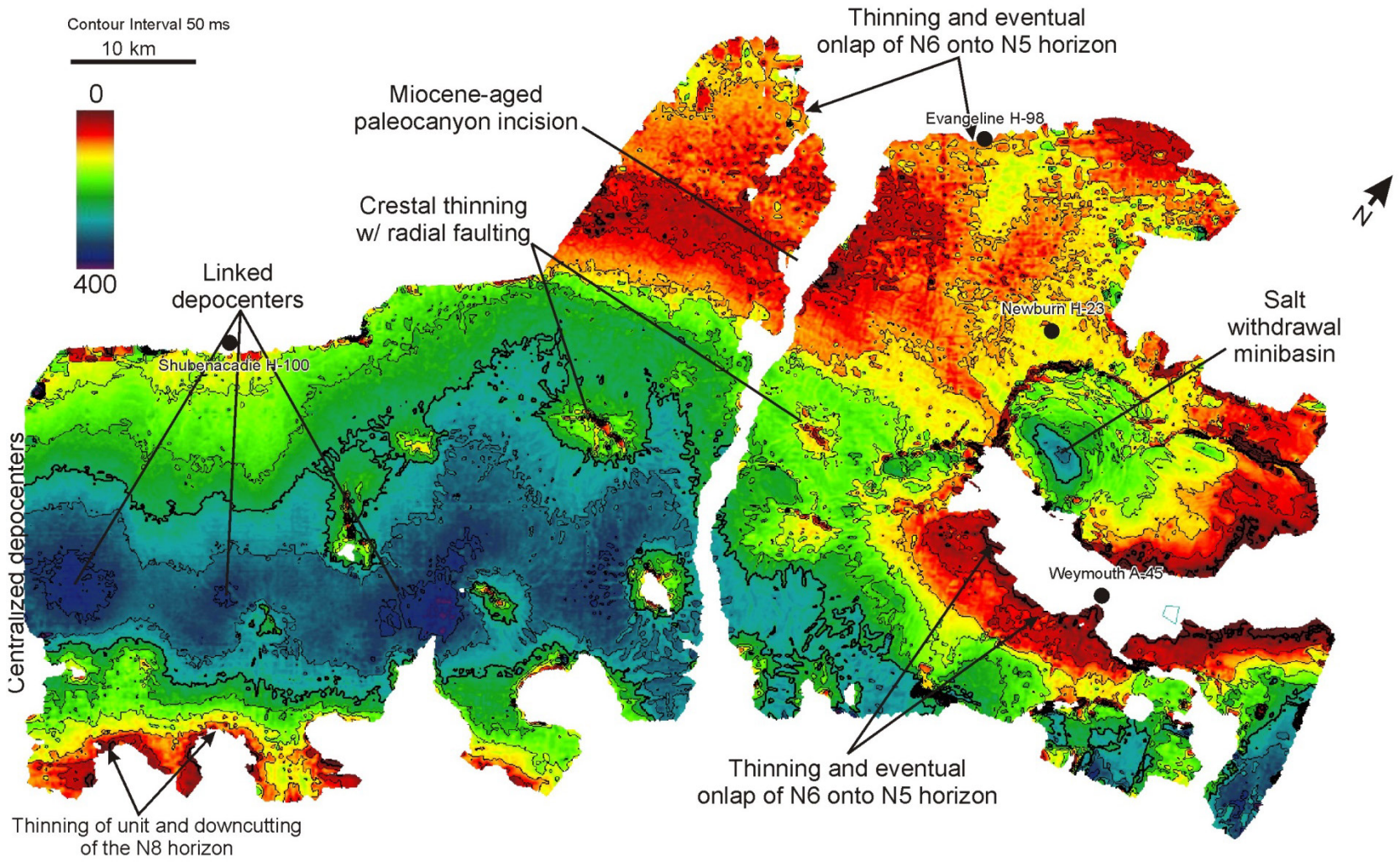

Figure 4.52: Isochron map of Unit 6 from N5 (Tortonian) to N6 (Tortonian).

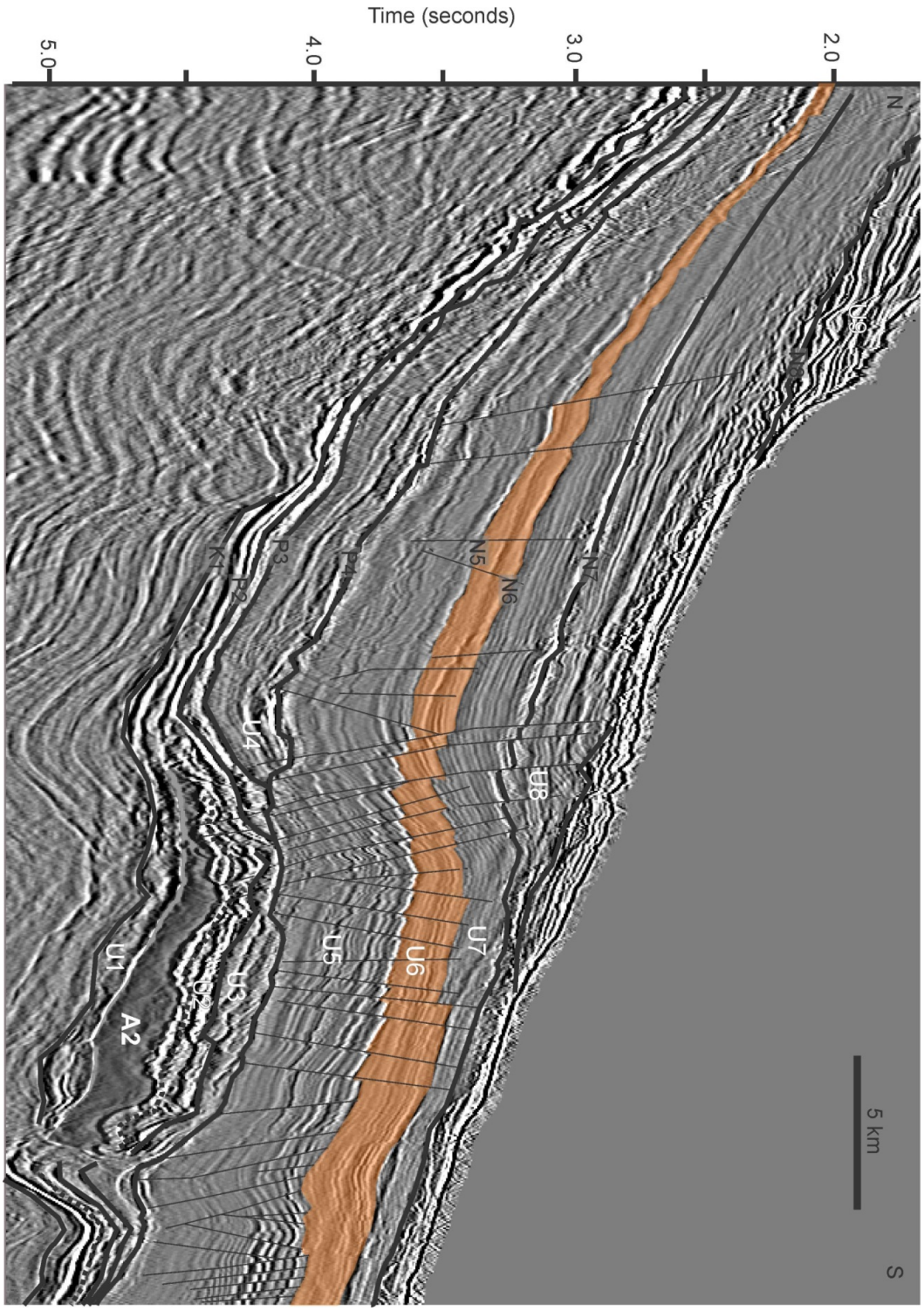

Figure 4.53: Tapering of the Unit 6 package upslope.

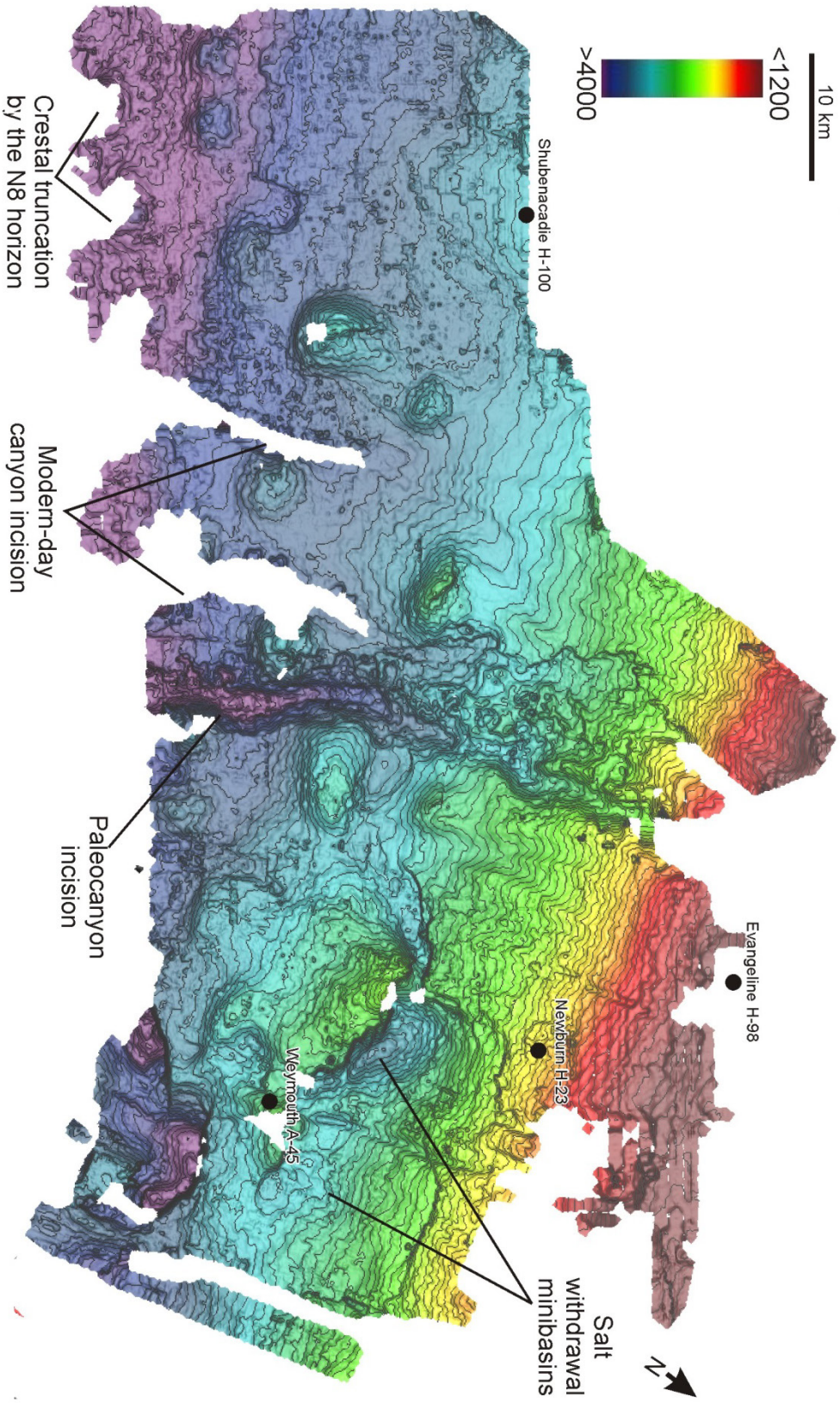

Figure 4.54: Time-structure of the N7 Horizon.

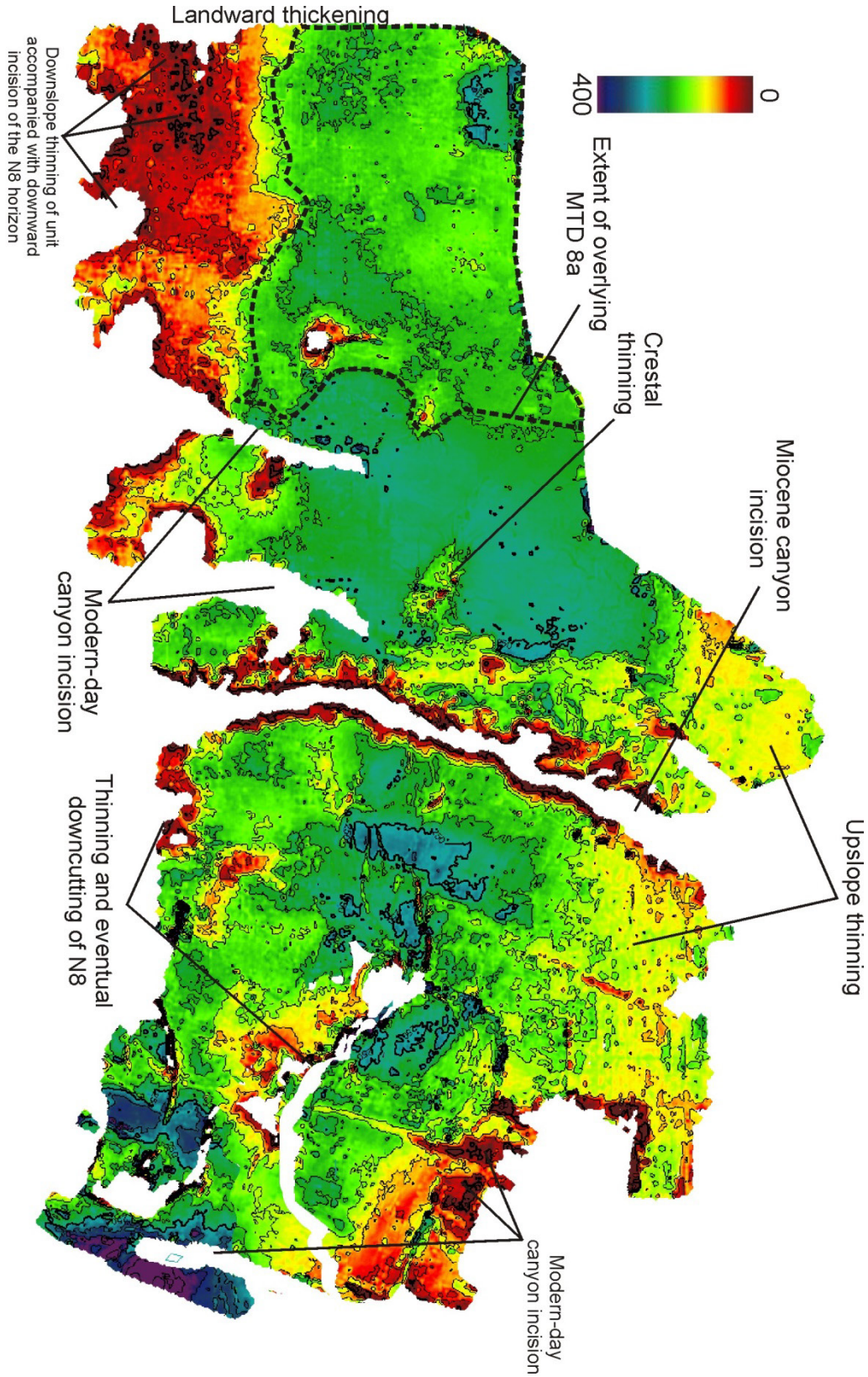

Figure 4.55: Isochron map of Unit 7 from the N6 (Tortonian) to N7 (Messinian) horizons.

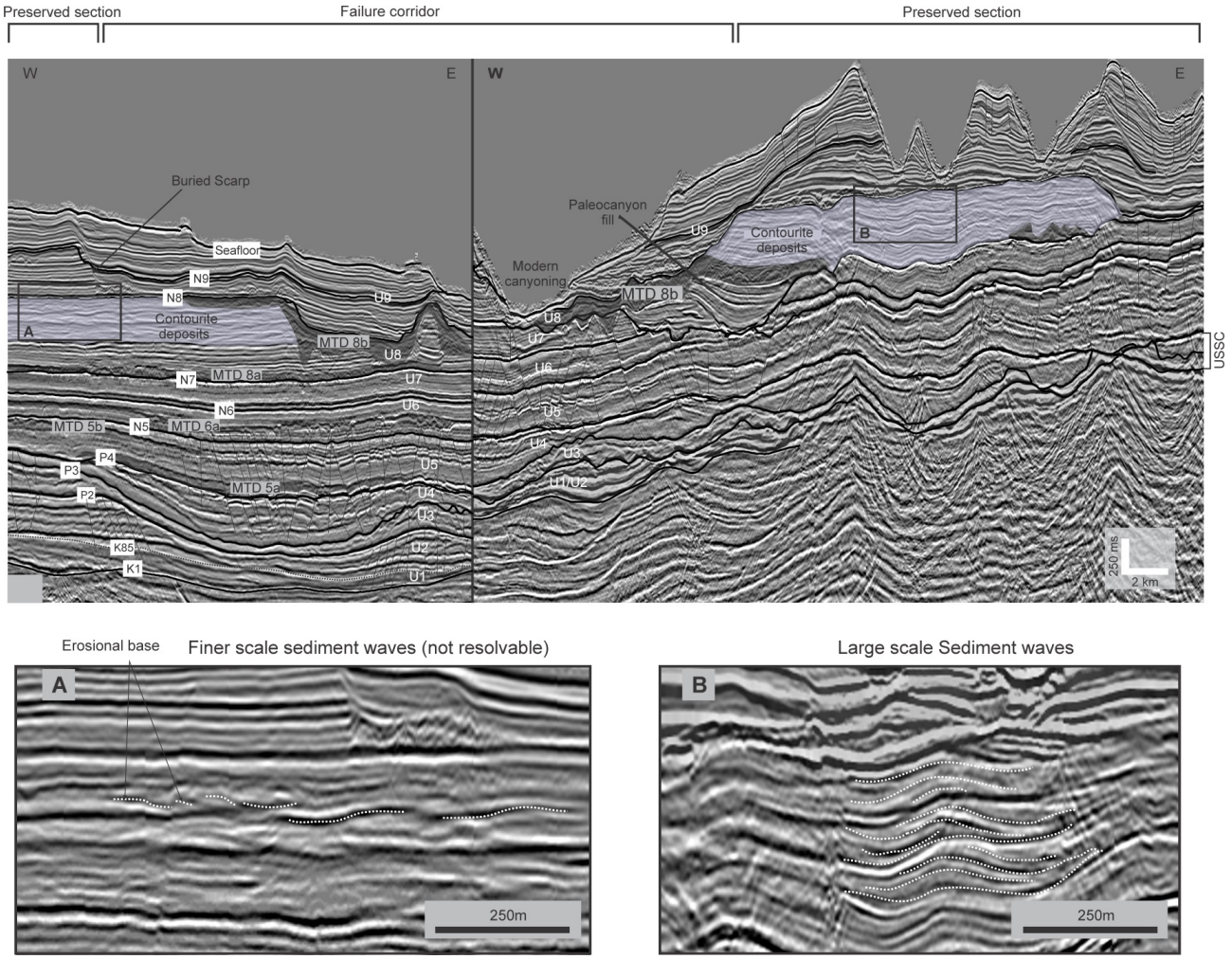

Figure 4.56: Cross sections showing the contourite distribution in areas of preserved section, erosional corridors, Miocene paleocanyon system and MTDs in throughout much of the study area. Note that the areas highlighted in mauve produce the northeast trending lineations on the coherence slice in Figure 4.57. These areas correspond to small scale bedforms that appear to climb up the slope. They are interpreted as contourite deposits. See Figure 4.9B for the location of this transect.

Unit 8: N7 to N8 (Messinian-Pliocene)

Unit 8 is bound below by the N7 horizon and above by the N8 horizon (Fig. 4.57). The N8 horizon has variable amplitudes throughout the study area and is defined by initial erosion into the underlying Unit 7. It is a time-transgressive surface that experienced repeated episodes of cut and fill. N8 is extensive throughout the study area and only absent in areas where it has been incised by modern-day canyon systems.

In plan view, large corridors of extensive erosion are present in the east and west shown as thinning on the isochron from the downcutting of the N8 horizon (Fig. 4.54). Thick sediment packages are present where the section is most preserved (i.e. the least amount of erosion from N8) in the northwest and northeastern-most part of the study area (Fig. 4.56). Max thicknesses in the interval are from a Miocene (Tortonian) paleocanyon (N7 Horizon) infill exceeding 750 ms (Figs. 4.34 and 4.58).

Where most preserved, dip lines in the west show a landward thickening succession (Fig. 4.31). In the western study area, the unit is composed of two distinctive acoustic packages. The upper section of the unit exhibits a low to medium amplitude with hummocky and sigmoidal cross sets identified as sediment waves with an irregular truncation surface at the base (Figs. 4.31 and 4.56). The lower section consists of parallel low amplitude facies that conformably overlie Unit 7 with the exception of the downcutting of an MTD in the northwest (see below).

Sediment waves are mostly preserved in areas of thickening above the A1 and A2 salt tongues i.e. centrally (north of M5) and in the western-most part of the study area (west of P1) (Figs. 4.15, 4.31, and 4.56). They vary in size from west to east and were previously identified as Miocene contourite drifts by Campbell (2011). These sediment waves are younger than the

Oligocene sediment waves visible in above the A2 allochthonous tongue in Unit 5. Generally, they are larger (sometimes exceeding 4-5 km in wavelength) above salt tongues in the east and in preserved sections in the vertical salt diapir province (Figs. 4.16 and 4.56). Orientations of wave crests infer a current direction of NW-SE. The westernmost preserved section shows smaller (<100 m in length), low amplitude, fine-scale sediment waves which can be difficult to resolve in seismic (Fig. 4.56).

There are 2 large MTDs in this unit. MTD 8a and 8b are confined to the vertical diapir province (Fig. 4.56). 8a is the deepest MTD and its extent (and erosion) are visible in the lower Unit 7 isochron (Figs. 4.55 and 4.56). Internal reflections in this MTD are chaotic and have low amplitudes with large blocks. Its upper surface produces a strong positive amplitude reflection in the east changing to a low amplitude reflection in the west where it becomes more irregular. The base of this MTD has scarps and is generally a strong negative reflection changing to a low amplitude reflection westward.

MTD 8b is truncated along the erosional corridor in the east. This MTD is only present around areas of preserved section around bathymetric highs in the eastern and western sections of the vertical salt diapir province (Fig. 4.55 and 4.56). It is a low amplitude chaotic deposit unconformably draping the Miocene paleocanyon system in Unit 7. Where preserved in the west, it incises into contourite deposits (Fig. 4.56).

In addition to the two MTDs described above, a series of stacked MTDs overlie the large Miocene paleocanyon (Fig. 4.19). These MTDs are generally limited to the axis of the paleocanyon and amplitudes of reflections in the fill vary highly throughout the succession. They incise down into one another and only remnants of some of the deposits remain.

When taking a coherence slice ~80 ms down from the N8 horizon, a series of scours become visible in the west (vertical salt diapir province) and northeast (upper slope) (Fig**.** 4.42). The base of the sediment waves coincides with the onset of scours and these sediment waves appear to unconformably overlie the scours. These scours are linear in plan view and although they show slight variations in directions, are generally oriented east-west and east-northeast to west-southwest. They are generally 5 to 10 km long and 50 to 250 m wide. They are visible in areas of preserved sections with contourite deposits and not present along the downslope erosional corridors. When stepping through the coherence volume, there appear to be several different phases of scour incision.

Unit 9: N8 to N10 (Pliocene to Present)

Unit 9 is bound below by the N8 horizon (explained in previous Unit 8) and above by the seafloor horizon (Fig. 4.61).

The N9 horizon extends between inter-canyon highs and terminates around the upper slope (Fig. 4.60). The seafloor horizon shows the modern day bathymetry (Fig. 4.61). The seafloor is expressed as a strong positive amplitude reflection that extends throughout the study area. Due to incision of modern-day canyon systems and concordant reflections, the N9 horizon was very difficult to map, which is why Unit 9 is based on horizons N8 to N10 instead (Figs. 4.27 and 4.60).

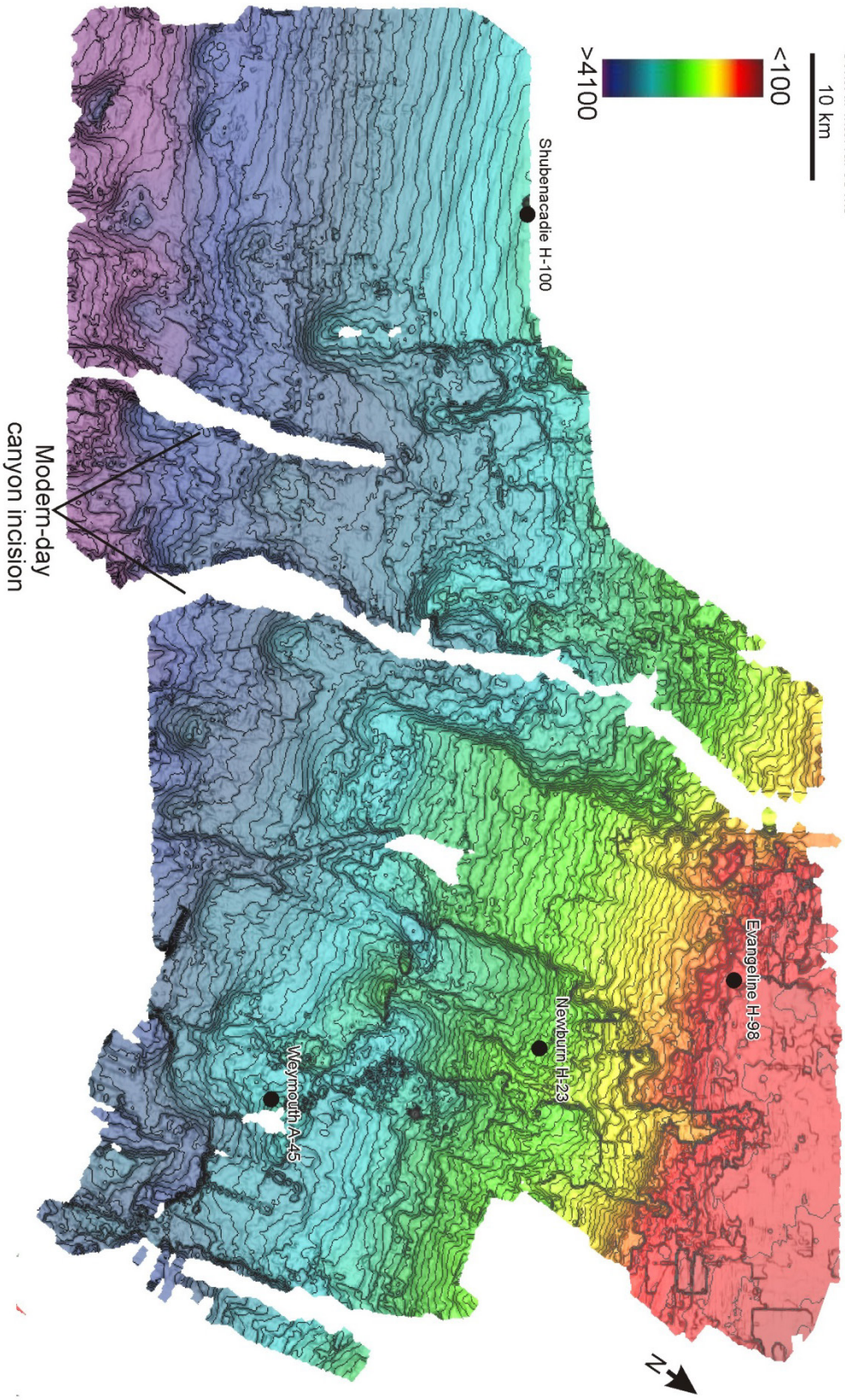

Figure 4.57: Time-structure map of the erosional N8 Horizon.

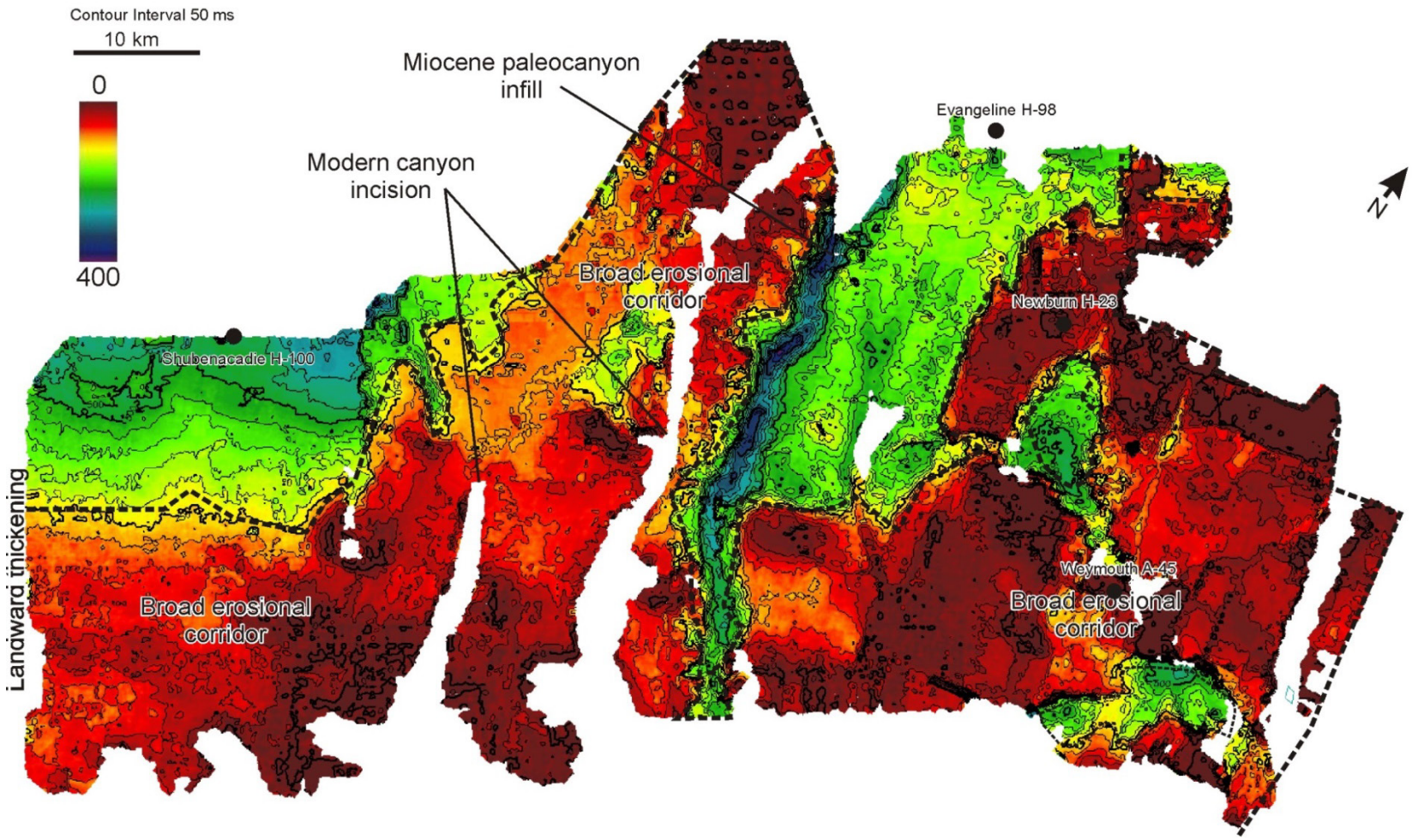

Figure 4.58: Isochron map of Unit 8 from the N7 (Messinian) to N8 (Pliocene) horizons.

Figure 4.59: Coherence slice taken 30 ms below N8 showing linear scours with varying orientations.

Modern canyons in the study area (e.g. Verrill and Dawson) incise into Units 7 and 8 in the south. These canyons are linear to gently curved in plan view and have several tributaries on the shelf edge feeding into larger canyon systems on the upper slope (Mosher et al. 2004; Piper et al. 2012) (Fig. 4.61). In cross section, modern day canyons are generally U to V shaped and slumping is common on the flanks of canyon walls (Fig. 4.27). Fill is mostly visible in the eastern section upslope, near the shelf edge (Fig. 4.27). Dawson Canyon is the largest canyon system with a maximum width of approximately 6 km and incision depths exceeding 700 ms (or 525 m).

Inter-canyon highs are intermittently truncated by modern-day canyon systems (Fig. 4.27). The lower portion of Unit 9 generally consists of a succession of stacked mass transport deposits. The upper portion of this unit has the highest amplitude reflections. When taking a dip line along an inter-canyon high, reflections are generally continuous downslope (Fig. 4.31). Internal reflections within these MTDs are highly variable, but generally consist of medium to high amplitude reflections. They generally erode into underlying strata across salt highs.

Between the modern day canyons, MTD accumulations are best preserved along the inter-canyon highs in the eastern and western sections of the study area (Fig. 4.63). These MTD accumulations are generally thicker in the west (~400 ms) than in the east and appear to have been deposited in areas of low paleo-seafloor relief or greater slope accommodation (e.g. salt withdrawal minibasins and on the downthrown side of growth faults). Thick sediment packages in Unit 9 originate from either stacked MTDs layered deposits or preservation on inter-canyon highs (Fig. 4.61). Thin sediment packages in this unit are generally associated with erosion along modern-day canyon axes (Fig. 4.63).

Unit 9 also contains a series of erosional scarps visible on the present day slope morphology in addition to older buried paleoscarps (Figs. 4.56, 4.60, 4.61, 4.64). The prevalence of scarps suggests that slope failure increased during this interval. These scarps are mainly preserved in the upper slope and may even be linked to MTD deposition in Unit 8.

4.5 Summary of seismic stratigraphic results

In summary, the nine units identified in this seismic stratigraphic framework can be separated into three main periods of development:

- Phase 1 (Units 1 to 4): Phase 1 comprises canyon bypass and infill spanning a time period between the Cenomanian to Rupelian. Unit 1 and 2 generally consist of hemipelagic sediments (with slow sedimentation rates) draping the seafloor and incised by a series of erosional canyons. These canyons provide evidence for multiple incision events starting along the K1 marker with repeated major incision events around P2 and P3, and this canyon relief was eventually infilled by the end of Unit 4.

- Phase 2 (Units 5 to 8): Phase 2 sees a gradual landward shift of depocenters during the Rupelian to Pliocene. The stratigraphy generally consists of sediment waves that are probably related to the contourite deposition previously studied by Campbell (2011). Additionally, this interval contains several interbedded MTDs and submarine channels that divert around salt structures in some cases.

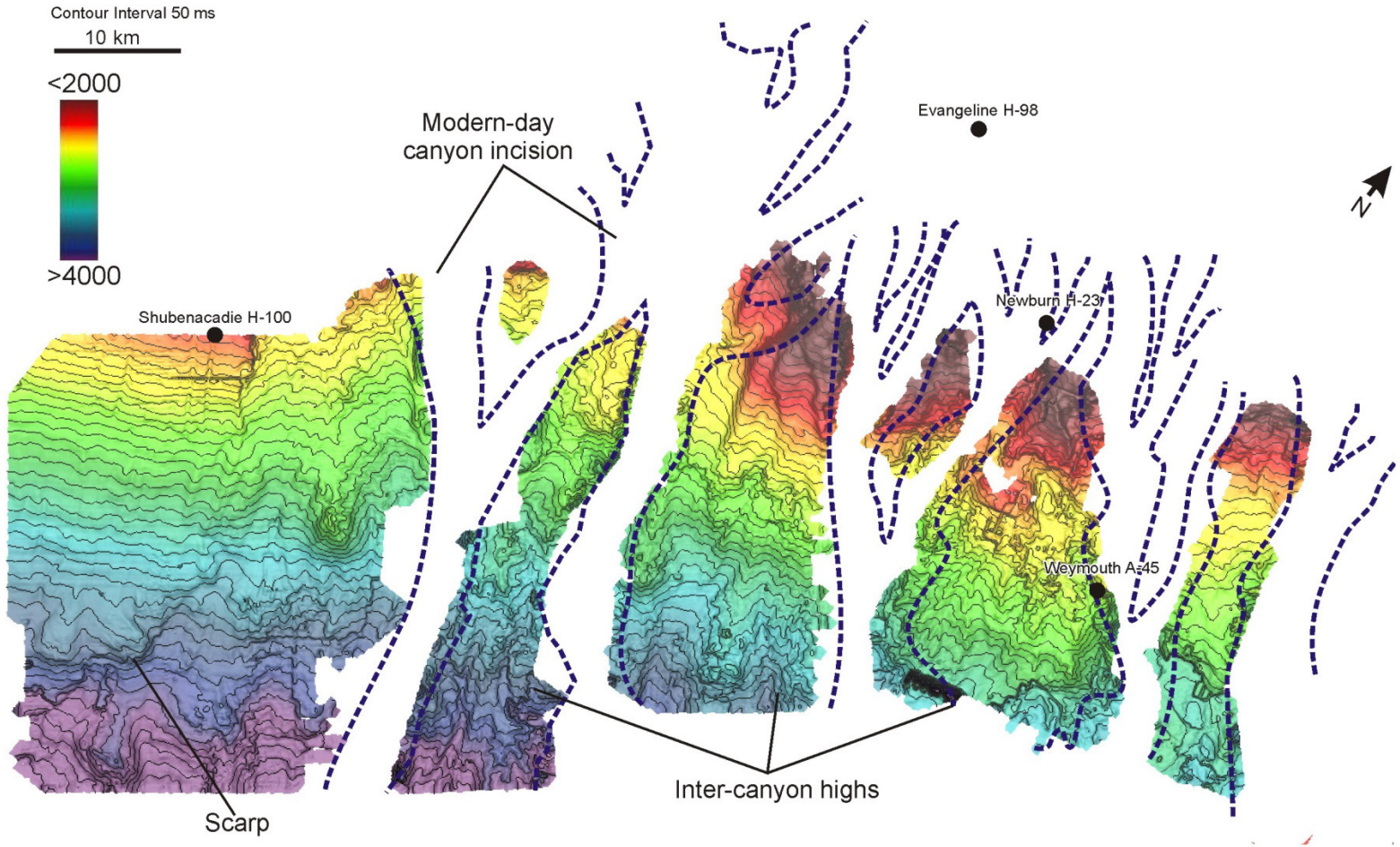

Figure 4.60: Time-structure of the N9 Horizon. Blue dashed lines represent trace of modern-day canyons (see next figure).

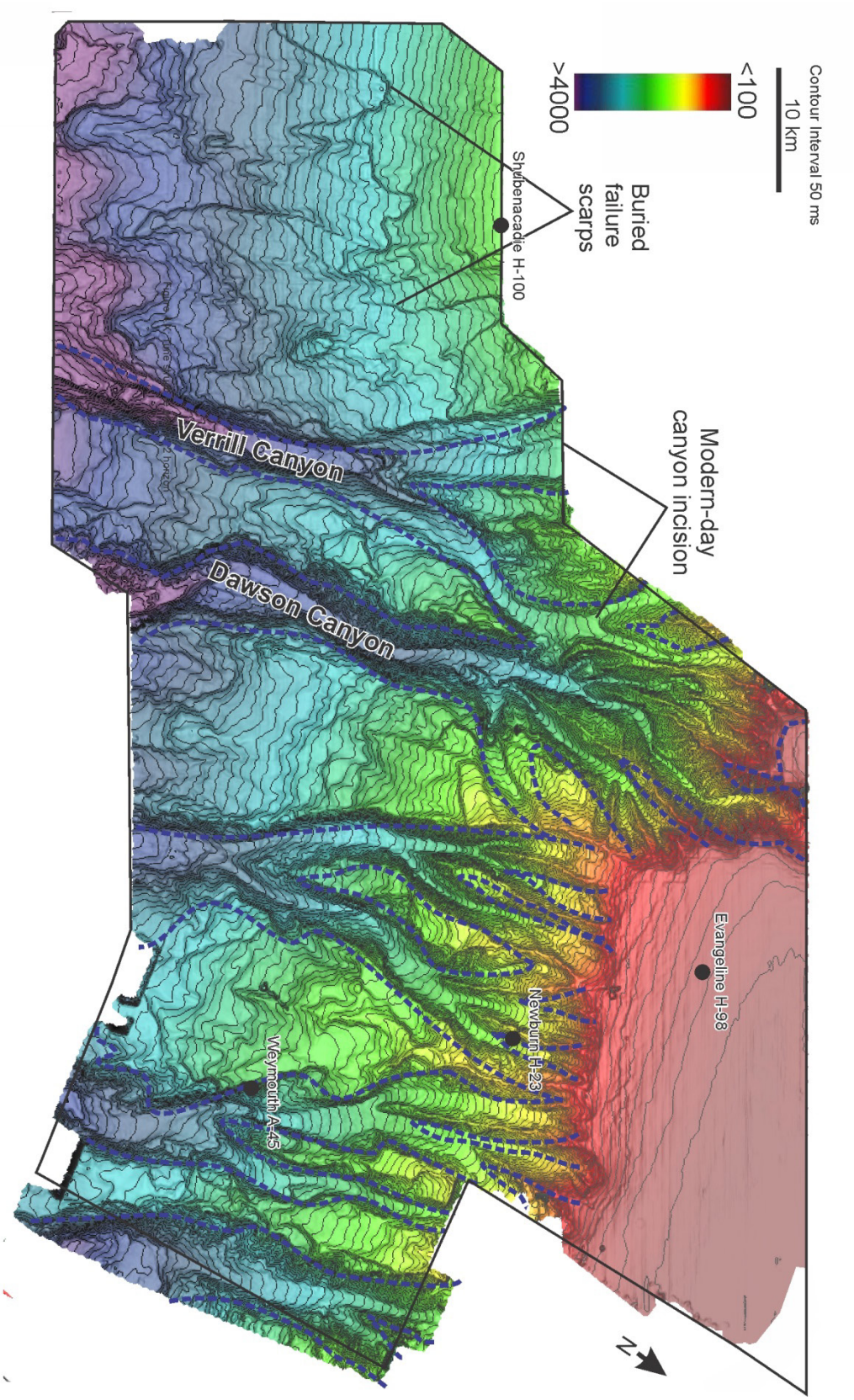

Figure 4.61: Time-structure of the seafloor horizon (mapped by M. Deptuck).

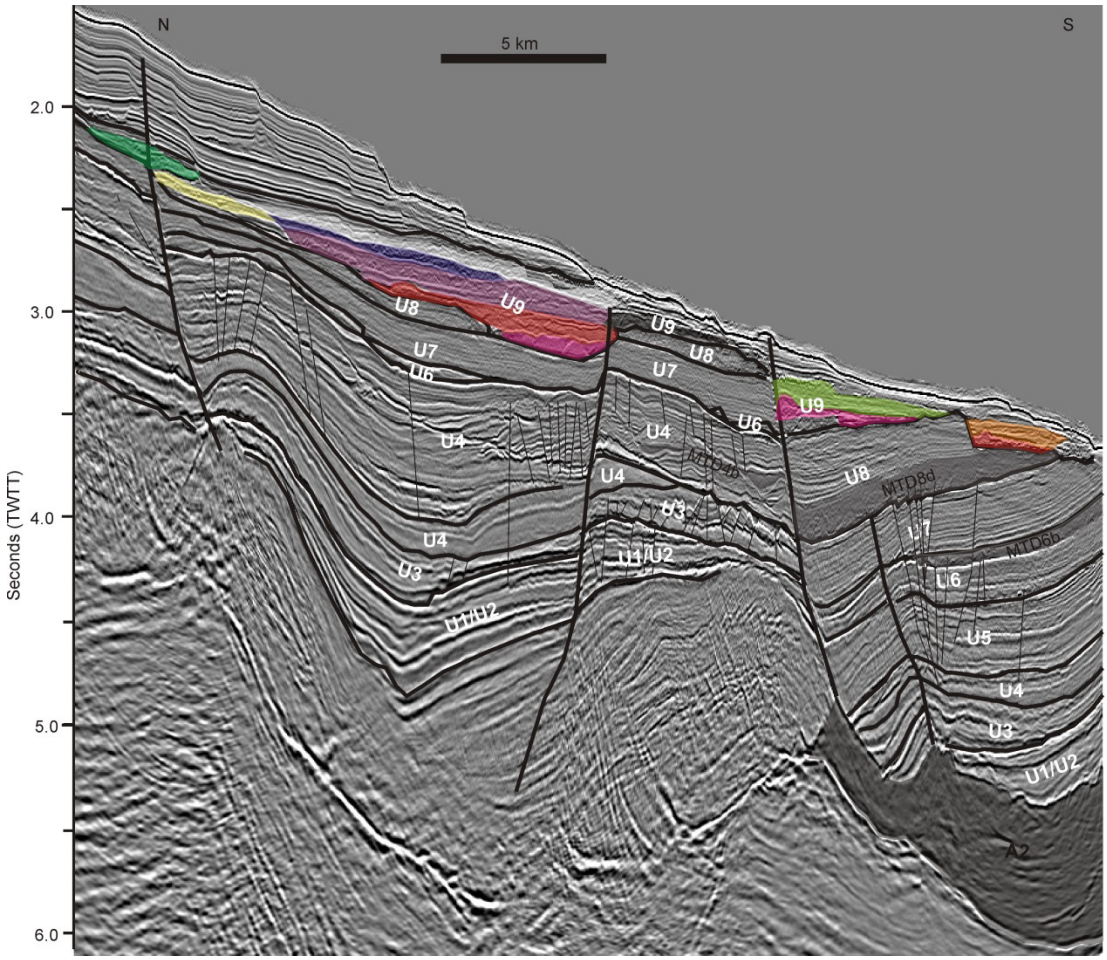

Figure 4.62: Seismic section showing a series of stacked MTDs (individual MTDs color-shaded) in the allochthonous tongue province. See Figure 4.9B for the location of this transect.

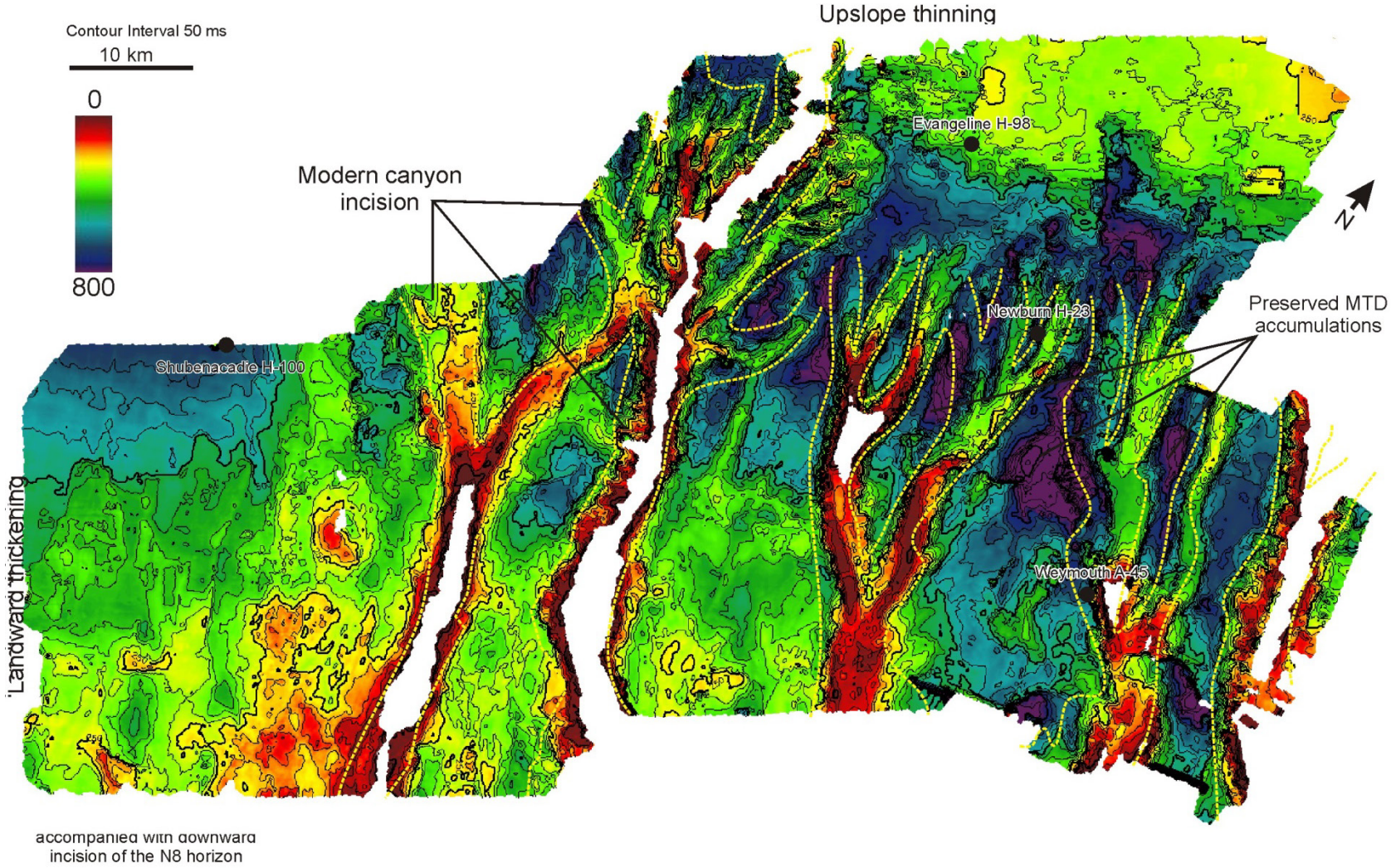

Figure 4.63: Isochron map of Unit 9 from the N8 (Pliocene) to N10 (present sea floor) horizons.

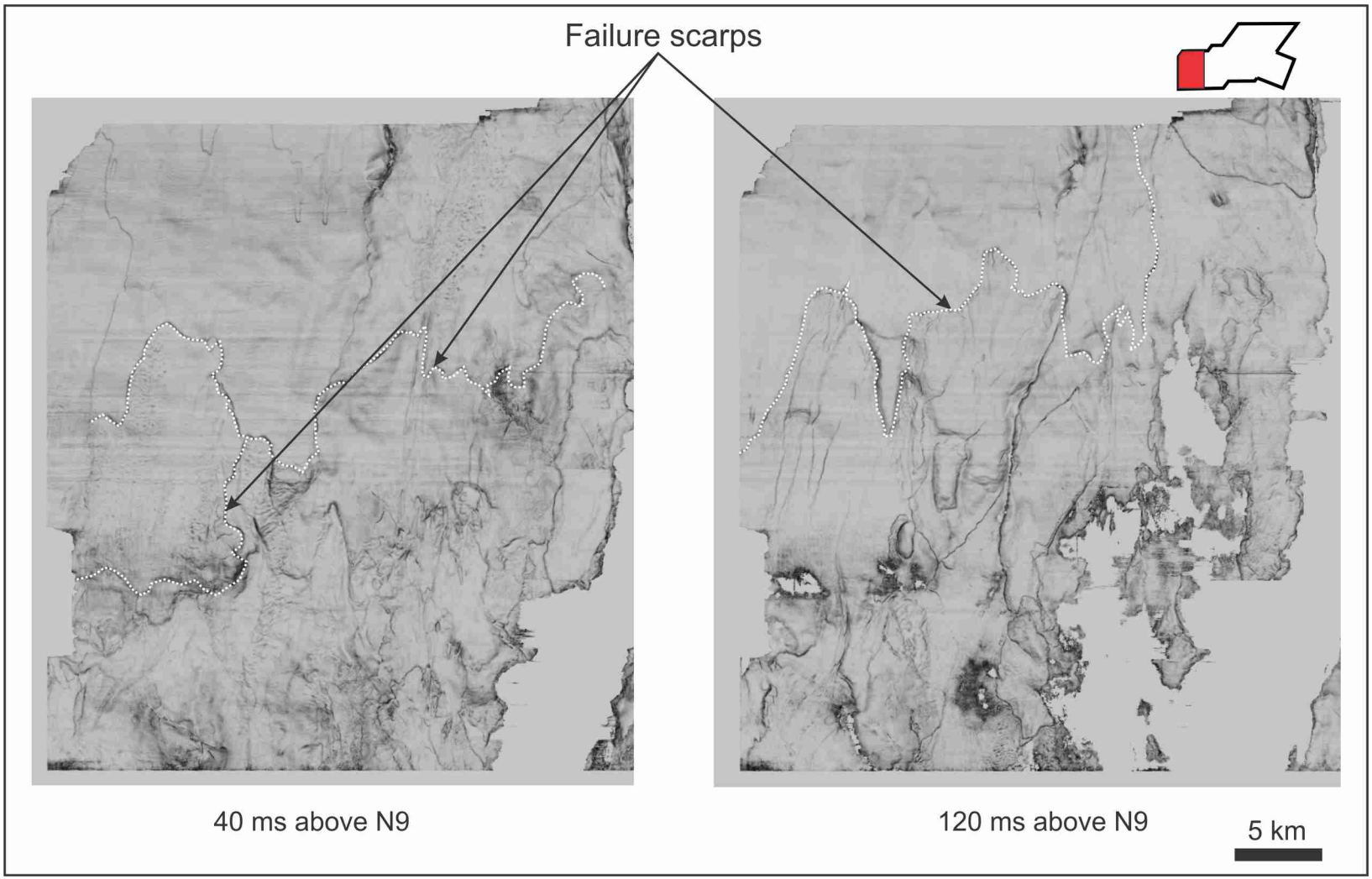

Figure 4.64: Coherence slices in Unit 9 showing the change in slope morphology as a result of scarps formed on the paleoslope. Location map shown on the top right.

- Phase 3 (Units 8 to 9): A transition from contourite deposition to a significant regional slope regrading event occurs somewhere between the Pliocene and the Present day. This unconformity (Horizon N8) is present throughout the study area and is a time-transgressive surface eroding up to 500 ms of strata away. The unconformity is overlain by a series of stacked mass transport deposits that have accumulated in topographic lows (minibasins). Finally, these deposits are draped, followed by modern day canyon development.

4.6 Faults

Fault history is complex in the study area mainly due to the nature of salt tectonics. Different areas are subject to different styles of faulting. The scale of faulting is subdivided into "major" and "minor" faults based on the magnitude of their throw. Major faults are categorized as faults with larger scale offsets (>150 ms) (e.g., the large counter-regional growth fault in the allochthonous salt tongue province; Fig. 4.65). These faults are typically immediately adjacent to or above salt structures. In contrast, minor faults generally have smaller offsets (<150 ms) and typically occur in a radial or polygonal pattern. Radial faults are confined to the overburden above salt bodies whereas polygonal faults are restricted to the intervening minibasins and the rest of the upper slope.

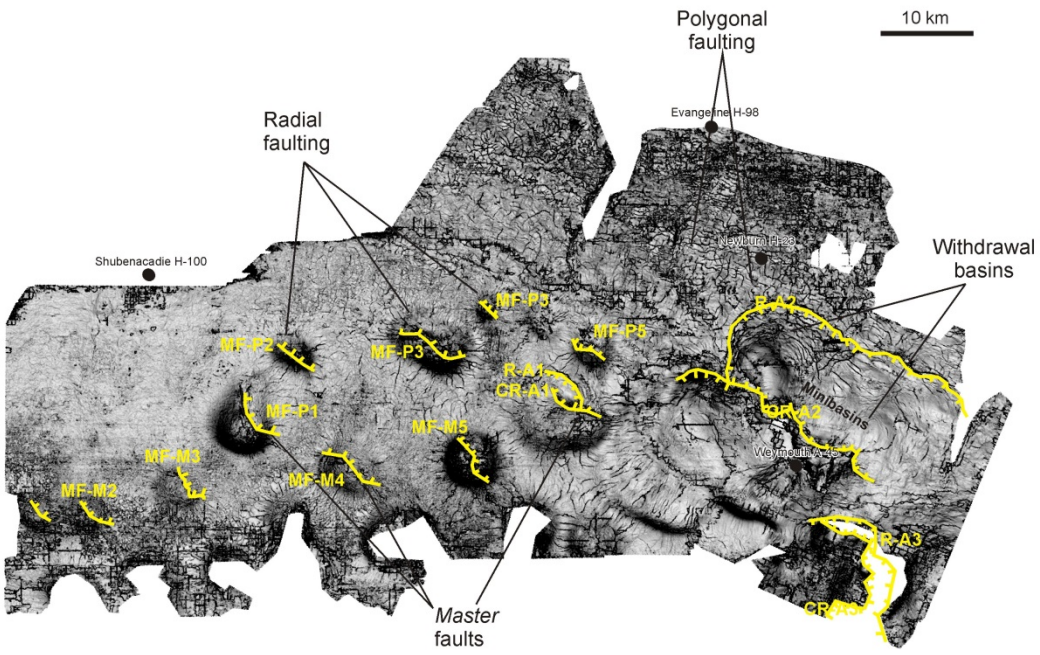

Figure 4.65: Dip map showing major faults (yellow lines), and smaller-scale minor faults (radial and polygonal) on the N5 Horizon (Tortonian). Individual major faults are labelled with "MF" codes and a dash to represent their association with individual diapirs (e.g., MF-P1 for "major fault, diapir P1)

4.7 Growth history across major faults

Major faults have significantly larger offsets (upwards of 150 ms) and form above or adjacent to salt structures in the vertical salt diapir and allochthonous tongue province as normal growth faults. Since salt movement is often synchronous with faulting, determining the timing of salt-related fault growth provides good chronological and geographic indications of salt migration.

Styles of faulting differ between the vertical and allochthonous salt provinces. Major faults are subdivided into both Master and Regional/Counter-regional growth faults. Master faults are confined to above vertical diapirs whereas Regional/Counter-regional growth faults are in the allocthonous tongue province and are related to salt withdrawal over time. Regional/Counter-regional faults in the allochthonous tongue province are generally of larger

scale (geographically and in terms of displacement) than other faults in the western study area. These Regional/Counter-regional faults typically trend east-west with growth intervals decreasing upward until Unit 8. In the vertical salt diapir province, growth faults are confined to the extent of a given vertical salt body in northwest-southeastern orientation. Offsets typically decrease stratigraphically upwards with the lower units showing the greatest amount of throw. Unit 8 shows the largest amount of growth across the study area in both Master and Regional/Counter-regional faults.

4.7.1 Master faults in the vertical salt diapir province

Master faults are present on the crests of vertical salt diapirs offsetting smaller radial faults. Where resolvable, these faults are present above all vertical salt diapirs. They are labelled according to the diapir name: MF-<diapir name>. Growth intervals occur in the upper units 5 to 8 but the resulting total offsets are largest in the lower units 1 to 4. These faults can sole into the salt body itself or its flanks, displacing all draping horizons. Crestal faulting can also penetrate upward to the seafloor (N10 horizon in Unit 9), although seafloor displacements are minimal (<200 ms or 160 m).

These faults commonly sole into the flank of the salt creating a ‘structural onlap’ contact (Figs. 4.16-4.18) where salt-sediment contacts deceivingly appear to onlap salt bodies, but in reality are truncated by a fault at the salt contact. Rafted units are affected most dramatically since they are mostly confined to the lower Units 1 to 4 that show the most offset. In these cases, fault displacement was a post-depositional process and these faults were likely active from at least the Mid-Late Miocene i.e. units 6 to 8. All master faults trend northwest-southeast in plan view.

In areas of increased localized erosion around the distal salt bodies, upper units (5 to 7) have been eroded away and therefore fault presence is difficult to determine in this younger interval over the diapirs. Similarly to other master faults, large offsets are still present in the lower Units 1 to 4, implying these growth faults were likely present but have since been eroded away in younger intervals.

4.7.2 Large offset growth faults in the allochthonous tongue province

In the allochthonous tongue province, larger salt structures generally have larger faults with greater offsets, map lengths, and offsets. Offsets here can be upwards of 700 ms. Faults in the allochthonous tongue province are labelled R (regional dipping)/CR (counter-regionally dipping)-<allochthonous tongue name> e.g. CR-A2 is a counter-regional fault above the A2 salt body.

There are 2 major growth faults around the A2 salt tongue: a counter-regional growth fault trending east-west and a regional-dipping growth fault trending northeast-southwest (Figs. 4.35 and 4.65). Both faults sole into pre-K1 strata. A regionally-dipping normal fault bounds the minibasins landward of A2 and trends east-west. This fault has been individually named R-MB (regionally dipping-minibasin) since it not located in close proximity to any particular salt body.

Between these faults are 3 intervening minibasins bounded by the R-A2 fault and a series of regional-dipping concentric faults. These are areas where salt has previously been evacuated and currently overlies the Balvenie Roho discontinuity (Fig. 4.22) Deptuck et al. 2011). These minibasins trapped sediment in paleoslope lows.

Unit thicknesses vary significantly across the CR-A2 fault. It is expected that the former bathymetric lows relate to minibasin subsidence and will accumulate more sediment than highs.

Units 1 to 4 show a thinner succession on the downthrown side of the fault likely indicating that the fault was not active during this time period or possibly even reversed. This relationship switches around in Units 4 to 8 where thickening occurs on the downthrown section of the fault and thinning on the upthrown as the fault became active. Unit 9 drapes the fault with little offset (<50 ms or approximately 40 m) although a minor step is present in the seafloor today.

4.8 Minor faults

Minor faults can be subdivided into radial and polygonal fault patterns. These faults are typically confined to Units 4 to 7. Work by Carruthers et al. (2013) suggests that radial faults are polygonal faults re-aligned around salt diapirs, and furthermore experience different spacing, length and throws.

4.8.1 Radial faults

Radial faults are faults that form roughly perpendicular to the concentric margin of the salt diapir in map view and diverge radially away from it (Fig. 4.66). Radial faulting is present around vertical diapirs where the relevant stratigraphic intervals, usually units 4 to 7, are preserved (Figs.4.15-4.18 and 4.66). Crestal erosion above distal salt bodies has eroded away the strata with most of the radial faults and only some are visible where overburden is most preserved. Generally these faults are 2 to 5 km long on the flanks of the salt body. They are densely spaced, often intersecting and merging into each other with offsets that are less than 100 ms.

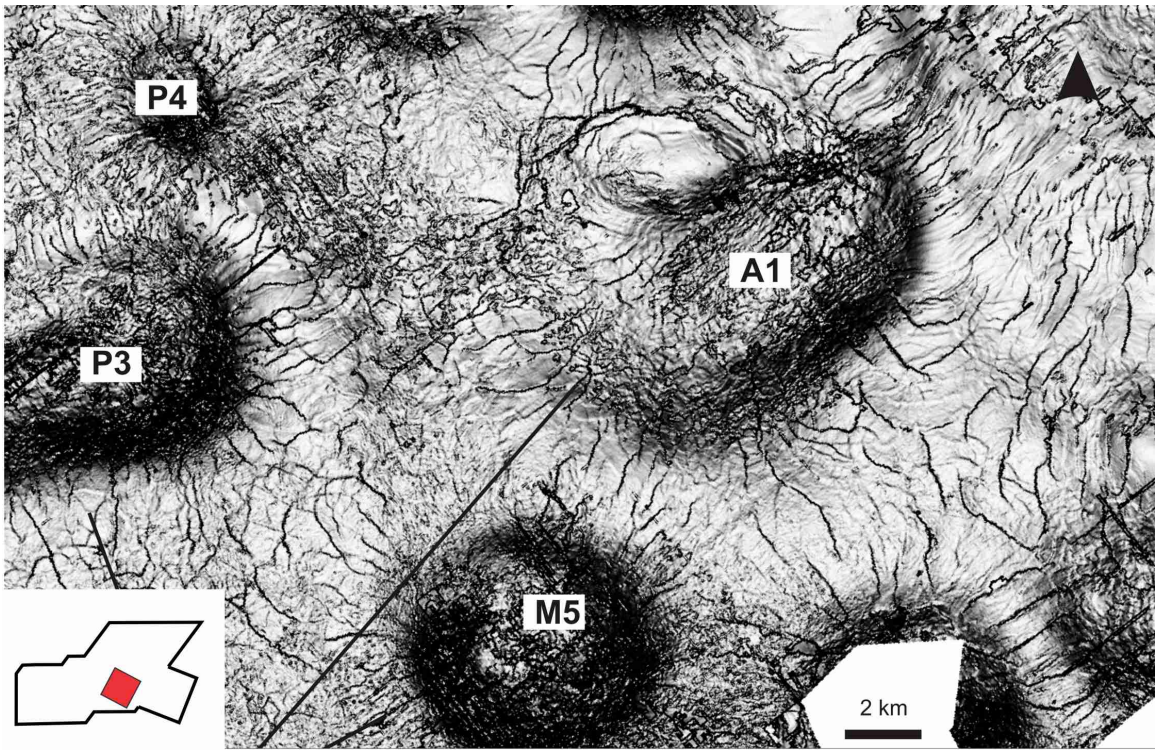

Figure 4.66: Dip map taken from the N5 Horizon. See Fig. 4.65 for a broader context. This enlarged area shows examples of radial faulting in the study area. Faults are located along the flanks of the salt bodies. Location map shown on the bottom left.

4.8.2 Polygonal faults

Polygonal faults are defined as small offset faults with less than 100 ms of throw and a more variable orientation. They are present throughout the study area but are densest around the upper slope domain. They are mostly confined to Units 4 to 6, sometimes extending into Unit 7. These faults do not extend above salt crests but are rather located at the flanks of salt bodies in the intervening minibasins and further upslope.

Polygonal faults are generally confined to one tier sometimes extending to parts of Unit 3 in the western portion of the study area (west of P3). Offsets across these faults are small, commonly less than 50 ms.

Chapter 5: Reconstructing salt-related deformation

There are several types of stratigraphic thickness variation ("thinning" or "thickening") in the study area and differentiating between these types is essential in order to distinguish the different processes responsible. For example: thinning of a stratal unit over a salt crest is an indicator of bathymetric relief over the diapir whereas thinning from canyon erosion is not. For the sake of simplifying these different types of thinning, a variety of terms are applied, and are listed in the table below (Table 5.1).

Types of stratigraphic thickness variation in the study area	
Term	**Process**
Stratal or depositional thinning	Thinning of a sedimentary unit over a salt structure due to bathymetric relief i.e. a fold or salt crest
Erosional thinning	Thinning due to erosional removal of strata, unrelated to diapir bathymetric relief (e.g., canyon erosion)
MTD tapering	Inherent thinning of a mass transport deposit with distance from its source due to the depositional process
Slope tapering	Regional-scale wedges of sediment that taper upslope or downslope
Minibasin thickening	Preferential infill of a minibasin as it subsides due to salt evacuation

Table 5.1: Classifications of stratal thinning and the different processes responsible in the study area.

5.1 Stratal thinning above salt bodies

In order to come up with a way to measure the magnitude and timing of the lateral compression (thought to be responsible for folding diapir crests and other structures), it was essential to measure the stratal thickness variations above salt diapirs relative to their flanks. The assumption is that more crestal thinning indicates more compression as the underlying salt diapir

displaces overburden upward on the seafloor creating a bathymetric high. Sediments, therefore, thin above the salt crest due to the effect of seafloor terrain on the depositional process.

A quantitative technique was attempted, but it proved too subjective to choose the location of measurements around the diapir structure and it was difficult to accommodate the effects of rafting, crestal erosion, depositional thickening/thinning (canyon/inter-canyon), and major crestal faults into the process. Instead, a simpler and qualitative approach was utilized, subdividing stratal/depositional thinning into 3 categories and explained with example seismic sections presented below (Figs. 5.1-5.5):

- Obvious diapir-related thinning (red)
- Subtle diapir-related thinning (yellow)
- Little to no diapir-related thinning (green)

The employment of a simpler approach allows each salt diapir to be color-coded (red, yellow and green) and plotted on a map through time (each stratigraphic unit). Such a technique can determine spatial patterns of implied salt motion during a period of lateral compression or other types of salt deformation. Example seismic sections are presented below (Figs. 5.1-5.5) to demonstrate the principles used and some of the challenges to proper interpretation.

Abbreviations were used for minor erosion to indicate the occurrence of erosion above the crest of the diapir (indicated as *ME* for minor erosion or *CE* for complete erosion of the unit above the crest of the salt diapir (Figs. 5.2 and 5.4). In the case of complete erosion (CE), stratal thinning of eroded units was extrapolated from the flanks where the unit is most preserved and may still show the initial stages of thinning towards the now-removed strata over diapir crests. Although speculative in some areas, a map of unit thicknesses (including areas of significant

crestal erosion) could be generated for each unit above salt bodies in the study area. In order to measure active diapirism, only salt bodies with diapir-related depositional thinning have been classified and not erosional thinning (Fig. 5.4). Salt bodies that show erosional thinning alone are in the green category with little to no depositional thinning since they are not related to active diapirism.

In contrast to thinning of stratigraphy over diapir crests, the 3 minibasins in the area of the allochthonous tongue province have variations in depositional thickness that relate to withdrawal of underlying salt ("minibasin thickening"), immediately adjacent to the corresponding allochthonous tongues themselves. The 3 minibasins are labelled B1, B2, and B3 and are colour-coded according to the amount of minibasin thickening (red), a moderate amount of thickening (yellow), and minor or no thickening (green) within a given unit compared to the area surrounding the minibasin. Although this colour coding is the opposite of that for thinning (e.g., red is the thickest for minibasins, thinnest for diapir crests), the colouring is consistent in terms of the relative amount of salt tectonic activity implied (i.e. red is greatest activity, green the least).

Within all the thickness measurements and map representations, Units 1 and 2 were lumped together within the study area because the surface dividing between these units (i.e. the K85 horizon) was only available in the vertical salt diapir province. Both the K1 and P2 horizons extend over the majority of both salt provinces and therefore stratal thinning could be determined across both salt provinces for this composite interval.

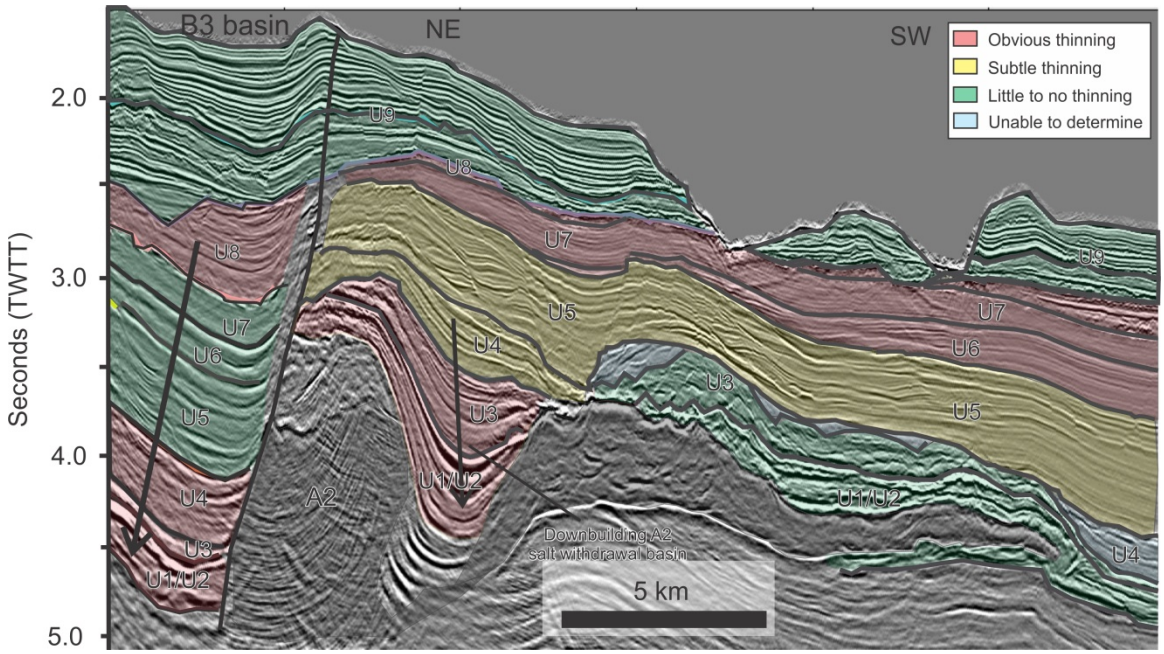

Figure 5.1: Cross section across the allochthonous tongue province (A2 tongue) through its withdrawal basin. Units 1-4 show no stratal thinning but rather minibasin thickening from downbuilding (see Table 5.1). Unit 5 shows some gradual (subtle) stratal thinning passing into obvious thinning in Units 6-8. Unit 9 is mostly eroded from modern canyon development and where preserved, no stratal thinning is obvious.

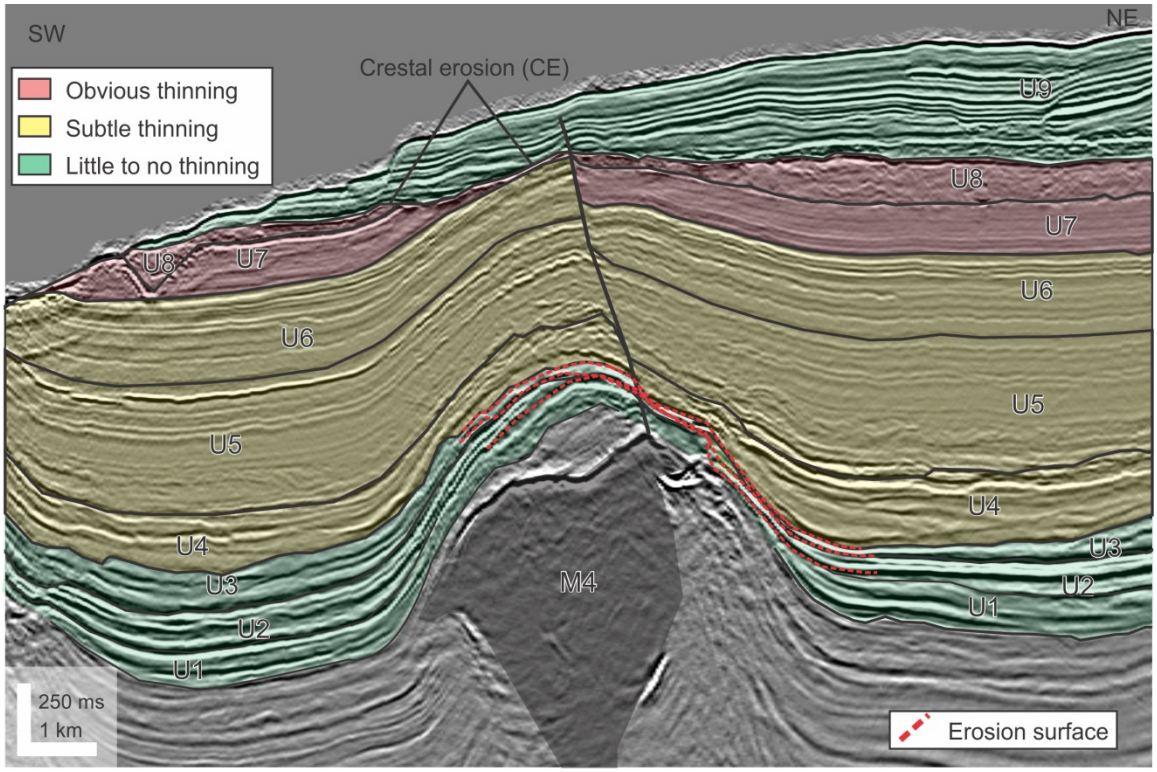

Figure 5.2: Cross section through the medial salt body M4. This salt body shows a variety of stratal variations. Again, Units 1 to 3 do not show any stratal thinning but rather erosional thinning related to canyon development (red lines; see Fig. 5.3 below). Thinning in Units 4-6 is subtle (yellow) passing into obvious thinning in Units 7 and 8. Units 7 and 8 are truncated by crestal erosion related to the widespread erosion and slope regrading that occurs at horizon N8. After the erosion, Unit 9 shows no stratal variations related to the salt diapir.

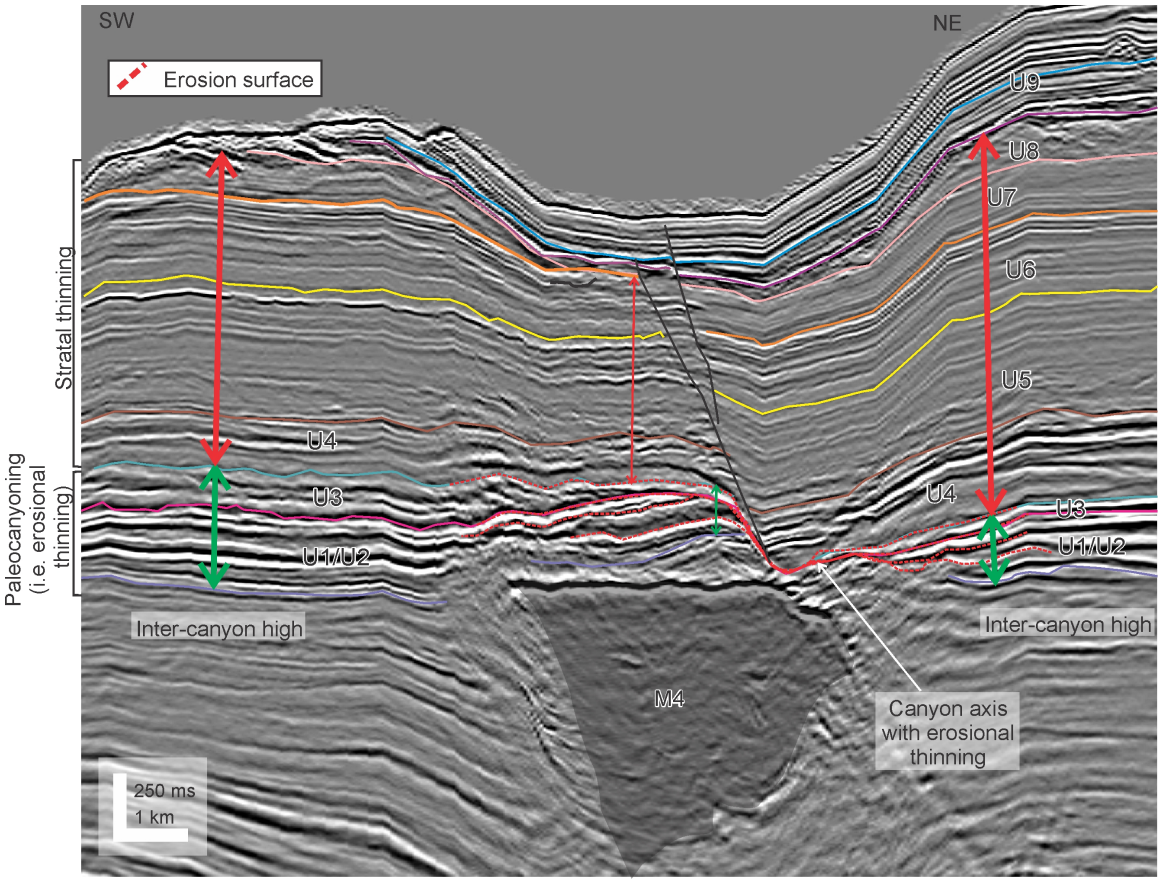

Figure 5.3: Flattened version of Figure 5.2 showing the canyon axis formed in Units 1 to 3 (red dotted lines) that has since been uplifted. Prior to uplift it would have likely looked similar to this. Note the thickening on the flanks of the diapir in Units 1 to 3 (green arrows) are inter-canyon highs and thinnning occurs along the canyon axis where it is the most eroded (red dotted lines). Thus stratal thinning in Units 1 to 3 in this diapir appears to be solely from canyon-related erosional thinning and not from diapir-related stratal thinning.

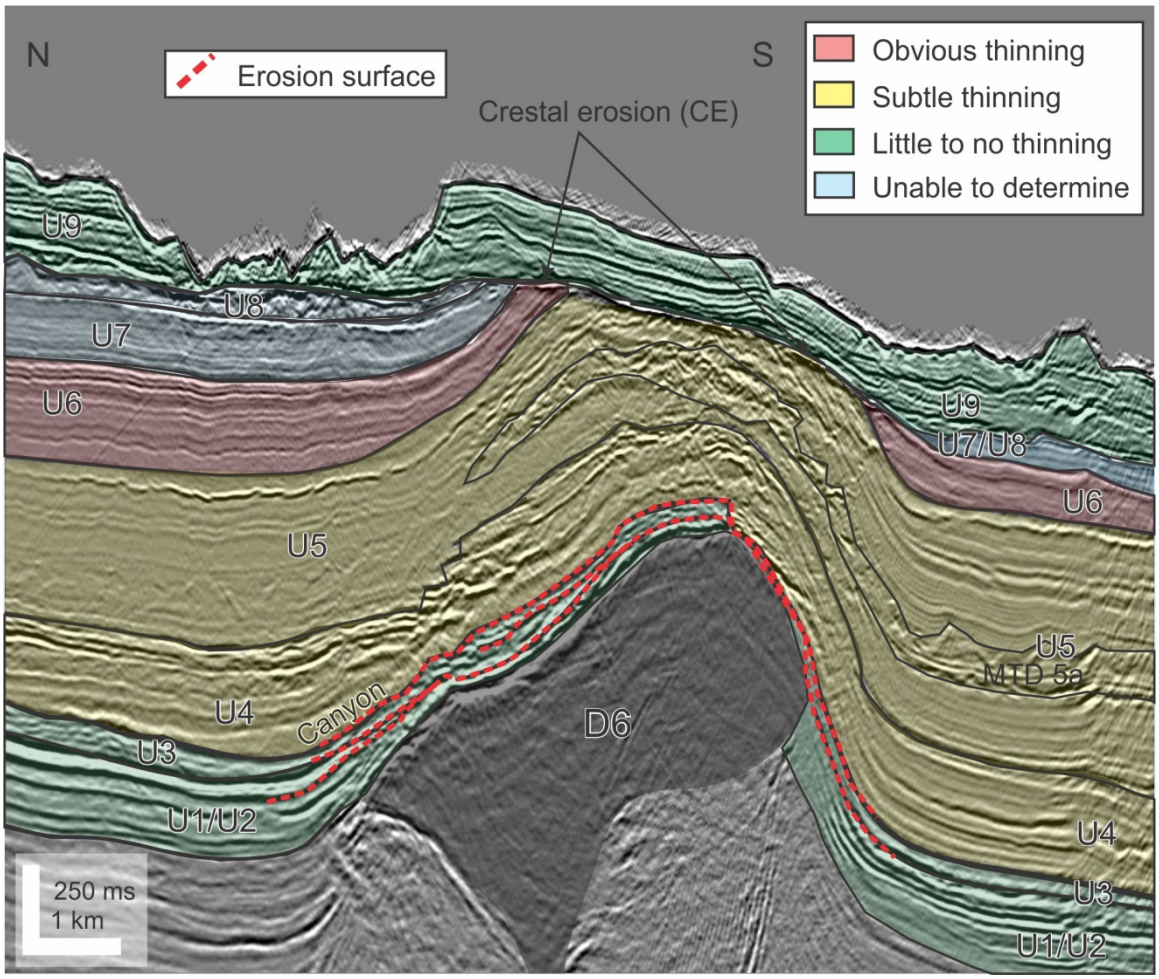

Figure 5.4: Cross section through the D6 salt body. Units 1-3 show canyon-related erosional thinning with several erosion surfaces cutting into the underlying stratigraphy (red dotted lines). Units 5-8 are truncated above the salt crest and thus diapir-related thinning is extrapolated from the flanks of the salt body where variations in thickness are evident well before reaching the crest. Units 4 and 5 show subtle diapir-related thinning passing into obvious thinning in Unit 6. Thickness variation in Units 7 and 8 was not confidently determinable because of excessive erosion around this area. This salt body is also very close to the edge of the survey making it difficult to determine regional thinning south of the salt body. No diapir-related stratal variations are present in Unit 9.

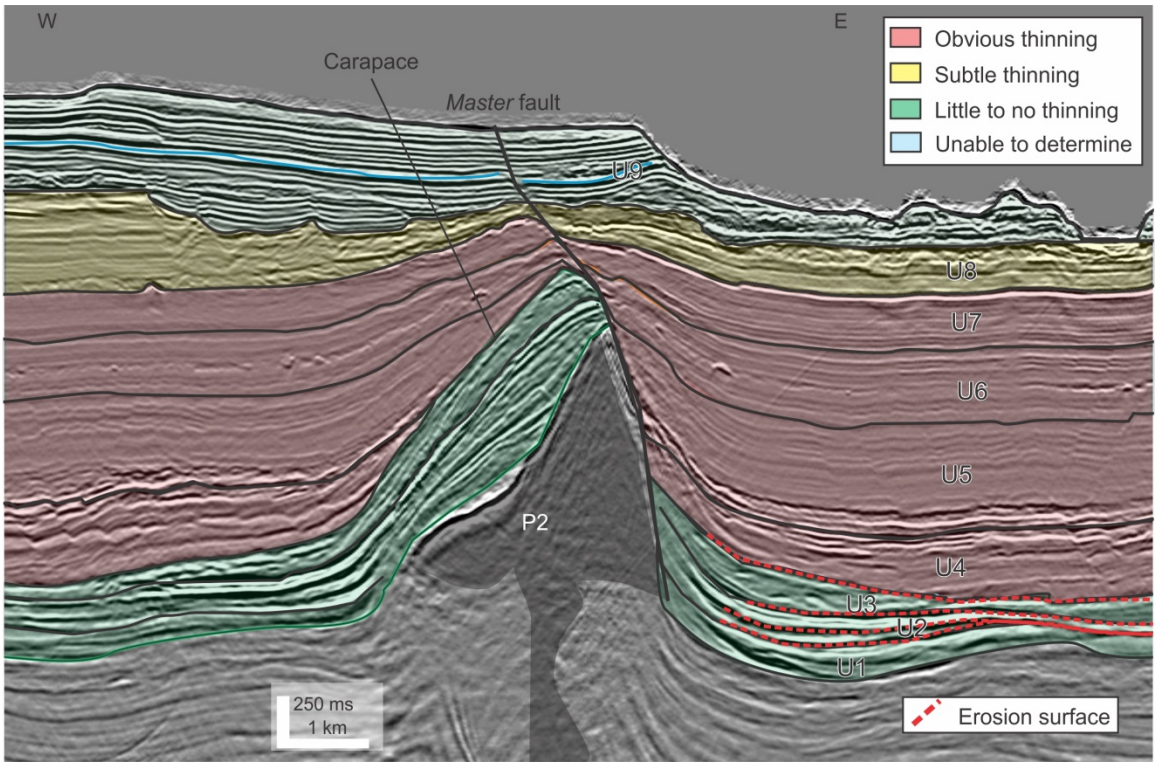

Figure 5.5: Cross section through the P2 salt body. No diapir-related stratal is present in Units 1 to 3. Obvious diapir-related stratal thinning is present in Units 4-7, changing to subtle thinning in Unit 8. No diapir-related stratal thinning appears to present in Unit 9.

5.2 Stratal thinning maps

Figures 5.6 to 5.13 are maps that summarize the presence of diapir-related stratal thinning and the thickening of minibasins over the time of each stratigraphic Unit, and thus show the timing of salt motion in the study area. Units 1 to 3 show no diapir-related stratal thinning, but do show widespread canyon-related erosional thinning. Depositional loading in minibasins is absent in the B2 basin during this time and thicker sedimentation and minibasin growth mostly takes place in B3 and B1 (Figs. 5.6-5.7). Both minibasins on top of A1 and A2 also show growth during this phase from downbuilding above the salt tongue.

Clear diapir-related stratal thinning above diapir crests begins within Unit 4 in the vertical salt diapir province (Fig. 5.8). Generally, salt diapirs west of diapir M4 and in the middle section of the study area show obvious diapir-related stratal thinning. In contrast, this unit has been

eroded away at the crest of the A1 and A2 tongues. It appears that some thinning is visible on the flanks of vertical saltdiapirs however the extent of erosional thinning from canyon development versus diapir-related thinning is cryptic and thus an accurate gauge of stratal thinning could not be obtained.

Minibasin A1 stops growing and is no longer active from Unit 4 onward. B1 and B2 show upslope loading during Unit 4 deposition. B2 shows minor sedimentation compared to adjacent basins B1 and B3. The minibasin in the A2 tongue shows subtle growth (yellow) during this phase from downbuilding above the salt tongue.

Unit 5 (Fig. 5.9) has similar patterns to Unit 4 with obvious thinning mostly west of A1. Salt bodies P3, M3, M4, P6, D8 and A2 show subtle diapir-related thinning while P4 and P5 show no thinning. Minibasin thickening has shifted to B2 and B3 in this interval. In contrast, minibasin thickening in the A2 withdrawal basin ceases in this interval and it is no longer active from this point on.

Unit 6 (Fig. 5.10) has a prominent regional trend of obvious diapir-related thinning across the study area with the exception of M3, P4 and P5 which show no stratal thinning. M4, P3 and D8 show subtle thinning. In the southern portion around the distal diapirs, minor erosion becomes apparent from the effects of erosion downcutting from the N8 horizon. In the allochthonous tongue province, minibasin thickening has preferentially shifted into the B1 and B2 basins and is largely absent in B3.

Unit 7 (Fig. 5.11) shows similar obvious thinning, again in the western portion of the study area (P1, M1, M2, M3, D1, D2, D3, D4 and D5) and the A2 allochthonous tongue. Diapirs P2, P4, P6, M4, D8 and salt tongue A1 show subtle thinning while diapir P3 shows no stratal

thinning. Diapir P5 is intersected in map view by a large Miocene canyon system eroding into Unit 7 significantly. This diapir lies along the axis of the canyon and therefore it was not possible to extrapolate thinning from its flanks. Diapirs D6 and D7 show significant erosion from modern day canyon development coupled with increased erosion from the N8 horizon. Preferential sediment accumulation is again focused in minibasins B1 and B2 and mostly absent in B3.

Similar to Unit 7, Unit 8 (Fig. 5.12) has obvious thinning confined to the west (west of M4, with the exception of P2/D4), also including M4, M5, D8 and A2 (in the east). D6 and D7 have been truncated significantly from modern canyon erosion, as has the P4 salt diapir from a Miocene paleocanyon system. Salt diapirs that show subtle thinning are only P2, D4 and A1 with proximal diapirs P3, P5, and P6 displaying no thinning. Minibasin thickening is focused in minibasins B1 and B2. Minibasin thickening favours the B1 and B2 basins.

Unit 9 (Fig. 5.13) shows some stratal thinning mostly confined to the western portion of the study area (i.e. P1, P3, M2, M3, D1 and D2) and M1, M5 and D4 show subtle thinning. The remainder of salt bodies show little or no thinning in this interval, where it is possible to determine. Documenting thinning in this interval was particularly difficult across much of the study area because of the variable topography caused by modern day canyon development and erosion.

Overall, proximal salt bodies P3 to P6 appear to have their own pattern of activity compared to the rest of the study area. Diapirs P4 to P5 are not ‘active’ for most of the units i.e. they generally show no thinning from Units 5 to 9 and salt bodies P3 and P6 (adjacent to P4 and P5) are less ‘active’ with subtle or no thinning between Units 5 to 9 (with the exception of P3 in Unit 6 and P6 in Unit 9).

There appear to be a few anomalies that do not follow the regional trend of activity when compared the surrounding salt bodies. They occur in M3, M4 and D8. For example, M3 shows no diapir-related thinning in the overall most 'active' interval Unit 6. Although proximal diapirs P3 to P6 show distinct results when compared to the regional trends, they are consistent with each other, and therefore appear to follow their own local trend in stratal thinning likely related to a large canyon system overlying them or some other factor. In contrast M3, M4 and D8 do not appear to follow any regional pattern.

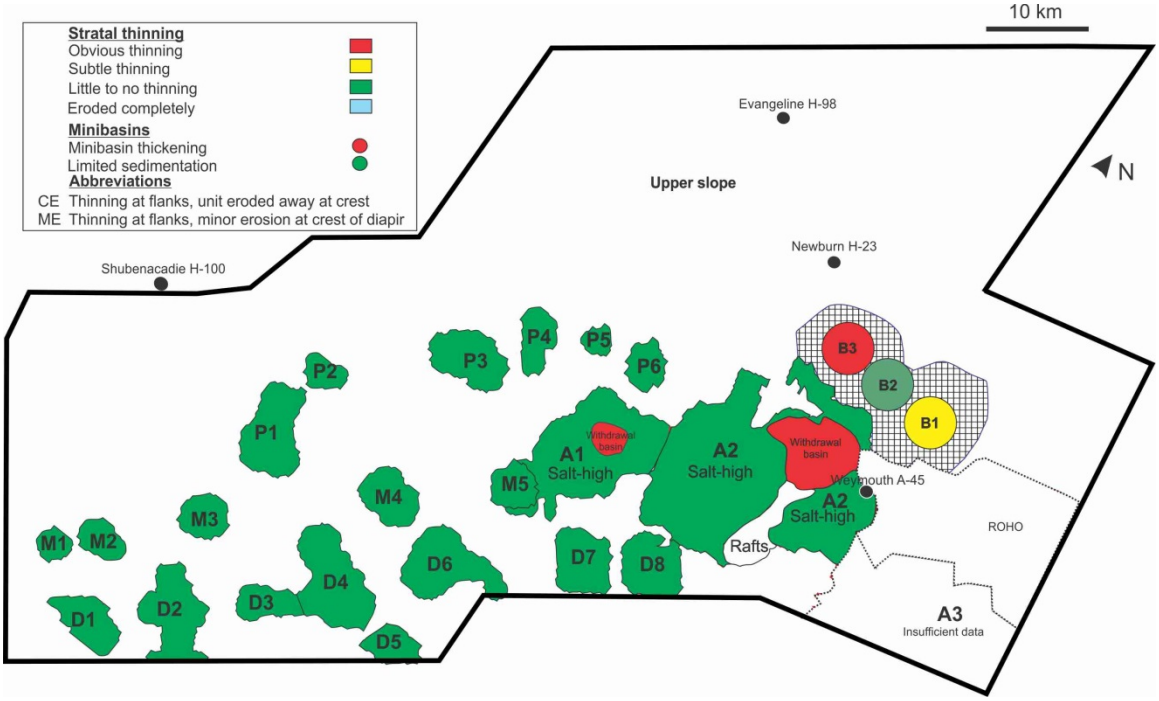

Figure 5.6: Diapir-related stratal thinning patterns over salt diapirs in Unit 1/2.

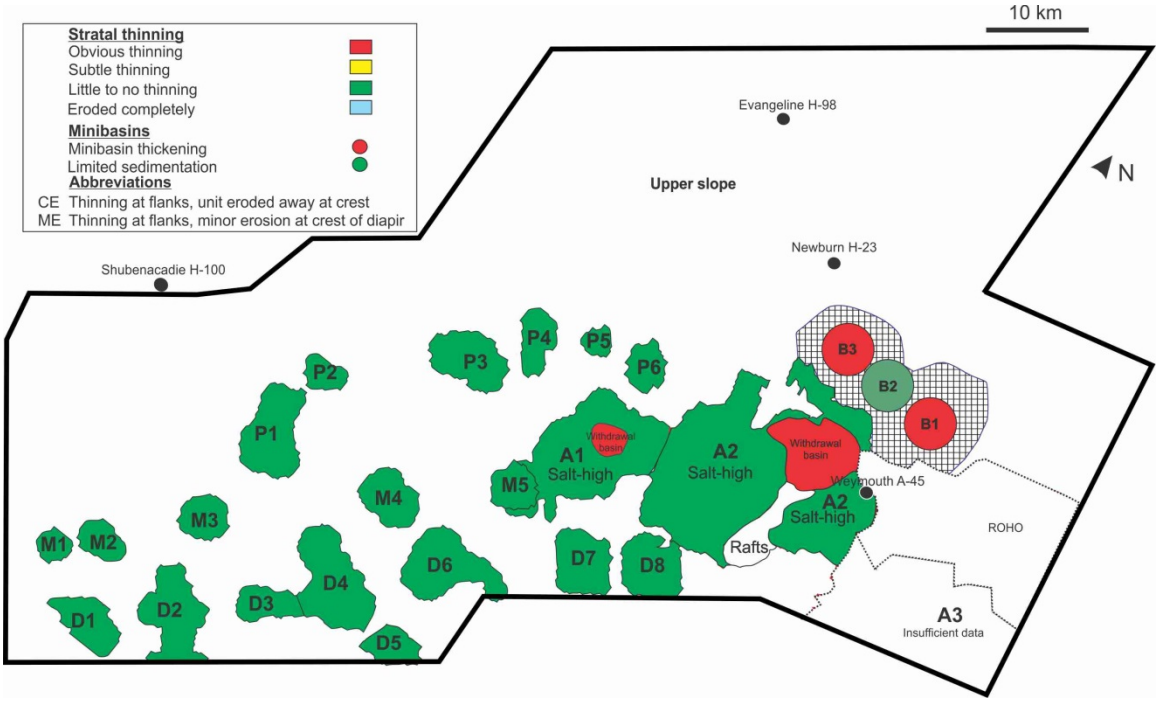

Figure 5.7: Diapir-related stratal thinning over salt bodies in Unit 3.

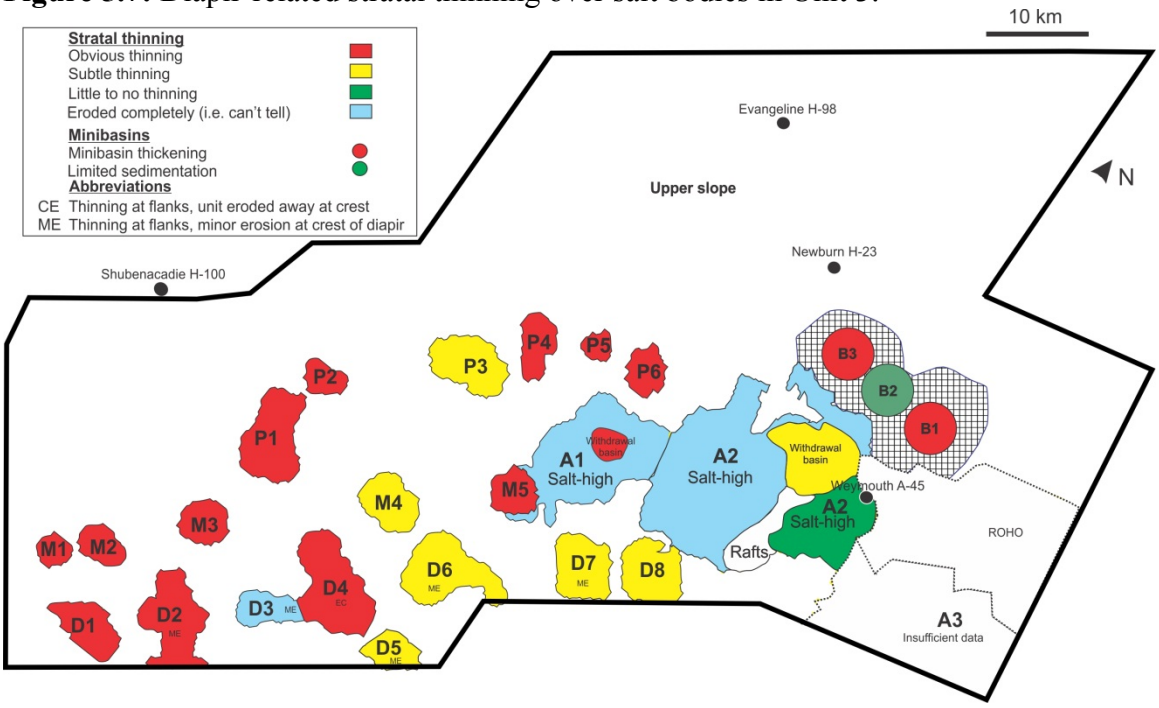

Figure 5.8: Diapir-related stratal thinning over salt bodies in Unit 4.

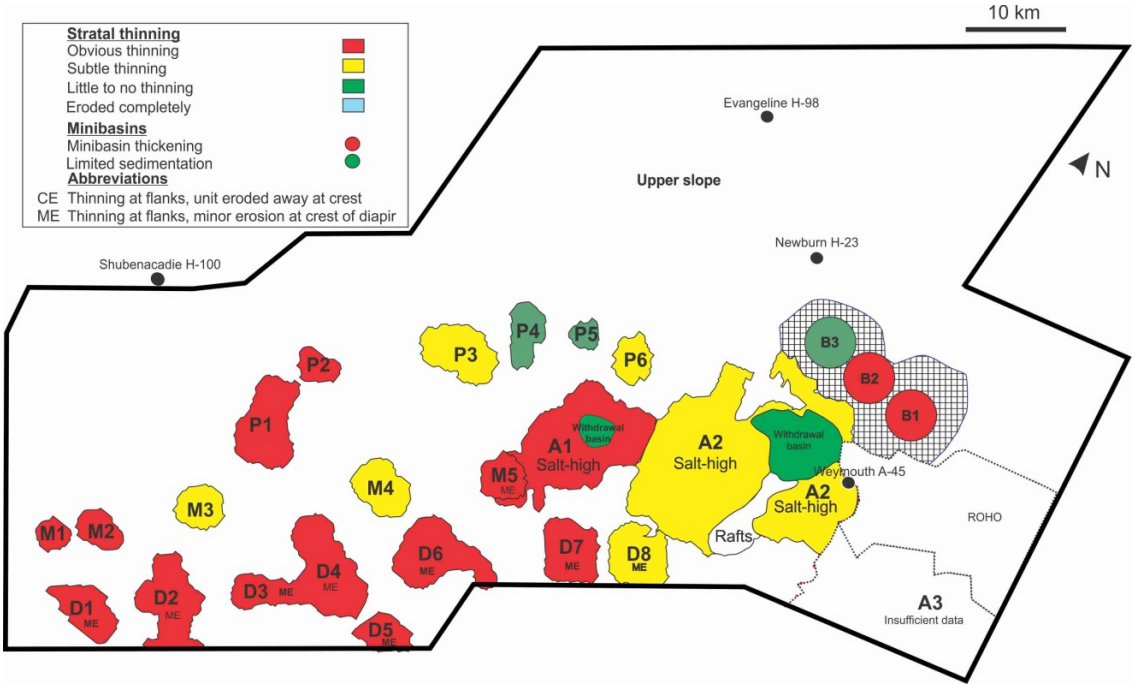

Figure 5.9: Diapir-related stratal thinning over salt bodies in Unit 5.

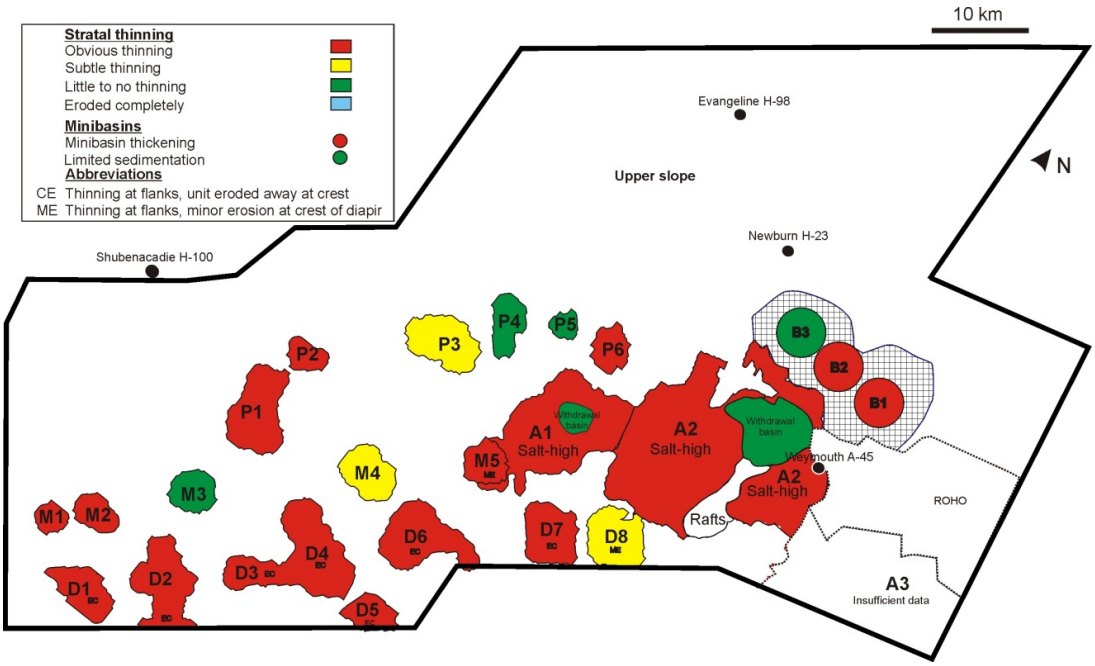

Figure 5.10: Diapir-related stratal thinning over salt bodies in Unit 6.

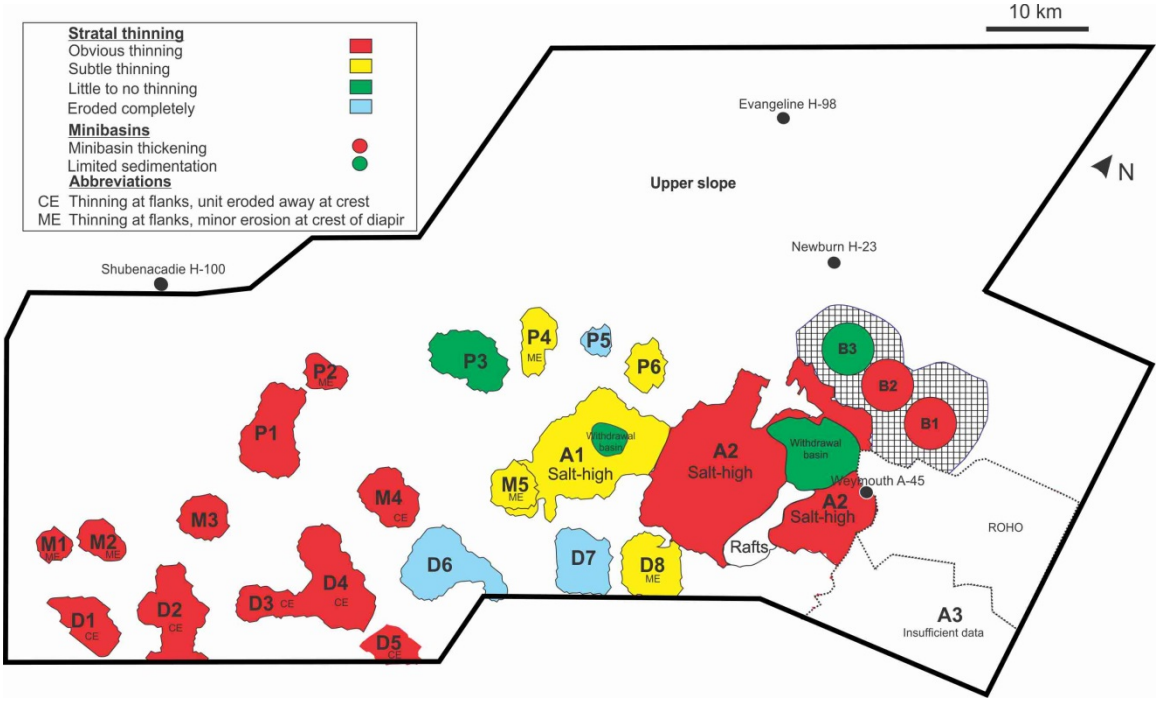

Figure 5.11: Diapir-related stratal thinning over salt bodies in Unit 7.

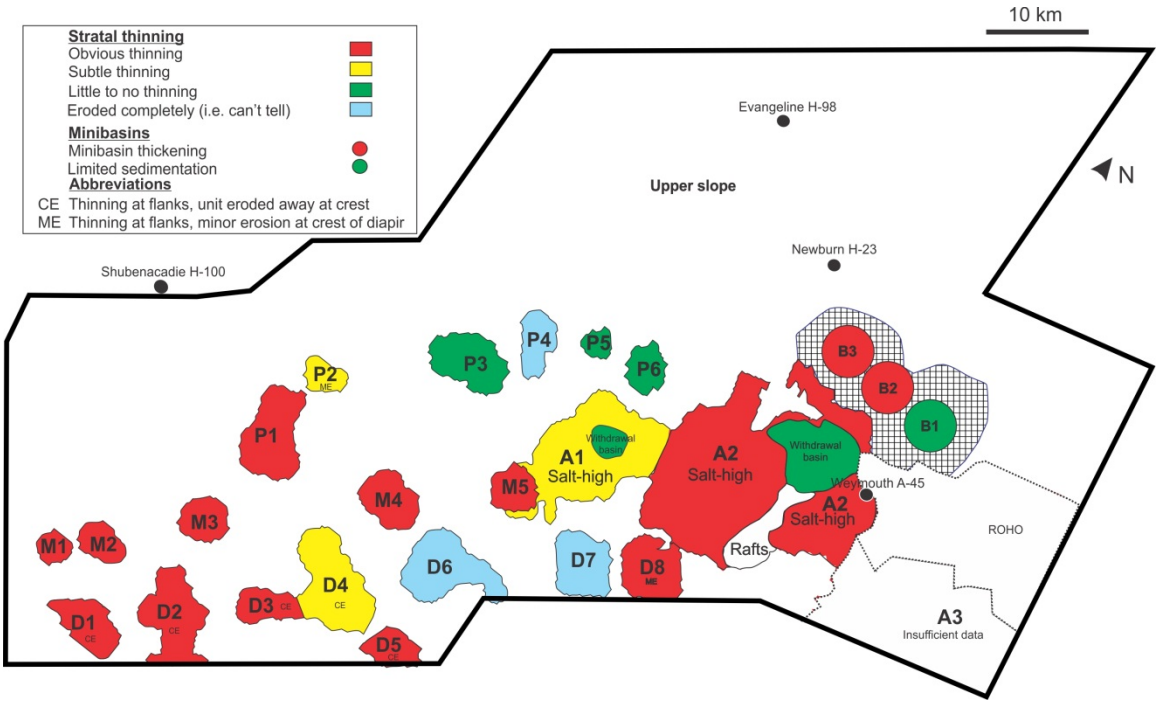

Figure 5.12: Diapir-related stratal thinning over salt bodies in Unit 8.

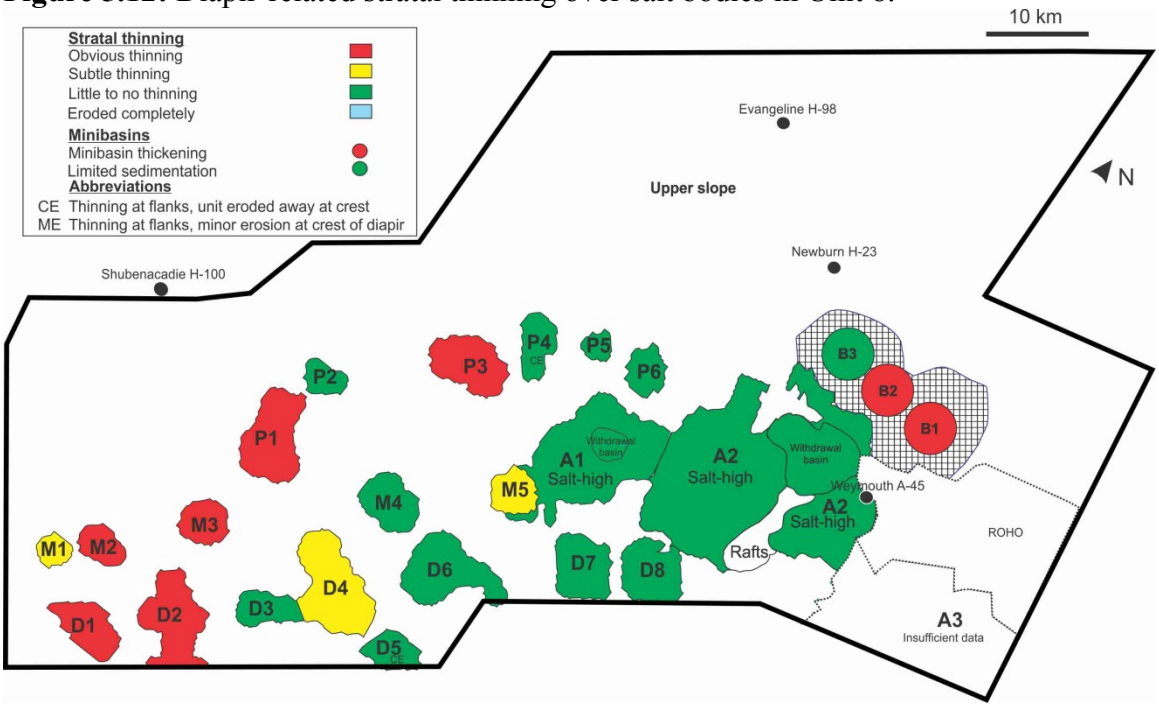

Figure 5.13: Diapir-related stratal thinning over salt bodies in Unit 9.

5.3 Challenges to determining diapir-related stratal thinning

Relationships between structural uplift of a raft/carapace and depositional thinning in units can be deceiving. Diapir-related thinning at the crest of diapirs is an important component of determining the extent of salt movement during active diapirism although it was often challenging to distinguish from other causes for variation in stratigraphic thickness. This section describes the nature of these challenges and how they were resolved. It also identifies discrepancies from the overall pattern observed in the relevant time intervals.

5.3.1 Units 1 to 3

Difficulties were encountered while attempting to distinguish diapir-related stratal thinning versus thinning in units due to erosion along canyon axes. For example, thinning of a stratal unit due to erosion along a canyon axis that has been subsequently lifted by active diapirism above a salt diapir can mimic the appearance of depositional stratal thinning of the unit around a topographic high. In order to try and correct for this issue, a time-thickness map (isochron) using Deptuck and Campbell's (2012) K-85 marker and the P3 horizon was used to determine the paleocanyon pathways in the interval of Units 2 and 3 (Fig. 5.14). Salt diapirs that intersect canyon systems were further examined to determine if these canyons show signs of being modified (uplifted) since deposition. It is expected that a canyon axis would show thinning above a salt diapir (in Units 2-3) and subsequent canyon infill (Unit 4) would be thicker. The opposite relationship would occur for inter-canyon highs over a diapir, which may correspond to a carapace if lifted during later compressional active diapirism.

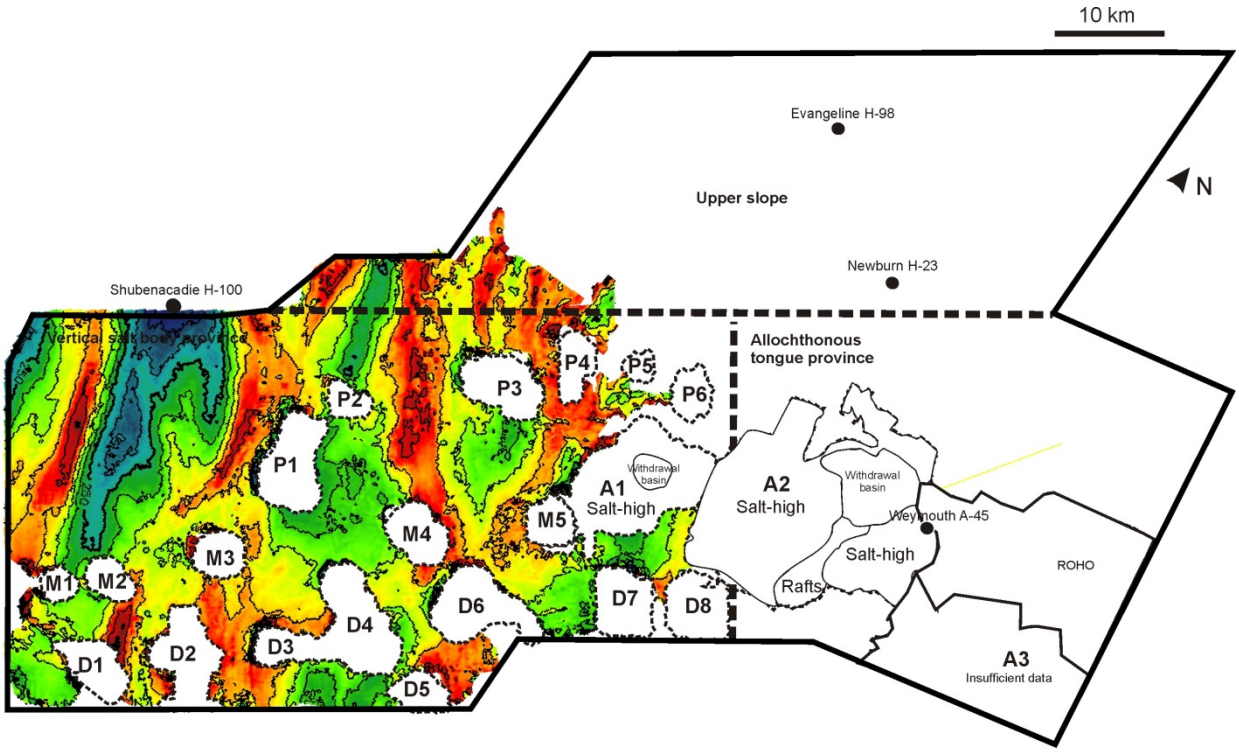

Figure 5.14: Isochron map of Units 1 to 3 showing paleocanyon development pathways in the study area affecting Units 1 to 3. In this rendition, infilled canyon thalwegs are red (thick) while inter-canyon highs are blue-green (thinning).

Diapirs that intersect canyons are P4, M3, D1, D2, D3, D5 and D6, and salt bodies partially affected by canyons are P1, P3, M1, M2, M4 and M5 (Fig. 5.14). Salt structures that do not intersect canyon axes at all are P2, D7 and D8 (Fig. 5.14). Salt bodies P5 and P6 are at the edge of the mapped horizons in the interval of Units 2 and 3 but appear to be intersected by smaller paleocanyon systems. With this information, the position of canyons and their effect on stratal thickness was carefully assessed for each diapir. This was done prior to assessing whether thickness variations were due paleo-bathymetric effects from uplift of the diapir alone.

With the consideration of canyon and inter-canyon thickness variations in mind, diapirs in Units 1 to 3 show no diapir-related stratal thinning when further examined and compared to the K85-P3 isochron. Canyons also show no notable relationship to the position of diapirs, and Units 1 to 3 occur as rafts/carapaces today further indicating these salt bodies were not

topographic highs or ‘active’ during this time period, but rather have been uplifted since deposition. The majority of present-day structural relief over the diapirs is therefore due to post-Unit 3 salt motion, and any relief that may have existed due to waning passive diapirism during Units 1-3 deposition was minor and not sufficient to affect canyon development.

Stratal thinning related to the structural uplift of the diapirs begins in Unit 4. When comparing canyon pathways and thinning of overburden in this unit, it would be expected that in this unit thickening would be seen along canyon axes and thinning would be along inter-canyon axes in a period of quiescence (no salt movement). Instead, stratal thinning is visible along both canyon axes (e.g. salt bodies P4 and M3) where thick packages are expected and along inter-canyon highs throughout most of the study area.

5.3.2 Units 4 to 8

Patterns of thinning in Units 4 to 8 suggest a period of active diapirism in both the vertical salt diapir and allochthonous tongue provinces with Unit 6 showing the greatest amount of depositional thinning across the study area. It is not possible to account for the observations with passive diapirism because of the clear indications that passive diapirism had ceased by this time (see Chapter 6 below). Although regional trends in stratal thinning can be deduced, the extent (or lack thereof) of stratal thinning in a given unit differs throughout the study area and some diapirs are active when others are not. For example, the M4 diapir shows different thinning patterns relative to the D4 diapirs which are less than 10 km away. M4 appears to be an outlier differing to the regional trends of other salt structures in the study area. The P4 and P5 (and partially P3 and P6) diapirs that show no thinning in comparison to the regional stratal thinning trends in the upper Units 4 to 8 also show different patterns relative to other salt bodies in the area. This may be related to the small size of these diapirs relative to the others.

5.3.3 Stratal thinning in mass transport deposits

Since mass transport deposits are instantaneous events (relative to geological time), thickness variations across a given MTD provide insight into paleo-seafloor bathymetry during their deposition; local thinning of these deposits should take place in areas of positive sea floor relief related to active diapirism.

In order to determine active diapirism, the extent of stratal thinning versus "MTD tapering" (Table 5.1) was important to quantify over the salt crests. MTDs taper outward as they pass downslope thinning away from the central flow axes. These other stratal variations across a salt diapir can be deceiving and stratal thinning from a paleo-topographic high can be easily confused for the natural tapering of the deposit. In order to correctly determine if stratal thinning is present it is important to get the distribution of the MTDs in plan view as well as several transects around the diapir to determine the direction of MTD tapering.

An example of this is shown from the large MTD 5a deposit that shows stratal thinning above the P3 diapir in the upper slope but none around the M3 diapir (Figs. 5.15 and 5.16). It can then be concluded that the M3 diapir formed more of a subtle topographic high than the P3 diapir. In other words, salt diapir P3 was more active during this time than the M3 diapir.

5.3.4 Slope tapering and stratal thinning

Stratal thinning related to diapirs versus broader regional "slope tapering" of a unit is also essential to differentiate in the study area. In this study, several units showed either thickening-landward (Unit 8) or thickening-seaward (Unit 5) successions. Broader tapering of units in either direction must be taken into account when analyzing localized stratal thinning from active diapirism. For example, it is expected that diapirs in a thickening-seaward succession would

show the depositional tapering above salt crests when taking dip lines (Fig. 5.15). In a strike line however, no such variation would be obvious. Although thinning due to broader regional thickness variations may be gradual, it is not a result of active diapirism but rather, the unit tapering downslope (Fig 5.16).

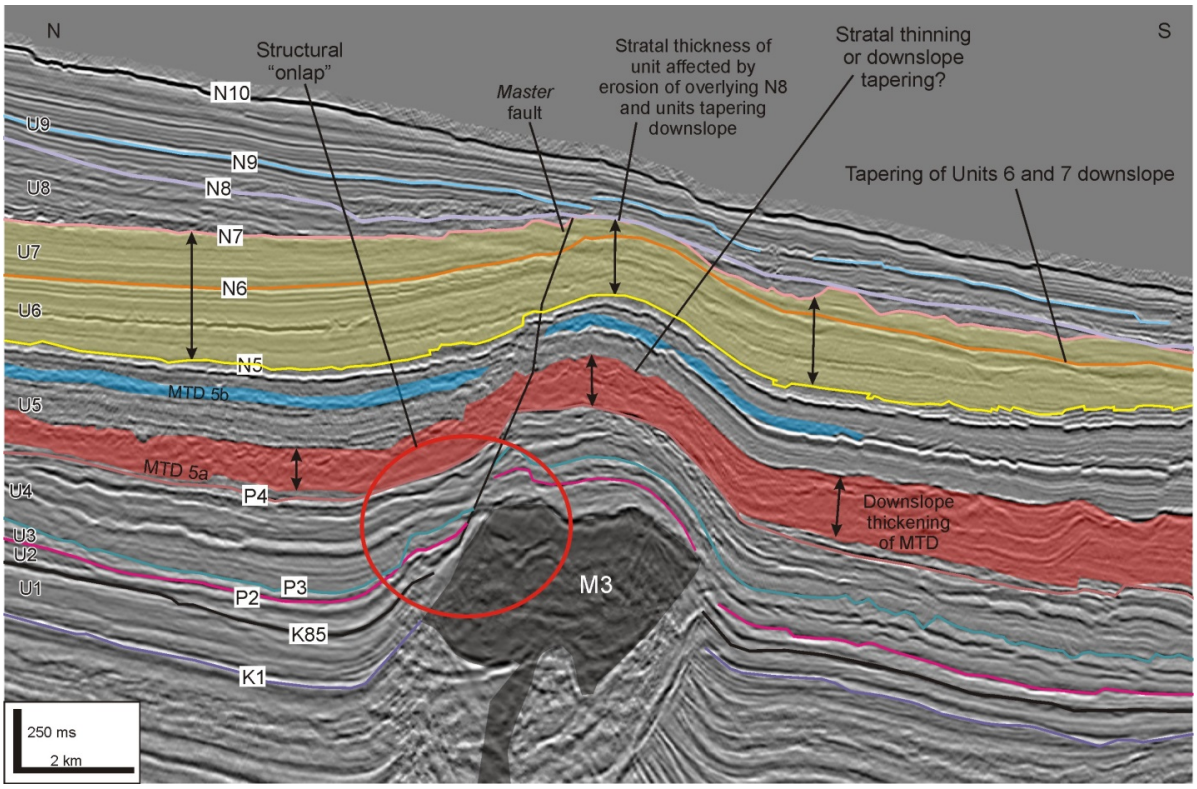

Figure 5.15: Seismic image showing the difficulty when determining stratal thinning in a given unit. A dip line such as this more readily shows the slope-tapering trend of Units 6-8. MTD 5a also has a thickening-seaward pattern that is obvious in a dip line.

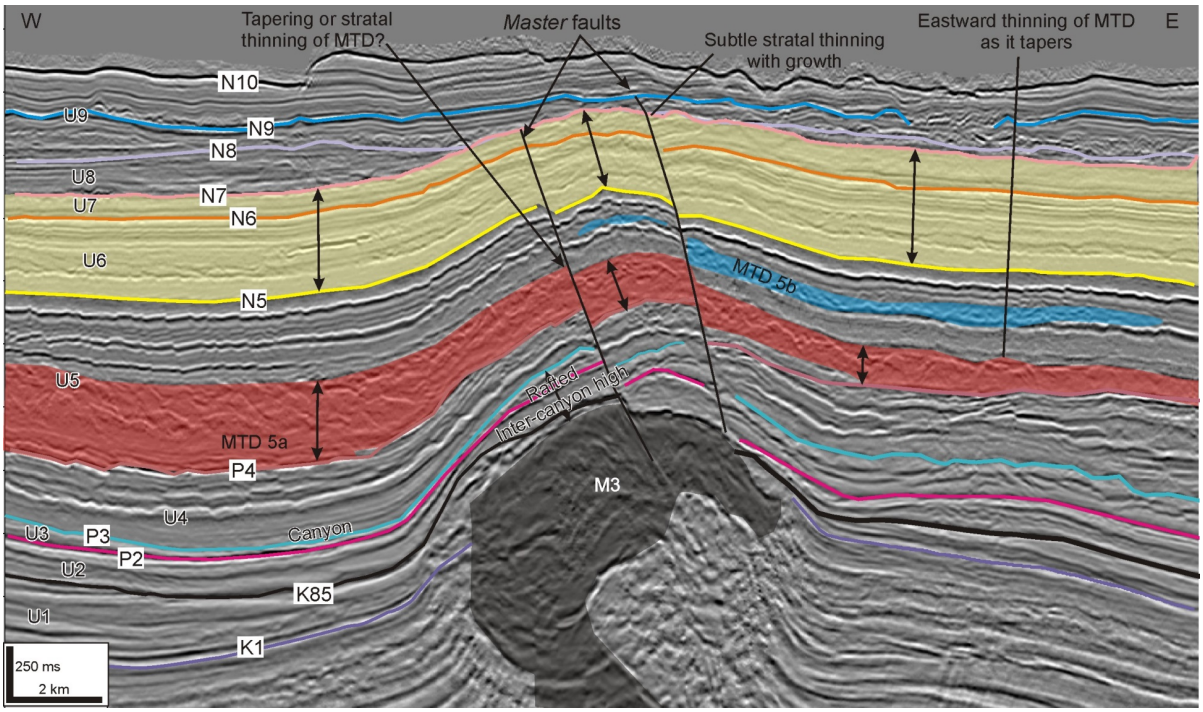

Figure 5.16: In a strike line, it is less easy to recognize stratal thinning due to inherent MTD processes versus structural/bathymetric relief. With the diapir-independent tapering of the MTD 5a, stratal thinning due to the structural relief of the diapir is also less obvious and difficult to determine. Slope tapering is less obvious in a strike line. What may look like subtle stratal thinning in this profile appears to be moreso related to varying regional depositional trends from minibasin to minibasin.

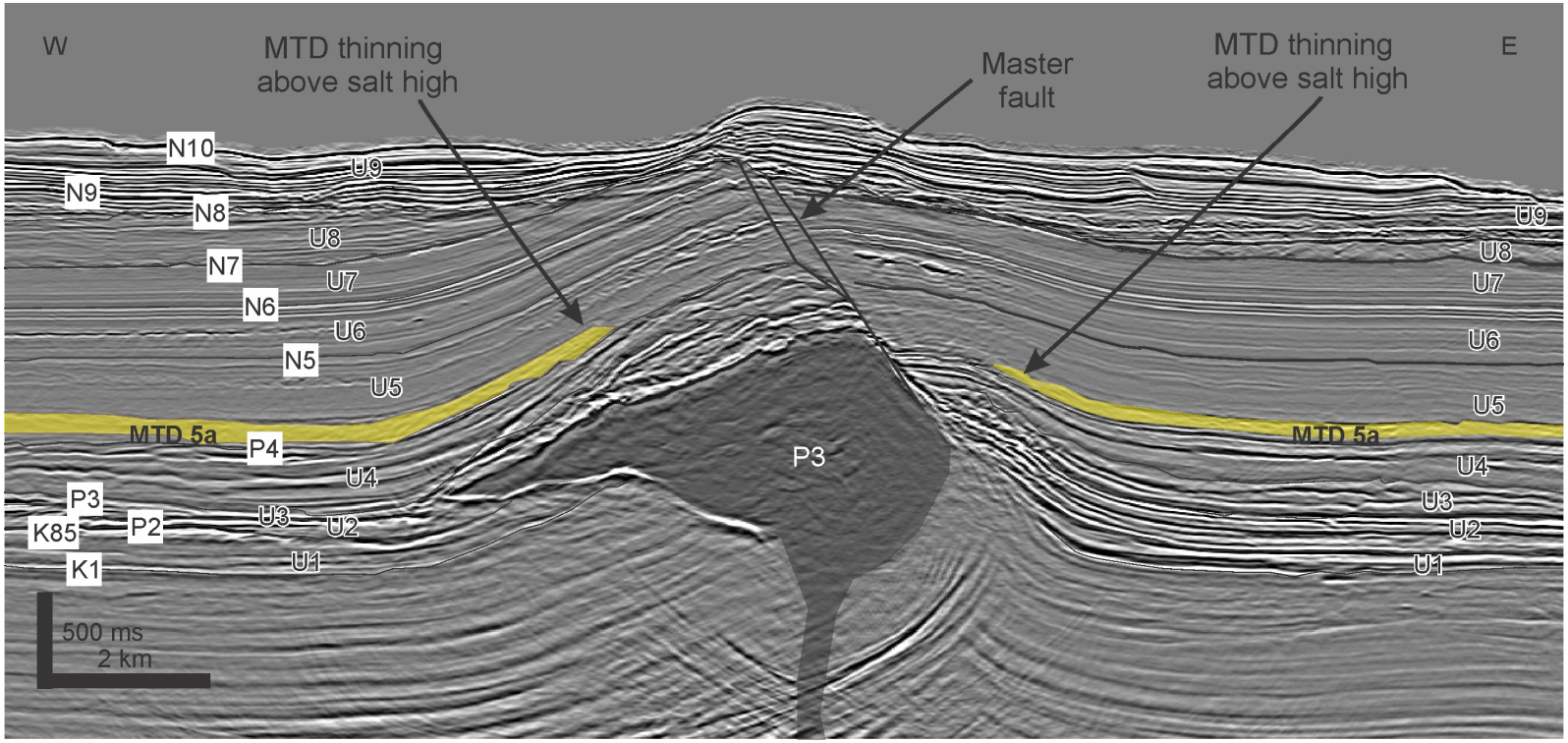

Figure 5.17: A strike line showing stratal thinning of the same MTD 5a over a diapir further upslope.

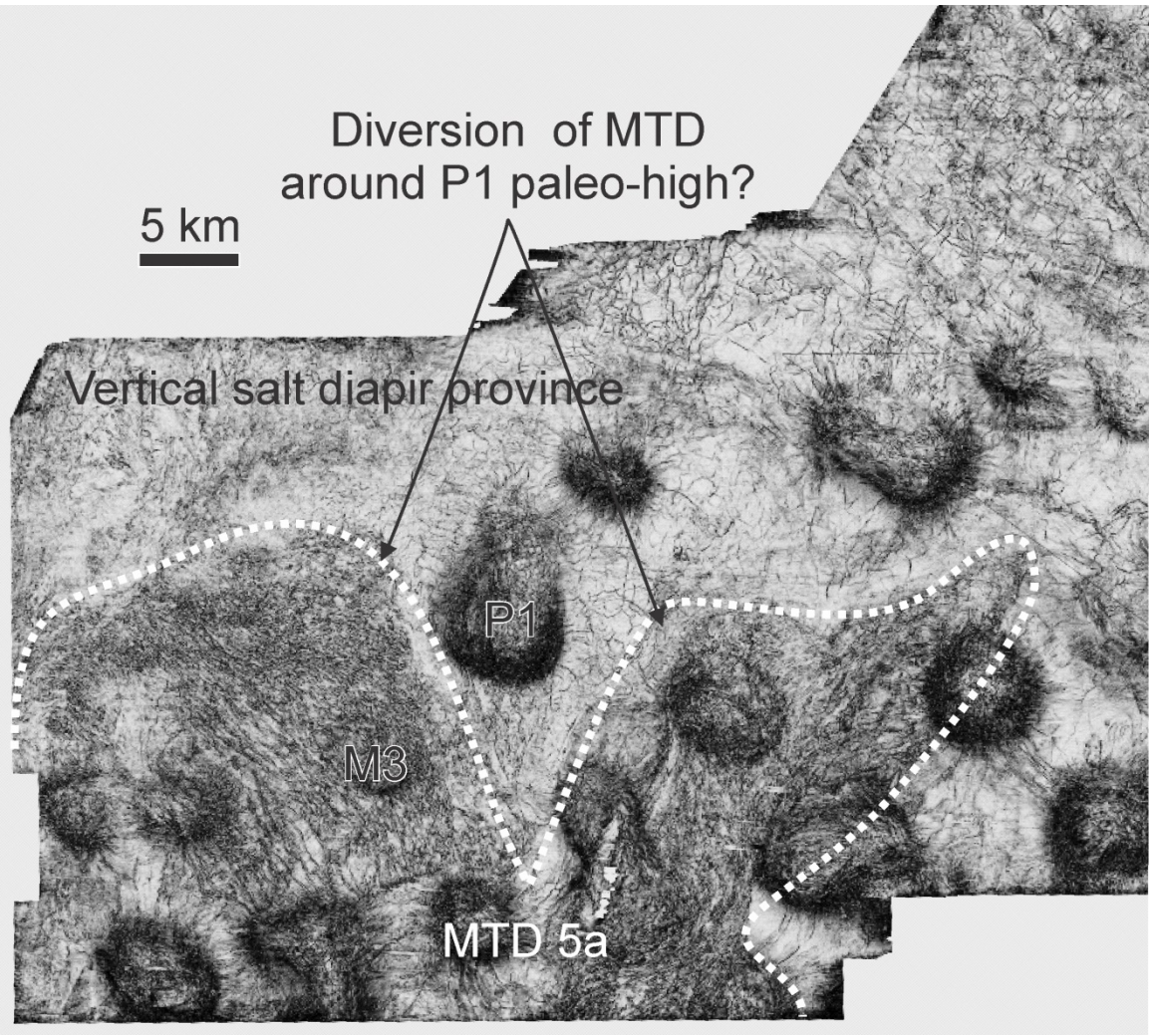

Figure 5.18: Coherence volume slice through MTD 5a showing its distribution. It appears that MTD 5a diverts around the P1 salt diapir perhaps indicating it was a bathymetric high and probably active during this time period. In contrast, M3 appears to be buried by the flow and barely visible indicating that it may have had little or no bathymetric relief on the paleoslope during this gravity flow.

Chapter 6: Discussion

6.1 Interpreted salt movement history in the study area during Units 1 to 3

The abundant occurrence of salt wings (section 4.4.3; Fig. 4.13) between Units 1 and 2 indicates that salt bodies in the study area were initially extruded passively across the seafloor (Cenomanian-Ypresian), and were eventually draped by sediment in Units 2 to 3 (Cenomanian-Bartonian) as the primary salt layer welded out.

In order for salt diapirs to grow passively and laterally expand, sedimentation rates must be less than salt growth rates (Hudec and Jackson 2007). For a salt body to stop growing while there is still an available salt supply from the primary salt layer, the diapir must be draped by thick enough sediment drape (sediment rates > salt extrusion rates) or alternatively the source layer may be depleted (salt extrusion rates drop to zero).

Although salt growth rates are not easily constrained during the Cenomanian to Ypresian, Deptuck and Campbell (2012) studied the composition of sedimentation in this interval (their Sub-units 1a, 1b, 1c corresponding to units 2, 3 and lower part of 4 in this study) and determined that they are composed of mainly background hemipelagic mudstones (Dawson Canyon Formation and most of the Banquereau Formation) and chalks (Wyandot and Ypresian Chalk) (Fensome et al. 2008; Weston et al. 2012; see also section 4.2). These sediments are typical of low energy environments and indicate that sedimentation rates were significantly reduced during this time. Doeven (1983) also demonstrates a decline in deposition rates from the Logan Canyon Formation in the Albian-Cenomanian (7-10 cm/ka) to the Dawson Canyon and Wyandot Formations in the Turonian-Maastrichtian (1-3 cm/ka) in multiple Scotian Margin wells. Given these significantly lowered rates of sedimentation, it is unlikely that salt bodies were rapidly draped or that passive diapirism ceased due to thick sediment cover. Thus, the formation of salt

wings during this time can be attributed to the interplay of slow sedimentation rates and passive salt expulsion from the autochthonous salt-supplying layer.

6.1.1 Salt wings in the study area

Salt wings represent the final phase of passive growth of diapirs from the Cenomanian to Ypresian during a period of slow sedimentation. Thus, the cessation of passive diapirism may be attributed to two possible scenarios:

1. There was a short pulse of lateral squeezing at some point during the deposition of Units 1 and 2 that laterally welded out the diapir stems.
2. The autochthonous salt layer has welded out due to depletion of the salt layer from continuous downbuilding (source layer depletion).

Squeezing of feeders would theoretically pinch stems and weld them out, impeding salt flow. Pinched stems are visible in the vertical salt diapir province and could have also taken place in the allochthonous tongue province, however, the lack of diapir-related stratal thinning above salt crests during the time of Units 1 to 3 (sections 5.2 and 5.3) or clear signs of crestal faulting do not suggest a period of squeezing took place during the deposition of Units 1 to 3.

Depletion of the source layer from continuous downbuilding seems the most viable cause for the cessation of salt body expulsion and draping of salt bodies by the Ypresian. Salt wings in the study area are indicators of the last pulse of passive salt movement in the study area and any movement after salt bodies were draped has to be from a different process.

6.2 History of salt movement in the study area

6.2.1 Vertical salt diapir province

Due to the complexity of this interval, the salt movement in the vertical salt diapir province is subdivided into several stages listed below, and each is described in detail on subsequent pages (Figs. 6.1 and 6.2):

Stage 1	Passive diapirism from downbuilding (units 1 to 3; Jurassic-Cenomanian/Turonian).
Stage 2	Passive salt expulsion whereby salt rates exceed sedimentation rates and extrude onto the seafloor, creating the lower part of salt wings (units 1 to 2; Cenomanian/Turonian-Ypresian). Canyon erosion and intercanyon deposits are synchronous with passive salt motion.
Stage 3	Welding out of the autochthonous salt layer and the cessation of salt expulsion onto the seafloor. The diapir is then draped at a time when several periods of canyon erosion occur on the upper to middle slope (units 2 to 3; Ypresian-Bartonian).
Stage 4	Lateral compression causes active diapirism and creates diapir-related stratal thinning of the overlying units as they drape the diapir (units 4 to 7; Bartonian-Pliocene).
Stage 5	Cessation of the main phase of lateral squeezing followed by a widespread slope re-grading event, commonly depositing MTDs in lows and eroding away salt highs (unit 8; Pliocene).
Stage 6	Drape and modern-day canyon development (Pliocene i.e. post-MTD deposition to modern day).

Table 6.1: Summary table detailing the evolution of the vertical salt diapir province.

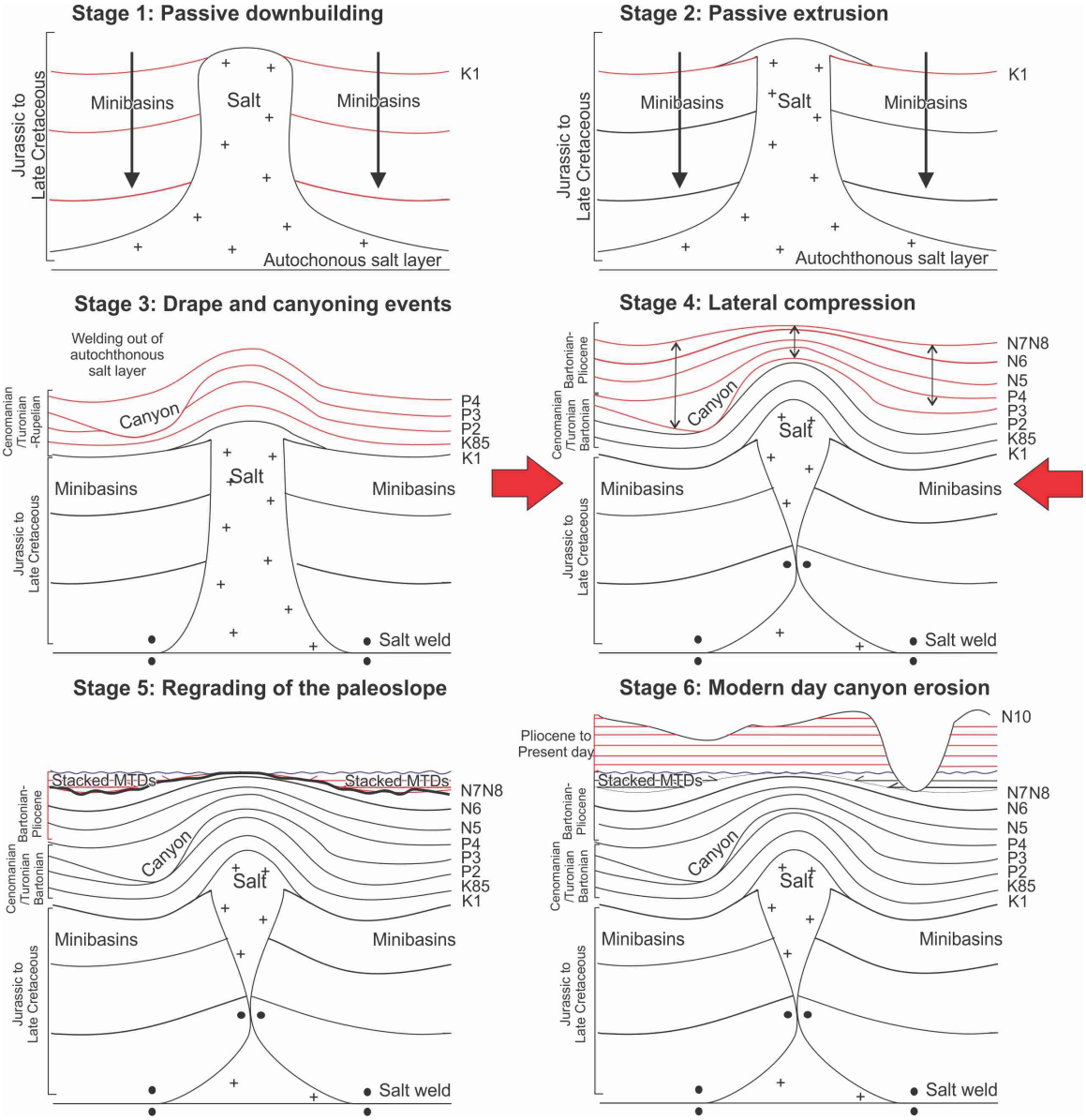

Figure 6.1: Summary diagram of the motion of vertical salt bodies in the study area.

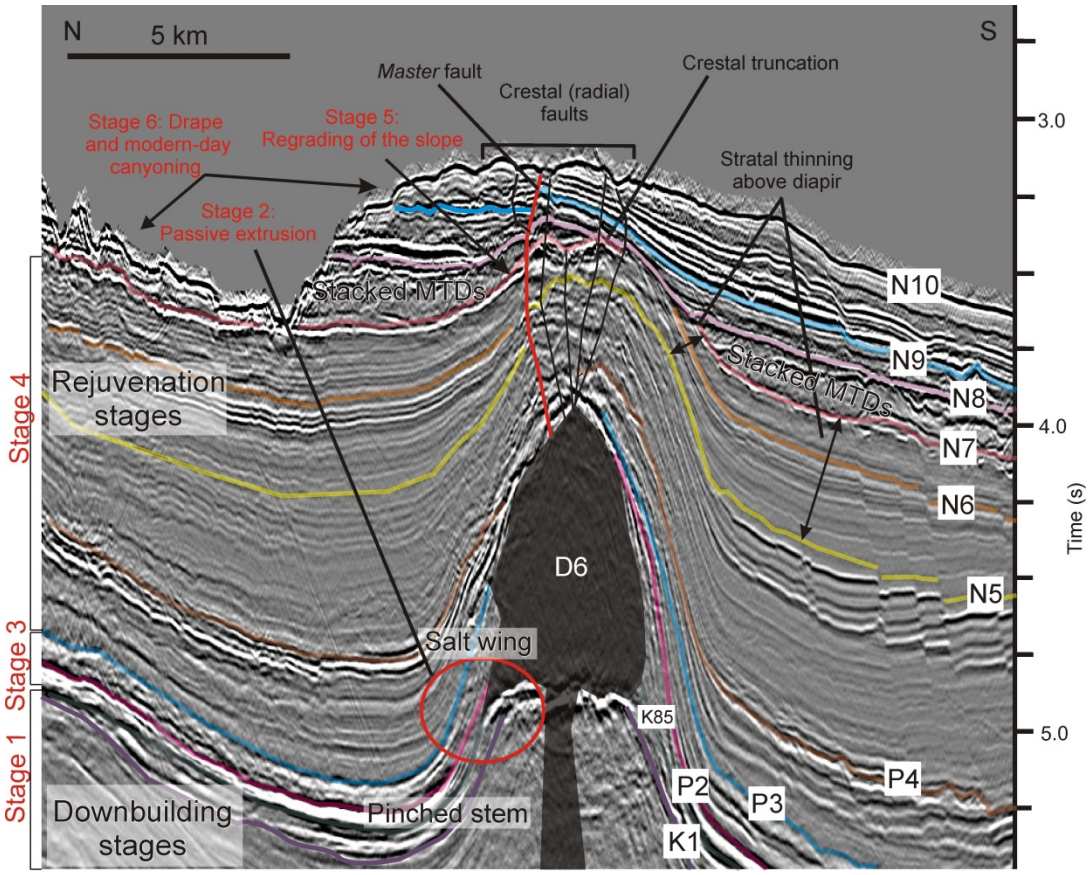

Figure 6.2: Illustration of a salt diapir and associated stages of salt movement.

Stage 1: Passive diapirism (pre-U1)

Salt-sediment contacts of the pre-K1 (pre-Cenomanian/Turonian) strata truncate vertical salt structures during the passive phase. This stage is coeval with the localized downbuilding of strata and creation of adjacent minibasins as the minibasin floor subsided as a result of salt evacuation. As passive downbuilding continued, salt continually kept pace with sedimentation rates or vice versa.

Stage 2: Passive extrusion (Units 1-2)

Salt flow rates eventually exceeded sedimentation rates, recorded in the presence of salt wings that taper onto the paleo-seafloor and that indicate expansion of the exposed salt area onto the sea floor. Generally, diapirs extruded between the K1 to P2 horizons (Units 1-2) from the Cenomanian/Turonian to Ypresian over a period of approximately 60 million years. Extrusion

periods widely vary throughout the study area based on the details of the salt wings (Table 6.1; Figs. 6.1 and 6.3). Using truncated contacts with salt and the point where the relationship changes to onlap and drape above, the relative ages of maximum extrusion are constrained for each diapir (Table 6.1).

Periods of extrusion	
At P2 (Ypresian)	P1, D2, D8
Between P2 and K-85	P3, D3
At K-85 (Santonian)	D7
Between K-85 and K1	A1, M3, M5, D6
At K1 (Cenomanian/Turonian)	P4, P5, A2
Diapirs between P2 and K1 (where K-85 is absent)	P5, D8
Not extruded	M1, M2, M4, D1, D4, D5

Table 6.2: Salt extrusion times interpreted from salt wings and the salt-sediment contacts.

Stage 3: Hemipelagic drape and canyon development (Units 2-3)

For salt to continue expelling and exceed sedimentation rates, it would need to have a higher rate of expulsion relative to the hemipelagic background. Eventually, salt growth rates were no longer able to keep pace with sedimentation and salt bodies were subsequently draped by sediment after the source layer welded out (see section 6.1). Drape consists of inter-canyon erosional remnants leftover from a series of canyon erosion events, with related thickening and thinning from erosion, inter-canyon deposition and eventual canyon axes infill.

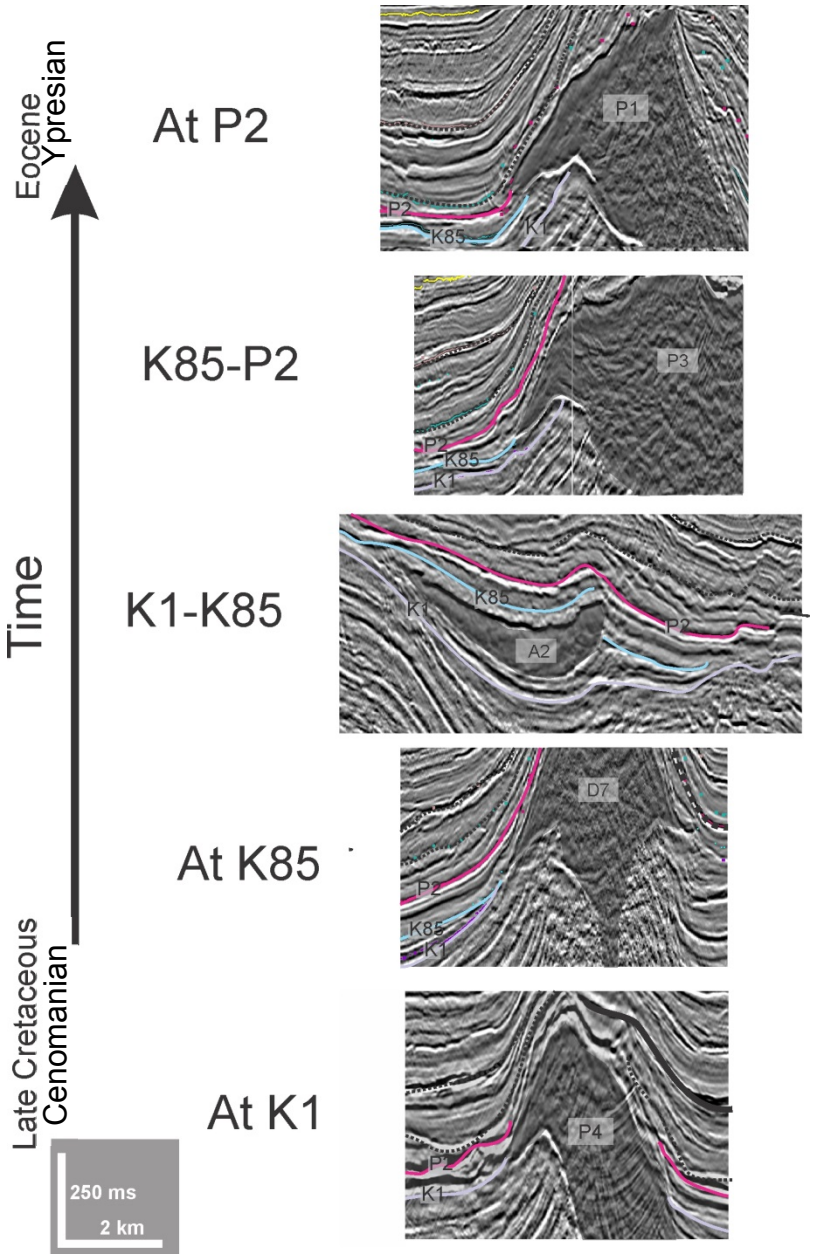

Figure 6.3: Examples of variation in wing terminations and extrusion timing for diapirs and allochthonous tongues across the study area, as indicated by the truncation of horizons beneath the salt wings, their termination at the lateral endpoint of the salt wings (end of extrusion), or drape and onlap above them. The horizon labels on the left represent the time of the switch from truncation beneath the salt wing to onlap above it.

Stage 4: Lateral compression (Units 4-8)

By the end of Unit 3, salt bodies have been buried, the autochthonous layer was welded out and the only way for salt to move after burial is from compression (see section 6.1). Lateral compression commenced in Unit 4, squeezing the diapir stems to create teardrop-shaped structures, and simultaneously uplifting Units 1-3 above salt structures in the form of rafts/carapaces, folding of salt tongues. The compressional active diapirism also caused associated faulting (growth/radial) and diapir-related stratal thinning above salt crests. Units 4 to 8 are the syn-kinematic deposits with Unit 6 (Tortonian) showing the greatest amount of thinning above salt structures, indicating it was likely one of the most active intervals of salt movement.

In the vertical salt diapir province, diapir-related stratal thinning appears to the most prominent west of P3. This is further evident from the diversion of a small submarine channel around M1 (see section 4.5, Unit 4). Unit 6 shows significant stratal thinning throughout the study area, and it is evident that compression was the most active in this interval in both provinces, as indicated mostly by stratal thinning and onlap that also occurs above salt highs. Unit 7 shows a period of some more modest stratal thinning, (perhaps a waning phase?) transitioning to Unit 8 that has a significant period of salt activity where MTDs onlap the paleo-relief of salt highs and infill topographic lows. It estimated that more than 600 ms (or 480 m) of overburden has been eroded over during this time.

The onset of active diapirism may coincide with deposition of MTD 4a, the oldest mass transport deposit found near the top of Unit 4, and restricted to areas immediately adjacent to the vertical diapirs indicating that salt bodies were likely topographic highs during this point. This is also the period of time when canyons were eroded and additionally, appear to divert around salt bodies, one of which was inverted. A small sinuous channel in the westernmost study area also

formed near the top of Unit 4, indicating that the depositional systems were quite complex during this period of time.

As a result of lateral compression, radial faults are created as overburden is domed and displaced upwards around all of the salt bodies in the study area. Where resolvable, growth faults are present above all salt bodies across the study area. They typically have stacked mass transport deposits that have accumulated on their hanging walls. These large faults are visible from Units 4 to 8 in coherence with little to no growth in earlier stratigraphic units (units 1 to 3).

Stages 5 and 6: Regrading of the paleoslope and modern day canyon development (Unit 9)

A substantial period of slope re-grading took place at the start of Unit 9, coincident with horizon N8 (Pliocene), and the onset of several stacked MTDs. The erosion planed off the slope, deposited MTDs in lows and thinned/eroded structural highs. While there is some bathymetric expression, relief from salt diapirism is minor along the modern seafloor in the study area and it appears that relatively little salt tectonic activity has affected the relief of the slope since the onset of Unit 9.

6.2.2 Salt evolution in the allochthonous tongue province

The A2 allochthonous tongue is the largest in the study area. It is structurally complex and has been subdivided into several structurally distinct parts. Two structural salt highs are present in A2 between a series of pre-K1 rafts/carapaces and lows created by minibasin loading into the underlying salt.

The A1 and A2 salt tongues appear to have been folded, and this is most evident at the toe of the A2 tongue which has rafted older (pre-K1) strata above the tongue. Landward of the A2 salt

diapir are 3 minibasins B1, B2 and B3. Deposition between these basins varies over each unit (i.e. minibasin thickening; see section 5.2).

Since the allochthonous tongue province is substantially more complex than the vertical salt diapir province, there are several more phases of evolution (Figs. 6.4-6.6). This is partially due to 2 separate types of compression that vary between north-south oriented and northwest-southeast oriented.

Stage 1	Passive diapirism from downbuilding (Pre-U1; Jurassic to Cenomanian/Turonian).
Stage 2	Passive extrusion (salt rates > sedimentation rates) (Units 1/2; between the Cenomanian Turonian-Ypresian).
Stage 3	Drape of the salt tongue (salt flow rates < sedimentation rates) (Units 1-4; Cenomanian/Turonian-Rupelian).
Stage 4	Simultaneous loading of Units 1 to 4 above the salt tongue triggered salt evacuation that formed a withdrawal basin. The salt tongue was thickly buried (i.e. locked in-place), so salt evacuation caused the adjacent tongue to inflate upwards creating thinning on the distal edges as the salt thrusted upwards (Cenomanian/Turonian-Rupelian).
Stage 5	Deposition of large-scale sediment waves from contour currents (Unit 5; Rupelian-Tortonian).
Stage 6	North-South trending compression further inflates the salt tongue from the Oligocene to Pliocene. Stacked MTDs deposit in the minibasin lows on the downthrown side of the counter-regional fault system. This is related to re-grading of the slope and subsequent infill of lows and erosion of highs (Units 5-8; Rupelian to Pliocene).
Stage 7	Similarly, a second phase of inflation of the salt tongue is evident, originating from a northeast-southwest linked system. These two compression phases occur at approximately the same time period and are difficult to differentiate.
Stage 8	Draping of the system and modern day canyon development (Unit 9; Pliocene to modern day).

Table 6.3: Summary table detailing the evolution of the allochthonous tongue province.

After passive downbuilding had ceased, the A2 salt tongue was extruded onto the seafloor between the Cenomanian/Turonian and the Ypresian (between the K1 and P2 markers) as is evident from the salt contacts below the tongue and the drape above it (stages 1 and 2). During

this time, passive diapirism forced salt to extrude onto the seafloor as salt rates exceeded sedimentation rates of hemipelagic drape (stage 2). Once the source layer had been depleted (indicated by the cessation of salt expulsion accompanied with low sedimentation rates; see section 6.2), downbuilding ceased and the tongue was draped. While being draped by sediments of Units 1 to 4, it began a new phase of passive downbuilding into the salt tongue itself in localized areas. This created downslope compression forcing the overlying sediments upwards (i.e. halokinetic active diapirism). Once the salt had been locally welded out (again), this second phase of downbuilding ceased. This process ultimately created a small minibasin approximately 5 km across with units 1 to 4 (Figs. 4.20 and 4.35) tapering in thickness towards the adjacent salt highs.

Unit 4 (Fig. 4.41) shows some salt-related deformation related to thinning at the flanks of the tongue where it is preserved. Unit 4 has been eroded above the majority of the salt tongue crests (A1 and A2) and whether or not the salt was entirely active during this phase is unclear. It is definitely apparent that by Unit 5, compressional active diapirism began, because of the apparent depositional thinning on the flanks of the salt highs (Fig. 4.44). Unit 5 is a thick contourite package with sediment waves with little thickness variation above the salt tongue; however, compared to its surroundings the unit over the tongue is thinner, as expected for the higher structural relief and confirming that some salt activity continued.

It is debatable how much of a topographic high the A2 salt tongue was during Unit 5. The inversion of a paleocanyon (see Unit 5 in Section 4.3) indicates that some salt growth in this area was at a later stage (i.e. post-Unit 5). This pattern is consistent with the presence of only subtle stratal thinning in Unit 5 (Fig. 5.9) and more obvious salt-deformation-related thinning visible in

Units 6, 7 and 8 above A2. This probably occurred as salt highs began to increase in height and invert the canyon (Figs. 5.10 and 5.12).

Dramatic thinning of Unit 6 (Figs. 4.52 and 4.53) indicates that salt had been compressed and displaced upwards at this time (U. Miocene). During Unit 6, the toe of the A2 tongue on the downslope portion inflates, as indicated by stratal thinning and folding of the toe in the downslope areas. This is likely related to upslope loading of the B1, B2 and B3 basins triggering downslope compression through gravity spreading (north-south oriented linked system).

In the north-south orientation a series of minibasins landward of the A2 tongue actively inflated the A2 salt high during deposition of Units 7 and 8. This also creates some downslope compression of the toe, although not as dramatic as the northwest-southeast oriented compression inferred earlier. This may be due to the intervening minibasin that is centrally located in A2, which could have confined the salt to that area or accommodated some of the deformation.

By the onset of Unit 9, a major regrading event took place depositing MTDs in lows, especially in minibasins. The final phase is the drape by slope sedimentation and eventual incision from modern day canyons.

6.2.3 A1 salt tongue

Similar to A2, A1 was passively extruded between the Cenomanian/Turonian and Santonian onto the seafloor until it was welded out (Units 1 to 3). Units 1-3 appear to drape the salt structure creating a minibasin that downbuilds into the tongue causing inflation of the salt adjacent to it. Since Unit 4 was mostly eroded above the salt tongue, changes in stratal thickness across this salt body could not be accurately quantified.

Although Unit 4 is mostly eroded away above this salt body, compression visibly initiated by Unit 5 likely originating from a linked system i.e. extensional faulting in the northeast, offset by squeezing in the southwest. Where resolvable, Unit 4 appears to have subtle thinning, passing upwards into Unit 5 which has dramatic structural thinning, and Unit 6 that eventually onlaps above the salt high in the northeast. Units 7 and 8 both show subtle thinning and Unit 9 shows no thinning with little topographic expression as the salt body became quiescent. Similar to the rest of the study area, the onset of a slope regrading event takes place at the base of Unit 9 (Horizon N8). The unconformity is overlain by a series of mass transport deposits and draped. Finally, a series of modern day canyon systems erode into the upper part of Unit 9.

6.3 Growth faults

Some workers have suggested that most extension in the brittle overburden of a diapir during a lateral compression phase is accommodated along large master faults across the crest of the diapir (Yin et al. 2009). These master faults are typically the first fault to form during a compressional phase and have achieved greater displacement than other subsidiary faults in part because their longer duration of activity (Yin et al. 2009; Carruthers et al. 2013).

Growth faulting can only be measured in areas where units are preserved on both sides of the fault. Since erosion is extensive around the medial and distal diapirs of this study, a comprehensive regional study of fault growth was not possible. Where preserved in some of the proximal diapirs, timing of fault growth is mostly constrained to the upper units (Units 5 to 8) and all salt bodies appear to show some variation of growth in Unit 8, suggesting a regional sense of movement (with the largest growth accumulations in the allochthonous salt tongue province along the margins of salt withdrawal minibasins).

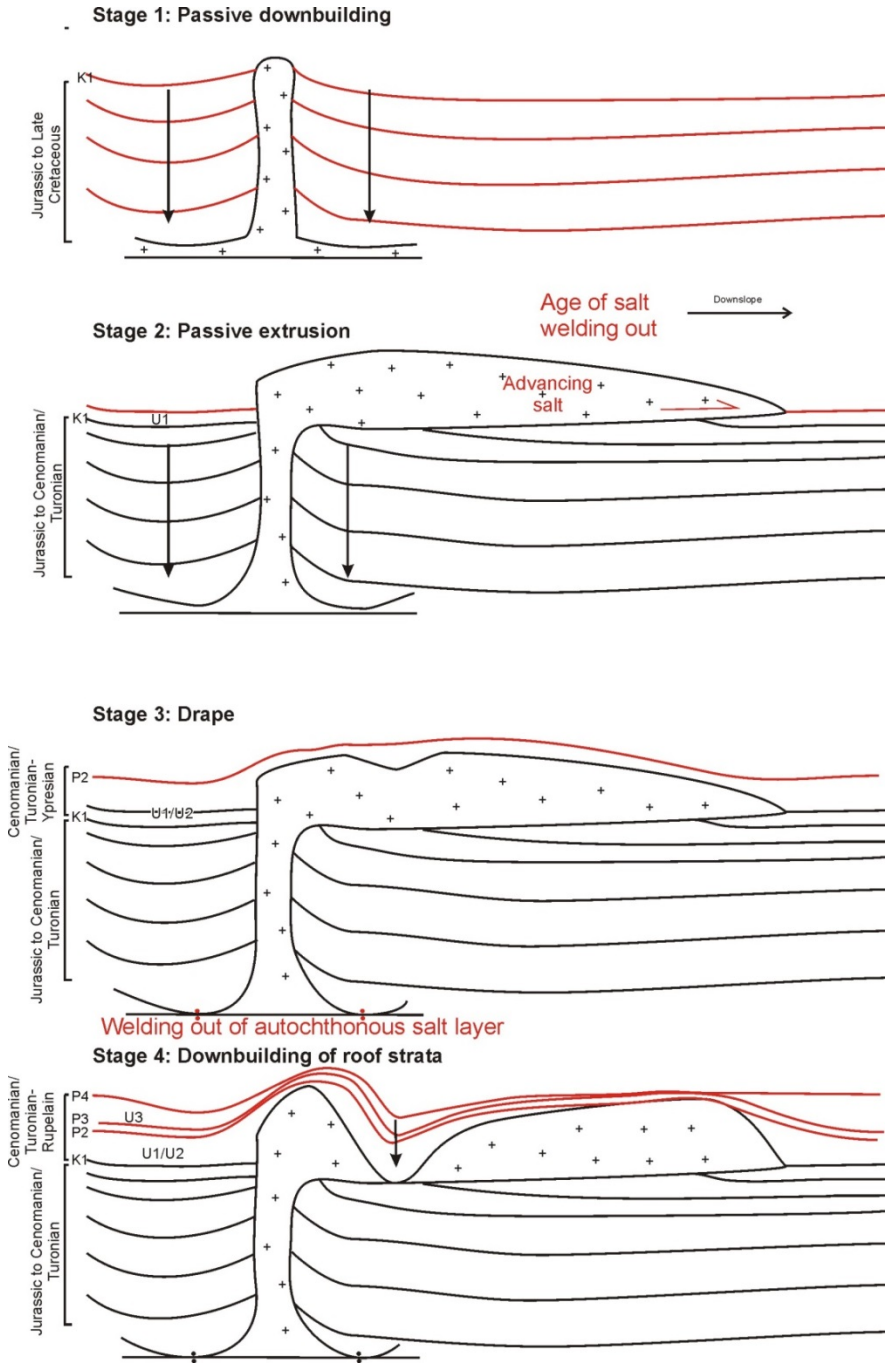
Stage 1: Passive downbuilding
K1
Jurassic to Late Cretaceous
Stage 2: Passive extrusion
Age of salt welding out
Downslope
Advancing salt
K1
U1
Jurassic to Cenomanian/ Turonian
Stage 3: Drape
Cenomanian/ Turonian- Ypresian
P2
K1
U1/U2
Jurassic to Cenomanian/ Turonian
Welding out of autochthonous salt layer
Stage 4: Downbuilding of roof strata
Cenomanian/ Turonian- Rupelain
P4
P3
P2
U3
U1/U2
K1
Jurassic to Cenomanian/ Turonian

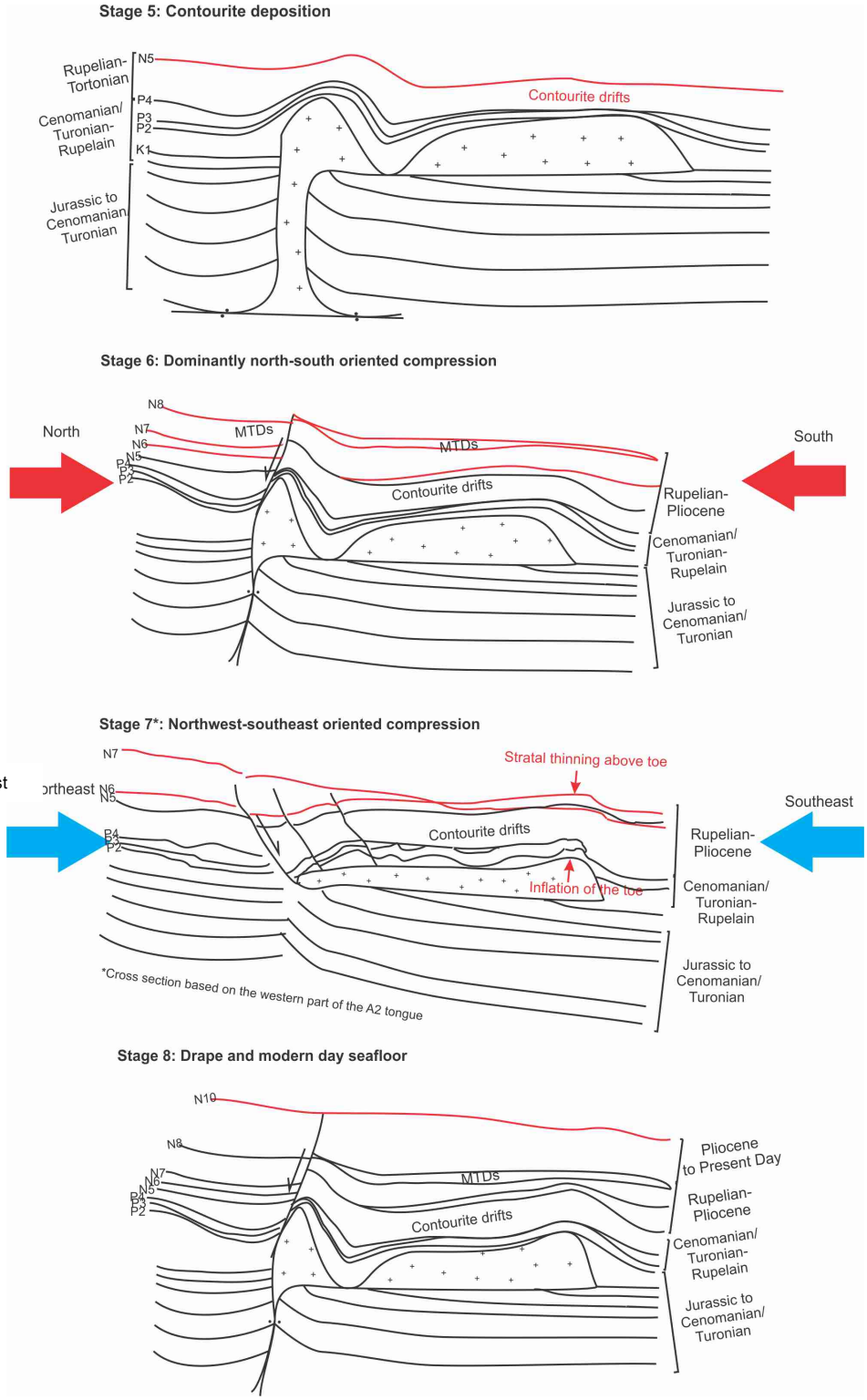

Figure 6.4: Summary figure of the allochthonous tongue evolution from the Cenomanian/Turonian to present day, based largely on the activity of the A2 tongue. Stage 7 depicts the western part of the A2 tongue (see Fig. 6.6).

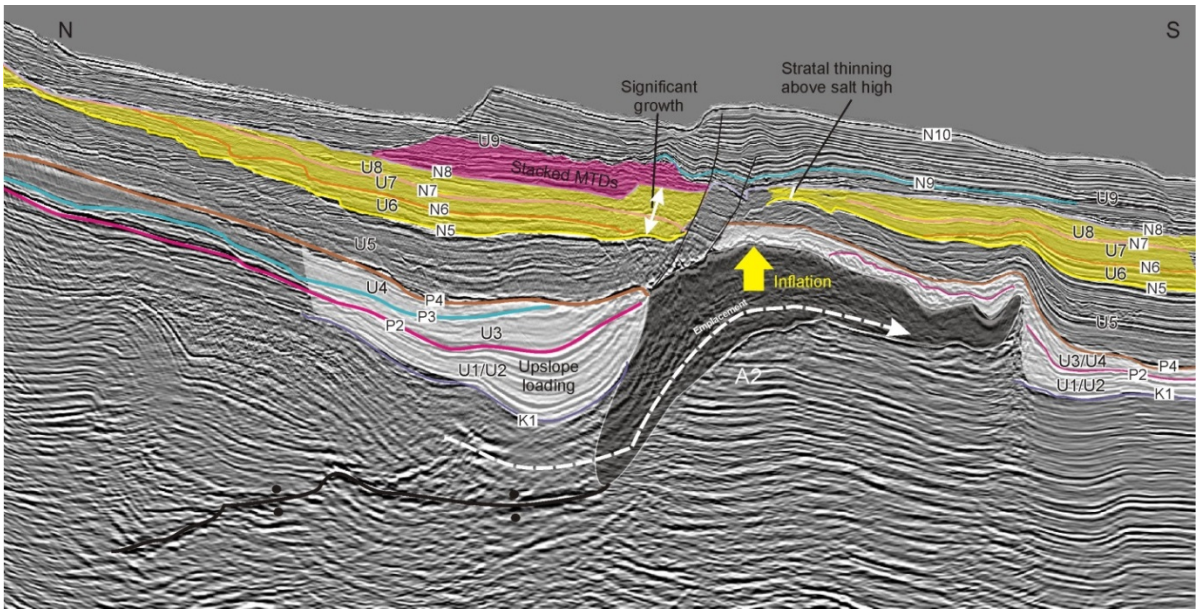

Figure 6.5: Early (Cenomanian/Turonian to Rupelian) downbuilding forced extrusion of the A2 allochthonous tongue onto the seafloor driven mainly by landward loading of sediments (light grey). By contrast, Unit 5 shows more subtle thinning over the tongue, implying less salt motion and less remaining relief at the time (Rupelian-Tortonian). Units 6 to 8 (yellow) show greater inflation of the salt tongue, folding, and structural thinning interpreted as the product of lateral compression in the Tortonian-Pliocene.

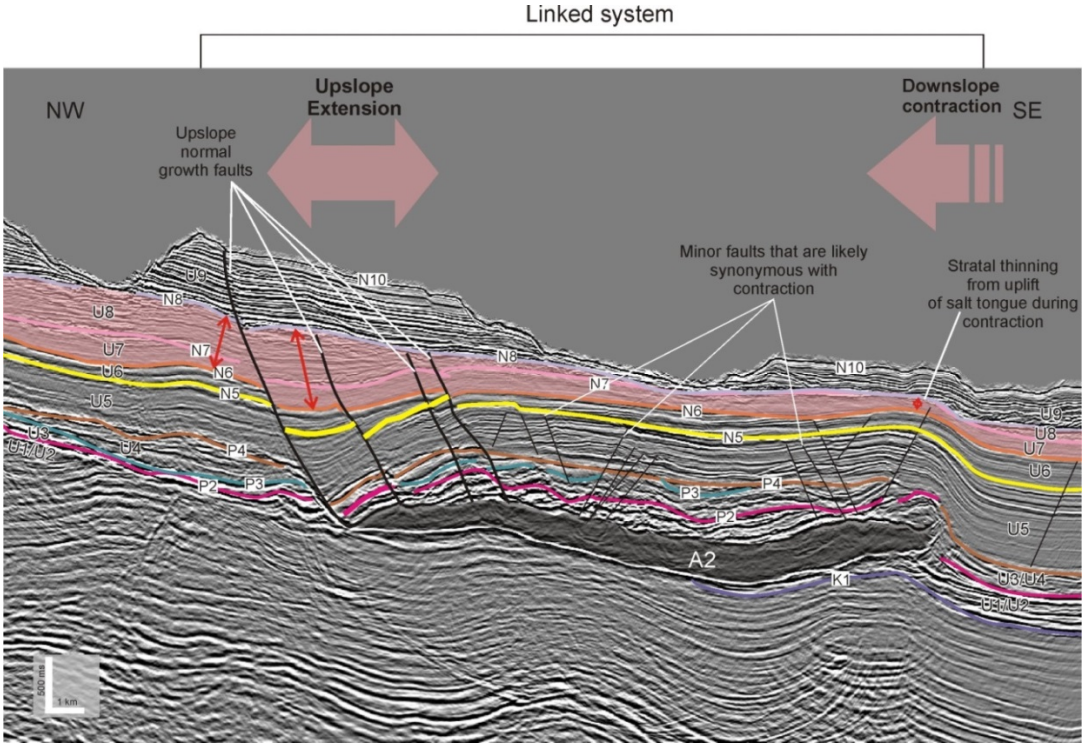

Figure 6.6: This cross section shows the western part of the A2 tongue. Downslope inflation of the toe of the A2 tongue is in a northwest-southeastern orientation (i.e. a linked upslope extension and downslope compression system).

The large master growth faults at the crest of vertical diapirs are thought to be related to crestal doming (extension) while the salt displaces sediment during its upward motion (Yin et al. 2009; Carruthers et al. 2011). The presence of such growth faults would only be possible if thrust motion and subsequent extension was very brief (insufficient time for accumulation of sediments that would indicate prolonged syn-depositional motion), and is therefore not a likely scenario given the ample evidence for syn-depositional growth even within the mapped units (e.g., individual MTD deposits responding to relief across faults).

Another possibility given the large offsets of these faults is that they may be related to a period of regional extension as a side effect of post-contraction relaxation. The faults could have been previously inverted, changing from an initial thrust motion during pulses of compression during the Miocene to normal faults post-contraction. Regardless of their motion, the uniform orientation (NW-SE) of these faults across the study area implies a regional scale of movement. Further investigation is required of salt bodies outside of the study area to assess how widespread the pattern of fault growth and their orientation is on a broader scale.

6.4 Origins of compressional active diapirism

6.4.1 One or more possible mechanisms?

As interpreted in section 6.2, the results of this study clearly indicate a period of lateral compression that resulted in rejuvenation of salt structures in the study area after earlier passive diapirism had ceased. This resulted in active diapirism between the Bartonian and Pliocene generally starting in Unit 4 in the salt diapir province (Unit 5 in the allochthonous tongue province) and ending in Unit 8. The question becomes: what process caused lateral compression and rejuvenation of salt tectonics in the study area? Figure 6.8 summarizes the timing of the salt

motion and compares it to the timing of other events in the region and globally, and Table 6.2 summarizes the processes considered below.

For a regional period of growth originating from one mechanism, it would be expected that all salt bodies are active at the same periods across the study area, i.e. all diapirs show diapir-related crestal stratal thinning in a given time period or none at all. Differences between these two areas may indicate separate origins of compression and any changes in slope morphology may have been triggered by adjacent shelf/upslope processes rather than processes strictly within the study area itself.

From the stratal thinning maps (Figs. 5.6-5.14), there appear to be recurring periods of activity, mainly west of diapir M4 in the vertical salt diapir province while the middle of the study area remained relatively inactive. The extent of thinning (i.e. obvious versus subtle thinning) also appears to be different between both provinces, while there is some evidence that limited compression has continued in the vertical salt body province to the present.

6.4.2 Possible origins of compression

Timing of salt diaprism is important to determine the possible mechanisms behind rejuvenation in the form of compressional active diapirism. The age of compression can be constrained to between the Bartonian and Pliocene across the study area (with most of the activity interval in the Miocene- Units 4 to 8). Assuming the process triggering compression is synchronous with downslope salt movement, activity must have initiated in the Bartonian, and ceased (or slowed down) by the Pliocene (after horizon N8).

Shelf-edge deltas

Two delta systems, the Sable and Banquereau Deltas have prograded to the shelf edge upslope of the study area, each of which consists of multiple stacked delta systems accumulated over time (Fig. 6.7). The Sable Delta system deposited several kilometres at the shelf-edge between Jurassic and Early Cretaceous. The upslope loading of these sediments during the Jurassic to Cretaceous triggered the downslope expulsion of salt forming the Sable Slope Canopy Complex today (Fig. 2.9) (Wade and MacLean 1990; Kendell 2012; Weston et al. 2012). These larger-scale linked systems (i.e. linked growth-fault and salt structures) pass from upslope extensional regimes to downslope compressional structures on the southwestern Scotian Slope i.e. loading from the upslope Sable Delta could have caused compression through a gravity spreading process.

The impact of upslope loading from the Sable Delta continued into the Cenozoic (i.e. downslope compression) (Deptuck et al. 2009; Deptuck 2011a), however, its impact on the study interval is debatable because of the expected declining effect after Sable Delta deposition ceased near the end of the Early Cretaceous. It would also be expected that this mechanism would be a continuous process and not episodic. A large pulse of shortening in the Miocene prior to a period of quiescence would be unlikely.

The younger Banquereau Delta was deposited as a prograding unit directly upslope of the study area in the Late Cretaceous and Paleogene (Fensome et al. 2008; Weston et al. 2012). Rapid deposition of the delta may have triggered a gravity spreading system, but no evidence of compression is observed between the Late Cretaceous to Eocene in the study area unless it is was accommodated solely in the salt. It appears that the Late Cretaceous was a period of relative tectonic quiescence in the study area with only passive expulsion and downbuilding of the source

layer. The delta may have been responsible for numerous periods of canyon erosion on the slope at this time, but does not appear to have triggered compressional active diapirism. In conclusion, the timing of the two main delta progradation episodes in the area does not match the timing of the main lateral compression phase in the Miocene (Figs. 6.8 and 6.9).

Thermal uplift

Periods of regional, crustal-scale tectonic uplift have been known to trigger downslope salt compression (Rowan et al. 2004). Based on models of apatite fission track data, Grist and Zentilli (2003) interpreted a period of post-Paleocene cooling related to erosion and uplift on mainland Nova Scotia and the Scotian Shelf. This period of tectonic uplift may have triggered

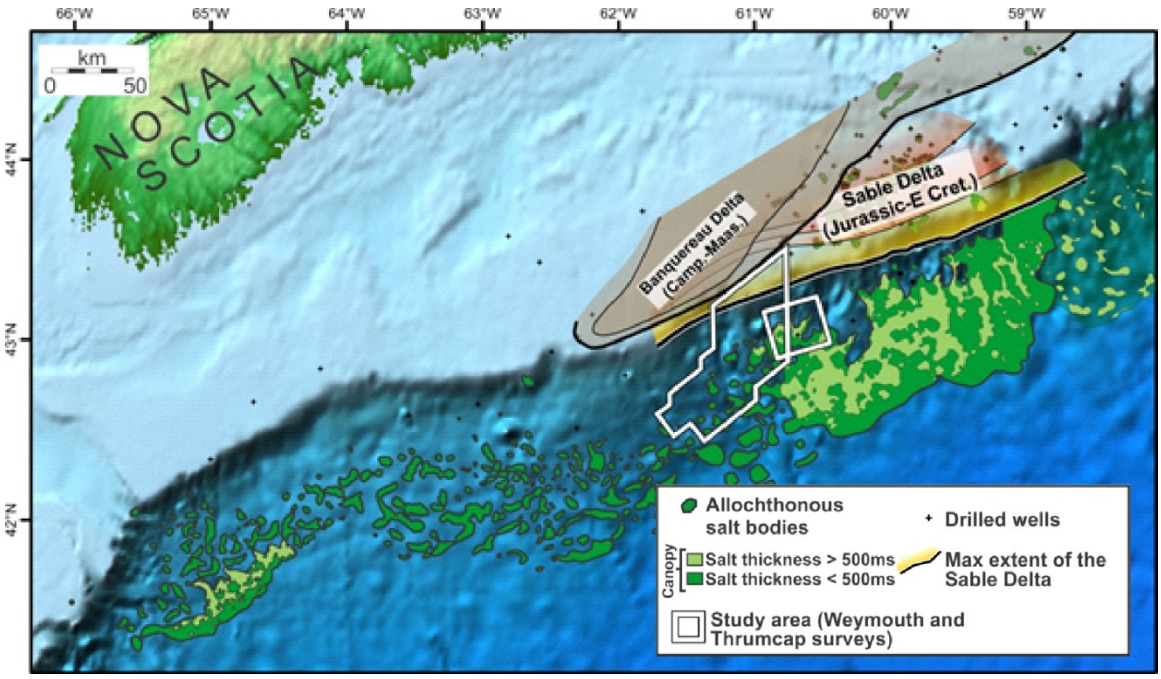

Figure 6.7: Upslope loading from deltas is one hypothetical cause for downslope compression in the study area via gravity spreading. Modified from Deptuck and Kendell (2012).

downslope rejuvenation of salt bodies on the slope via tilting of the margin. The timing of a period of uplift roughly aligns with this study because the lateral compression of salt structures took place in post-Paleocene times, but coincidence of timing is not sufficient to establish it as the cause. It only leaves it as a candidate. Other tectonic tilting processes are also possible.

Loading by an ice sheet

A diapir can rise in response to loading of its source layer from a glacial icesheet (Lang et al. 2014). The Scotian Margin has been host to series of glaciations during the Pleistocene. Timing of the first shelf-crossing glaciation has been estimated at around 500 ka (Piper et al. 1994) and loading from the weight of a heavy glacial ice sheet could have triggered downslope compression. Although this process seems possible in principle, the timing of compressional active diapirism in the study area is constrained from the Bartonian to Pliocene (i.e. pre-500 ka). Since shelf-crossing glaciations have been only previously been documented by authors to post-500 ka (Piper et al. 1994), compression from an upslope glaciation is an unlikely scenario.

Localized linked systems

It is likely that compression in the allochthonous tongue province is part of a localized linked system separate from other vertical salt bodies in the west. In this case, upslope extensional features are observed in the form of growth faults and downslope contraction is observed in the form of stratal thinning, folding and faulting of the salt. The compression in the allochthonous tongue province can be directly tied to upslope extension along growth faults. No other readily apparent upslope deposits are present in this area during the Cenozoic. Therefore, the compression in this area may be geologically localized sediment loading in the study area and not caused by a larger regional system such as loading from an upslope delta.

Sediment loading and contourites

Sediment deposition and differential loading has the potential to rejuvenate salt tectonic systems even if salt has welded out. Campbell (2011) studied the deposition of contourites during the Miocene, and observed up to 1500 m of strata deposited landward of the isolated diapirs in the western study area (section 4.5). The relatively rapid deposition of contourites from the Oligocene to Pliocene (units 4 to 8) is roughly coincident with the start of downslope

compressional active diapirism in the vertical salt diapir province. These thick contourite deposits taper downslope and could have created downslope contraction in response to upslope loading (Deptuck et al. 2009). However, no upslope extensional faults have been observed that could have complemented contraction.

Determining timing provides a test of possible processes behind rejuvenation. Several options can be eliminated because they are not synchronous with the compression event (Table 6.2) Three separate mechanisms are not eliminated by timing constraints: crustal-scale regional uplift and tilting in the post-Paleocene, contourite deposition in the west, and an individual linked system in the east (Fig. 6.8 and 6.9). The rapid deposition of a thick contourite package in the western part of the study (upslope of P1 to P3) between the Oligocene and Pliocene seems like the most likely trigger for downslope contraction in the western section of the study area where the contourites are best preserved. In contrast, compression in the allochthonous tongue province is most likely related to a localized linked system independent of the vertical salt diapir province (Figs. 6.8 and 6.9).

6.5 Comparisons to the North Sea

Rejuvenation of salt structures was previously documented by Davison et al. (2000) and Carruthers et al. (2011) in the Central Graben, North Sea. Salt bodies in that area have experienced episodic squeezing with pinched stems, master faults, stratal thinning at the diapir crests, and associated radial/concentric faults. In comparison, salt bodies on the Scotian Slope have experienced squeezing and exhibit many of the same characteristics although in a slope setting with allochthonous tongues, vertical diapirs, and many complicating factors such as canyon erosion and other processes causing thickness variations in the study interval. Davison et

al. (2000) recorded compression as a series of episodic events with periods of drape or onlap between periods of compression.

6.6 Future work

More recent work has studied the mechanisms behind salt movement in the Central Graben and whether or not the Cenozoic reactivation is linked to larger scale crustal tectonism or localized salt tectonics (Clausen et al. 2012; Rasmussen 2013; Clausen et al. 2013). Clausen et al. (2012) argues that differential loading originating from sequences of prograding Cenozoic deposits is the primary mechanism behind the reactivation of salt bodies in the Central Graben. Rasmussen (2013) counters that the causes behind rejuvenation are more complicated and related to episodes of tectonic inversion (uplift) previously documented by many other workers. Analogous issues can be carried over to this study i.e. whether compression is related to localized linked systems or a more broad process such as the post-Paleocene uplift previously studied by Grist and Zentilli (2003). It appears the relationships between sediment loading, salt movement and regional tectonism in salt tectonics are complicated and subtle, leaving ample room for further study.

In order to determine the process responsible for salt deformation, analogue or numerical modelling experiments would be required to quantify the contourite, growth faults, upslope deltas and post-Paleocene uplift relation to downslope salt structures. Since the exact mechanism behind compression is not well understood and several scenarios are presented, numerical modelling analogue system would probably be the most effective way to determine if the process

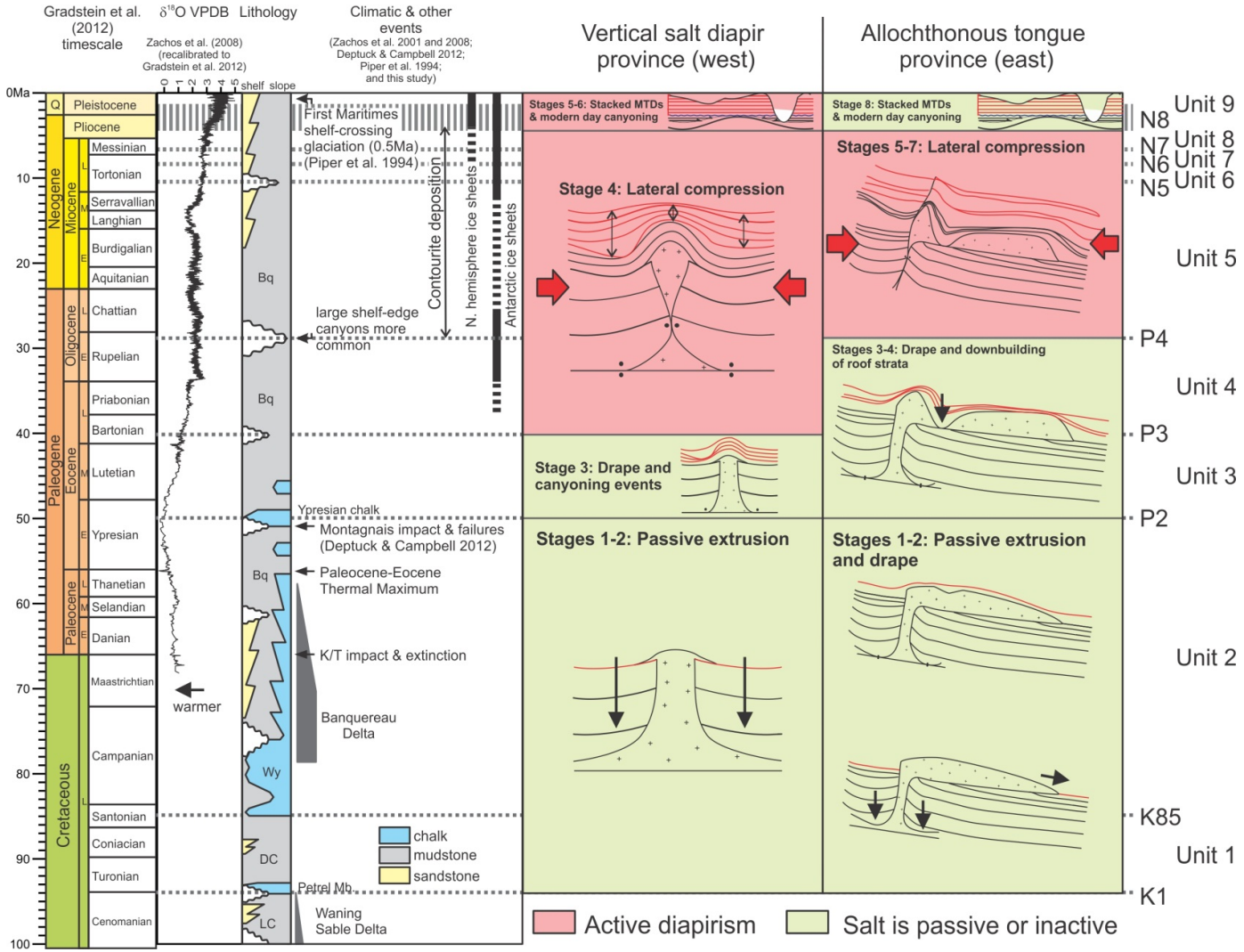

Figure 6.8: Summary diagram of salt evolution in the study area and important regional/global events between Late Cretaceous and Cenozoic. Red shaded squares indicate time periods when salt was being squeezed by compressional active diapirism. Greens are periods of quiescence or passive expulsion. Horizon names and intervening units are listed on the right.

Possible causes behind downslope compression	Plausible?
Shelf Crossing Glaciations (post-500ka)	No
Contourite Deposition (Oligocene-Pliocene) (Campbell 2011)	Yes
Linked System (Oligocene-Pliocene)	Yes
Post-Paleocene Uplift (Grist and Zentilli 2003)	Yes
Banquereau Delta (Late Cretaceous-Paleogene)	No
Sable Delta (Jurassic-Late Cretaceous)	No

Table 6.4: Processes and their plausibility based on timing relative to the compressive active diapirism rejuvenation event.

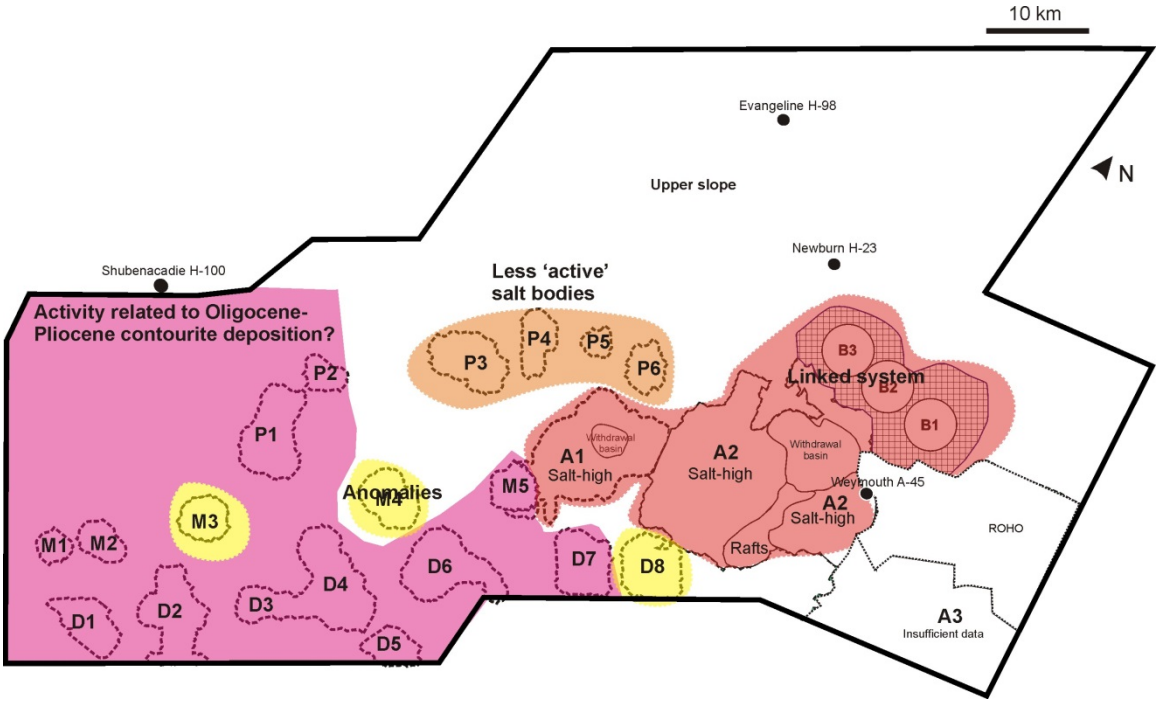

Figure 6.9: Summary figure highlighting the different patterns of salt deformation in the study area and possible driving mechanisms. Areas highlighted in purple indicate salt bodies in the west that may have experienced deformation from an upslope contourite deposit. Contrastingly in the east, salt movement in A1 and A2 is likely caused from a linked system (highlighted in pink). Salt bodies P3, P4, P5 and P6 (highlighted in orange) are salt structures that have a separate pattern from the rest of the salt bodies, likely related to infill in a Miocene canyon system that intersects them. Yellow highlighted salt bodies are anomalous with no consistent pattern when compared to the other salt structures.

is related to an upslope gravity spreading system or thermal uplift. In contrast, an analogue system would capture the style of deformation over each salt body and these results can be compared and contrasted with this study. Additionally it could also take into account the uplift of local carapaces/rafts.

Finally, the examination of other seismic datasets using similar techniques on the Scotian Slope to determine the regional extent of the lateral compression event would also clarify whether the cause is due to more local or regional processes.

6.7 Implications for petroleum system elements

Salt movement has implications for the distribution of hydrocarbons today. On a bumpy slope, minibasins between salt highs have the potential to trap sands and this was likely the case between the Oligocene and Pliocene in the allochthonous tongue province given the evidence for significant (>100 ms) diapir and minibasin-related bathymetric relief at this time. Similarly, the Bartonian to Pliocene (units 4-8) interval in the vertical salt diapir province has a gradual landward shift of depocenters which has implications for the sand distribution, i.e. where the gravity flows preferentially deposited in lows. By the time of the Pliocene, a slope re-grading phase had taken place, erasing most of the bumpy topography (i.e. salt highs) and reverting the slope back to a graded geometry (i.e. mainly bypass) slope. The presence of a widespread unconformity with drape may trap hydrocarbons or other fluids migrating upwards from greater depths which may also prove to be shallow hazards for drilling. Minibasins between salt bodies could contain a series of fan systems that would have otherwise deposited at the toe of the slope prior to the generation of the relief. If these sands were present, salt bodies could potentially trigger formation of hydrocarbon traps.

Although reservoir potential exists on this part of the upper slope, the overburden around the salt structures in the study area has been extensively faulted through radial and large-scale master faults. These faults would likely facilitate leaking of potential hydrocarbons above salt structures that might otherwise act as seals. Units at the crest of salt bodies in this interval are therefore a risky target. Furthermore, fault activity late in the sedimentary history could also give clues to the presence of a deeper hydrocarbon system in the area (i.e. seeps). While individual traps may be breached because of younger salt tectonic activity, sites of active shallow faults could be targets for shallow sampling to characterise the broader petroleum potential on the Scotian Slope, however, the presence of faults themselves may prove a shallow hazard for exploration possibly affecting seafloor stability, trapping shallow gas or causing abnormal pressure differentials. Careful mapping of the shallow faults in the interval and a more detailed study of their activity would be useful both for exploration targets and safety.

Chapter 7: Conclusions

1. *Three phases of deposition*- Seismic stratigraphy in the study area is complex, but it can be subdivided into 3 main phases:
    a. Phase 1 spans from the Late Cretaceous (Cenomanian) to the Oligocene (Priabonian/Rupelian) and is characterized by bypass canyon development and later infill. Sedimentation rates in these lower units (1-4) were reduced and consist of hemipelagic and pelagic muds and chalks (Deptuck and Campbell 2012). Canyon development began around the Late Cretaceous continuing into the Eocene (Units 2 and 3) with draping in Unit 4 filling canyon lows and thinning above canyon highs.
    b. Phase 2 shows a change from a thickening-seaward to thickening-landward geometry during deposition of Units 5 to 8. These shifting depocenters largely consist of contourite deposits with sediment waves previously recognized by Campbell (2011), that preferentially migrated landward from the Oligocene to Pliocene.
    c. Phase 3 marks a significant slope regrading event and ponding of MTDs in minibasins, followed by drape and modern canyon development within Unit 9. The regionally extensive unconformity marking the planing event (N8 Horizon) shows the greatest degree of erosion around distal salt bodies and has removed at least 500 metres of pre-existing bathymetric relief over some salt structures.

2. *The end of passive salt diapirism*- Salt diapirs were passively extruded onto the paleoseafloor at different times between the Late Cretaceous (Cenomanian) and Early Eocene (Ypresian). Sedimentation rates were particularly slow during this time (Deptuck

and Campbell 2012), indicating that salt extrusion rates (although also slow), exceeded sedimentation rates during this time. At various times in this interval depending on the salt structure, the salt eventually welded out and stopped passively extruding, such that the diapirs were slowly draped by Units 1 to 3 across the study area, beginning a period of relative salt tectonic quiescence.

3. *Compressional active diapirism in the study area*- The history of compressional active diapirism is expressed by depositional features such as the diversion of canyons, stratal thinning of overburden, pinched stems, crestal faulting, and other features. Compressional active diapirism initiated in Unit 4 in the vertical salt diapir province and Unit 5 in the allochthonous tongue province, culminating at Unit 6 and mostly ending by the end of Unit 8. The degree of stratigraphic thinning varies across the study area with no distinct pattern. There appears to be a difference between the timing and extent of active diapirism in the vertical salt diapir province versus the allochthonous tongue province possibly indicating different mechanisms on either side of this structural boundary.

4. *Recognizing active diapirism*- Evidence for the extent of compressional active diapirism is mostly provided by stratal thinning above salt bodies in this study. Stratigraphic thinning above a given diapir can be affected by many other factors such as broader depositional trends (e.g. thickening-seaward successions), lateral pinching out of MTDs, regional and localized unconformities, crestal faulting and modern/paleocanyon erosion. Recognizing signs of active diapirism is not always straightforward, particularly in areas

where crestal erosion is prominent. A unified approach of employing regional and localized depositional trends across a group of salt bodies is needed to determine the presence of active diapirism and specifically compressional active diapirism versus halokinetic active diapirism.

5. There seem to be differences between processes driving the eastern and western portions of the study area as previously inferred by Deptuck et al. (2009). Several variations on the general pattern exist. Salt tongues in the east appear to be part of a localized linked system with upslope extension (growth faults) and downslope compression. Contourite deposition in the west was synchronous with the onset of compressional active diapirism suggesting possible sediment-loading. However, no extensional faults are seen upslope in the study area in conjunction with downslope compression. Despite these local variations, the general similarity of timing between lateral compression in both eastern and western areas could still indicate a single cause. Broader investigation of salt bodies across the slope region is needed to tie in this framework on a broader scale and thoroughly test the remaining hypothetical causes, such as regional crustal uplift and tilting.

References

Albertz, M., Beaumont, C., Shimeld, J.W., Ings, S.J., and Gradmann, S. 2010. An investigation of salt tectonic structural styles in the Scotian basin, Offshore Atlantic Canada: 1. Comparison of observations with geometrically simple numerical models. Tectonics, 29: 1-29.

Booth, J.R., Dean, M.C., DuVernay, A.E., and Styzen, M.J. 2003. Paleo-bathymetric controls on the stratigraphic architecture and reservoir development of confined fans in the Auger Basin: Central Gulf of Mexico slope. Marine and Petroleum Geology, 20: 563-586.

Bouma, A.H., 1962. Sedimentology of some flysch deposits: A graphic approach to facies interpretations. Elsevier, Amsterdam.

Brackenridge, R., Stow, D.A., and Hernández-Molina, F.J. 2011. Contourites within a deep-water sequence stratigraphic framework. Geo-Marine Letters, 31: 343-360.

Bull, S., Cartwright, J., and Huuse, M. 2009. A review of kinematic indicators from mass-transport complexes using 3D seismic data. Marine and Petroleum Geology, 26: 1132-1152.

Catuneanu, O., V. Abreu, J.P., Bhattacharya, M.D., Blum, R.W., Dalrymple, P.G., Eriksson, C.R. Fielding, W.L., Fisher, W.E., Galloway, M.R., Gibling, K.A., Giles, J.M., Holbrook, R., Jordan, C.G.St.C. Kendall, B., Macurda, O.J., Martinsen, A.D., Miall, J.E. Neal, D., Nummedal, L., Pomar, H.W., Posamentier, B.R., Pratt, J.F., Sarg, K.W., Shanley, R.J., Steel, A., Strasser, M.E., Tucker, and C., Winker. 2009. Towards the standardization of sequence stratigraphy. Earth Science Reviews, 92: 1-33.

Campbell, D.C. 2011. The Late Cretaceous and Cenozoic geological history of the outer continental margin off Nova Scotia, Canada: Insights into margins evolution from a

mature passive margin. Ph.D. Dissertation, Department of Earth Sciences, Dalhousie University, Halifax, Nova Scotia: 1-285.

Campbell, C., and Deptuck, M. 2012. Alternating Bottom-Current-Dominated and Gravity-Flow-Dominated Deposition in a Lower Slope and Rise Setting—Insights from the Seismic Geomorphology of the Western Scotian Margin, Eastern Canada. SEPM Special Publication, 99: 329-346.

Clausen, O., Nielsen, S., Egholm, D., and Goledowski, B. 2013. Reply to rasmussen (this volume): Cenozoic structures in the eastern north sea basin-A case for salt tectonics: Discussion. Tectonophysics, 601: 234-235.

Cronin, B.T., Akhmetzhanov, A.M., Mazzini, A., Akhmanov, G., Ivanov, M., and Kenyon, N.H. 2005. Morphology, evolution and fill: Implications for sand and mud distribution in filling deep-water canyons and slope channel complexes. Sedimentary Geology, 179: 71-97.

Dalla Valle, G., Gamberi, F., Rocchin, F., Minisini, D., Errera, A., Baglioni, L., Trincardi, F. 2013. 3D seismic geomorphology of mass transport complexes in a foredeep basin: Examples from the Pleistocene of the Central Adriatic Basin (Mediterranean Sea). Sedimentary Geology, 294: 127-141.

Deptuck, M.E. 2003. Post-rift geology of the Jeanne D'Arc Basin, with a focus on the architecture and evolution of early Paleogene submarine fans, and insights from modern deep-water systems. Ph.D. Dissertation, Department of Earth Sciences, Dalhousie University, Halifax Nova Scotia: 1-366.

Deptuck, M.E., Sylvester, Z., Pirmez, C., and O'Byrne, C. 2007. Migration–aggradation history and 3-D seismic geomorphology of submarine channels in the Pleistocene Benin-major canyon, Western Niger Delta Slope. Marine and Petroleum Geology, 24: 406-433.

Deptuck, M.E., Kendell, K., and Smith, B. 2009. Complex deepwater fold-belts in the southwest Sable Subbasin, Offshore Nova Scotia (extended abstract). Canadian Society of Exploration Geologists, Canadian Society of Exploration of Geophysicists, Canadian Well Logging Society Convention, Calgary, Alberta, Canada, 4p.

Deptuck, M.E. 2011a. Proximal to distal postrift structural provinces of the western Scotian Margin, Offshore Eastern Canada: Geological context and parcel prospectivity for Call for Bids NS11-1. Canada-Nova Scotia Offshore Petroleum Board, Geoscience Open File Report, 2011-001.

Deptuck, M.E. 2011b. Potential shelf sources for deepwater reservoirs along the southwestern Scotian Margin. 2011 AAPG ICE: Nova Scotia Play Fairway Analysis Seminar Technical Presentations (Talk).

Deptuck, M.E., and Campbell, D.C. 2012. Widespread erosion and mass failure from the ~51 ma Montagnais marine bolide impact off southwestern Nova Scotia, Canada. Canadian Journal of Earth Sciences, 49: 1567-1594.

Deptuck, M. E., and Kendell, K. 2012. Contrasting salt tectonic styles on the western versus central parts of the Scotian Margin, offshore Nova Scotia, CNSOPB Open File Poster 2012-001PF, 2 panels.

Doeven, P.H., 1983. Cretaceous nannofossil stratigraphy and paleoecology of the Canadian Atlantic Margin. Bulletin of the Geological Survey of Canada, 356: 1-70.

Dooley, T.P., Jackson, M.P., and Hudec, M.R. 2009. Inflation and deflation of deeply buried salt stocks during lateral shortening. Journal of Structural Geology, 31: 582-600.

Faugères, J., Stow, D.A.V., Imbert, P., and Viana, A. 1999. Seismic features diagnostic of contourite drifts. Marine Geology, 162: 1-38.

Fensome, R., Crux, J., Gard, G., MacRae, A., Williams, G., Thomas, F., Fiorini, F., and Wach, G. 2008. The last 100 million years on the Scotian margin, Offshore Eastern Canada: An event-stratigraphic scheme emphasizing biostratigraphic data. Atlantic Geology, 44: 93-126.

Gauley, B-J.L., 2001. Lithostratigraphy and sediment failure on the central Scotian Slope. M.Sc. thesis, Dalhousie University, Halifax, N.S., Canada, 214 p.

Grist, A.M., and Zentilli, M. 2003. Post-Paleocene cooling in the southern Canadian Atlantic region: evidence from apatite fission track models. Canadian Journal of Earth Sciences, 40: 1279-1297.

Hart, B.S. 2000. 3-D seismic interpretation: A primer for geologists. Society for Sedimentary Geology (SEPM), Volume 48, 123p.

Hay, D. 2012. Stratigraphic evolution of a tortuous corridor from the stepped slope of Angola. SEPM Special Publication, 99: 163-180.

Hilgen, F. J., Schwarzacher, W., and Strasser, A. 2004. Concepts and definitions in cyclostratigraphy. SEPM. Special Publication, 81: 303–305.

Hudec, M.R., and Jackson, M.P. 2007. Terra infirma: Understanding salt tectonics. Earth-Science Reviews, 82: 1-28.

Hudec, M. R., and Jackson, M. P. 2011, The salt mine: a digital atlas of salt tectonics. The University of Texas at Austin, Bureau of Economic Geology, Udden Book Series No. 5; AAPG Memoir 99, 305 p.

Ings, S.J., and Shimeld, J.W. 2006. A new conceptual model for the structural evolution of a regional salt detachment on the northeast Scotian margin, Offshore Eastern Canada. AAPG Bulletin, 90: 1407-1423.

Jackson, M.P., Vendeville, B.C., and Schultz-Ela, D.D. 1994. Structural dynamics of salt systems. Annual Review of Earth and Planetary Sciences, 22: 93-117.

Jackson, C.A., Barber, G.P., and Martinsen, O.J. 2008. Submarine slope morphology as a control on the development of sand-rich turbidite depositional systems: 3D seismic analysis of the Kyrre Formation (Upper Cretaceous), Måløy Slope, Offshore Norway. Marine and Petroleum Geology, 25: 663-680.

Jansa, L. and Wade, J. 1975. Geology of the continental margin Offshore Nova Scotia and Newfoundland. Offshore geology of Eastern Canada, 2: 74-30.

Kendell, K.L. 2012. Variations in salt expulsion style within the Sable Canopy Complex, central Scotian margin. Canadian Journal of Earth Sciences, 49: 1504-1522.

Kneller, B. 2003. The influence of flow parameters on turbidite slope channel architecture. Marine and Petroleum Geology, 20: 901-910.

Labails, C., Olivet, J., Aslanian, D., and Roest, W.R. 2010. An alternative early opening scenario for the central Atlantic Ocean. Earth and Planetary Science Letters, 297: 355-368.

Lang, J., Hampel, A., Brandes, C., and Winsemann, J. 2014. Response of salt structures to ice-sheet loading: Implications for ice-marginal and subglacial processes. Quaternary Science Reviews, 101: 217-233.

Lines, L.R. and Newrick, R.T. 2004. Fundamentals of geophysical interpretation. Geophysical monograph series,13: 1-274.

Lowe, D. 1982. Sediment gravity flows: II: Depositional models with special reference to the deposits of high-density turbidity currents. Journal of Sedimentary Petrology, 52: 279-297.

Lowe, D.R. 1976. Grain flow and grain flow deposits. Journal of Sedimentary Research, 46.

MacDonald, A.W. 2005. Cenozoic seismic stratigraphy of the central Nova Scotian Continental Margin: the interplay of erosion, deposition and salt tectonics. MSc. Thesis, Geology Department, Saint Mary's University, Halifax, Nova Scotia: 1-152.

MacRae, R.A., Pe-Piper, G., Deptuck, M.E., and Decoste, A. 2014. Stratigraphic revelations regarding Mesozoic salt on the Scotian Margin and implications for early trans-Atlantic basin history (abstract). Canadian Society of Exploration Geologists, Canadian Society of Exploration of Geophysicists, Canadian Well Logging Society Convention, Calgary, Alberta, Canada, 2p.

Mayall, M., Jones, E., and Casey, M. 2006. Turbidite channel reservoirs—key elements in facies prediction and effective development. Marine and Petroleum Geology, 23: 821-841.

McHargue, T., Pyrcz, M.J., Sullivan, M.D., Clark, J., Fildani, A., Romans, B., Covault, J., Levy, M., Posamentier, H., and Drinkwater, N. 2011. Architecture of turbidite channel systems on the continental slope: Patterns and predictions. Marine and Petroleum Geology, 28: 728-743.

Meckell III, L.D. 2011. Sand-prone submarine mass-transport deposits: reservoir characteristics and classification of an underappreciated deepwater facies. Houston Geological Society Bulletin, 52: 17-23.

Mitchum, R.M. Jr., P.R. Vail, and S. Thompson, III, 1977. Seismic stratigraphy and global changes of sea level; Part 2, The depositional sequence as a basic unit for stratigraphic analysis: AAPG Memoir 26, p. 53-62.

Mosher, D.C., Piper, D.J., Campbell, D.C., and Jenner, K.A. 2004. Near-surface geology and sediment-failure geohazards of the central Scotian Slope. AAPG Bulletin, 88: 703-723.

Mulder, T. 2011. Gravity processes and deposits on continental slope, rise and abyssal plains: Chapter 2 *In* Deep-sea Sediments. *Editted by* H. Hüneke,and T. Mulder. Developments in Sedimentology 63, Elsevier, Amsterdam: 25-148.

Nelson, C. H., Escutia, C., Damuth, J. E., and Twichell, D. C. 2011. Interplay of mass-transport and turbidite-system deposits in different active tectonic and passive continental margin settings: External and local controlling factors. Sedimentary Geology, 96: 39-66.

Normark, W.R., and Piper, D.J.W. 1991. Initiation processes and flow evolution of turbidity currents: implications for the depositional record, *In*: From Shoreline to Abyss: Contributions in Marine Geology in Honor of Francis Parker Shepard, Society for Sedimentary Geology (SEPM): 207-230.

Offshore Energy Technical Research (OETR) Association. 2011. Play Fairway Analysis Atlas. Available from http://www.novascotiaoffshore.com/analysis [accessed 14 Dec. 2012].

Olafiranye, K., Jackson, C.A., and Hodgson, D.M. 2013. The role of tectonics and mass-transport complex emplacement on upper slope stratigraphic evolution: A 3D seismic case study from Offshore Angola. Marine and Petroleum Geology, 44: 196-216.

Piper, D.J.W., and A.E. Aksu. 1987. The source and origin of the 1929 Grand Banks turbidity current inferred from sediment budgets. Geomarine Letters 7:177–182.

Piper, D.J., Normark, W.R., and Sparkes, R. 1987. Late Cenozoic stratigraphy of the central Scotian Slope, Eastern Canada. Bulletin of Canadian Petroleum Geology, 35: 1-11.

Piper, D.J. and Normark, W.R. 2009. Processes that initiate turbidity currents and their influence on turbidites: A marine geology perspective. Journal of Sedimentary Research, 79: 347-362.

Porter, M.J., Brien S.O., and Brealey, C. 2002. Thrumcap Geophysical Report: Volume 1. 3D seismic survey over liceneses EL 2359, EL2381, and EL2382, Offshore Nova Scotia; Program No. NS24-S6-1E.

Postma, G. 1986. Classification for sedimentary gravity-flow deposits based on flow conditions during sedimentation. Geology, 14: 291-294.

Prather, B.E. 2000. Calibration and visualization of depositional process models for above-grade slopes: A case study from the Gulf of Mexico. Marine and Petroleum Geology, 17: 619-638.

Prather, B.E. 2003. Controls on reservoir distribution, architecture and stratigraphic trapping in slope settings. Marine and Petroleum Geology, 20: 529-545.

Pyles, D.R., Syvitski, J.P., and Slatt, R.M. 2011. Defining the concept of stratigraphic grade and applying it to stratal (reservoir) architecture and evolution of the slope-to-basin profile: An outcrop perspective. Marine and Petroleum Geology, 28: 675-697.

Rasmussen, E.S. 2013. Cenozoic structures in the eastern north sea Basin—A case for salt tectonics: Discussion. Tectonophysics, 601: 226-233.

Ross, W., Halliwell, B., May, J., Watts, D., and Syvitski, J. 1994. Slope readjustment: A new model for the development of submarine fans and aprons. Geology, 22: 511-514.

Rowan, M.G., Peel, F.J., and Vendeville, B.C. 2004. Gravity-driven fold belts on passive margins. AAPG Memoir, 82: 157-182.

Schultz-Ela, D.D., Jackson, M.P., and Vendeville, B.C. 1993. Mechanics of active salt diapirism. Tectonophysics, 228: 275-312.

Shanmugam, G. 2006. Deep-water processes and facies models: Implications for sandstone petroleum reservoirs: Implications for sandstone petroleum reservoirs. .

Shaw, J., Piper, D., Fader, G., King, E., Todd, B., Bell, T., Batterson, M., and Liverman, D. 2006. A conceptual model of the deglaciation of Atlantic Canada. Quaternary Science Reviews, 25: 2059-2081.

Shimeld, J. 2004. A comparison of Salt Tectonic Subprovinces beneath the Scotian Slope and Laurentian Fan. *In* Salt-sediment interactions and hydrocarbon prospectivity. *Edited by* P.J. Post, D.L. Olson, K.T. Lyons, S.L. Palmes, P.F. Harrison, and N.C. Rosen. 24th Annual Research Conference, Gulf Coast Section, SEPM Foundation: 502-532.

Smith, R. 2004. Silled sub-basins to connected tortuous corridors: Sediment distribution systems on topographically complex sub-aqueous slopes. Geological Society, London, Special Publications, 222: 23-43.

Stea, R.R., Piper, D., Fader, G., and Boyd, R. 1998. Wisconsinan glacial and sea-level history of maritime Canada and the adjacent continental shelf: A correlation of land and sea events. Geological Society of America Bulletin, 110: 821-845.

Stow, D. and Holbrook, J. 1984. North Atlantic contourites: An overview. Geological Society, London, Special Publications, 15: 245-256.

Stow, D.A. and Mayall, M. 2000. Deep-water sedimentary systems: New models for the 21st century. Marine and Petroleum Geology, 17: 125-135.

Swift, S.A. 1987. Late Cretaceous-Cenozoic development of outer continental margin, southwestern Nova Scotia. AAPG Bulletin, 71: 678-701.

Thomas, F.C. 2001. Cenozoic micropaleontology of three wells, Scotian Shelf and Slope. GSC Open File Report #4014.

Vendeville, B.C. and Jackson, M. 1992. The rise of diapirs during thin-skinned extension. Marine and Petroleum Geology, 9: 331-354.

Vendeville, B.C., and Nilsen, K.T. 1995. Episodic growth of salt diapirs driven by horizontal shortening. GSC CSEPM Foundation 16th Annual Research Conference: Salt Sediment and Hydrocarbons, 3-6 December 1995.

Viana, A.R. and Rebesco, M. 2007. Economic and palaeoceanographic significance of contourite deposits. Geological Society Special Publication 276.

Wade, J.A., and MacLean, B.C. 1990. Chapter 5-The geology of the southeastern margin of Canada. Part 2: Aspects of the geology of the Scotian Basin from recent seismic and well data. *In* Geology of the continental margin of eastern Canada. *Edited by* M.J. Keen and G.L. Williams. Geological Survey of Canada, Geology of Canada No. 2: 190-238.

Weston, J.F., MacRae, R.A., Ascoli, P., Cooper, M.K.E., Fensome, R.A., Shaw, D., Williams, G.L., Dehler, S., Deptuck, M., and Karim, A. 2012. A revised biostratigraphic and well-log sequence-stratigraphic framework for the Scotian margin, Offshore Eastern Canada. Canadian Journal of Earth Sciences, 49: 1417-1462.

Williams G.L. 1991. Palynological analysis of the interval 995-5040 m in Husky-Bow Valley et al. Evangeline H-98, Scotian Shelf. GSC Internal Report: BAS-PAL.2-91GLW.

Yilmaz, Ö. 1987. Investigations into Geophysics, Volume 2: Seismic Data Processing. Society of Exploration Geophysicists, Tulsa, Oklahoma.

Yilmaz, Ö. 2001. Seismic data analysis. Society of Exploration Geophysicists, Tulsa, Oklahoma.

Appendix 1

Profile examples showing details across vertical diapirs in the study area. Figures are generally ordered from proximal to distal (i.e. proximal diapir P1 is first and distal salt body D8 is last). Conventions for Horizon and Unit labels are explained in Chapter 4.4 and a chart with their age assignments is in Figure 4.2 or Figure 6.8. Transects were generally taken to capture each salt body's characteristics.

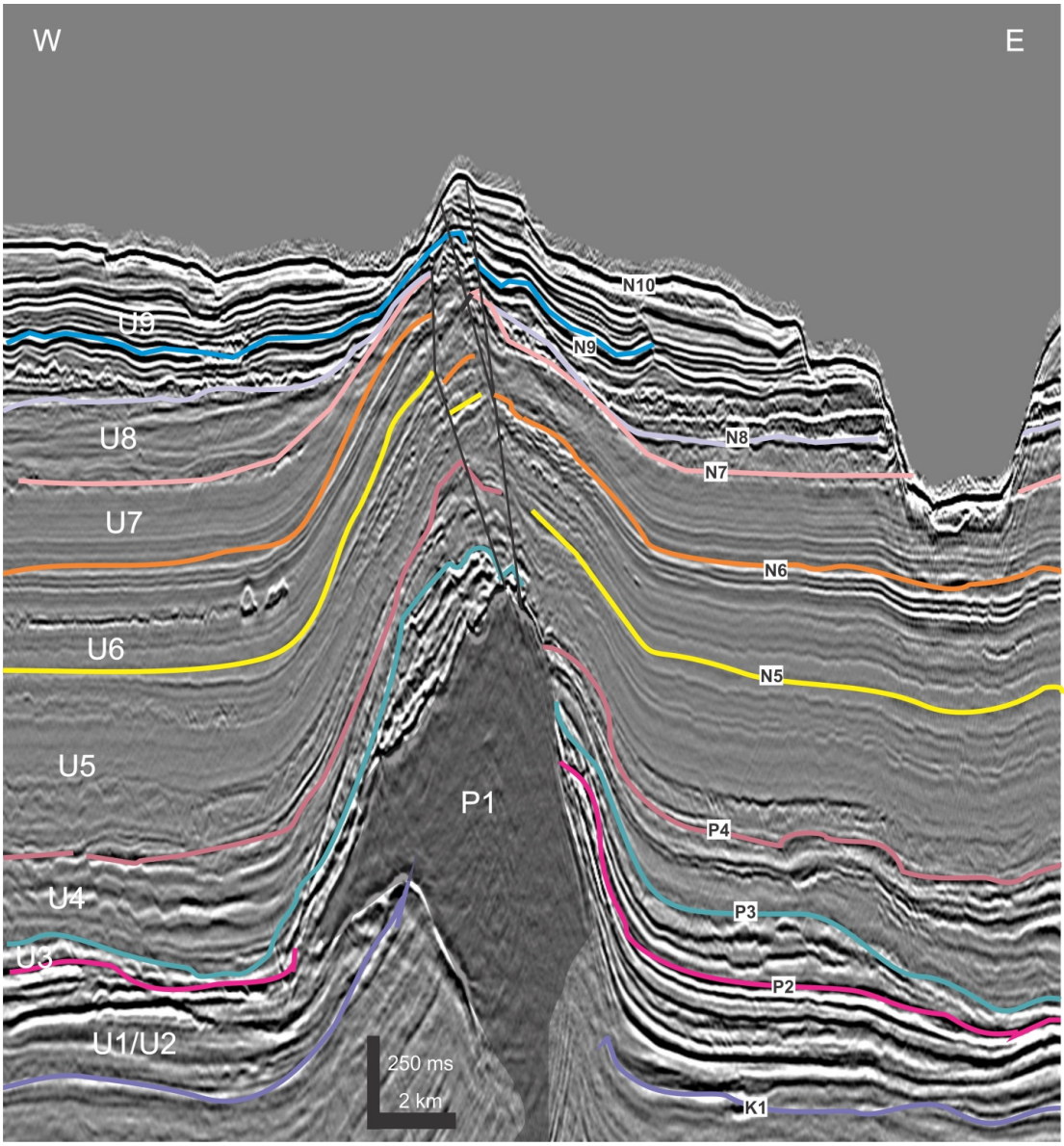

Figure A-1: Salt diapir P1 (strike line).

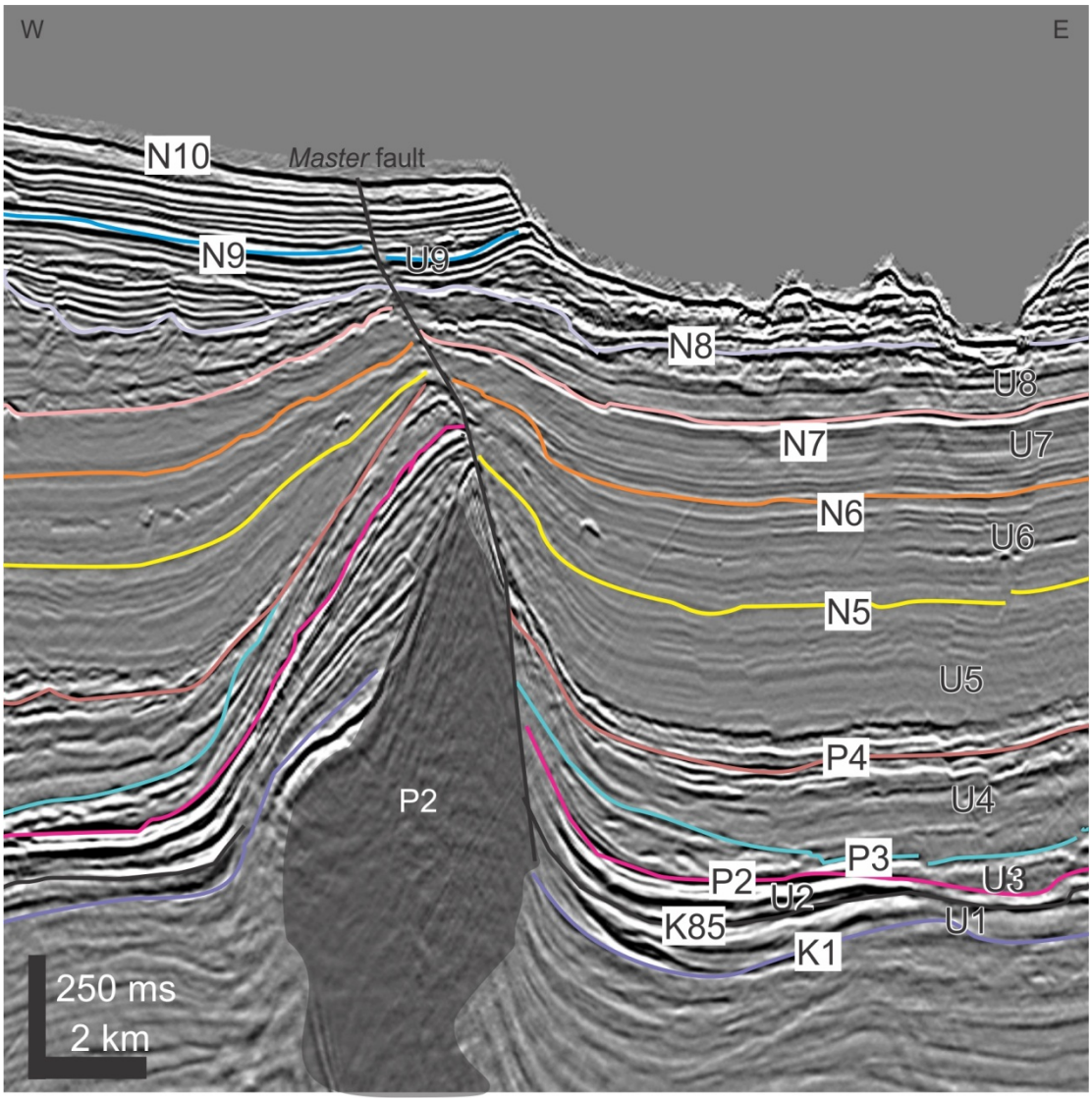

Figure A-2: Salt diapir P2 (strike line).

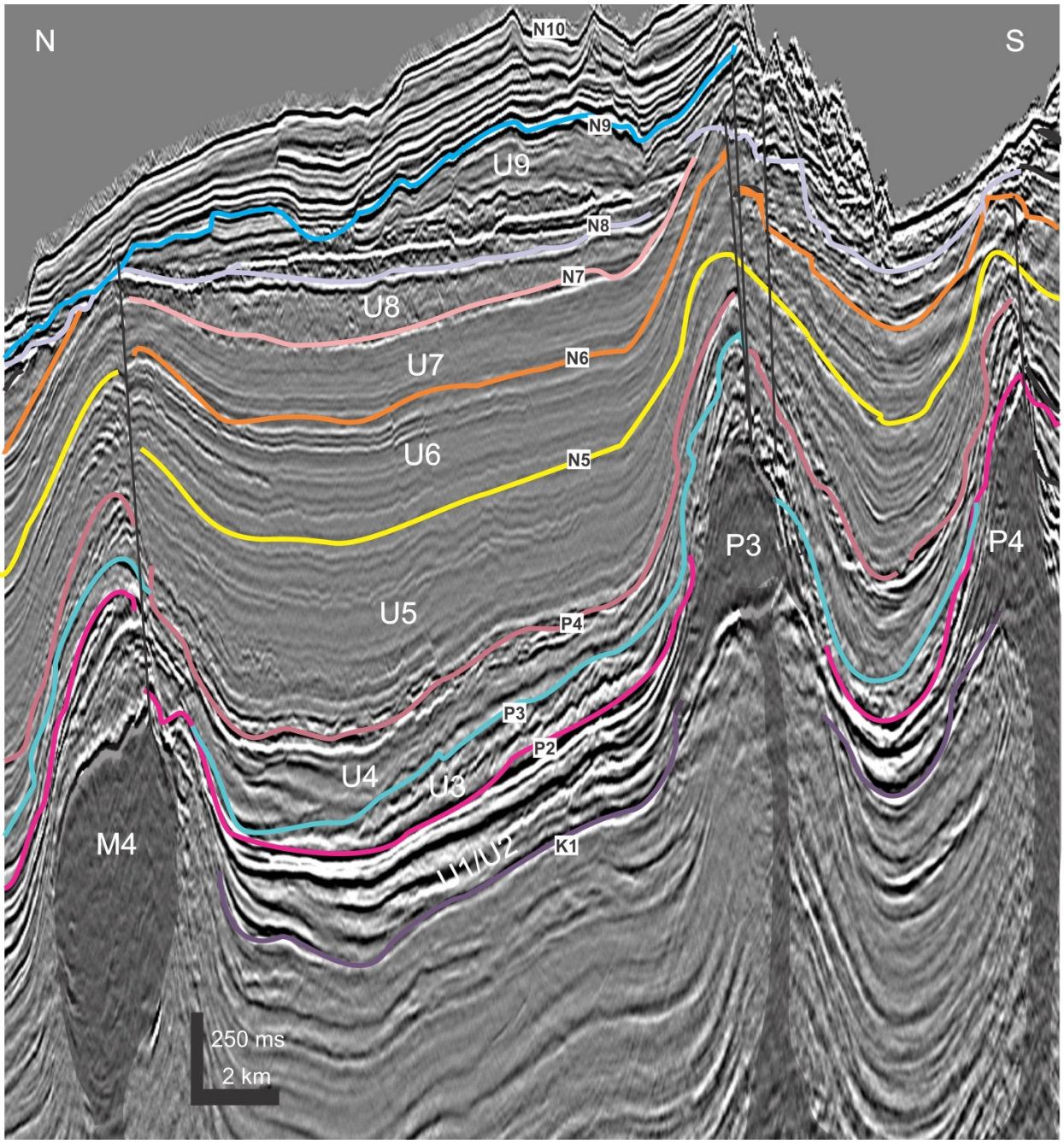

Figure A-3: Salt diapirs P3, P4 and M4 (dip line).

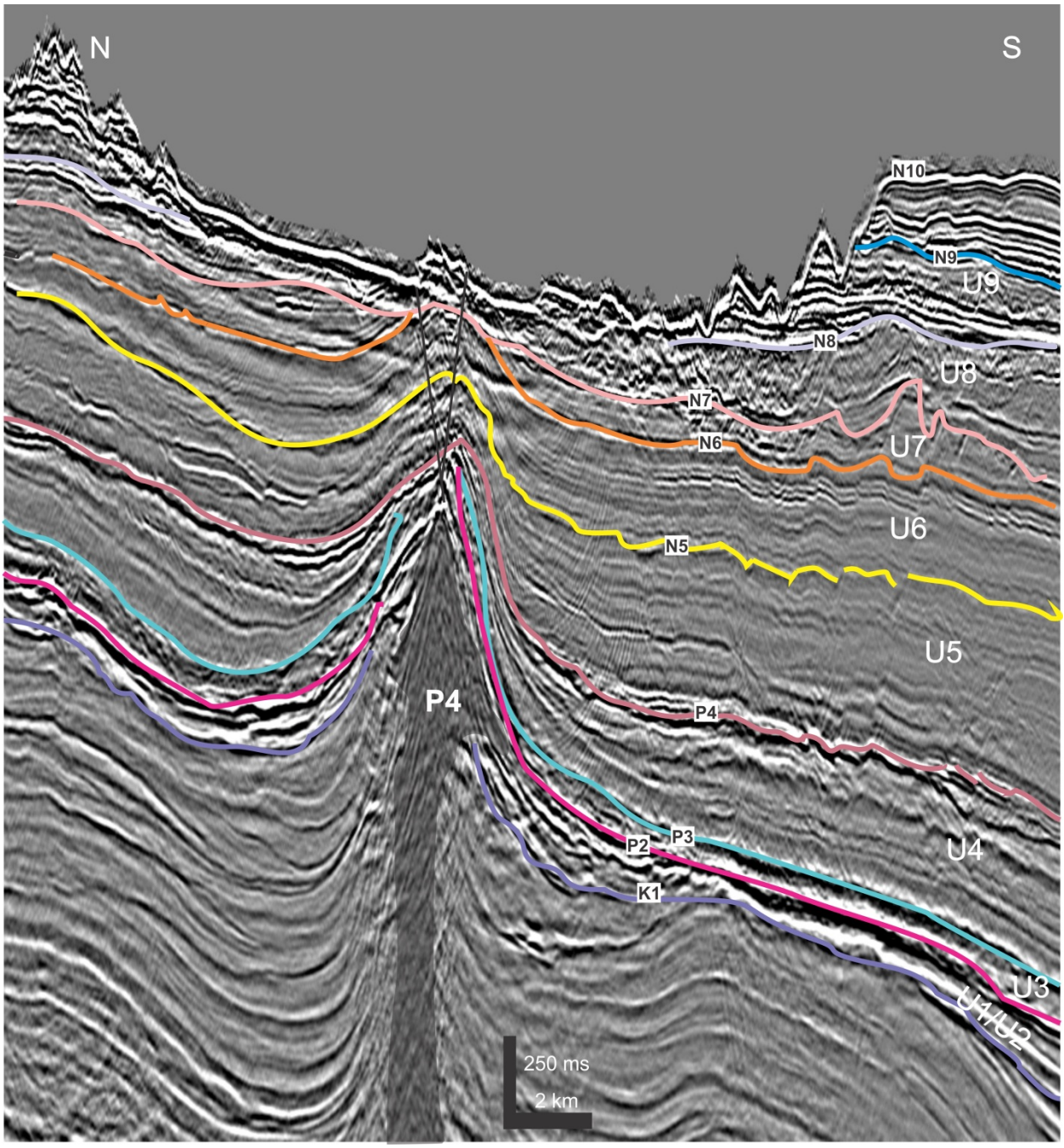

Figure A-4: Salt diapir P4 (dip line).

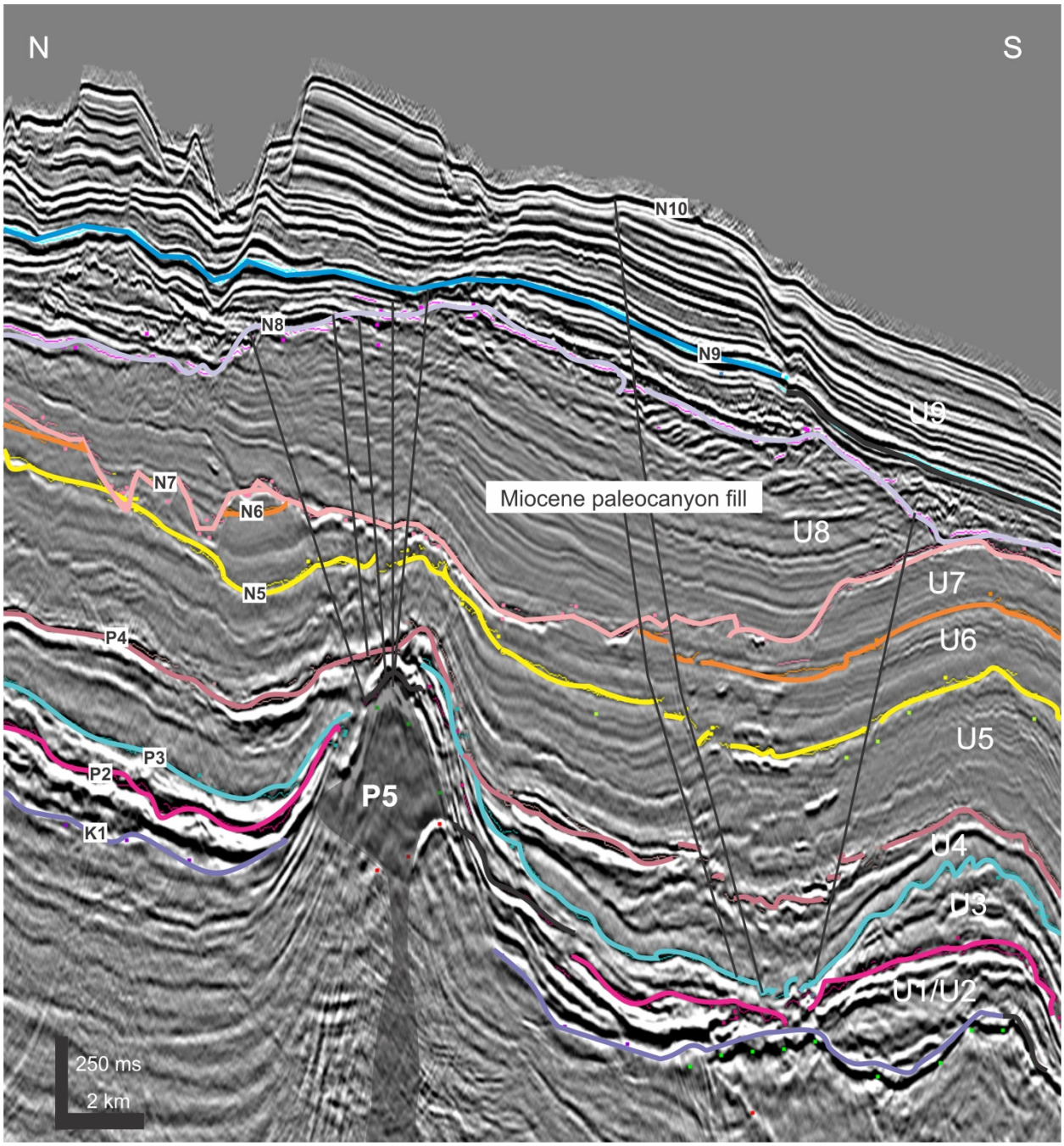

Figure A-5: Salt diapir P5 (dip line).

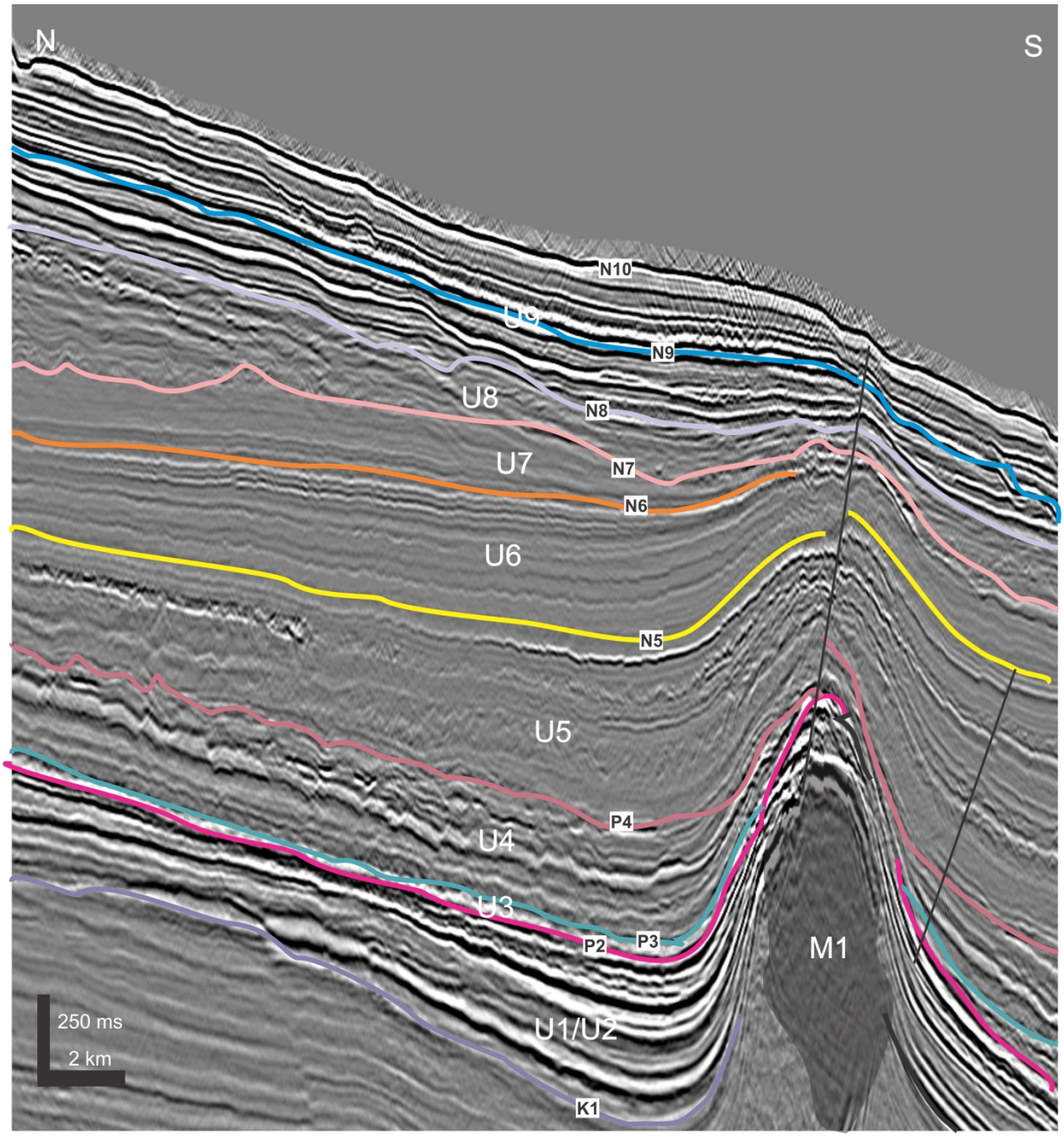

Figure A-6: Salt diapir M1 (dip line).

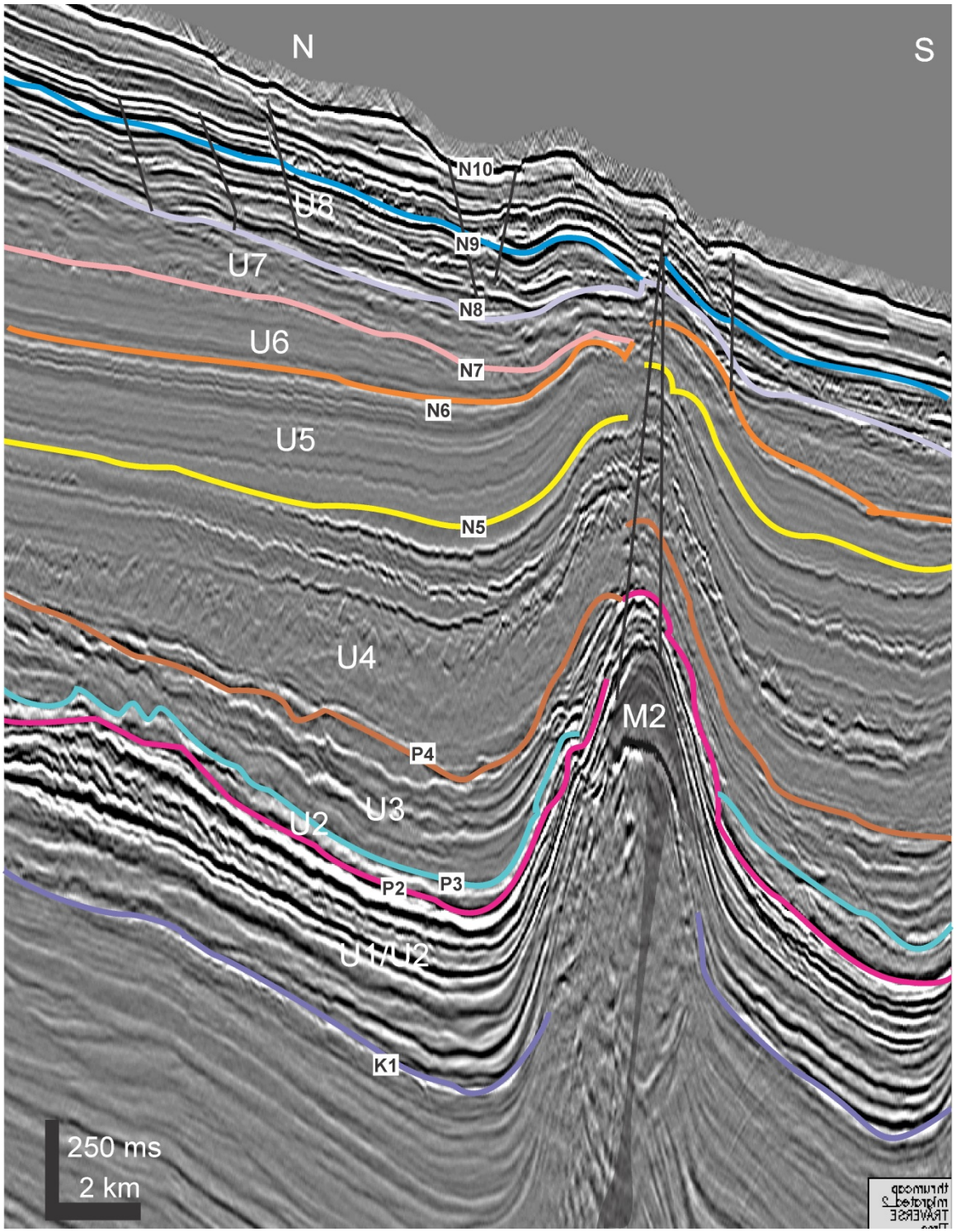

Figure A-7: Salt diapir M2 (dip line).

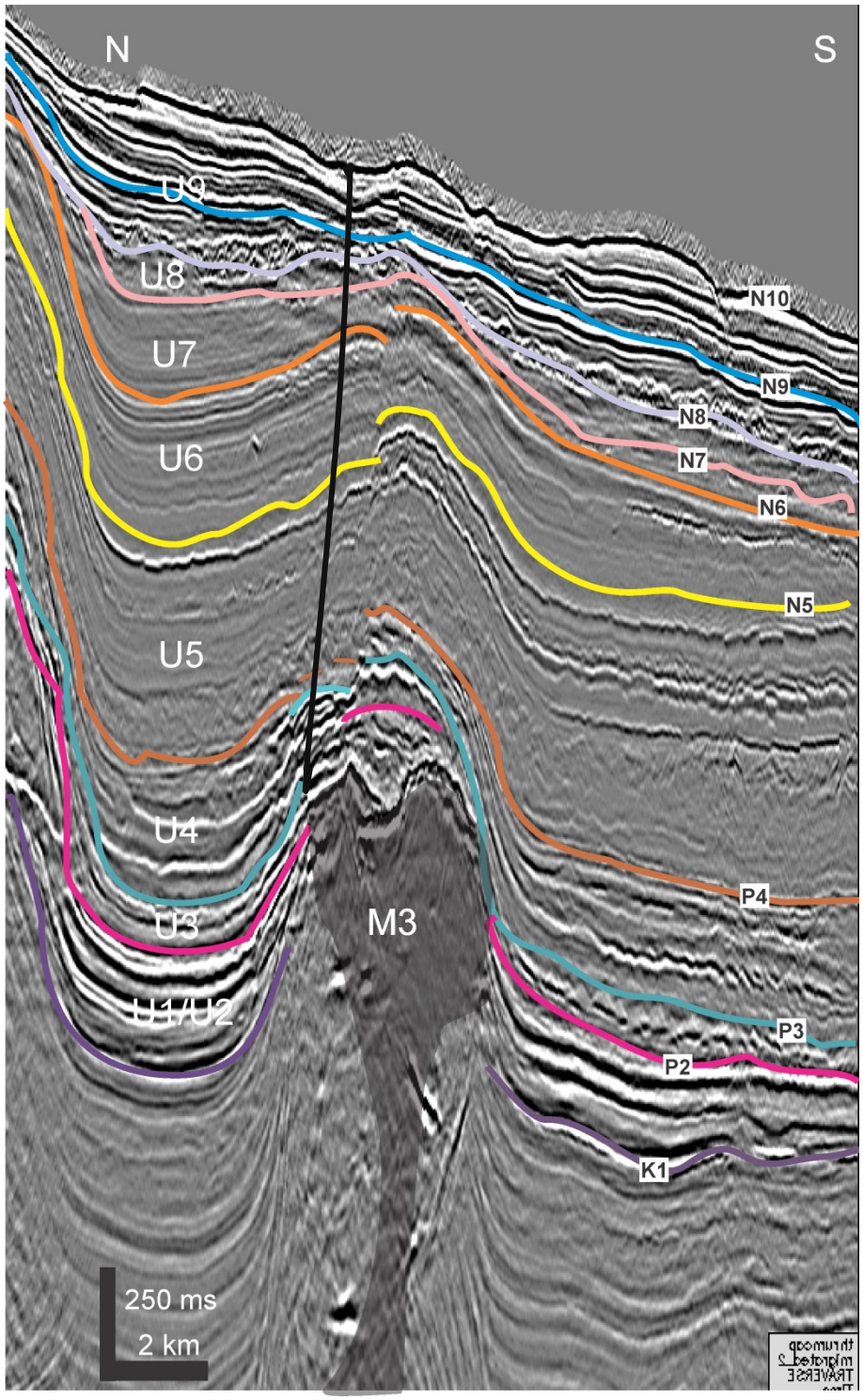

Figure A-8: Salt diapir M3 (dip line).

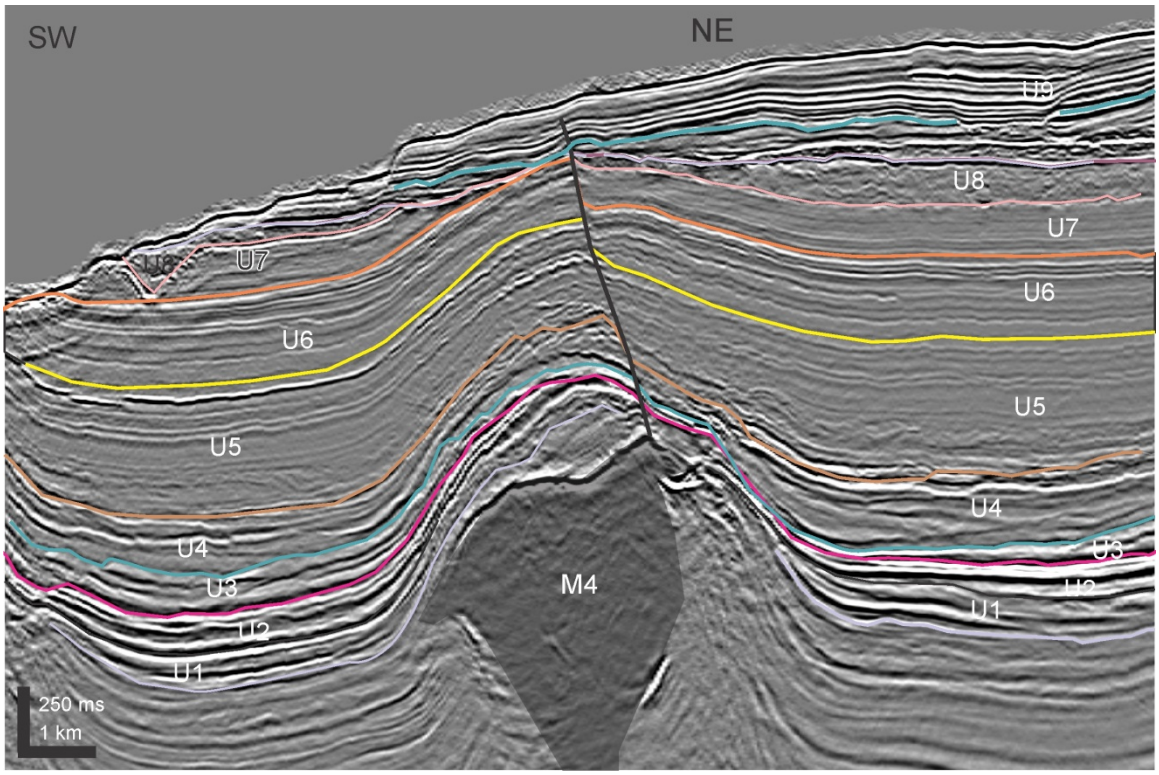

Figure A-9: Salt diapir M4 (strike line).

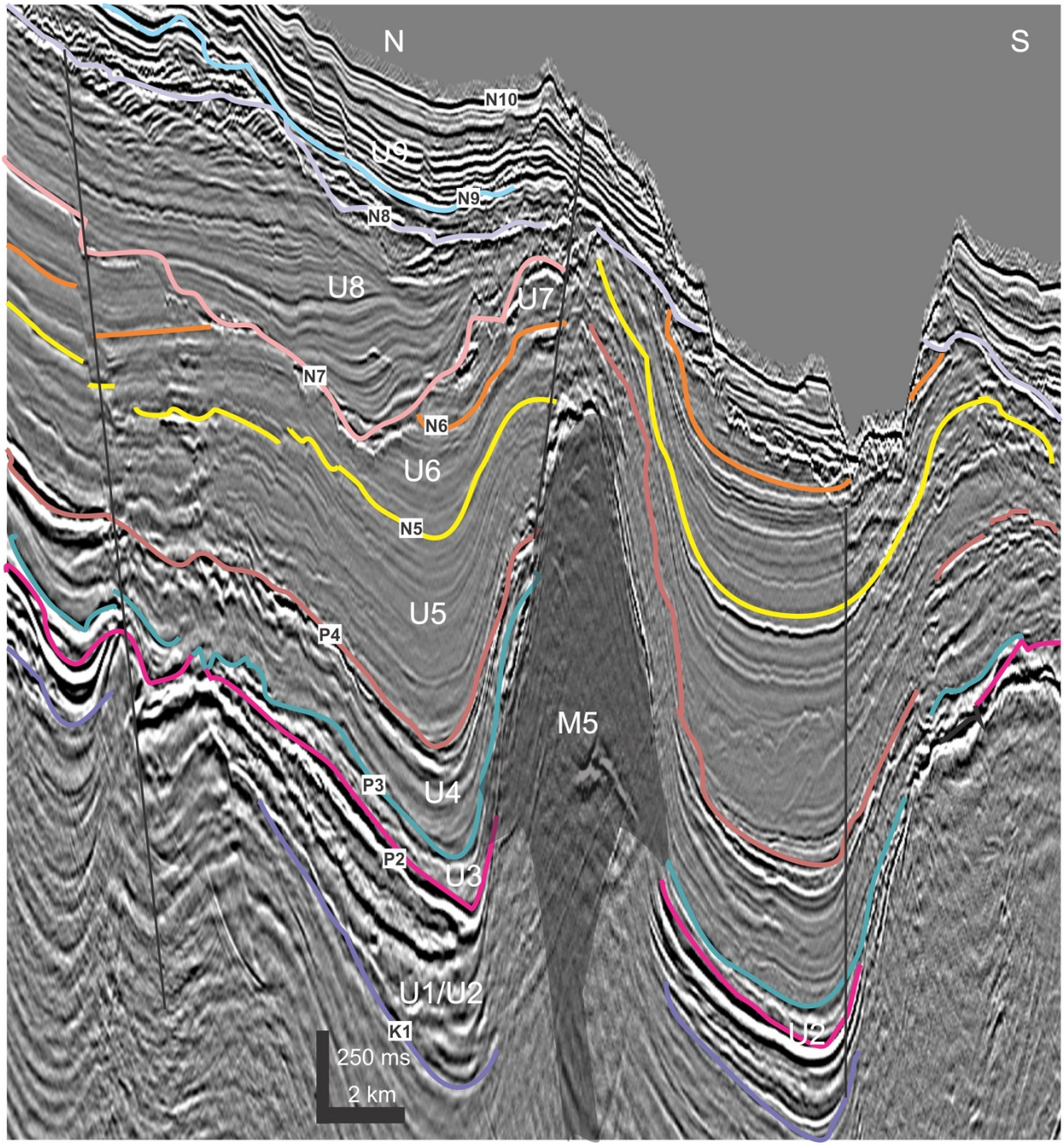

Figure A-10: Salt diapir M5 (dip line).

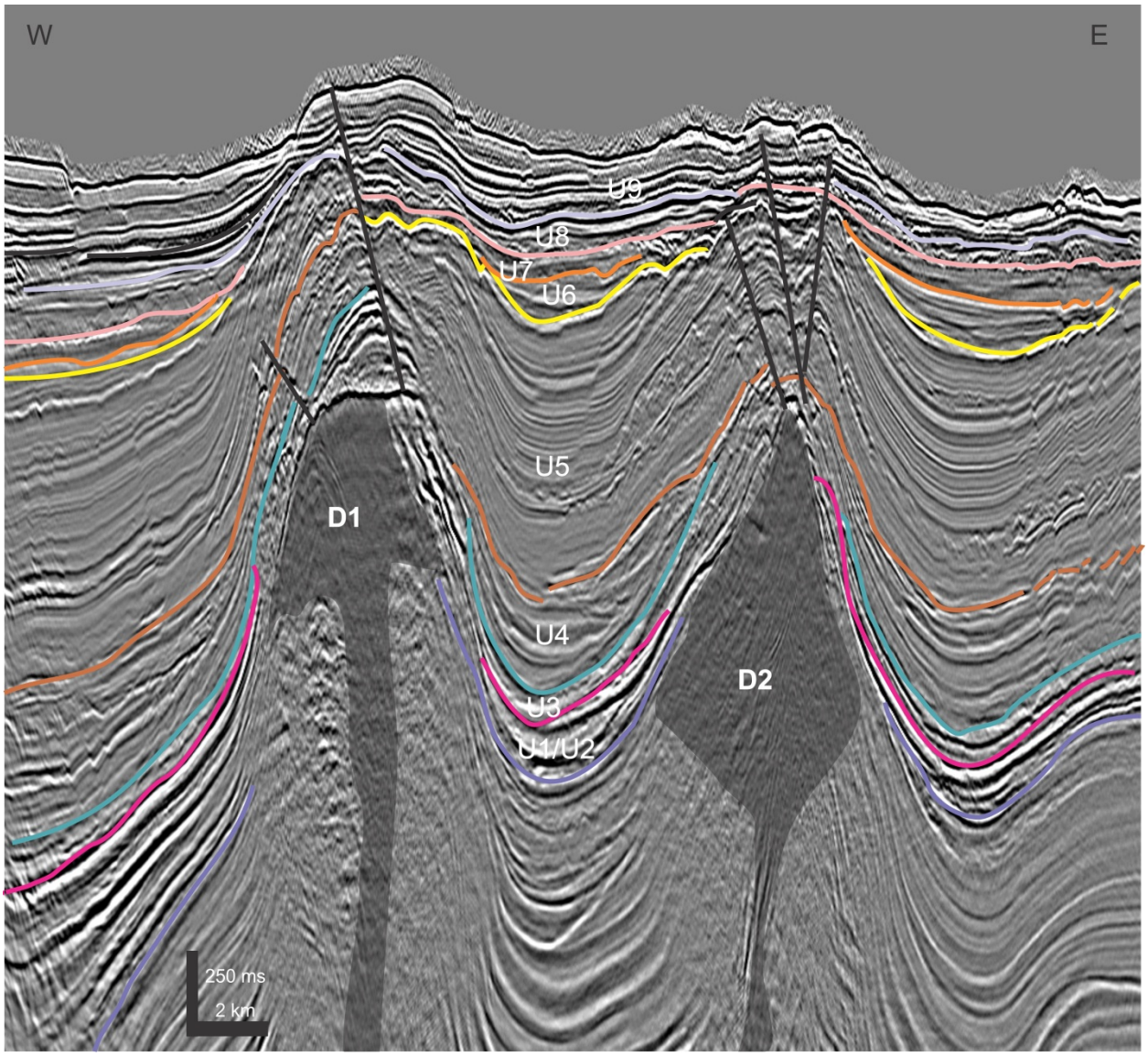

Figure A-11: Salt diapirs D1 and D2 (strike line).

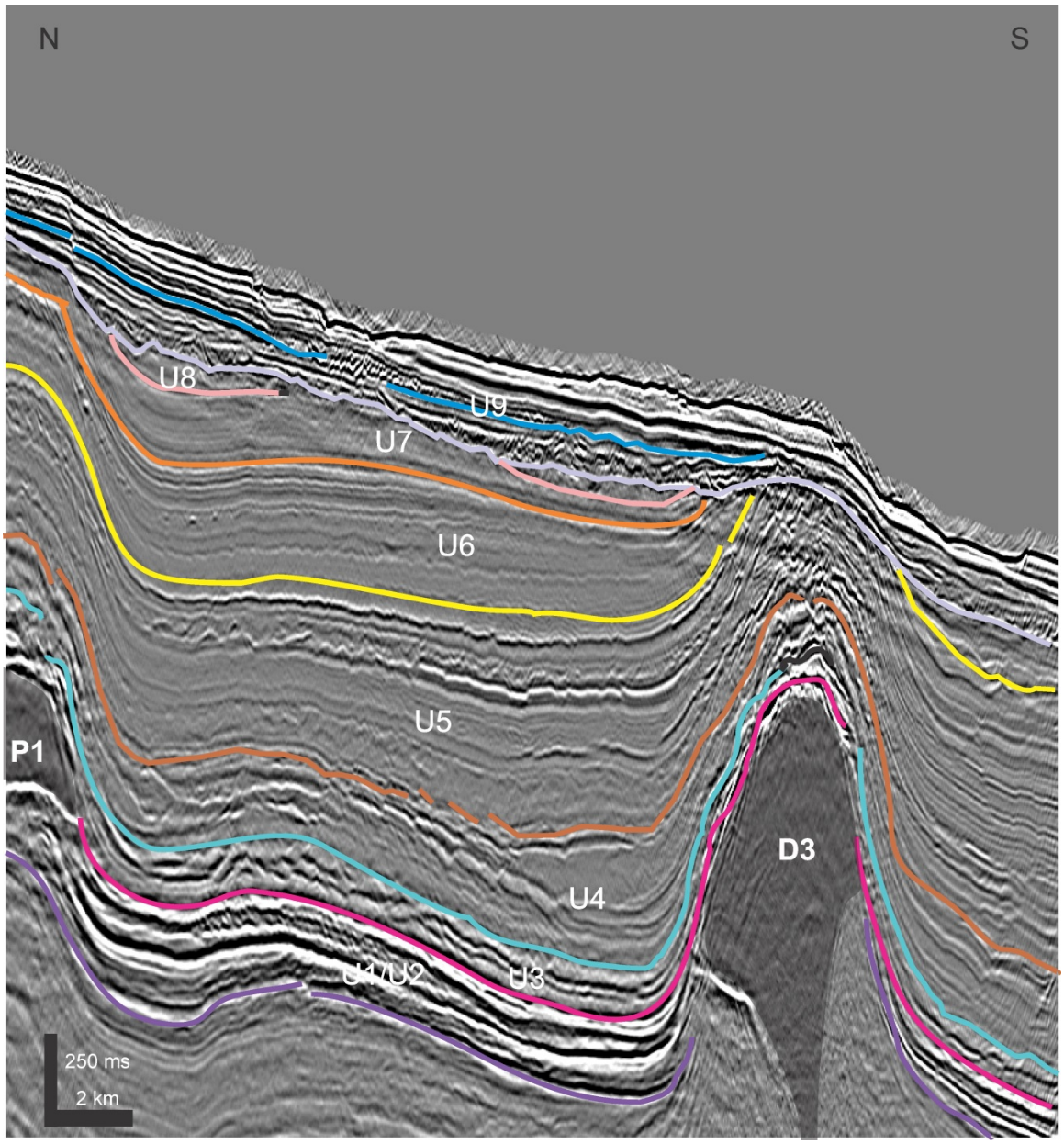

Figure A-12: Salt diapirs P1 (partial) and D3 (dip line).

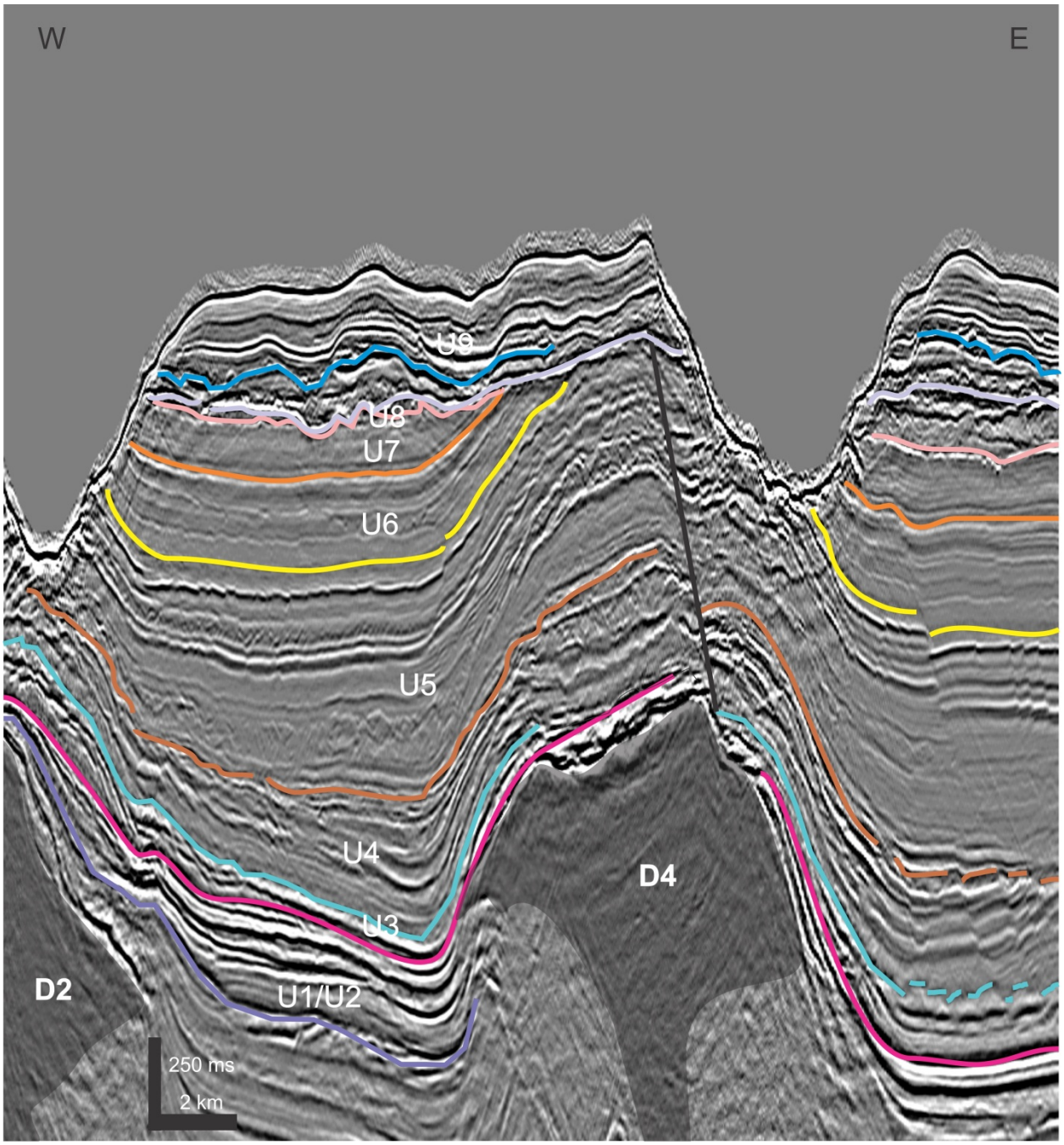

Figure A-13: Salt diapirs D2 (partial) and D4 (strike line).

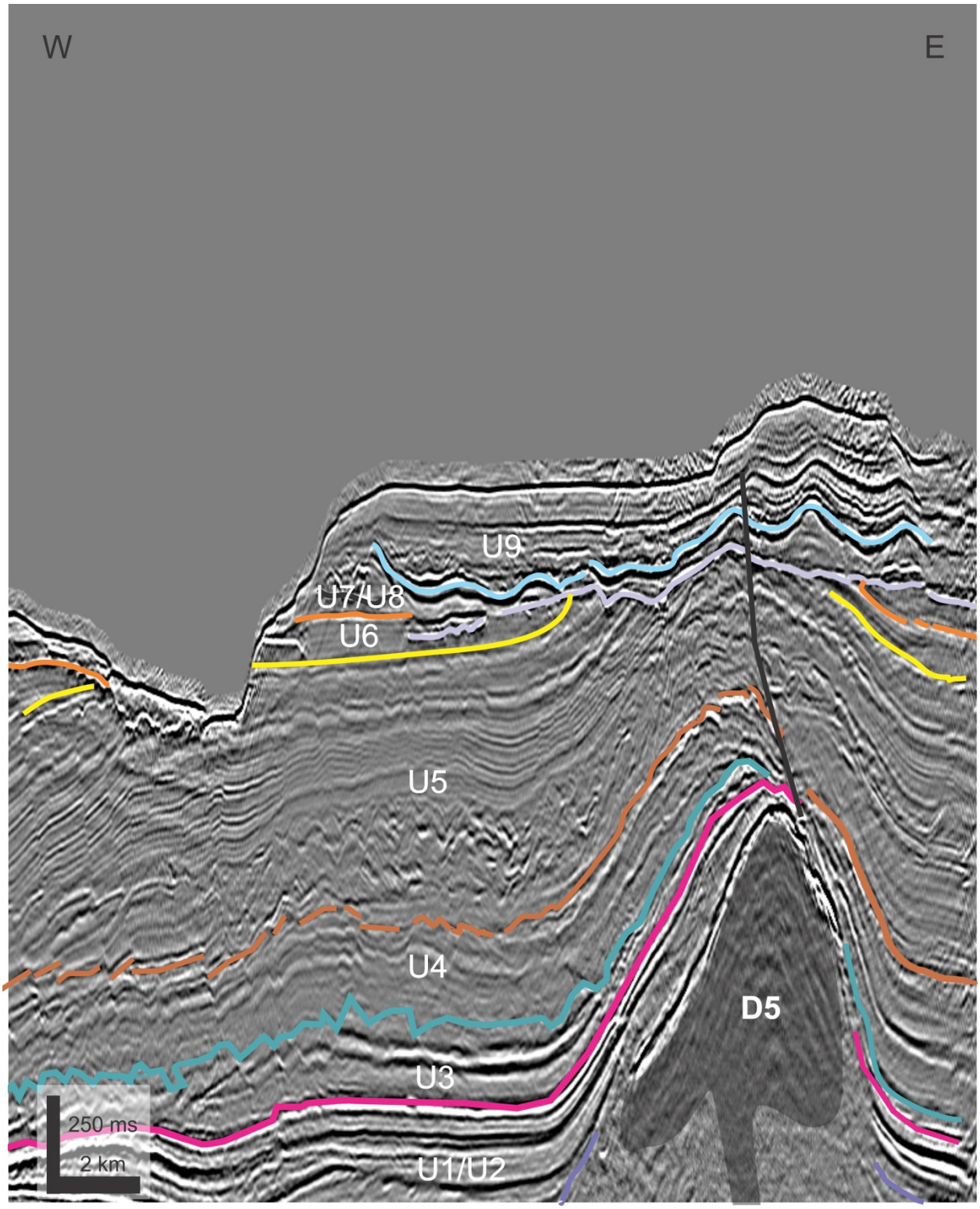

Figure A-14: Salt diapir D5 (strike line).

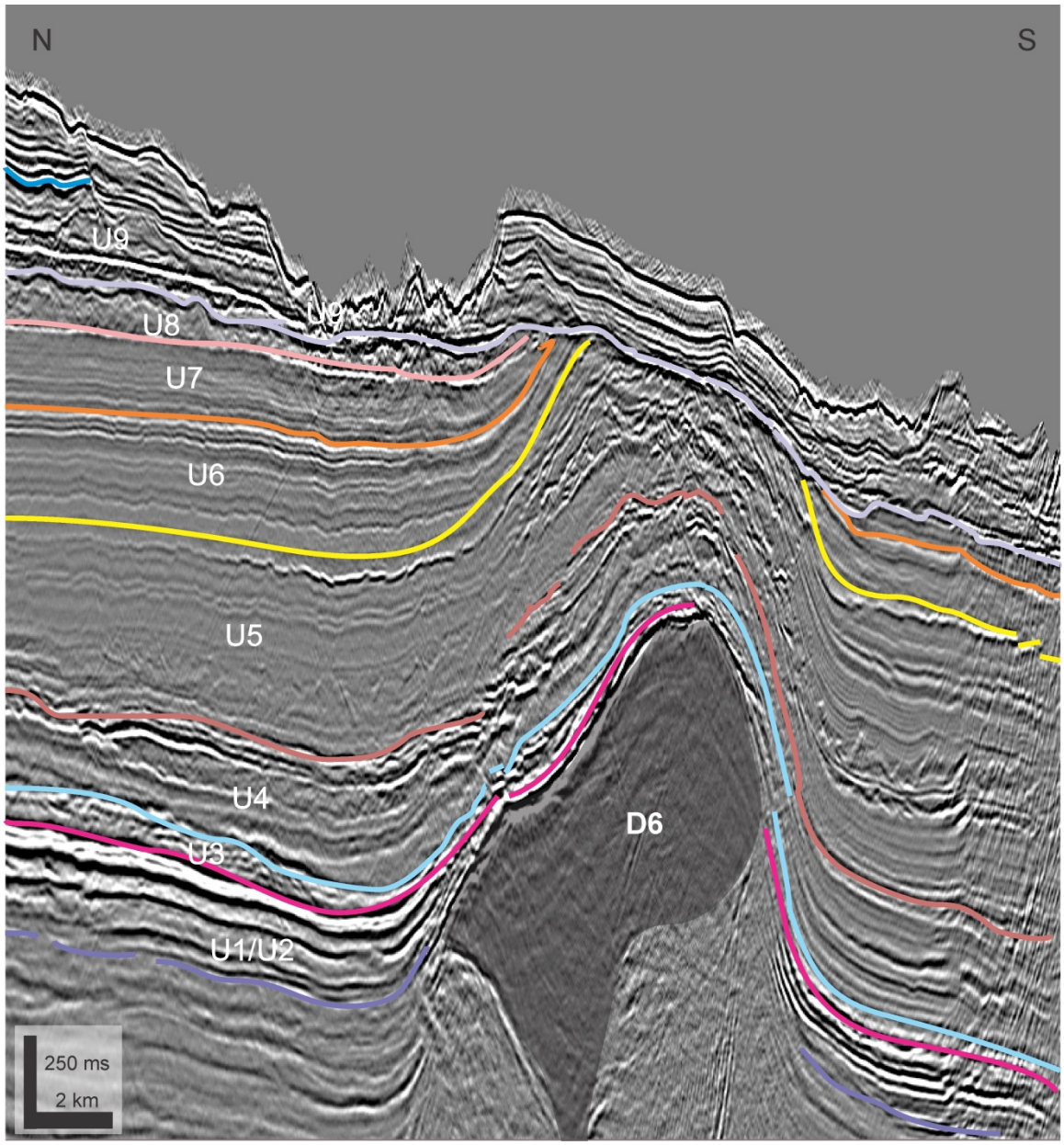

Figure A-15: Salt diapir D6.

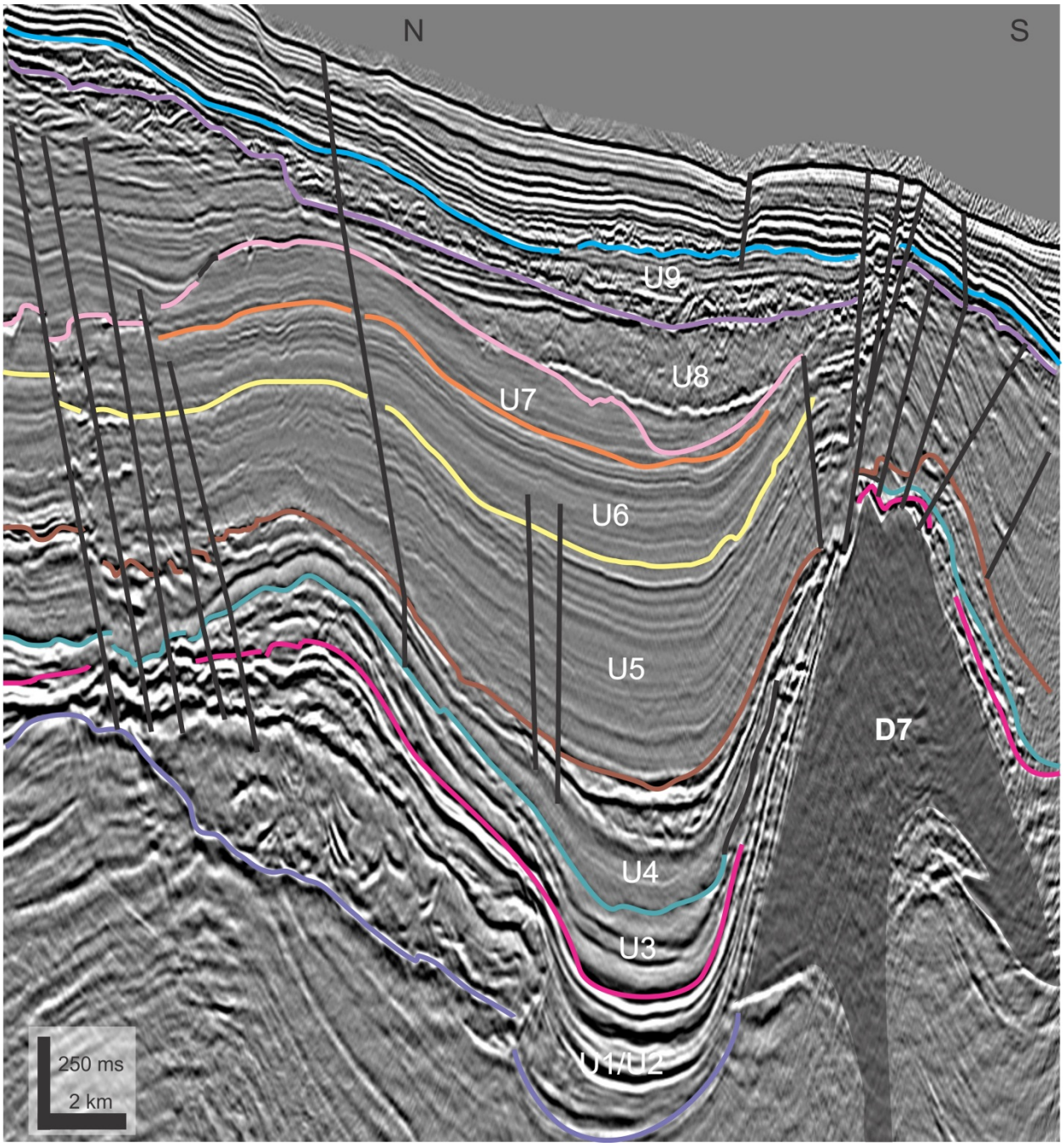

Figure A-16: Salt diapir D7.

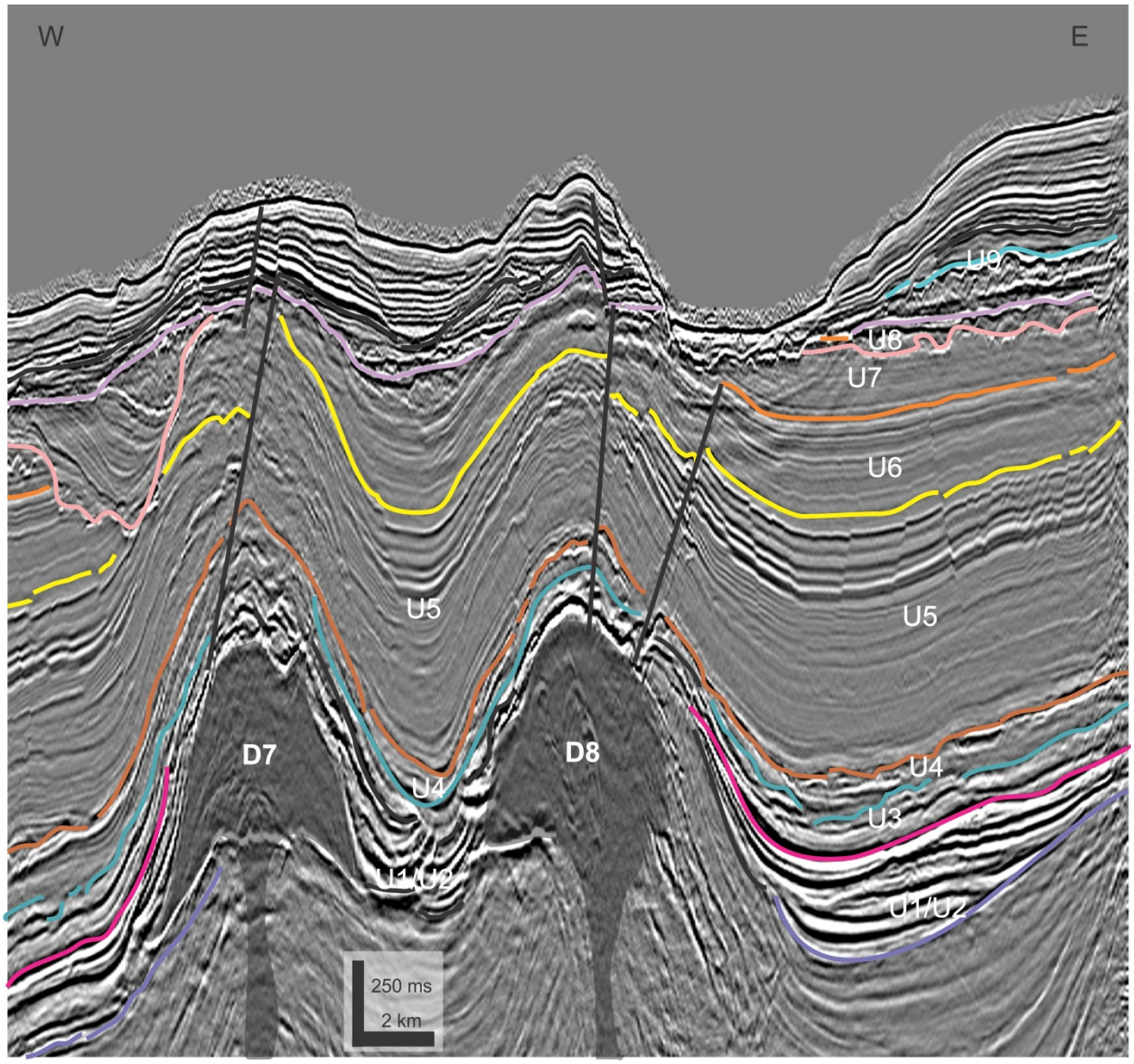

Figure A-17: Salt diapir D7 and D8 (strike line).